



MINISTÉRIO DA
CIÊNCIA, TECNOLOGIA
E INOVAÇÕES



sid.inpe.br/mtc-m21d/2021/11.25.20.43-TDI

SYNCHRONIZATION IN OSCILLATOR NETWORKS AND APPLICATIONS IN ENERGY TRANSMISSION NETWORKS

Juliana Cestari Lacerda

Doctorate Thesis of the Graduate Course in Applied Computing, guided by Drs. Elbert Einstein Nehrer Macau, and Celso Bernardo da Nobrega de Freitas, approved in November 17, 2021.

URL of the original document:

<<http://urlib.net/8JMKD3MGP3W34T/45RUNQ8>>

INPE
São José dos Campos
2021

PUBLISHED BY:

Instituto Nacional de Pesquisas Espaciais - INPE
Coordenação de Ensino, Pesquisa e Extensão (COEPE)
Divisão de Biblioteca (DIBIB)
CEP 12.227-010
São José dos Campos - SP - Brasil
Tel.:(012) 3208-6923/7348
E-mail: pubtc@inpe.br

**BOARD OF PUBLISHING AND PRESERVATION OF INPE
INTELLECTUAL PRODUCTION - CEPPII (PORTARIA Nº
176/2018/SEI-INPE):****Chairperson:**

Dra. Marley Cavalcante de Lima Moscati - Coordenação-Geral de Ciências da Terra
(CGCT)

Members:

Dra. Ieda Del Arco Sanches - Conselho de Pós-Graduação (CPG)
Dr. Evandro Marconi Rocco - Coordenação-Geral de Engenharia, Tecnologia e
Ciência Espaciais (CGCE)
Dr. Rafael Duarte Coelho dos Santos - Coordenação-Geral de Infraestrutura e
Pesquisas Aplicadas (CGIP)
Simone Angélica Del Ducca Barbedo - Divisão de Biblioteca (DIBIB)

DIGITAL LIBRARY:

Dr. Gerald Jean Francis Banon
Clayton Martins Pereira - Divisão de Biblioteca (DIBIB)

DOCUMENT REVIEW:

Simone Angélica Del Ducca Barbedo - Divisão de Biblioteca (DIBIB)
André Luis Dias Fernandes - Divisão de Biblioteca (DIBIB)

ELECTRONIC EDITING:

Ivone Martins - Divisão de Biblioteca (DIBIB)
André Luis Dias Fernandes - Divisão de Biblioteca (DIBIB)



MINISTÉRIO DA
CIÊNCIA, TECNOLOGIA
E INOVAÇÕES



sid.inpe.br/mtc-m21d/2021/11.25.20.43-TDI

SYNCHRONIZATION IN OSCILLATOR NETWORKS AND APPLICATIONS IN ENERGY TRANSMISSION NETWORKS

Juliana Cestari Lacerda

Doctorate Thesis of the Graduate Course in Applied Computing, guided by Drs. Elbert Einstein Nehrer Macau, and Celso Bernardo da Nobrega de Freitas, approved in November 17, 2021.

URL of the original document:

<<http://urlib.net/8JMKD3MGP3W34T/45RUNQ8>>

INPE
São José dos Campos
2021

Cataloging in Publication Data

Lacerda, Juliana Cestari.

L116s Synchronization in oscillator networks and applications in energy transmission networks / Juliana Cestari Lacerda. – São José dos Campos : INPE, 2021.
xxiv + 166 p. ; (sid.inpe.br/mtc-m21d/2021/11.25.20.43-TDI)

Thesis (Doctorate in Applied Computing) – Instituto Nacional de Pesquisas Espaciais, São José dos Campos, 2021.

Guiding : Drs. Elbert Einstein Nehrer Macau, and Celso Bernardo da Nobrega de Freitas.

1. Synchronization. 2. Power Grids. 3. Kuramoto models.
I.Title.

CDU 621.316.729:004



Esta obra foi licenciada sob uma Licença [Creative Commons Atribuição-NãoComercial 3.0 Não Adaptada](https://creativecommons.org/licenses/by-nc/3.0/).

This work is licensed under a [Creative Commons Attribution-NonCommercial 3.0 Unported License](https://creativecommons.org/licenses/by-nc/3.0/).



INSTITUTO NACIONAL DE PESQUISAS ESPACIAIS

DEFESA FINAL DE TESE DE JULIANA CESTARI LACERDA BANCA Nº 284/2021 REG 133138/2017

No dia 17 de novembro de 2021, às 09h, por teleconferência, o(a) aluno(a) mencionado(a) acima defendeu seu trabalho final (apresentação oral seguida de arguição) perante uma Banca Examinadora, cujos membros estão listados abaixo. O(A) aluno(a) foi APROVADO(A) pela Banca Examinadora, por unanimidade, em cumprimento ao requisito exigido para obtenção do Título de Doutora em Computação Aplicada. O trabalho precisa da incorporação das correções sugeridas pela Banca e revisão final pelo(s) orientador(es).

Título: "SYNCHRONIZATION IN OSCILLATOR NETWORKS AND APPLICATIONS IN ENERGY TRANSMISSION NETWORKS"

Dr. Lamartine Nogueira Frutuoso Guimarães - Presidente - IEAV
Dr. Elbert Einstein Nehrer Macau - Orientador - INPE
Dr. Celso Bernardo da Nobrega de Freitas - Orientador - Ericsson
Dr. Marcos Gonçalves Quiles - Membro Interno - UNIFESP
Dr. Ricardo Luiz Viana - Membro Externo - UFPR
Dr. José Mario Vicensi Grzybowski - Membro Externo - UFFS



Documento assinado eletronicamente por **Lamartine Nogueira Frutuoso Guimarães (E), Usuário Externo**, em 24/11/2021, às 08:16 (horário oficial de Brasília), com fundamento no § 3º do art. 4º do [Decreto nº 10.543, de 13 de novembro de 2020](#).



Documento assinado eletronicamente por **Marcos Gonçalves Quiles (E), Usuário Externo**, em 24/11/2021, às 10:04 (horário oficial de Brasília), com fundamento no § 3º do art. 4º do [Decreto nº 10.543, de 13 de novembro de 2020](#).



Documento assinado eletronicamente por **José Mario vicensi grzybowski (E), Usuário Externo**, em 25/11/2021, às 09:34 (horário oficial de Brasília), com fundamento no § 3º do art. 4º do [Decreto nº 10.543, de 13 de novembro de 2020](#).



Documento assinado eletronicamente por **Ricardo luiz viana (E), Usuário Externo**, em 30/11/2021, às 13:25 (horário oficial de Brasília), com fundamento no § 3º do art. 4º do [Decreto nº 10.543, de 13 de novembro de 2020](#).



Documento assinado eletronicamente por **Celso Bernardo da nobrega de**



freitas (E), Usuário Externo, em 13/12/2021, às 09:42 (horário oficial de Brasília), com fundamento no § 3º do art. 4º do [Decreto nº 10.543, de 13 de novembro de 2020](#).



A autenticidade deste documento pode ser conferida no site <http://sei.mctic.gov.br/verifica.html>, informando o código verificador **8578610** e o código CRC **F5171C08**.

Referência: Processo nº 01340.008231/2021-14

SEI nº 8578610

“Eppur si muove”.

GALILEO DI VINCENZO BONAULTI DE GALILEI

*To my father **Judson.***

ACKNOWLEDGEMENTS

I thank advisors Dr. Elbert Einstein Nehrer Macau and Dr. Celso Bernardo da Nóbrega de Freitas.

I thank my family, friends and pets. Especially Judson, Rosangela, Leonardo, Lenir, Psiu, Chapolin, Espiriguidiberto, Quark, Ivana, Jéssica, Juliana Marino, Luciano and Sabrina.

I also thank CNPq for the financial support with grant 141138/2017-3.

ABSTRACT

Synchronization is a process in which dynamic units coordinate some intrinsic property of the system. It is a universal behavior that takes place in many natural and artificial systems, such as electric power transmission networks, also called *power grids*. In order to study synchronization in systems of interacting dynamical units, it has been shown to be useful to describe the system as a complex network of interacting oscillators, where nodes represent the dynamical units and the connections between them express their interacting channels. Some of the most widely used models of phase oscillators to study synchronization in complex networks are the first and second order Kuramoto models. When a synchronized oscillator network is subjected to a perturbation, like a sudden change of a component's frequency or the addition of a new edge in the network's topology, it can eventually lead the whole system out of the synchronous state. The impact that the topology and its changes have on the synchronization of a network is the object of intense studies as it has been shown that small changes on its structure may desynchronize the system. This doctoral thesis aims to study synchronization of dynamical systems whose components are described by the first and second order Kuramoto models, more specifically, the role that topology plays on the synchronization of these systems by taking distinct approaches. First, we focus on the synchronization of power transmission networks, which are, in a first approximation, well represented by the second order Kuramoto model. In order to be fully functional, the components of the power transmission network must present synchronization in their frequencies. Power grids are subject to local instabilities that can eventually lead to failures throughout the entire network, due to the loss of synchronization of its components, causing, for example, blackouts. An evolutionary optimization method used to generate topologies that favor the synchronization of power grids is presented, as well as the study of the stability of these networks. We also show that a simple change in the network topology can cause nonlocal failures and even destroy the synchronous state of the system. A more general approach in the study of synchronization in oscillator networks is also presented, in a way that nodes are represented by the first order Kuramoto model and the influence of cycles and heterogeneity between connections in the synchronization of the system is studied. We find an indication that a network topology with a reduced number of cycles and with a high number of connections between high and low degree nodes tends to favor synchronization.

Keywords: Synchronization. Power Grids. Kuramoto models.

SINCRONIZAÇÃO EM REDES DE OSCILADORES E APLICAÇÕES EM REDES DE TRANSMISSÃO DE ENERGIA

RESUMO

Sincronização é um processo no qual unidades dinâmicas coordenam alguma propriedade intrínseca do sistema. É um comportamento universal que ocorre em muitos sistemas naturais e artificiais, como nas redes de transmissão de energia elétrica, também chamadas de *power grids*. Para estudar a sincronização em sistemas dinâmicos, mostrou-se útil descrever o sistema como uma rede complexa de osciladores que interagem entre si, onde os nós representam as unidades dinâmicas e as conexões entre elas expressam seus canais de interação. Alguns dos modelos de osciladores de fase mais utilizados para estudar a sincronização em redes complexas são os modelos de Kuramoto de primeira e segunda ordem. Quando uma rede de osciladores sincronizados é submetida a uma perturbação, como uma mudança repentina na frequência de um componente ou a adição de uma nova aresta na topologia da rede, isso pode eventualmente levar todo o sistema para fora do estado síncrono. O impacto que a topologia e suas mudanças têm na sincronização de uma rede é objeto de intensos estudos, pois tem sido demonstrado que pequenas mudanças em sua estrutura podem dessincronizar o sistema. Esta tese de doutorado tem como objetivo estudar a sincronização de sistemas dinâmicos cujos componentes são descritos pelos modelos de Kuramoto de primeira e segunda ordem, mais especificamente, o papel que a topologia desempenha na sincronização desses sistemas por meio de abordagens distintas. Primeiramente, focamos na sincronização de redes de transmissão de energia, que são, em uma primeira aproximação, bem representadas pelo modelo de Kuramoto de segunda ordem. Para serem totalmente funcionais, os componentes da rede de transmissão de energia devem apresentar sincronização em suas frequências. As redes de transmissão elétricas estão sujeitas a instabilidades locais que podem eventualmente levar a falhas em toda a rede, devido à perda de sincronização de seus componentes, causando, por exemplo, apagões. É apresentado um método de otimização evolutiva utilizado para gerar topologias que favoreçam a sincronização de redes elétricas, bem como o estudo da estabilidade dessas redes. Também mostramos que uma simples mudança na topologia da rede pode causar falhas não locais e até mesmo destruir o estado síncrono do sistema. Uma abordagem mais geral no estudo da sincronização em redes de osciladores também é apresentada, de forma que os nós são descritos pelo modelo de Kuramoto de primeira ordem e a influência dos ciclos e da heterogeneidade entre as conexões na sincronização do sistema é estudada. Encontramos uma indicação de que uma topologia de rede com um número reduzido de ciclos e com um grande número de conexões entre nós de alto e baixo grau tende a favorecer a sincronização.

Palavras-chave: Sincronização. Redes de transmissão de energia elétrica. Modelos de Kuramoto.

LIST OF FIGURES

	<u>Page</u>
2.1 Definition of stability (a) when the initial conditions are different but close and (b) close to the equilibrium point.	10
2.2 Order parameters R and ψ represented as a vector that points from the center of the unit circle. The length of the vector is given by $ R $ and the direction by ψ . Oscillators are represented by points in the circle.	14
2.3 Order parameter R as a function of time. As its value is constant, the system is in <i>phase locking</i> and $S = 1$	15
2.4 Edge evolution according to the Edge Snapping method. The gain k_{mn} is represented on the x-axis and the potential $V(k_{mn})$ on the y-axis.	17
2.5 Schematic representation of the evolutionary Edge Snapping strategy. Step 1 (variation): calculate edge activation probabilities (represented by the color bar), starting from n_T distinct initial conditions. Step 2 (selection): select the edges whose activation probability is greater than a threshold f^* , thus giving rise to the final topology of the network.	18
2.6 Network generated by Step 1 of the Edge Snapping method. The probability of activation F of the edges are represented by colors.	20
2.7 Seven node ES network created by the Edge Snapping method with (a) probability of activation of the edges and (b) natural frequencies of the nodes represented, respectively, by colors. The threshold of the probability of activation is $f^* = 0.58$	21
3.1 Diagram of an electric power plant composed by a generator (G) (with phase θ_1) and a consumer (C) (with phase θ_2) connected by a transmission line. The full definition of this system can be found in Section 3.2.	24
3.2 $(\theta_n - \theta_m)_{opt}$ and E_{max} as a function of the total number N of oscillators.	34
3.3 Values of couplings P_{max}^* , P_{max}^{**} and P_{max}^{***} as a functions of the number N of oscillators in a fully connected network with parameters $\alpha = 0.2$, $\Delta\nu_{max} = 2$	36
3.4 Network composed of a generator that supplies a power $P_1 = 2$ and a consumer that uses a power $P_2 = -1$	37
3.5 (a) Phase of generator (blue) and consumer (red), (b) angular velocity of oscillator 1 (generator), (c) angular velocity of oscillator 2 (consumer) and (d) order parameter as a function of time for a fixed coupling $P_{max} = 1.5$	38

3.6	(a) Phase of generator (blue) and consumer (red), (b) angular velocity of oscillator 1 (generator) and 2 (consumer) and (c) order parameter as a function of time for a fixed coupling $P_{max} = 1.49$	39
3.7	Fully connected networks with 5 consumers (C, red square) each consuming a power $P_C = -1$ and (a) 5 generators (G, blue circle), each providing a power $P_G = 1$, (b) 3 generators with $P_{G1} = P_{G2} = 2, P_{G3} = 1$, (c) 2 generators with $P_{G1} = 3, P_{G2} = 2$ and (d) 1 generator with $P_G = 5$	40
3.8	System without perturbation. (a) Three node transmission network composed of a consumer (C, red) connected to two generators (G, blue). (b) is the power absorbed by the consumer, (c) the order parameter as a function of time and (d) is the instantaneous frequency of all nodes as a function of time.	42
3.9	System with perturbation $\Delta P_C = -1$ during (marked in yellow) $\Delta t = 2$ time units. (a) Three node transmission network composed of a consumer (C, red) connected to two generators (G, blue). (b) is the power absorbed by the consumer, (c) the order parameter as a function of time and (d) is the instantaneous frequency of all nodes as a function of time.	43
3.10	System with perturbation $\Delta P_C = -3$ during (marked in yellow) $\Delta t = 2$ time units. (a) Three node transmission network composed of a consumer (C, red) connected to two generators (G, blue). (b) is the power absorbed by the consumer, (c) the order parameter as a function of time and (d) is the instantaneous frequency of all nodes as a function of time.	44
3.11	Minimum value (threshold) of ΔP_C that leads the system out of the synchronous state as a function of the coupling P_{max} for distinct values of the duration of the perturbation Δt that hits the system.	45
3.12	Basin of attraction (yellow) of a single node dynamics for the coupling P_{max} equal to (a) 4, (b) 12, (c) 24 and (d) 65. The attracting fixed point is plotted as a red dot.	47
3.13	Basin stability E of the one-node model as a function of the maximum capacity of the transmission line (coupling) P_{max}	49
3.14	(a) Histogram of the basin stability E . (b) Mean and standard deviation (light color) of basin stability $\langle E \rangle$ of all networks as a function of the nodes' degree g . Light colors indicate standard deviation.	51
3.15	(a) Average of the basin stability $\langle E \rangle$ of nodes with degree 1 and 2, (b) 3 and 4, (c) 5 and 6 and (d) 7 and 8, as a function of the average degree of the neighbors g_{av} . Light colors indicate standard deviation.	52

3.16	(a) Average basin stability $\langle E \rangle$ as a function of the betweenness b . Light colors indicate standard deviation. (b) Typical examples of nodes (red) that have certain distinct betweenness values b , this values of betweenness are marked as red points in (a); the boxes on the right of the red nodes represent the rest of the network whose number of nodes is written inside them.	53
3.17	(a) Average of the basin stability $\langle E \rangle$ of all generated networks as a function of the degree g of the nodes that are adjacent (red) or not (blue) of dead trees and dead ends. Lighter colors indicate standard deviation. (b)-(d) Average basin stability $\langle E \rangle$ as a function of the neighbors degree plotted for nodes with distinct degrees and that are adjacent (red) and not adjacent (blue) to dead trees.	54
3.18	(a) Histogram of basin stability E and measure of nodes' (b) basin stability, (c) degree, (d) betweenness and (e) average neighbors' degree values, divided between nodes adjacent (Y, red) and not (N, blue) to dead trees or dead ends.	56
3.19	(a) Model A, with $P_{max} = 3.2$, (c) Model B with $P_{max} = 3.2$ in the edges marked in black and $P_{max}^B = 2P_{max}$ in the dashed green edge and (e) Model C with $P_{max} = 3.2$. The instantaneous frequencies of models A, B and C are plotted in (b), (d) and (f), respectively. (g) Partial synchronization index for all the three models as a function of the coupling.	59
4.1	Network topology generated by the Edge Snapping method. (a) Shows the power generated or consumed by all nodes and (b) shows the probability of activation of all edges.	64
4.2	(a) Nodes degree g as a function of the power generated or consumed P . (b) Probability of edge activation of each edge of the network F_{mn} as a function of the absolute value of the power difference between nodes m and n , $ P_{mn} $. (c) Standard deviation of the probability of activation σ_F of all edges as a function of the number of trials n_T	65

4.3	Characteristics of a network topology generated by the Edge Snapping method along with the second order Kuramoto model where the power consumed or generated are set by a Gaussian distribution with zero mean and standard deviation equal to 0.2, without the constraint $\sum_{m=1}^N P_m = 0$. (a) Nodes degree g as a function of the power generated or consumed P . (b) Probability of edge activation of each edge of the network F_{mn} as a function of the absolute value of the power difference between nodes m and n , $ P_{mn} $	66
4.4	Random network with the same number of nodes, power consumed or generated and edges as the ES network (Figure 4.1).	67
4.5	Average instantaneous frequency ν_{avg} of all nodes as a function of the transmission capacity P_{max} for the (a) ES network and (b) random network where consumers are marked in red and generators in blue. (c) Partial synchronization index S of the ES network (red) and random network (green), order parameter R of the ES network (blue) and random network (black) as a function of the transmission capacity.	68
4.6	(a) Distribution of the values, their kernel density estimate and (b) box plot of the basin stability E of all nodes of the ES (red) and random (blue) networks presented in Figures. 4.1 and 4.4, respectively. (c-d) The same as (a-b), but now with of four ES and random networks. The median of the boxplots is 1, the mean is shown as a white square.	70
4.7	Degree g , neighbors degree g_{av} and betweenness centrality b of the nodes as a function of each other and kernel density estimate of the histogram in the diagonal for the ES (red) and random (blue) networks.	71
5.1	Original random network with $N = 50$ nodes, $N_G = 25$ generators (blue circle) and $N_C = 25$ consumers (red square).	76
5.2	Critical coupling P_{max}^c as a function of the number of generators for the power grid topology presented in Figure 5.1 with some generators being replaced at random by consumers.	78
5.3	(a) Instantaneous frequency of all nodes as a function of time for the coupling fixed at $P_{max} = P_{max}^c = 5.26$, (b) partial synchronization index S and (c) average instantaneous frequency as a function of the coupling P_{max} for the original network topology.	79

5.4	Original network (Figure 5.1) with a few changes: a new transmission line (red) connecting nodes 36 (G) and 38 (G), a removed transmission line (dashed green) disconnecting nodes 0 (C) and 20 (C) and a transmission line (purple) with doubled transmission capacity between nodes 1(C) and 13(C). Note that none of these changes are considered together.	80
5.5	(a) Instantaneous frequency as a function of time for the coupling fixed at $P_{max} = 5.26$, (b) partial synchronization index S_{mn} of all nodes, for a coupling also fixed at $P_{max} = 5.26$ for the network topology depicted in Figure 5.4 taking into account only the added edge (red) and (c) the same network topology but with the nodes that lost the synchronous state marked in black. The partial synchronization index for this configuration is $S = 0.78$	81
5.6	Partial synchronization index S as a function of coupling P_{max} for network configurations that present an advantage and disadvantage into reaching the synchronous state when compared to the original network topology. In (a) all the topology modifications leads the system out of the synchronous state, while in (b), all the modifications performed improve the synchronization of the system as a lower coupling is required to reach this state.	82
5.7	(a) Fraction of edges that increases (green), decreases (brown) and does not change (black) the value of P_{max}^c as a function of the number of generators of the network when one new edge is added at a random position in all of the sixteen topologies. (b) Fraction of edges that connect a generator to another generator (blue), a consumer to a consumer (red) and a consumer to a generator (black), only in relation to those who increase P_{max}^c	83
5.8	(a) Fraction of edges that increases (green), decreases (brown) and does not change (black) the value of P_{max}^c as a function of the number of generators of the network when an edge is removed at a random position in all of the sixteen topologies. (b) Fraction of edges that connect a generator to another generator (blue), a consumer to a consumer (red) and a consumer to a generator (black), only in relation to those who increase P_{max}^c	84

5.9	(a) Fraction of edges that increases (green), decreases (brown) and does not change (black) the value of P_{max}^c as a function of the number of generators of the network when the maximum transmission capacity of an edge is doubled at a random position in all of the sixteen topologies. (b) Fraction of edges that connect a generator to another generator (blue), a consumer to a consumer (red) and a consumer to a generator (black), only in relation to those who increase P_{max}^c	85
6.1	Histograms of Erdős-Rényi (orange), Watts-Strogatz (green) and Barabási-Albert (blue) networks in relation to (a) assortativity (ρ) and (b) clustering coefficient (C). One million networks were generated to compute each histogram.	94
6.2	(a)-(b) BA, (c)-(d) ER and (e)-(f) WS networks with low and high values of clustering coefficient C . The Similar \mathcal{S} (ν_{min}), Neutral \mathcal{N} (ν_{ini}) and Dissimilar \mathcal{D} (ν_{max}) patterns of dissonance ν are also showed for each network (from top to bottom, respectively). ω_i is the natural frequency of the nodes and the size of the nodes is proportional to the degree.	96
6.3	(a)-(b) BA, (c)-(d) ER and (e)-(f) WS networks with low and high values of assortativity ρ . The Similar \mathcal{S} (ν_{min}), Neutral \mathcal{N} (ν_{ini}) and Dissimilar \mathcal{D} (ν_{max}) patterns of dissonance ν are also showed for each network (from top to bottom, respectively). ω_i is the natural frequency of the nodes and the size of the nodes is proportional to the degree.	97
6.4	(a-c) Mean of the order parameter $\langle R \rangle$ and (d-f) the total partial synchronization index S as a function of the coupling for networks with low (dashed line) and high (continuous line) values of assortativity ρ and patterns Neutral (black), Similar (blue) and Dissimilar (red) of natural frequency distribution.	99
6.5	(a-c) Mean of the order parameter $\langle R \rangle$ and (d-f) the total partial synchronization index S as a function of the coupling for networks with low (dashed line) and high (continuous line) values of clustering coefficient C and patterns Neutral (black), Similar (blue) and Dissimilar (red) of natural frequency distribution.	100
6.6	Contour plot of the assortativity ρ and the neighborhood patterns in relation to the (a,c,e) coupling λ_{PL} and (b,d,f) order parameter R_{PL} at phase locking for the models BA, ER and WS of networks.	101
6.7	Contour plot of the clustering coefficient C and the neighborhood patterns in relation to the (a,c,e) coupling λ_{PL} and (b,d,f) order parameter $\langle R \rangle_{PL}$ at phase locking for the models BA, ER and WS of networks.	102

LIST OF TABLES

	<u>Page</u>
3.1 Comparison between different coupling values required for synchronization as a function of the network topologies shown in Figure 3.7.	41

CONTENTS

	<u>Page</u>
1 INTRODUCTION	1
1.1 Synchronization	1
1.2 Power grids	2
1.3 Contributions	4
1.4 Thesis structure	6
2 SYNCHRONIZATION	9
2.1 Dynamical systems	9
2.2 Synchronization and the Kuramoto models	11
2.3 Edge Snapping method	14
2.3.1 Evolutionary Edge Snapping	17
3 ENERGY TRANSMISSION NETWORKS	23
3.1 Introduction	23
3.2 Modelling power grids	25
3.3 Necessary conditions for synchronization	28
3.3.1 Numerical simulations	37
3.4 Network topology and system stability	41
3.4.1 Perturbations	42
3.4.2 Basin stability	45
3.4.2.1 One-node model	46
3.4.2.2 Multi-node model	49
3.4.3 Braess's paradox	55
3.5 Conclusion	58
4 SYNCHRONIZATION OF ENERGY TRANSMISSION NETWORKS AT LOW VOLTAGE LEVELS	61
4.1 Introduction	61
4.2 Models and methods	61
4.3 Results and discussion	63
4.4 Conclusion	72

5	ELEMENTARY CHANGES IN TOPOLOGY AND POWER TRANSMISSION CAPACITY CAN INDUCE FAILURES IN POWER GRIDS	73
5.1	Introduction	73
5.2	Models and methods	73
5.3	Results and discussion	76
5.3.1	A fixed network topology	76
5.3.2	Several network topologies	80
5.4	Conclusion	85
6	HOW HETEROGENEITY IN CONNECTIONS AND CYCLES MATTER FOR SYNCHRONIZATION OF COMPLEX NETWORKS	87
6.1	Introduction	87
6.2	Models and methods	90
6.2.1	Total dissonance	90
6.2.2	Assortativity and clustering coefficient	91
6.2.3	Generating network configurations	92
6.3	Results and discussion	93
6.4	Conclusion	103
7	CONCLUSION	105
	REFERENCES	107
	APPENDIX A - VULNERABILITY AND STABILITY OF POWER GRIDS MODELED BY SECOND ORDER KURAMOTO MODEL - A MINI REVIEW.	119
	APPENDIX B - SYNCHRONIZATION OF ENERGY TRANSMISSION NETWORKS AT LOW VOLTAGE LEVELS.	133
	APPENDIX C - ELEMENTARY CHANGES IN TOPOLOGY AND POWER TRANSMISSION CAPACITY CAN INDUCE FAILURES IN POWER GRIDS.	143
	APPENDIX D - HOW HETEROGENEITY IN CONNECTIONS AND CYCLES MATTER FOR SYNCHRONIZATION OF COMPLEX NETWORKS.	155

1 INTRODUCTION

1.1 Synchronization

Complex networks have been shown to be appropriate for modeling phenomena composed by several dynamic units where it is intended to capture the global and emergent properties of these systems (ARENAS et al., 2008). Thus, a vertex or node represents a dynamic unit and its interactions are represented by the edges of the network. Complex networks whose nodes are described by oscillators have been an extensively studied topic in recent decades (ARENAS et al., 2008; OSIPOV et al., 2007; BOCCALETTI et al., 2006), being used in various areas of science such as: biology (ULLNER et al., 2008), climatology (DONGES et al., 2009), neuroscience (BULLMORE; SPORNS, 2009), neurocomputation (FOLLMANN et al., 2015), applied mathematics (LACERDA et al., 2016; FREITAS et al., 2019; LACERDA et al., 2020), social systems (GIL; ZANETTE, 2006) and chemistry (KURAMOTO, 2012; MAGRINI et al., 2021).

When considering complex networks of oscillators, an interesting phenomenon to be studied is synchronization, which is a process in which dynamic units coordinate some property due to interactions between them (PIKOVSKY et al., 2003; LACERDA et al., 2017; LACERDA et al., 2019). It is a universal behavior in many natural and artificial systems and appears in areas such as biology (LEEUEWEN et al., 2009; VARELA et al., 2001), neuroscience (VICKHOFF et al., 2013), social systems (PLUCHINO et al., 2005; NÉDA et al., 2000) and physics (FORTUNA; FRASCA, 2007; PANTALEONE, 2002).

One of the most widely used oscillator models in the literature is the first order Kuramoto model, which describes self-sustained phase oscillators that have arbitrary intrinsic frequencies and are coupled in its classic version through the sine difference of their phases. This model is relatively simple, but it manages to describe a wide variety of synchronization patterns and is general enough to be adapted to different contexts. The collective behavior, or synchronization of oscillators, is achieved after a phase transition for a given critical coupling (ACEBRÓN et al., 2005; KURAMOTO, 1975). Applications of the first order Kuramoto model includes opinion formation (PLUCHINO et al., 2005), lasers (HOPPENSTEADT; IZHIKEVICH, 2000) and neurocomputation (FOLLMANN et al., 2015).

One of the wide applications of Kuramoto's model is in the study of electric energy transmission networks or *power grids*, where the system can be described by a second-order Kuramoto model (LACERDA et al., 2021b; GRZYBOWSKI et al., 2016; FILATRELLA et al., 2008). In this model, the phase and angular velocity (or instant-

neous frequency) evolve over time, the synchronization is damped by an inertia term and the coupling constant relates to the maximum power transmission capacity of the transmission lines. This model was first proposed to study the synchronization of some species of fireflies that manage to synchronize their light emissions (ERMEN-TROUT, 1991). The second-order Kuramoto model can also be used in the study of other physical systems, such as the forced pendulum dynamics (STROGATZ, 2014) and the Josephson junctions (TREES et al., 2005).

Since Kuramoto's models were used in the study of scale-free networks to analyze the role of *hubs* in the dynamics of nodes (MORENO; PACHECO, 2004), many studies have focused on the influence that the topology of networks has on the emergence of synchronization, where properties such as the occurrence of triangles, existence of communities, correlations between degrees and distribution of sub-graphs are used. The study of temporal networks, whose structures change over time, has led to the conception of new versions of Kuramoto's models. New properties have also been added to the study of this model, such as delay and repulsive coupling. (RODRIGUES et al., 2016)

1.2 Power grids

Electric energy can be generated in several ways, for example, by hydroelectric (which is currently the main source of energy generation in Brazil (GRZYBOWSKI et al., 2016; RIBEIRO et al., 2016)) and nuclear power plants. It can also be generated from the wind, through solar energy and by coal and gas-based thermoelectric plants, for example. This generated power is taken through transmission lines to consumers, covering long distances. Transmission lines are high-voltage lines that run across the country and are a link between energy generating sources and distributors, which can be energy concessionaires or, for example, consumers who receive high-voltage energy such as steel mills. The transmission lines cross the country, passing through fields, valleys, mountains, where there are chances of occurrence of numerous disturbances. A simple interruption in a certain segment of transmission can leave entire cities without electricity. For example, a minor interruption of one minute in the transmission of energy can cause losses in the order of thousands of dollars (MARTINHO, 2009; KOÇ et al., 2013).

Power grids are naturally complex as they are one of the biggest constructions ever made and are a typical example for the study of the collective behavior of interconnected dynamic units. In order to be fully functional, all of its components must be in a synchronous state and they must be robust enough to go back to this

state even when subjected to failures and disturbances (GRZYBOWSKI et al., 2018), which represents an enormous challenge for stability analysis. Therefore, engineers and researchers must accurately analyze the stability of power systems, taking into consideration scenarios that can cause disturbances in the network, implying local failures and in some cases, blackouts of high proportions (ALHELOU et al., 2019).

Instabilities in power grids can be caused, for instance, by the malfunctioning of some of its components, due to climatic factors such as fire, rain and lightning (ESPINOZA et al., 2016; PANTELI; MANCARELLA, 2015) or if a renewable source of energy becomes unavailable (INFIELD; FRERIS, 2020). Interruptions in energy transmission due to climatic problems have a great impact on the network infrastructure, being disturbed one of the main causes of problems in power grids world wide (WARD, 2013; BORGHETTI et al., 2006).

Extreme weather events have a great influence on the operation of the electrical components that make up the energy transmission network, which can affect the entire network infrastructure. Some issues related to weather events that affect the functioning of the power grid are: high temperatures and heat waves, that limit the power transfer capacity of transmission lines; strong winds during storms, that can lead to failures and damage transmission and power distribution lines; cold waves can cause transmission line failures; lightning on or near conductors can cause a short circuit (PANTELI; MANCARELLA, 2015).

Global warming is expected to have a major impact on the climate parameters discussed above and consequently will also have an impact on the operation of power grids (PACHAURI et al., 2014). The operation of various components, such as transformers and transmission lines, is governed by operating at the highest possible temperature, and an increase in ambient temperature affects operation and possibly limit their capabilities. Changes in precipitation patterns, as well as in the frequency and intensity of drought periods, can impact hydropower generation (PANTELI; MANCARELLA, 2015).

The growing integration of renewable energy sources in transmission networks is stimulated by environmental and economic issues. However, the generation of renewable energy is intermittent, stochastic and subject to climatic conditions, so it can cause unforeseen fluctuations in the system and is one of the major causes of instability in transmission networks today (ZHU; HILL, 2018). The addition of renewable sources to existing power grids makes the topology and functionality of the electrical grid to change dramatically. Energy production becomes increasingly

decentralized and heterogeneous, which can degrade the synchronous state, that is, compromise the fully functioning state of the power grid. The impact that the network topology has on the collective dynamics and stability of the power grid operation is still the object of intense studies (LACERDA et al., 2021a; ROHDEN et al., 2014).

By the use of the second order Kuramoto model to study power grids, the authors of (MENCK et al., 2013) built a model of basin stability in relation to large perturbations to analyze electric networks stability, which may be applied to other dynamical systems. It was shown that there are some patterns called dead ends and dead trees in power grids that reduce the overall dynamic stability of the system (MENCK et al., 2014). The role of the change in the topology of power grids was also studied, where it was shown that the addition or removal of a single transmission line can destabilize the entire network (WITTHAUT; TIMME, 2012; YANG et al., 2016; YANG; JIANG, 2017).

The main objective of this thesis is to better understand the role that topology plays in the synchronization of complex systems as it is still the object of intense studies. Some of the questions we answer are the following: Could there be an optimal topology that favors the synchronization of a complex network? Can the removal or addition of an edge disturb the system and lead it out of the synchronous state? How heterogeneity in connections and the existence of cycles affect the synchronization of the system?

1.3 Contributions

In this work, by taking distinct approaches, we study the role that topology plays on the synchronization of dynamical systems whose dynamics are described by the first and second order Kuramoto models. In summary, we apply an evolutionary optimization method to generate topologies that favor synchronization in power grids, we show that very simple changes in the topology of power grids can lead the system out of the synchronous state and how this phenomenon relates to the nature of the nodes being connected by the perturbed edge and level of decentralization of energy generation. Finally, the impact of the presence of cycles and heterogeneity between connections of nodes whose dynamics are described by the first order Kuramoto model on synchronization is studied, as we note that this approach could be applied to the problem of reaching of an agreement in a discussion on a polemic subject.

The first contribution of this thesis is presented in Chapter 3 and was published

in the journal **The European Physical Journal Special Topics** with the title *Vulnerability and stability of power grids modeled by second-order Kuramoto model: a mini review*, (LACERDA et al., 2021b). In this chapter, an extended version of the paper is presented, where a model to study and simulate power grids is derived, necessary conditions for synchronization and the study of the stability of networks are also presented.

The second contribution of our present work is presented in Chapter 4 and was published in the journal **Applied Mathematical Modelling** with the title *Synchronization of energy transmission networks at low voltage levels*, (LACERDA et al., 2021a). In this work, we show how to build a power grid topology that presents relatively low number of edges and favors synchronization, as a lower value of coupling is required to reach the synchronous state. As the coupling is related to the maximum transmission capacity of a transmission line, lower coupling in this context means lower voltage levels and therefore cheaper transmission lines. The basin stability of this network is also calculated as it appears to have a higher quantity of stable nodes when compared to a random network with the same number of nodes and edges. The methodology used in this work is based on an evolutionary optimization framework and would be of great interest when building power grids due to the costs involved in the construction of transmission lines, as there would be less lines and they would be required to operate in a lower voltage level.

The third contribution is presented in Chapter 5 and was submitted to publication in the journal **Physica A: Statistical Mechanics and its Applications** with the title *Elementary Changes in Topology and Power Transmission Capacity Can Induce Failures in Power Grids*. We show that elementary changes in the topology of power grids, like the addition or removal of a single transmission line or the increase of its maximum transmission capacity can cause failures in the network. Besides, we show that the probability of the occurrence of these failures can be related to the level of centralization of energy generation and to the nature of the nodes being connected by the transmission line being perturbed, although failures related to the increase in the transmission capacity does not seem to be much affected by the level of centralization. When considering a centralized power grid, that is, one grid whose power is supplied by just a few generators, one must be very careful when contemplating a change between two consumers, being an addition, removal or increase in the transmission capacity of the transmission line connecting them, as there is a considerable probability that this change may cause a network failure. In the decentralized power grid, the modification that cause most of the failures in

the grid is between a consumer and a generator when the removal or increase in the transmission capacity is being considered. Therefore, one must be very cautious when planning an update in an existing power grid or when building a new one as a single modification in the grid may lead the system out of the synchronous state.

The forth and last contribution also focus on the impact of the network topology on the synchronization of the system but here the dynamical units are described by the first order Kuramoto model. It is presented in Chapter 6 and was published in the journal **Chaos: An Interdisciplinary Journal of Nonlinear Science** with the title *How Heterogeneity In Connections And Cycles Matter For Synchronization Of Complex Networks*, (LACERDA et al., 2021b). In this work, the complex network metrics assortativity and clustering coefficient are used in order to generate network topologies of Erdős-Rényi, Watts-Strogatz and Barabási-Albert types that present high, intermediate and low values of these metrics. We also employ the total dissonance metric for neighborhood similarity, which generalizes to networks the standard concept of dissonance between two non-identical coupled oscillators. Based on this quantifier and using an optimization algorithm, we generate Similar, Dissimilar and Neutral natural frequency patterns, which correspond to small, large and intermediate values of total dissonance, respectively. The emergency of synchronization is numerically studied by considering these three types of dissonance patterns along with the network topologies generated by high, intermediate and low values of the metrics assortativity and clustering coefficient. We find that, in general, low values of these metrics, that is, a network with reduced number of cycles and with a high number of connections between nodes with high and low degree appear to favor synchronization, especially for the Similar dissonance pattern. We note that this approach can be applied to the problem of reaching of an agreement in a discussion on a polemic subject.

1.4 Thesis structure

This thesis is divided into two parts. The first one presents the theoretical foundations of this work and is composed by Chapters 2 and 3. Synchronization metrics, the first and second order Kuramoto models and the evolutionary optimization method Edge Snapping are discussed in Chapter 2. Power grids are the focus of Chapter 3, where a model to study its dynamics is derived and necessary conditions for synchronization are presented and the stability of this system is also studied.

The second part is composed of Chapters 4, 5 and 6, where the contributions of this work are presented. Power grids are the main topic of discussion in Chapters 4

and 5 while a more general approach to the synchronization paradigm is taken in Chapter 6 where the topological effects of cycles and connection heterogeneity on the synchronization of networks whose oscillators' dynamics are described by the first order Kuramoto model are studied. Final remarks are presented in Chapter 7.

2 SYNCHRONIZATION

In this chapter, we introduce the concept of dynamical systems and system stability in Section 2.1. The definition of synchronization and some of its metrics can be found in Section 2.2, along with the first and second order Kuramoto models. Finally, in Section 2.3 a method to generate network topologies that favor synchronization is presented.

2.1 Dynamical systems

A *system* is a set of physical elements that act together, accomplishing a common goal. A mathematical model is created, based on the structure and physical laws that coordinate this system, and is used to analyze it. In the case of overly complicated systems, mathematical models may reflect only a few phenomena of interest. A system can be *static*, when its state variables (minimum set of variables that uniquely define the state of a system) x_1, x_2, \dots, x_n are time-invariant, or, *dynamic*, when the state variables are functions of time $x_1(t), x_2(t), \dots, x_n(t)$ (MACHOWSKI et al., 2020).

In this work, we deal only with nonlinear dynamical systems, which can be modeled by differential equations of the form:

$$\dot{\mathbf{x}}(t) = \frac{d\mathbf{x}(t)}{dt} = \mathbf{F}(\mathbf{x}(t)), \quad (2.1)$$

where $\mathbf{x} = [x_1(t), \dots, x_n(t)]^T$ is the vector of the state variables and $\mathbf{F}(\mathbf{x}) = [F_1(x_1, \dots, x_n), \dots, F_n(x_1, \dots, x_n)]^T$ is a vector of nonlinear functions, $\mathbb{R}^n \rightarrow \mathbb{R}^n$. The variables $x_1(t), \dots, x_n(t)$ can represent, for example, populations of different species in an ecosystem or the position and velocity of planets in the solar system. The functions $F_1(x_1, \dots, x_n), \dots, F_n(x_1, \dots, x_n)$ are determined by the problem to be considered (STROGATZ, 2014).

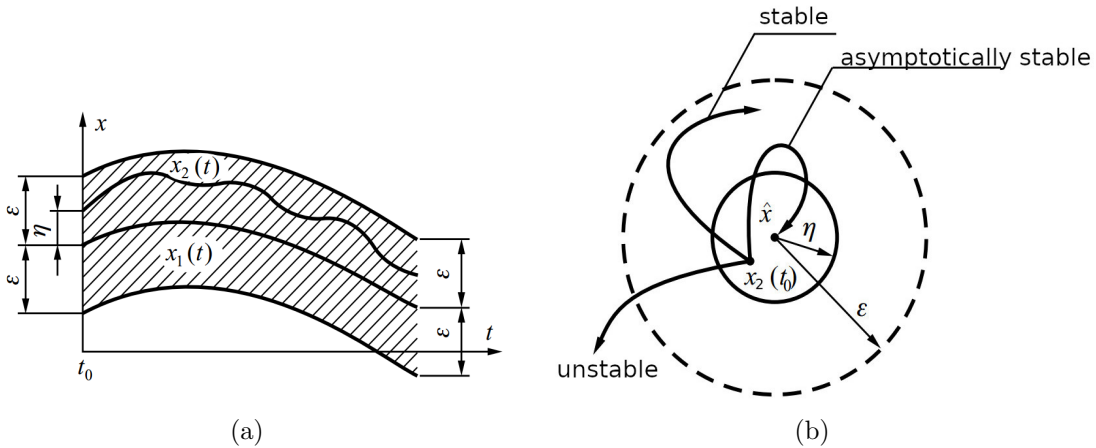
A coordinate space corresponding to state variables is called *phase space*. Each point in the phase space represents a single system state. The curve $\mathbf{x}(t)$ in phase space that contains the states of the system in consecutive times is called the *trajectory* or *orbit* of the system. When this trajectory consists of only one point, that is, $\mathbf{x}(t) = \hat{\mathbf{x}}$ is constant, this point is called *equilibrium point* if, at that point, all partial derivatives are zero, $\dot{\mathbf{x}} = 0$. Using Equation 2.1, one can find the coordinates of this equilibrium point, as they satisfy the equation:

$$\mathbf{F}(\hat{\mathbf{x}}) = 0. \quad (2.2)$$

The equilibrium point may not be unique as nonlinear equations may have more than one solution. Excluding equilibrium points, all states of a dynamical system are dynamic states because the derivatives $\dot{\mathbf{x}}$ are nonzero.

Consider the trajectory of a dynamical system given by $\mathbf{x}_1(t)$, which started from a certain initial condition $\mathbf{x}_1(0)$, and also another trajectory of the same system, given by $\mathbf{x}_2(t)$ that started from another initial condition $\mathbf{x}_2(0)$, both trajectories are shown in Figure 2.1 (a). A system is considered stable in the Lyapunov sense if the beginning of the trajectory of $\mathbf{x}_2(t)$ is close enough to the beginning of the trajectory of $\mathbf{x}_1(t)$ and they remain close even over time. That is, for any t_0 , it is possible to choose a number η such that for all other initial conditions that satisfy the condition $\|\mathbf{x}_2(t_0) - \mathbf{x}_1(t_0)\| < \eta$, the expression $\|\mathbf{x}_2(t) - \mathbf{x}_1(t)\| < \varepsilon$ is valid for $t_0 \leq t < \infty$. If the trajectory $\mathbf{x}_2(t)$ over time tends to the trajectory $\mathbf{x}_1(t)$, that is, $\lim_{t \rightarrow \infty} \|\mathbf{x}_2(t) - \mathbf{x}_1(t)\| = 0$, the dynamic system is said to be *asymptotically stable* (MACHOWSKI et al., 2020).

Figure 2.1 - Definition of stability (a) when the initial conditions are different but close and (b) close to the equilibrium point.



Adapted from : Machowski et al. (2020).

Consider $\mathbf{x}_1(t)$, whose trajectory starts at t_0 at the equilibrium point $\hat{\mathbf{x}}$ and therefore remains there with the passage of time, in a way that its trajectory consists of just one point, as we can see in Figure 2.1(b). Consider $\mathbf{x}_2(t)$ whose trajectory starts at t_0 at the initial condition given by $\mathbf{x}_2(t_0)$ which lies within the neighborhood defined by η . The system is said to be stable at the equilibrium point if, for $t_0 \leq t < \infty$,

the trajectory $\mathbf{x}_2(t)$ does not exceed the area determined by ε . If the trajectory $\mathbf{x}_2(t)$ tends to the equilibrium point $\hat{\mathbf{x}}$ over time, that is, $\lim_{t \rightarrow \infty} \|\mathbf{x}_2(t) - \hat{\mathbf{x}}\| = 0$, the system is said to be *asymptotically stable at the equilibrium point*. On the other hand, if the trajectory $\mathbf{x}_2(t)$ tends to leave the area defined by ε over time, the dynamic system is said to be unstable at the equilibrium point $\hat{\mathbf{x}}$. The stability of nonlinear systems usually depends on the size of the perturbation, that is, it can be stable for small perturbations (low values of η) and unstable for high perturbations (MACHOWSKI et al., 2020).

2.2 Synchronization and the Kuramoto models

The first use of the verb *to synchronize* that is reported dates back to 1624 with the meaning of *occurring at the same time* (PICKETT, 2018). Synchronization is understood as a collective state of coupled systems, that is, it is a process in which coupled oscillatory systems adjust their individual frequencies in an organized manner (BOCCALETTI et al., 2018). It was first studied by Christiaan Huygens in 1665 (HUYGENS, 1986) by observing the collective behavior pendulums hanging on the same wall. In a few words, synchronization is a process in which dynamical systems manage to coordinate some dynamical property, either because they are coupled or because they are driven by a common force (PIKOVSKY et al., 2003).

In order to model synchronization in large groups, Arthur Winfree developed a method where the system is described by self-sustained oscillators in which the rate of change of the phase of each oscillator is determined by the action of all the other system components (WINFREE, 1967; ACEBRÓN et al., 2005). Yoshiki Kuramoto showed that the dynamics of this system can be described as (KURAMOTO, 1975; STROGATZ, 2000)

$$\dot{\theta}_m = \omega_m + \sum_{n=1}^N \Gamma_{mn}(\theta_n - \theta_m), \quad (2.3)$$

where N is the number of oscillators, $m = 1, \dots, N$, Γ_{mn} is the interaction function and determines the type of coupling between the oscillators m and n . θ_m and ω_m are the phase and the natural frequency of oscillator m , respectively. Kuramoto then assumed that each oscillator is affected by the others in an interaction called global coupling λ and that these interactions related only on the sinusoidal phase difference

$$\Gamma_{mn}(\theta_n - \theta_m) = \frac{\lambda}{N} \sin(\theta_n - \theta_m). \quad (2.4)$$

Taking into account that we are not necessarily dealing with a fully connected network, we make use of the adjacency matrix A that indicates if nodes m and n are

connected ($A_{mn} = 1$) or not ($A_{mn} = 0$). The first order Kuramoto model can then be written as:

$$\dot{\theta}_m = \omega_m + \frac{\lambda}{g_m} \sum_{n=1}^N A_{mn} \sin(\theta_n - \theta_m), \quad (2.5)$$

where the coupling λ is constant and g_m is the degree of node m , that is, the number of edges connected to that node. Each oscillator has its own natural frequency ω_m which tries to dictate its independent movement but the oscillator is also affected by the movement of the others through the coupling constant which tries to synchronize them. When the coupling is not strong enough, the oscillators move incoherently but when this coupling goes beyond a certain threshold, collective movement and, therefore, synchronization emerges. (ACEBRÓN et al., 2005)

In this phase oscillator model, three types of behavior can be highlighted. If all oscillators move with angular velocity very close to their own natural frequencies, this phenomenon is called *incoherence*. It occurs when the magnitude of the difference between natural frequencies is large in relation to the coupling applied in the system. If the phase difference between all oscillators is constant over time, we have a phenomenon called *phase locking* and this happens when the coupling is strong relative to the magnitude of the differences in natural frequencies. If the phase of all oscillators is the same and does not change overtime, then we say that the system presents *phase synchronization* (MATTHEWS et al., 1991; PIKOVSKY et al., 2003).

The first order Kuramoto model is rich enough to display a large variety of synchronization patterns and very flexible to be adapted to many different contexts, but it does not take into account the dynamics of the corresponding frequencies (as it is required in the study of power transmission networks, for example) because it is a phase oscillator model. One can accomplish this by inserting inertial effects to the model which in turn is called second order Kuramoto model (ACEBRÓN et al., 2005).

In the second-order Kuramoto model, the phase θ_m and the angular velocity or instantaneous frequency $\dot{\theta}_m$ evolve over time and the synchronization is dampened by an inertia term. It is defined as:

$$\ddot{\theta}_m = -\alpha \dot{\theta}_m + \omega_m + \frac{\lambda}{g_m} \sum_{n=1}^N A_{mn} \sin(\theta_n - \theta_m), \quad (2.6)$$

for $m = 1, \dots, N$, where N is the total number of oscillators, $\alpha \in \mathbb{R}$ is the dissipation parameter, λ is the coupling constant, ω_m and g_m are the natural frequency and degree of the m oscillator, respectively. A_{mn} are the inputs of the adjacency matrix,

being equal to 1 if the oscillators m and n are connected and equal to 0 otherwise. Bidirectional networks without self loops are considered in this work. In a mechanical analog, $\ddot{\theta}$, $\dot{\theta}$ and ω , relate to inertia, damping and driving torque of a rotor (TANAKA et al., 1997a).

In addition to its use in modeling power grids (GRZYBOWSKI et al., 2016; PAGANI; AIELLO, 2013; FILATRELLA et al., 2008), which is an object of our study, the Kuramoto models can also be used to describe other dynamical systems, as in the study of some species of fireflies that manage to synchronize their light emissions (ERMENTROUT, 1991), in the modeling of the forced pendulum (STROGATZ, 2014) and in the study of electrochemical chaotic oscillators (MAGRINI et al., 2021).

Equation 2.6 can also be written as two first-order differential equations:

$$\begin{aligned}\dot{\theta}_m &= \nu_m, \\ \dot{\nu}_m &= -\alpha\nu_m + \omega_m + \frac{\lambda}{g_m} \sum_{j=1}^N A_{mj} \sin(\theta_j - \theta_m),\end{aligned}\tag{2.7}$$

where ν_m is the angular velocity of oscillator m .

To quantify the synchronous states between phase locking and phase synchronization, we define a couple of metrics. The order parameter \hat{R} is defined as

$$\hat{R}e^{i\psi} = \frac{1}{N} \sum_{m=1}^N e^{i\theta_m},\tag{2.8}$$

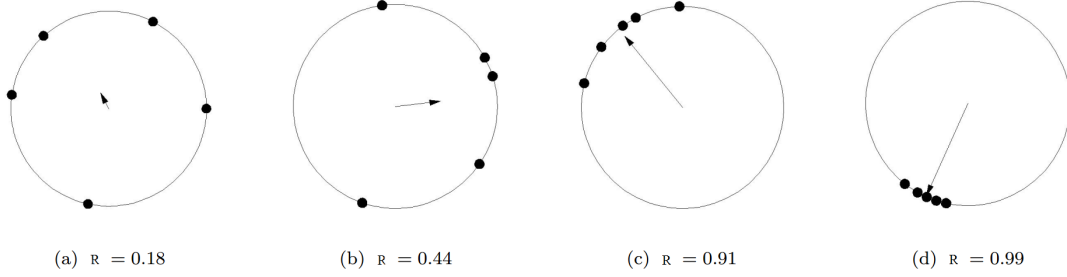
where $R = |\hat{R}|$ is given by

$$R = R(t) = \left| \frac{1}{N} \sum_{m=1}^N e^{i\theta_m} \right|.\tag{2.9}$$

$R \in [0, 1]$ measures the collective behavior of the system and ψ gives the average phase of all oscillators (DANIELS, 2005). Let us imagine oscillators as points that move around a unit circle over time, the parameters \hat{R} and ψ correspond to a vector fixed at the center of the circle Figure 2.2, where $R = |\hat{R}|$ is the vector's size and the phase ψ represents its direction. R tends to the value 1 as the oscillators come together in the unit circle. In this work, whenever we refer to the order parameter, we are referring to the R parameter. The parameter R is used to measure the phase synchronization, that is, when the average of this parameter over a certain period of time is constant and reaches the value 1, we say that the system is in phase

synchronization (DANIELS, 2005). Since the previous measurement alone cannot tell

Figure 2.2 - Order parameters R and ψ represented as a vector that points from the center of the unit circle. The length of the vector is given by $|R|$ and the direction by ψ . Oscillators are represented by points in the circle.



Source: Daniels (2005).

us whether the system has converged to a *phase locking* state, where oscillators do not have the same phase but present the same instantaneous frequency, so the distance between them remains constant is the unit circle. We introduce a new quantifier called *partial synchronization index* (GÓMEZ-GARDENES et al., 2007)

$$S_{mn} = \left| \lim_{\Delta t \rightarrow \infty} \frac{1}{\Delta t} \int_{t_r}^{t_r + \Delta t} e^{i[\theta_m(t) - \theta_n(t)]} dt \right|, \quad (2.10)$$

where t_r is a long enough transient time. When two oscillators m and n are in *phase locking*, $S_{mn} = 1$. To measure the degree of partial synchronization of the entire network, we use the arithmetic mean

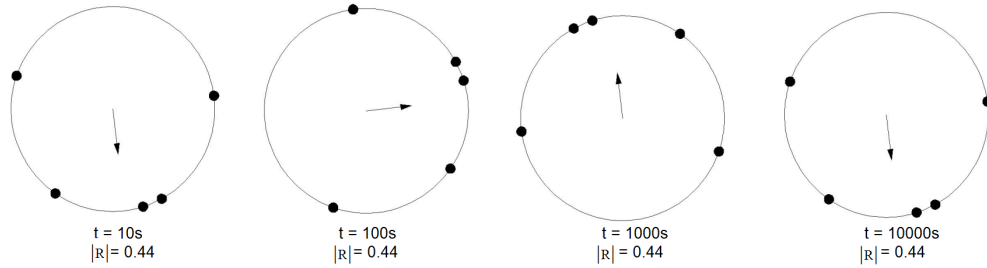
$$S = \frac{1}{N^2} \sum_{m,n=1}^N S_{mn}. \quad (2.11)$$

Note that, unlike the order parameter R , S is not time dependent. In order to visualize what it means for the network to present a partial synchronization index $S = 1$, one can look at Figure 2.3. Note that the phase difference between all oscillators remains constant, that is, they all have the same angular velocity.

2.3 Edge Snapping method

In this section, we introduce the evolutionary optimization method called Edge Snapping (DELELLIS et al., 2010) that allows the generation of complex networks that

Figure 2.3 - Order parameter R as a function of time. As its value is constant, the system is in *phase locking* and $S = 1$.



Source: Adapted from Daniels (2005).

favor synchronization and present a relatively low number of edges. This method has already been applied to networks of oscillators whose dynamics is described by the first-order Kuramoto model (SCAFUTI et al., 2015b) and by the Rossler oscillator model (SCAFUTI et al., 2015a). As one of the contributions of this thesis, we apply this method to networks of oscillators whose dynamics are described by the second-order Kuramoto model. Our objective is to use the networks created by this method to model power grids and analyze their stability.

Dynamical systems can be modeled as networks of oscillators where each one of them is described by a nonlinear differential equation. When studying the synchronization of these systems, in general, one seeks to find a network topology and a coupling value that make all oscillators share a dynamic property (DELELLIS et al., 2010).

In order to find a network structure that optimizes synchronization, several methods have been proposed such as the Monte Carlo method (GOROCHOWSKI et al., 2010; YANAGITA; MIKHAILOV, 2010; RAD et al., 2008; DONETTI et al., 2005) or gradient-based learning strategies (TANAKA; AOYAGI, 2008; SKARDAL et al., 2014). These methods use some objective function such as the order parameter R to guarantee system synchronization where the system is composed of a network with an optimized structure. The Monte Carlo method is usually very time-consuming, which makes it difficult to apply in large networks. Gradient-based methods assume some restrictions in the derivation of the coupling evolution rule and generally a global information of the entire network is used (SCAFUTI et al., 2015b). The *Edge Snapping* (DELELLIS et al., 2010) method is an adaptive strategy for the evolution of a weightless network topology that is more efficient than Monte Carlo and does not require global information network, such as gradient-based. It is an adaptive method that

is based on the use of a second-order model to model the evolution of the network edges, here called *gain*, and this gain model has two stable fixed points that lead to the formation of the network topology. Edges are activated or deactivated (removed from the network) according to local conditions that ensure a common evolution of the system.

Consider a network of nonlinear coupled oscillators whose nodes' dynamics is given by

$$\dot{x}_m = f_m(x_m) + \lambda \sum_{n=1}^N k_{mn} G(x_m, x_n) \quad (2.12)$$

where $x_m \in \mathbb{R}^p$ is the state variable with dimension p of the m oscillator, f_m represents the dynamics of each oscillator, note that they do not need to be identical. G is a generic coupling function and k_{mn} (which initially have the value zero) are the time-varying coupling gains associated with the edge (m, n) and λ is the coupling constant.

To characterize the evolution in the gain k_{mn} , we use a second-order model with damping subject to a bistable potential V forced by h . This model is defined as: (DELELLIS et al., 2010; SCAFUTI et al., 2015a)

$$\ddot{k}_{mn} + d\dot{k}_{mn} + \frac{\partial V(k_{mn})}{\partial k_{mn}} = h(\|\theta_m - \theta_n\|) \quad (2.13)$$

where $h(\|x_m - x_n\|)$ is a generic increasing function of class k_∞ ¹, such that $h(0) = 0$, $\|\cdot\|$ is the Euclidean norm, d is the damping constant, and the bistable potential V is defined as:

$$V(k_{mn}) = bk_{mn}^2(k_{mn} - 1)^2 \quad (2.14)$$

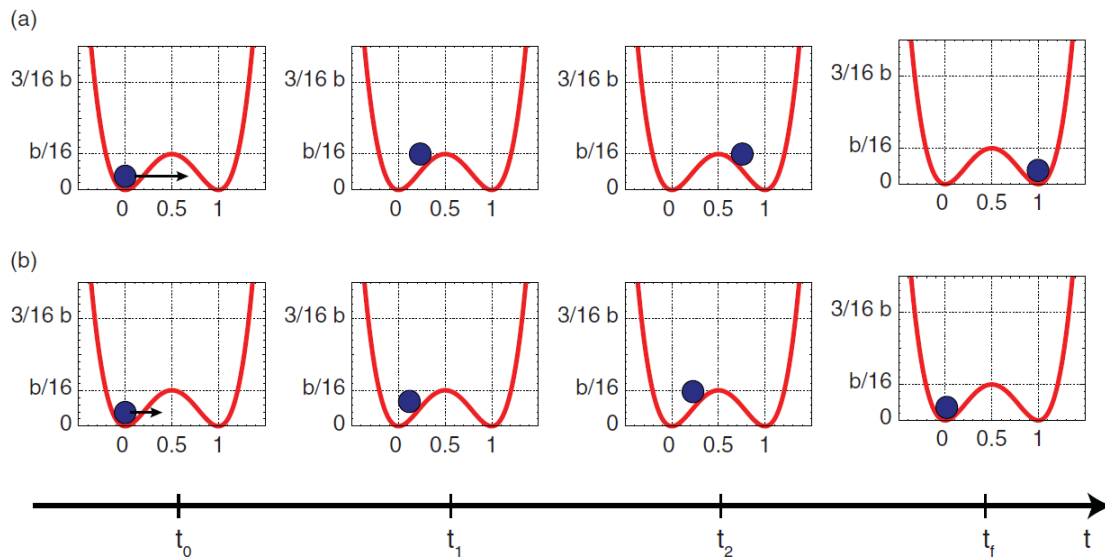
where $b > 0$ is a constant. V is a bistable potential with two local minima that correspond to the desired equilibria for the system, $k_{mn} = 0$ (nonexistent edge) and $k_{mn} = 1$ (existing edge). At the beginning of the evolution of the gain, all nodes are disconnected and based on the external forcing h , the edges may move out of their initial equilibrium point ($k_{mn} = 0$).

The dynamics of the gains k_{mn} , given by Equation 2.13, depends on the dynamics of the oscillators x_m defined by Equation 2.12. Thus, the resulting topology is the consequence of the dynamic evolution given by these two equations. The gain mimics

¹A function $F : \mathbb{R}_{\geq 0} \rightarrow \mathbb{R}_{\geq 0}$ is of class k if it is continuous, positive definite and strictly increasing. An unbounded function of class k belongs to class k_∞ . A function $F : I \rightarrow R$ is positive defined if $F(x) > 0 \forall x, x \neq 0$ and $F(0) = 0$.

the damped motion of a particle in one dimension subjected to a double well potential as we can see in Figure 2.4. In Figure 2.4(a), the force is large enough to move the particle from the initial equilibrium point $k_{mn} = 0$ (nonexistent edge) to the equilibrium point corresponding to $k_{mn} = 1$ (existing edge). This does not happen in Figure 2.4(b), as the force is not big enough. Note that the height of the barrier between the two equilibrium points is proportional to the constant b of Equation 2.14.

Figure 2.4 - Edge evolution according to the Edge Snapping method. The gain k_{mn} is represented on the x-axis and the potential $V(k_{mn})$ on the y-axis.



Fonte: Scafuti et al. (2015b)

2.3.1 Evolutionary Edge Snapping

The Edge Snapping method is now used in the context of evolutionary optimization, where variation and selection rules are applied to generate the complex network topology.

The evolutionary Edge Snapping strategy is composed of two fundamental rules, called *variation* and *selection* (SCAFUTI et al., 2015a), which are described below and illustrated in Figure 2.5.

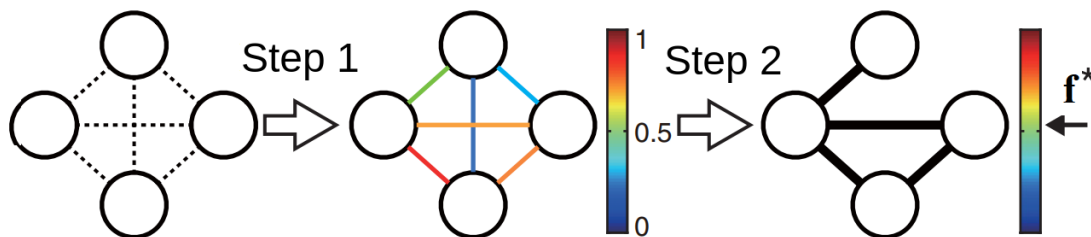
Step 1 - Variation rule: A set of weightless topologies is generated using Equations 2.12 and 2.13 starting from different initial conditions (a set of n_T initial conditions is randomly generated from a uniform distribution between $[0, 2\pi)$). From this set of n_T topologies, we calculate the fraction between the number of topologies where the edge between nodes m and n is present (n_{mn}) and the total number of generated topologies. This fraction is the probability of activation of the edge between nodes m and n , given by

$$F_{mn} = \frac{n_{mn}}{n_T}. \quad (2.15)$$

As a result of this Step 1, we have a matrix F of size $N \times N$ that is symmetric and stochastic, where N is the total number of oscillators, whose elements are the activation probability of all possible edges.

Step 2 - Selection rule: Only the edges whose activation probabilities F_{mn} are greater than a certain threshold value f^* , that is, only if $F_{mn} > f^*$, edges are marked as active in the network. This threshold value is chosen in a way to ensure that the resulting network topology is connected (no node is allowed to have zero degree), synchronized and presents the fewest edges possible. This network is referred to as minimal or *ES* network.

Figure 2.5 - Schematic representation of the evolutionary Edge Snapping strategy. Step 1 (variation): calculate edge activation probabilities (represented by the color bar), starting from n_T distinct initial conditions. Step 2 (selection): select the edges whose activation probability is greater than a threshold f^* , thus giving rise to the final topology of the network.



Source: Adapted from Scafuti et al. (2015b).

Using the second-order Kuramoto model, the equation that describes the dynamics of the network, generically defined in Section 2.3 as Equation 2.12, is now defined by Equation 2.6 with the adjacency matrix A_{mn} replaced by the gain k_{mn} . The dynamics of the network is then be given by

$$\ddot{\theta}_m = -\alpha\dot{\theta}_m + \omega_m + \frac{\lambda}{g_m} \sum_{n=1}^N k_{mn} \sin(\theta_n - \theta_m). \quad (2.16)$$

The generic function $h(|\theta_m - \theta_n|)$ in Equation 2.13 is defined as

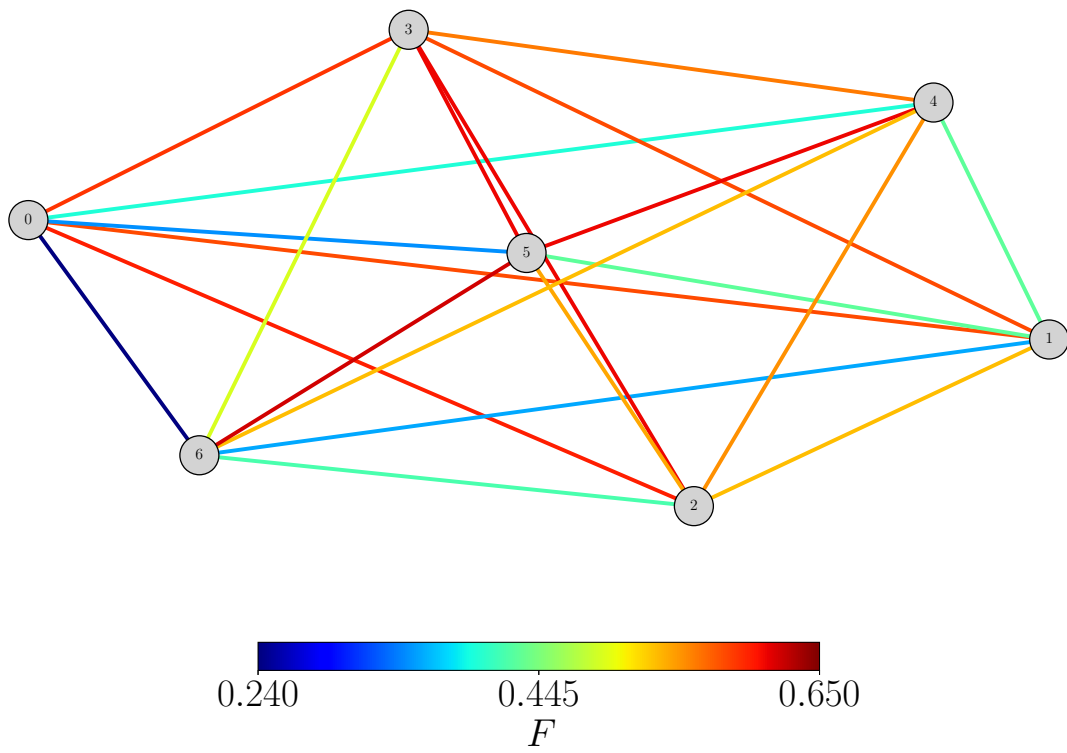
$$h(|\theta_m - \theta_n|) = 1 - |\theta(n) - \theta(m)|. \quad (2.17)$$

Now, we illustrate this technique with a small graph. A seven node network topology is generated by the use of this method. The nodes' natural frequency are selected are set as $\omega = [-1.00, -0.67, -0.33, 0.00, 0.33, 0.66, 1.00]$. The other model parameters are fixed as $n_T = 100$, $b = 1.0$, $d = 1.0$ for the edge snapping method and $\alpha = 0.1$, $\theta_m = 0.5$ and $\nu_m = 0$ for $m = 1, \dots, N$ in relation to the second order Kuramoto model.

The network topology generated by the Step 1 of the Edge Snapping method is shown in Figure 2.6. The activation probability of the edges are represented by colors, as reddish ones indicate high and bluish ones indicate low activation probabilities. Step 2 is now applied as the edges with the lowest values of F are removed (snapped), one by one. After each edge removal, we check if the network is still connected and if it is still in the synchronous state. When one of these two conditions is not satisfied, the method stops the edge removal and the remaining, final topology is referred to as *ES network* (Edge Snapping network).

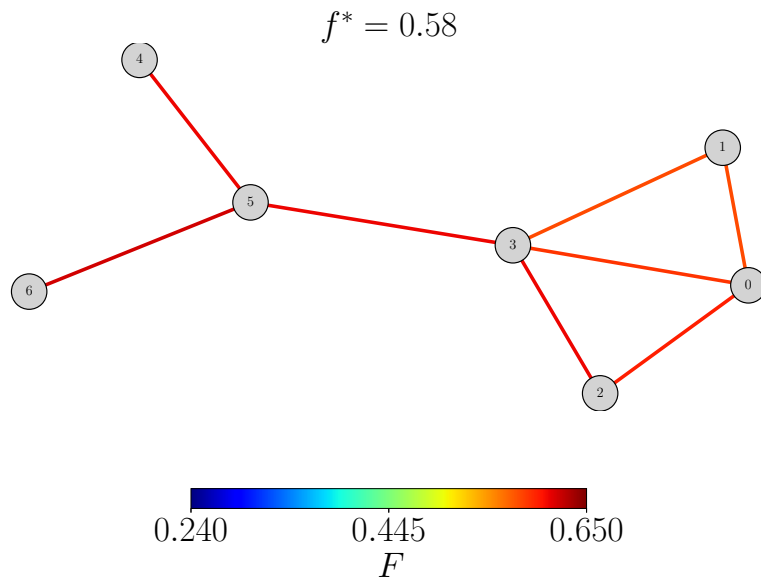
The seven node ES network can be seen in Figure 2.7, where the threshold of the probability of activation is $f^* = 0.58$, that is, all edges with probability of activation equal or lower than f^* were removed from the network created at Step 1 (Figure 2.6). The probability of activation of the edges of the ES network are depicted by colors in Figure 2.8(a) and the natural frequencies of the nodes are depicted in Figure 2.8(b). Note that this method generates networks with a relatively low number of edges as only 8 out of the 21 possible edges were marked as active. An application of this method is presented in Chapter 4.

Figure 2.6 - Network generated by Step 1 of the Edge Snapping method. The probability of activation F of the edges are represented by colors.

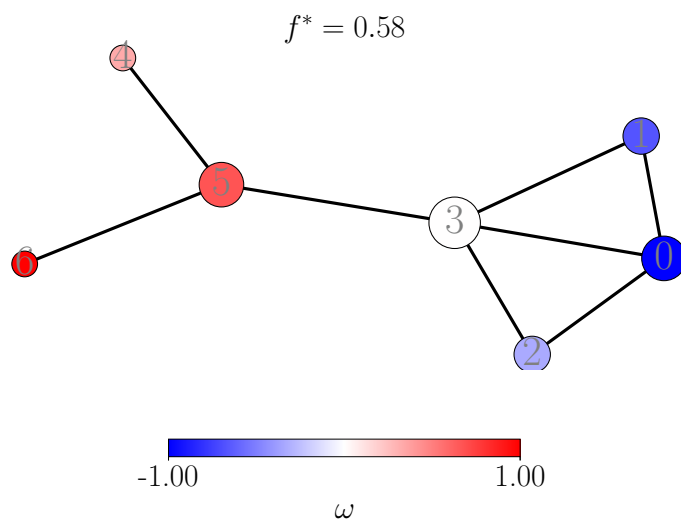


Source: Author production.

Figure 2.7 - Seven node ES network created by the Edge Snapping method with (a) probability of activation of the edges and (b) natural frequencies of the nodes represented, respectively, by colors. The threshold of the probability of activation is $f^* = 0.58$.



(a)



(b)

Source: Author production.

3 ENERGY TRANSMISSION NETWORKS

In this chapter, we present an extended version of a mini review (except for the vulnerability part which is not the scope of this work) published in the journal **The European Physical Journal Special Topics** with the title *Vulnerability and stability of power grids modeled by second-order Kuramoto model: a mini review*, (LACERDA et al., 2021b). This paper can be found in Appendix A.

An introduction is made in Section 3.1, modelling power grids is presented in Section 3.2, the conditions for synchronization are presented in Section 3.3 and, finally, in Section 3.4 we study how the system responds to perturbations and how it is affected by the system's topology.

3.1 Introduction

Electric power transmission network systems are non-linear dynamic systems, whose stability, that is, the ability to return to the equilibrium state, depends on the initial conditions and the intensity of the disturbances suffered by the network, due to several factors (MACHOWSKI et al., 2020).

The transmission of electrical power between generators and consumers that are geographically distant from each other is essential these days. These electric transmission networks or *power-grids* are dynamic systems whose transmission lines can exceed thousands of kilometers and the growing demand for electric energy has brought new challenges such as expansion strategies and evaluation of the stability of the grid. In the current power grid model, the energy generated must be produced according to the demand, forcing the grid to be sufficiently interconnected (CARARETO et al., 2013).

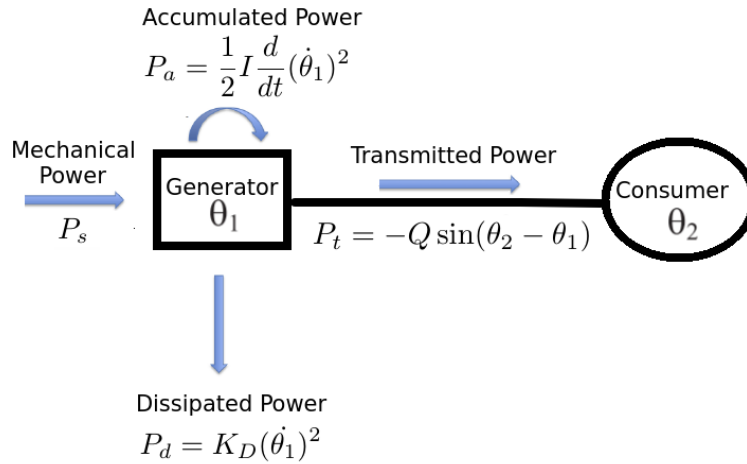
Transmission in power grid occurs mainly through alternating current, which has an oscillatory nature. For the electrical system to work perfectly, it is necessary that the entire network operates at the same frequency, that is, it is necessary that all dynamic systems that make up the network are synchronized (POURBEIK et al., 2006). If there is a high demand for energy and this demand is not adequately supplied or a network failure occurs, a network component (oscillator) can lose synchronization, which may eventually lead to a blackout (FILATRELLA et al., 2008).

Taking into account that electrical networks are expanding and becoming more and more complex with the addition of small energy sources, it is relevant to study the aspects that can favor and, most importantly, disfavor the synchronization of this

network (FILATRELLA et al., 2008). Electric transmission networks have been studied for more than ten years from a topological point of view with the use of complex networks and important results were found, such as vulnerability to attacks and cascading failures (CARARETO et al., 2013).

An electrical power plant is characterized by having a constant energy source and being equipped with generators, composed of a large magnet and rotor formed by a set of wound coils on a rotating shaft. When this rotor rotates within the magnetic field, its coils generate electromotive force in the form of alternating current in which the rotation frequency and the number of coils determine the frequency Ω of the generated electric current. A diagram of a generator (turbine) (G), with phase θ_1 and a consumer (C) with phase θ_2 is shown in Figure 3.1. We then have an energy source that feeds the rotation within the turbine, this energy can be accumulated as rotational energy or be dissipated due to friction (D). The remaining energy becomes available to the user as long as there is a phase difference between them. (FILATRELLA et al., 2008)

Figure 3.1 - Diagram of an electric power plant composed by a generator (G) (with phase θ_1) and a consumer (C) (with phase θ_2) connected by a transmission line. The full definition of this system can be found in Section 3.2.



Source: Author production.

In this chapter, by using a power balance equation, we present a mathematical derivation of a model that represents the dynamics of power grids, it turns out to be the second order Kuramoto model. To arrive at this model, we make two approximations as we assume that: (1) the electrical network is operating at a frequency

close to its standard frequency Ω (50 or 60 Hz), that is, the system is on the verge of small disturbances; (2) the rate in which kinetic energy is stored is always much smaller than the rate of the dissipated energy due to friction. We use here the unit of measure called *per units* (p.u.) which is usually adopted in studies of power grids (KUNDUR et al., 1994).

3.2 Modelling power grids

A power plant (Figure 3.1) is characterized by having a mechanical energy input and is equipped with a generator (G , rotor) that converts this mechanical energy into electrical energy. A consumer (C), on the other hand, does the reverse process. The rate at which energy is supplied to the generator, that is, the power of the source, is indicated by P_s . The generator produces electrical power with a constant frequency Ω and has a phase given by

$$\theta_1 = \Omega t + \tilde{\theta}_1 \quad (3.1)$$

where t is time and $\tilde{\theta}_1$ is a small perturbation.

In the process of converting mechanical to electrical power, there is power dissipation due to friction (FILATRELLA et al., 2008)

$$P_d = K_D(\dot{\theta}_1)^2, \quad (3.2)$$

where K_D is a dissipation constant. There is also the accumulation of kinetic energy at a rate

$$P_a = \frac{1}{2}I \frac{d}{dt}(\dot{\theta}_1)^2 = I\dot{\theta}_1\ddot{\theta}_1, \quad (3.3)$$

where I is the moment of inertia. The power remaining in the system, P_t , is transmitted to the consumer. In Figure 3.1 the generator has a phase θ_1 and the consumer θ_2 and the power flows between them as long as there is a difference between these phases since power transmitted is defined as

$$P_t = -Q \sin(\theta_2 - \theta_1), \quad (3.4)$$

where Q is a constant.

Using the Equations 3.2, 3.3 and 3.4, we can describe the dynamics of a generator (or consumer) by writing the power balance equation (FILATRELLA et al., 2008)

$$\begin{aligned} P_s &= P_d + P_a + P_t \\ &= K_D(\dot{\theta}_1)^2 + I\dot{\theta}_1\ddot{\theta}_1 - Q \sin(\theta_2 - \theta_1) \end{aligned} \quad (3.5)$$

Assuming that the power grid is operating at a frequency close to Ω , that is, that we are in limit of small perturbations:

$$\dot{\tilde{\theta}}_1 \ll \Omega. \quad (3.6)$$

Substituting Equation 3.1 into Equation 3.5:

$$\begin{aligned} P_s &= K_D(\Omega + \dot{\tilde{\theta}}_1)^2 + I[(\Omega + \dot{\tilde{\theta}}_1)\ddot{\tilde{\theta}}_1] - Q \sin(\tilde{\theta}_2 - \tilde{\theta}_1), \\ &= K_D(\dot{\tilde{\theta}}_1)^2 + I\Omega\ddot{\tilde{\theta}}_1 + \dot{\tilde{\theta}}_1(I\ddot{\tilde{\theta}}_1 + 2K_D\Omega) + K_D\Omega^2 - Q \sin(\theta_2 - \theta_1). \end{aligned} \quad (3.7)$$

Note that $\ddot{\tilde{\theta}}_1 = \frac{d}{dt}(\Omega) + \ddot{\tilde{\theta}}_1 = \ddot{\tilde{\theta}}_1$ and that $\theta_2 - \theta_1 = (\Omega t + \tilde{\theta}_2) - (\Omega t + \tilde{\theta}_1) = \tilde{\theta}_2 - \tilde{\theta}_1$. Considering Equation 3.6, the term $K_D(\dot{\tilde{\theta}}_1)^2$ can be neglected:

$$P_s \cong I\Omega\ddot{\tilde{\theta}}_1 + \dot{\tilde{\theta}}_1(I\ddot{\tilde{\theta}}_1 + 2K_D\Omega) + K_D\Omega^2 - Q \sin(\theta_2 - \theta_1). \quad (3.8)$$

In mechanical systems, it is common for the rate at which kinetic energy is stored ($P_a \cong I\Omega\ddot{\tilde{\theta}}_1$) to be much lower than the rate at which energy is dissipated by friction ($P_d \cong K_D\dot{\tilde{\theta}}_1^2$). Due to Equation 3.6 we can then write:

$$I\Omega\ddot{\tilde{\theta}}_1 \ll K_D(\dot{\tilde{\theta}}_1)^2 \ll K_D\Omega. \quad (3.9)$$

Therefore, the accumulated power is much less than $K_D\Omega^2$:

$$I\Omega\ddot{\tilde{\theta}}_1 \ll K_D\Omega. \quad (3.10)$$

We can then neglect the term $I\ddot{\tilde{\theta}}_1$ in the coefficient of the first derivative in Equation 3.8 and this equation becomes

$$P_s \cong I\Omega\ddot{\tilde{\theta}}_1 + 2K_D\Omega\dot{\tilde{\theta}}_1 + K_D\Omega^2 - P \sin(\theta_2 - \theta_1). \quad (3.11)$$

Isolating $\ddot{\tilde{\theta}}_1$ e neglecting the approximation sign:

$$\ddot{\tilde{\theta}}_1 = \frac{P_s}{I\Omega} - \frac{2K_D}{I}\dot{\tilde{\theta}}_1 - \frac{K_D\Omega}{I} + \frac{Q}{I\Omega} \sin(\theta_2 - \theta_1). \quad (3.12)$$

Normalizing time as a function of the common frequency Ω^{-1} (FILATRELLA et al., 2008):

$$\ddot{\tilde{\theta}}_1 = \left(\frac{P_s\Omega}{I} - \frac{K_D\Omega^3}{I} \right) - \frac{2K_D\Omega}{I}\dot{\tilde{\theta}}_1 + \frac{P\Omega}{I} \sin(\theta_2 - \theta_1). \quad (3.13)$$

For better visualization, we define the following constants:

$$P_1 = \frac{P_s \Omega}{I} - \frac{K_D \Omega^3}{I}, \quad (3.14)$$

$$\alpha = \frac{2K_D \Omega}{I}, \quad (3.15)$$

$$P_{max} = \frac{Q \Omega}{I}, \quad (3.16)$$

where P_1 is the generated power, α is the dissipation parameter and P_{max} is the maximum power transmission capacity of the transmission line. Equation 3.13 can then be written as

$$\ddot{\theta}_1 = P_1 - \alpha \dot{\theta}_1 + P_{max} \sin(\theta_2 - \theta_1). \quad (3.17)$$

Equation 3.17 describes the dynamics of the generator in Figure 3.1, that is, it is connected to just one consumer. In turn, the dynamics of this consumer is given by:

$$\ddot{\theta}_2 = P_2 - \alpha \dot{\theta}_2 + P_{max} \sin(\theta_1 - \theta_2). \quad (3.18)$$

Generalizing these equations for a network with N dynamical systems, where not all nodes necessarily have the same degree and assuming that all transmission lines have the same maximum capacity:

$$\ddot{\theta}_m = P_m - \alpha \dot{\theta}_m + \frac{P_{max}}{g_m} \sum_{m=1}^N A_{mn} \sin(\theta_n - \theta_m). \quad (3.19)$$

This differential equation is the celebrated second-order Kuramoto model (RODRIGUES et al., 2016; GRZYBOWSKI et al., 2016; TANAKA et al., 1997a; TANAKA et al., 1997b) presented in Chapter 2, in which the dynamics of generators and consumers is described by non-linear oscillators. Note that to arrive at the second-order Kuramoto model, we made two approximations by assuming that we are at the limit of small perturbations and that the rate at which kinetic energy is stored is always less than the rate at which energy is dissipated by friction.

In this work, we consider an electrical network represented by a network of oscillators whose dynamics is described by the second order Kuramoto model, given by Equation 3.19 and written here as two first-order differential equations (GRZYBOWSKI et

al., 2016; FILATRELLA et al., 2008):

$$\dot{\theta}_m = \nu_m, \quad (3.20)$$

$$\dot{\nu}_m = P_m - \alpha\nu_m + \frac{P_{max}}{g_m} \sum_{n=1}^N A_{mn} \sin(\theta_n - \theta_m). \quad (3.21)$$

where $m = 1, \dots, N$ and N is the number of oscillations. θ_m , ν_m and g_m are the phase, angular velocity (or instantaneous frequency) and degree of the oscillator m , respectively, α is the dissipation parameter, P_m denotes a power consumed ($P_m < 0$) or generated ($P_m > 0$), which corresponds to the natural frequency of the oscillator m , P_{max} is the coupling constant, which corresponds to the maximum transmission capacity of the transmission line (we assume here that all lines have the same transmission capacity), and A is the adjacency matrix that has input $A_{mn} = 1$ if oscillators m and n are connected and input $A_{mn} = 0$ otherwise. More specifically, $\dot{\nu}_m$ is the accumulated rotational power, $\alpha\nu_m$ is the dissipated power due to friction, P_{max} is directly related to the maximum power that can be transmitted by a network line and

$$F_{L_{mn}} = P_{max} A_{mn} \sin(\theta_n - \theta_m) \quad (3.22)$$

is the flow or power transmitted from node n to node m (CARARETO et al., 2013).

3.3 Necessary conditions for synchronization

Synchronization of power grids is very dependent on the power transferred between its components, which in turn also depends on the capacity of the transmission lines, that is, on the coupling. If the coupling is weaker than a certain threshold, synchronization does not take place. If the coupling is greater than this threshold but still less than a second threshold, synchronization occurs but eventually breaks down due to disturbances, we say that this synchronized state is locally stable. If the coupling is large enough, the system becomes synchronized regardless of disturbances and initial conditions. In this case, we say that the synchronized state is globally stable (CARARETO et al., 2013).

In this section, some conditions necessary for the system synchronization are calculated analytically. For the sake of the calculations, we omit the degree g_m term and

the second order Kuramoto model is given by:

$$\dot{\theta}_m = \nu_m, \quad (3.23)$$

$$\dot{\nu}_m = P_m - \alpha\nu_m + P_{max} \sum_{n=1}^N A_{mn} \sin(\theta_n - \theta_m). \quad (3.24)$$

In a network of generators and consumers, the synchronous state needs to be maintained for the network to properly function. As the power transmission only occurs if the phases of the oscillators are different from each other, that is, if $\theta_m \neq \theta_n$, the phase synchronization never exists. On the other hand, the oscillators need to have the same fixed angular velocity, so it is possible for them to synchronize in *phase locking*, with $\nu_m = \nu_S$ for $m = 1, \dots, N$, where ν_S is the synchronous angular velocity and since it does not vary with time, we have $\dot{\nu}_m = 0$.

Substituting the synchronous angular velocity ν_S in Equation 3.24, the network dynamics is given by:

$$\dot{\theta}_m = \nu_S, \quad (3.25)$$

$$0 = -\alpha\nu_S + P_m + P_{max} \sum_{n=1}^N A_{mn} \sin(\theta_n - \theta_m). \quad (3.26)$$

Equation 3.26 corresponds to a system of N equations. Adding all these equations:

$$\sum_{m=1}^N [-\alpha\nu_S + P_m + P_{max} \sum_{n=1}^N A_{mn} \sin(\theta_n - \theta_m)] = 0, \quad (3.27)$$

that is,

$$\sum_{m=1}^N [-\alpha\nu_S + P_m] + P_{max} \sum_{m=1}^N [\sum_{n=1}^N A_{mn} \sin(\theta_n - \theta_m)] = 0. \quad (3.28)$$

As the adjacency matrix of the network is symmetric, the second term of Equation 3.28 is equal to zero:

$$\sum_{m=1}^N \sum_{n=1}^N A_{mn} \sin(\theta_n - \theta_m) = 0. \quad (3.29)$$

Then, Equation 3.28 becomes

$$\sum_{m=1}^N (-\alpha\nu_S + P_m) = 0. \quad (3.30)$$

As the term $\alpha\nu_S$ does not depend on m

$$-N\alpha\nu_S + \sum_{m=1}^N P_m = 0. \quad (3.31)$$

The synchronous angular velocity is then given by

$$\nu_S = \frac{\sum_{m=1}^N P_m}{N} \frac{1}{\alpha} = \frac{\bar{P}}{\alpha}, \quad (3.32)$$

where $\bar{P} = \frac{\sum_{m=1}^N P_m}{N}$ is the average value of all natural frequencies of the oscillators. In the power grid, there is a balance between the rate of energy supplied by generators and consumed by consumers, in a way that all supplied energy is consumed and no part is stored, so $\sum_{m=1}^N P_m = 0$ and $\nu_S = 0$. However, the rate of energy required by consumers changes over time and this causes generators to continually change the rate of energy produced, which implies that the synchronous angular velocity ν_S can change over time (GRZYBOWSKI et al., 2016).

The phase of oscillator m in the synchronous state is defined as (MENCK et al., 2014; ROHDEN et al., 2012)

$$\theta_m^S = \arcsin\left(\frac{P_m}{P_{max}}\right). \quad (3.33)$$

We now deduce two necessary conditions for synchronization, that is, *phase locking*, called P_{max}^* and P_{max}^{**} and a condition in which only the difference between the instantaneous frequencies remains constant, given by P_{max}^{***} , in the system given by Equations 3.23 and 3.24.

The degree of the node m is defined as the number of edges g_m connected to it, that is, $g_m = \sum_{n=1}^N A_{mn}$. It can then be noted that

$$\sum_{n=1}^N A_{mn} \sin(\theta_n - \theta_m) \in [-g_m, g_m], \quad (3.34)$$

since the sine function is limited. A necessary condition for the existence of a synchronous state is that there is a real solution for the Equations 3.25 and 3.26 and this can be achieved using Equation 3.34 above. Isolating P_{max} in Equation 3.26, we have:

$$P_{max} = \frac{\alpha\nu_S - P_m}{\sum_{n=1}^N A_{mn} \sin(\theta_n - \theta_m)}. \quad (3.35)$$

Now using Equation 3.34:

$$P_{max} \geq \max \left(\frac{|\alpha \nu_S - P_m|}{g_m} \right). \quad (3.36)$$

From Equation 3.32, we know that $\alpha \nu_s = \bar{P}$:

$$P_{max} \geq \max \left(\frac{|\bar{P} - P_m|}{g_m} \right) = P_{max}^*, \quad (3.37)$$

for $m = 1, \dots, N$. That is, there is no synchronous state in the model represented by Equations 3.23 and 3.24 for a coupling value lower than P_{max}^* . The difference between the rates of consumed and generated energy, P_m , has to be compensated by a high coupling or by a high connectivity between the nodes of the network.

We now derive another necessary condition for synchronization. Consider a fully connected network (where all nodes have degree equal to $N - 1$), and, by the use of Equations 3.23 and 3.24 we consider the difference equations given by $\ddot{\theta}_m - \ddot{\theta}_n$: (GRZYBOWSKI et al., 2016)

$$\ddot{\theta}_m - \ddot{\theta}_n = \dot{\nu}_m - \dot{\nu}_n = P_m - P_n - \alpha(\nu_m - \nu_n) + P_{max}E(\theta_m, \theta_n, \theta_q), \quad (3.38)$$

where

$$E(\theta_m, \theta_n, \theta_q) = 2 \sin(\theta_n - \theta_m) + \sum_{q=1, q \neq m, n}^N \sin(\theta_q - \theta_m) + \sin(\theta_n - \theta_q). \quad (3.39)$$

The maximum of the function $E(\theta_m, \theta_n, \theta_q)$, given by Equation 3.39, corresponds to the state of maximum power transfer.

If the oscillators enter the synchronous state, we get $\nu_m = \nu_n = \nu_S$ fixed for $m = 1, \dots, N$ and therefore $\dot{\nu}_m = \dot{\nu}_n = 0$. Then, using the Equation 3.38:

$$0 = P_m - P_n - \alpha(\nu_S - \nu_S) + P_{max}E(\theta_m, \theta_n, \theta_q), \quad (3.40)$$

$$\Rightarrow P_n - P_m = P_{max}E(\theta_m, \theta_n, \theta_q). \quad (3.41)$$

Assuming, without loss of generality, that $P_n > P_m$, we calculate the lower bound for the coupling P_{max} that satisfies Equation 3.41. We then need to maximize $E(\theta_m, \theta_n, \theta_q)$ given by Equation 3.39. The first-order conditions necessary for this to

happen are given by (CHOPRA; SPONG, 2005):

$$\frac{\partial E}{\partial \theta_m} = -2 \cos(\theta_n - \theta_m) - \sum_{q=1, q \neq m, n}^N \cos(\theta_q - \theta_m) = 0, \quad (3.42)$$

$$\frac{\partial E}{\partial \theta_n} = 2 \cos(\theta_n - \theta_m) + \sum_{q=1, q \neq m, n}^N \cos(\theta_n - \theta_q) = 0, \quad (3.43)$$

$$\frac{\partial E}{\partial \theta_q} = \cos(\theta_q - \theta_m) - \cos(\theta_n - \theta_q) = 0. \quad (3.44)$$

By Equation 3.44, one can see that

$$\theta_q = \frac{\theta_m + \theta_n}{2} \quad \text{or} \quad \theta_m = \theta_n \quad (3.45)$$

If we substitute $\theta_m = \theta_n$ directly into Equation 3.39, we see that $E = 0$, which is expected since there is only power transfer between two oscillators if there is a non-zero phase difference between them (GRZYBOWSKI et al., 2016). If we replace the critical point $\theta_q = \frac{\theta_m + \theta_n}{2}$ in Equation 3.39:

$$E(\theta_m, \theta_n, \theta_q) = 2 \sin(\theta_n - \theta_m) + \sum_{q=1, q \neq m, n}^N \sin\left(\frac{\theta_n - \theta_m}{2}\right) + \sin\left(\frac{\theta_n - \theta_m}{2}\right) \quad (3.46)$$

$$= 2 \sin(\theta_n - \theta_m) + 2(N - 2) \sin\left(\frac{\theta_n - \theta_m}{2}\right) \quad (3.47)$$

Now we find the value of $(\theta_n - \theta_m)$ that maximizes Equation 3.47. If we replace $\theta_q = \frac{\theta_m + \theta_n}{2}$, in Equation 3.42:

$$2 \cos(\theta_n - \theta_m) + \sum_{q=1, q \neq m, n}^N \cos\left(\frac{\theta_n - \theta_m}{2}\right) = 0 \quad (3.48)$$

$$\Rightarrow 2 \cos(\theta_n - \theta_m) + (N - 2) \cos\left(\frac{\theta_n - \theta_m}{2}\right) = 0 \quad (3.49)$$

$$\Rightarrow 2 \left[2 \cos^2\left(\frac{\theta_n - \theta_m}{2}\right) - 1 \right] + (N - 2) \cos\left(\frac{\theta_n - \theta_m}{2}\right) = 0 \quad (3.50)$$

$$\Rightarrow 4 \cos^2\left(\frac{\theta_n - \theta_m}{2}\right) - 2 + (N - 2) \cos\left(\frac{\theta_n - \theta_m}{2}\right) = 0 \quad (3.51)$$

Substituting $\theta_q = \frac{\theta_m + \theta_n}{2}$, in Equation 3.43:

$$2 \cos(\theta_n - \theta_m) + \sum_{q=1, q \neq m, n}^N \cos\left(\frac{\theta_n - \theta_m}{2}\right) = 0, \quad (3.52)$$

which is analogous to Equation 3.48.

Solving then Equation 3.51 as a function of $\cos\left(\frac{\theta_n - \theta_m}{2}\right)$:

$$\cos\left(\frac{\theta_n - \theta_m}{2}\right) = \frac{-(N-2) \pm \sqrt{(N-2)^2 + 32}}{8}, \quad (3.53)$$

and therefore, the value of $\theta_n - \theta_m$, which is a candidate to maximize Equation 3.39, is given by

$$(\theta_n - \theta_m)_{opt} = 2 \arccos\left(\frac{-(N-2) + \sqrt{(N-2)^2 + 32}}{8}\right). \quad (3.54)$$

The second order conditions that need to be satisfied to find the maximum of Equation 3.39 are given by:

$$\frac{\partial^2 E}{\partial \theta_i \partial \theta_j} \leq 0, \quad (3.55)$$

is checked for $(\theta_n - \theta_m)_{opt}$ (CHOPRA; SPONG, 2005), where $i, j = \{m, n, q\}$, and therefore, the maximum value of Equation 3.39 is obtained when we replace $(\theta_n - \theta_m)_{opt}$ in Equation 3.47:

$$E_{max} = 2 \sin(\theta_n - \theta_m)_{opt} + 2(N-2) \sin\left(\frac{(\theta_n - \theta_m)_{opt}}{2}\right) \quad (3.56)$$

Functions $(\theta_n - \theta_m)_{opt}$ and E_{max} as a function of the number of oscillators is plotted in Figure 3.2 for $N = 2, \dots, 32$.

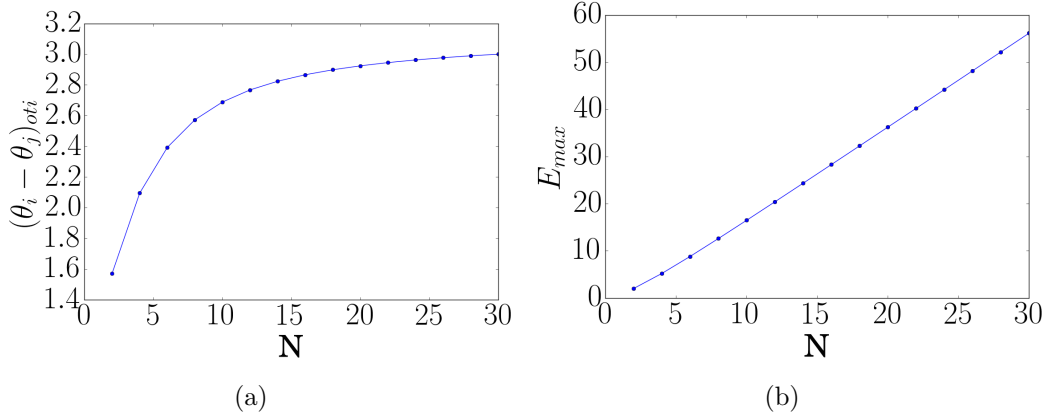
Taking into consideration Equation 3.56, the lower bound for the P_{max} coupling so that we have phase locking and which satisfies Equation 3.41 is given by

$$P_{max} \geq \max\left(\frac{|P_n - P_m|}{E_{max}}\right) = P_{max}^{**}, \quad (3.57)$$

where P_m and P_n is the rate of energy generated or consumed by the oscillators m and n , respectively, and $(\theta_n - \theta_m)_{opt} \in [\frac{\pi}{2}, \pi]$.

We deduce now a necessary condition so that the difference between the instantaneous frequencies ν_m and ν_n is constant. Let $\Delta\nu_{mn} = \nu_m - \nu_n$, considering again

Figure 3.2 - $(\theta_n - \theta_m)_{opt}$ and E_{max} as a function of the total number N of oscillators.



Source: Author production.

Equation 3.38 we can rewrite it: (GRZYBOWSKI et al., 2016)

$$\Delta \dot{\nu}_{mn} + \alpha \Delta \nu_{mn} = P_m - P_n + P_{max} E, \quad (3.58)$$

whose solution is given by

$$\Delta \nu_{mn} = \frac{P_m - P_n + P_{max} E}{\alpha} + \Delta \nu_0 e^{-\alpha t}, \quad (3.59)$$

where $\Delta \nu_0$ is a constant. It can be noted that the last term tends to zero, $\Delta \nu_0 e^{-\alpha t} \rightarrow 0$, when $t \rightarrow \infty$. Discarding then the last term of Equation 3.59, we can rewrite it as:

$$P_{max} = \frac{\alpha \Delta \nu_{mn} - P_m + P_n}{E}. \quad (3.60)$$

Considering $E = E_{max}$ and, as P_m and P_n are constant, the minimum value of P_{max} that enables synchronization must take into account the largest deviation between $\Delta \nu_{mn}$. Considering that the instantaneous frequencies are distributed in the range $[\nu_{min}, \nu_{max}]$, we can define the largest deviation between them as $\Delta \nu_{max} = \nu_{max} - \nu_{min}$. We thus obtain the necessary condition for the difference between the instantaneous frequency of the network oscillators to be constant:

$$P_{max} > \max \left(\frac{|\alpha \Delta \nu_{max} - P_m + P_n|}{E_{max}} \right) = P_{max}^{***}. \quad (3.61)$$

In Figure 3.3 one can see the values of the couplings P_{max}^* , P_{max}^{**} and P_{max}^{***} as a function of the number of oscillators in a fully connected network. The parameters

used are $\alpha = 0.2$, $\nu_m \in [-1, 1]$ and therefore $\Delta\nu_{max} = 2$. In Figure 3.3(a) the number of generators is defined as $\frac{N}{2}$ that provide an energy rate $P_m = +1$ with $m = 1, \dots, \frac{N}{2}$ and $\frac{N}{2}$ consumers using an energy rate given by $P_m = -1$ with $m = \frac{N}{2} + 1, \dots, N$. Note that in this case, where $|P_m| = |P_n|$ for $m, n = 1, \dots, N$, between the two conditions necessary for synchronization, P_{max}^{**} has a value greater than P_{max}^* for all values of N . In Figure 3.3(b), the number of generators is defined as $\frac{N}{3}$ that provide an energy rate $P_m = +1$ with $m = 1, \dots, \frac{N}{3}$ and $\frac{2N}{3}$ consumers who consume an energy rate $P_m = -0.5$ with $m = \frac{N}{3} + 1, \dots, N$. Note that here $|P_m| \neq |P_n|$ for $m, n = 1, \dots, N$, and, contrary to what happened in the previous case, between the two conditions necessary for synchronization, P_{max}^{**} has a value lower than P_{max}^* for all values of N . Therefore, the maximum value between P_{max}^* and P_{max}^{**} must be used as a necessary condition for synchronization.

It should be remembered that for the deduction of P_{max}^* and P_{max}^{**} , we assumed that the angular velocities were equal, since the system was synchronized. If, however, the system is affected by some perturbation, the angular velocities will no longer be the same and the Equations 3.37 and 3.57 cannot be used anymore. In this case, we can use the P_{max}^{***} coupling given by Equation 3.61 which gives maximum transmission capacity of the transmission lines that is needed for the network to resume the synchronization state after a disturbance. From the numerical approximations in Figure 3.3 it can be noted that the coupling P_{max}^{***} is always greater than or equal to the couplings considered previously.

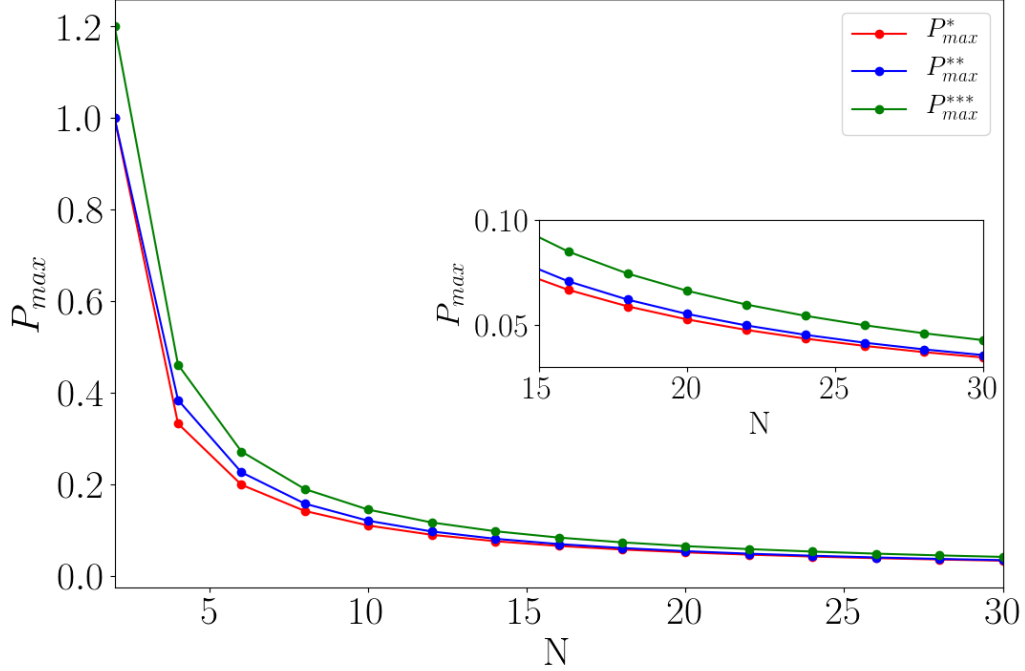
So far, we have assumed that we are dealing with fully connected electrical networks but, to relate our results to real electrical networks, we need to relate the results to other network topologies. For this, consider the Laplacian matrix G given by

$$G = D - A, \quad (3.62)$$

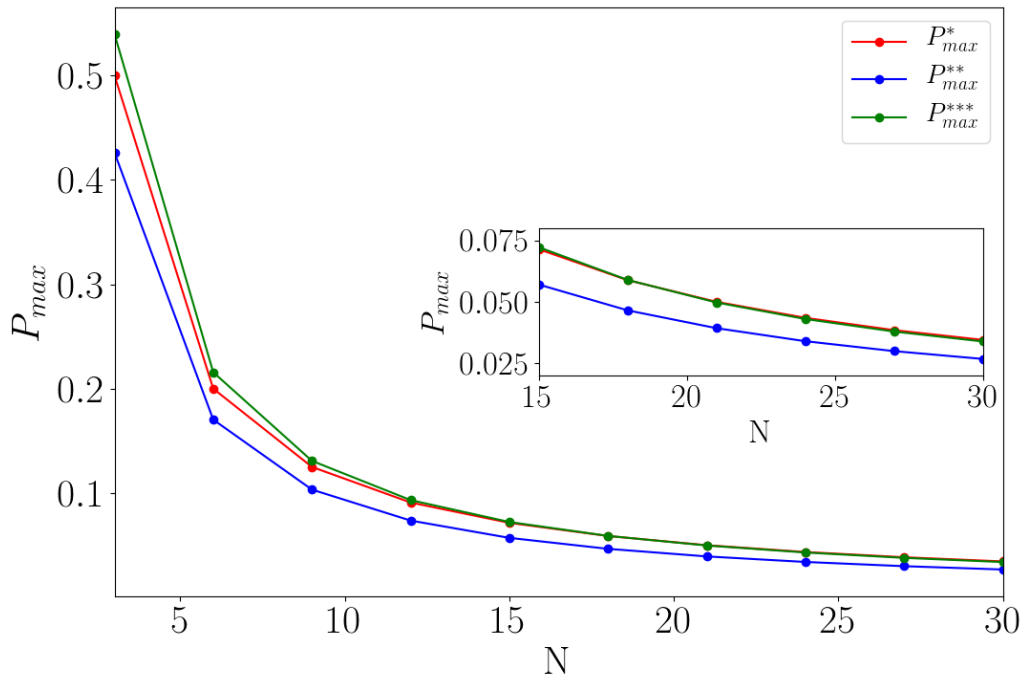
where A is the adjacency matrix and D is the degree matrix, which is a diagonal matrix defined as $D_{mm} = \sum_{n=1}^N A_{mn}$. Consider an undirected, strongly connected network with N nodes, such that λ is its second-smallest eigenvalue, also known as algebraic connectivity. Now consider a fully connected network with the Laplacian matrix given by G^F and its second smallest eigenvalue given by λ^F . We can generalize the results obtained previously to a fully connected network by (GRZYBOWSKI et al., 2016; CARARETO et al., 2013)

$$\lambda P_{max} = \lambda^F P_{max}^F, \quad (3.63)$$

Figure 3.3 - Values of couplings P_{max}^* , P_{max}^{**} and P_{max}^{***} as a functions of the number N of oscillators in a fully connected network with parameters $\alpha = 0.2$, $\Delta\nu_{max} = 2$.



(a) $\frac{N}{2}$ consumers and $\frac{N}{2}$ generators.



(b) $\frac{2N}{3}$ consumers and $\frac{N}{3}$ generators.

Source: Author production.

where P_{max} is the coupling of the highly connected network.

3.3.1 Numerical simulations

As a first approach, we consider a network with only two nodes, represented in Fig 3.4 with one generator (blue) and one consumer (red). The constants are supplied power $P_1 = 2$ and consumed power $P_2 = -1$, initial phase given by $(\theta_n - \theta_m)_{opt}$ and initial angular velocity given by $\nu_m = \nu_n = 0$. Regarding the coupling P_{max} , using the Equation 3.37, we have

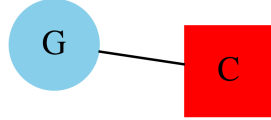
$$P_{max}^* = \max(|\bar{P} - P_m|) = 1.5.$$

By Equation 3.57 we see that

$$P_{max}^{**} = \frac{|P_1 - P_2|}{E_{max}} = \frac{3.0}{2.0} = 1.5.$$

In this case, $P_{max}^* = P_{max}^{**} = 1.5$ is the coupling required for the system to come into synchronization. We then fix the coupling as $P_{max} = 1.5$.

Figure 3.4 - Network composed of a generator that supplies a power $P_1 = 2$ and a consumer that uses a power $P_2 = -1$.

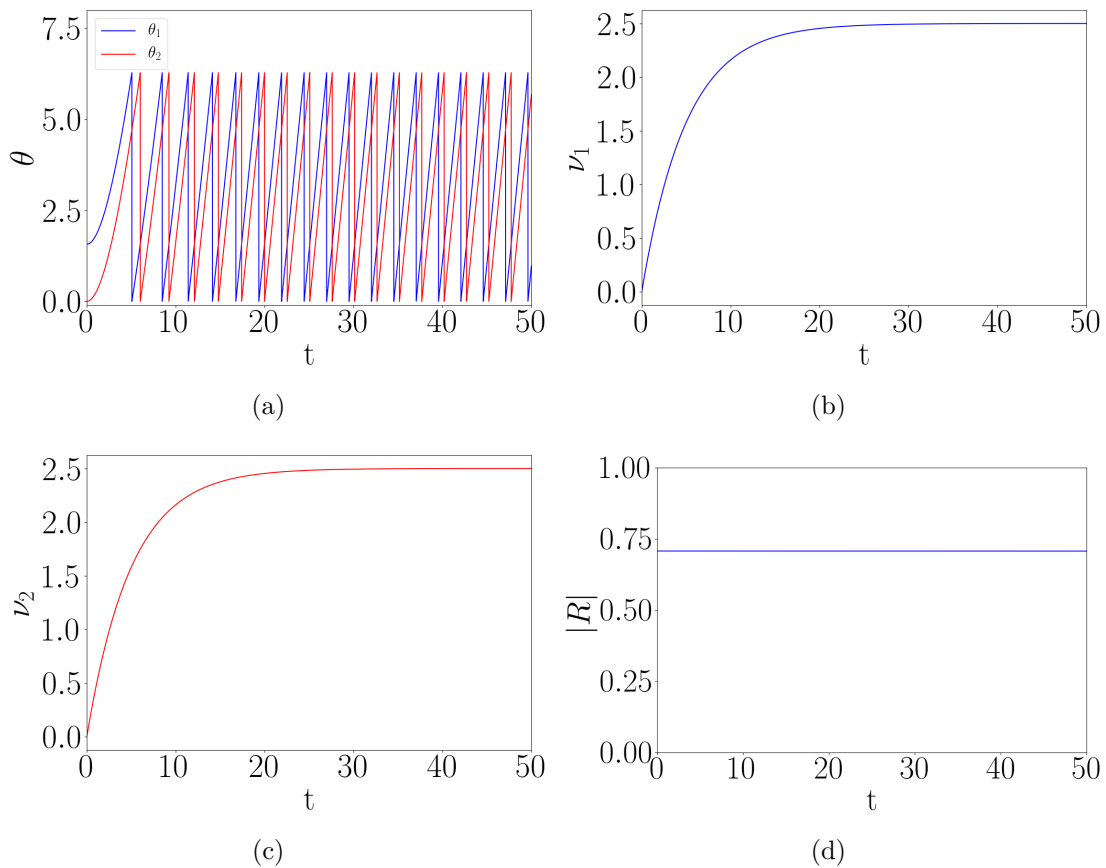


Source: Author production.

The behavior of the system composed by a generator and a consumer with $P_{max} = 1.5$ is shown in Figure 3.5. It can be seen in Figure 3.5(a) that, although the phases do not coincide, their behavior is qualitatively equal and this is confirmed when we see the plots of the angular velocities $\nu_{1,2} = \dot{\theta}_{1,2}$ in Figure 3.5(b,c), where both converge to the same value, indicating phase locking. As expected, both angular velocities reach the synchronous angular velocity value given by Equation 3.32, $\nu_S = \frac{\bar{P}}{\alpha} = \frac{0.5}{0.2} = 2.5$. In Figure Figure 3.5(d) we have the magnitude of the order parameter R , given by Equation 2.8, as a function of time, indicating that the phases of the oscillators are not equal as $|R| < 1$ but at the same time, giving indications that

there is a synchronous instantaneous frequency as its value is constant over time. This fact is confirmed when we calculate the value of the partial synchronization index, given by Equation 2.11, that is equal to one, $S = 1$.

Figure 3.5 - (a) Phase of generator (blue) and consumer (red), (b) angular velocity of oscillator 1 (generator), (c) angular velocity of oscillator 2 (consumer) and (d) order parameter as a function of time for a fixed coupling $P_{max} = 1.5$.

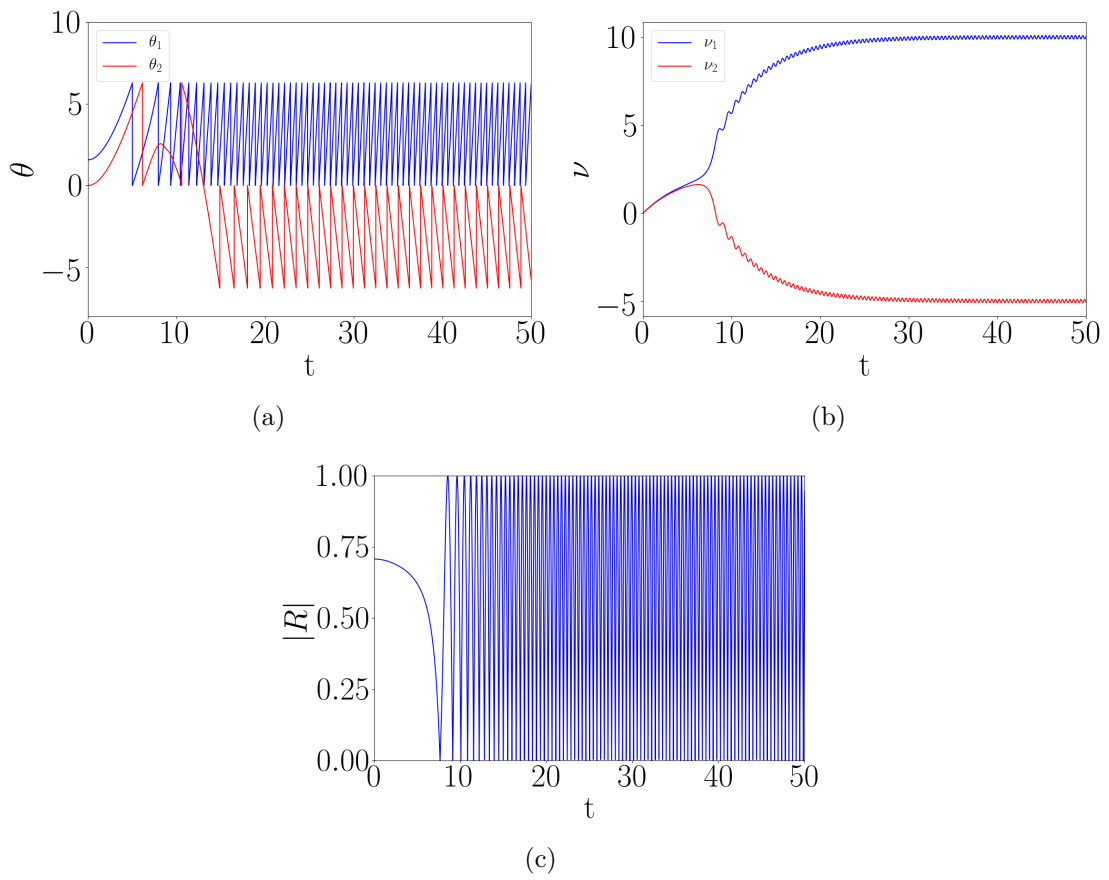


Source: Author production.

We can see that $P_{max} = 1.5$ is really a necessary condition for synchronization when we integrate the same system, with the same parameters, but now with $P_{max} = 1.49$. The result is shown in Figure 3.6. It can be noticed that the angular velocities present very distinct values. The order parameter is not constant and the partial sync index value is $S = 0.54$.

We now analyze what happens to the synchronous state of the power grid when there is fixed power consumption and generation but the network topology changes in a

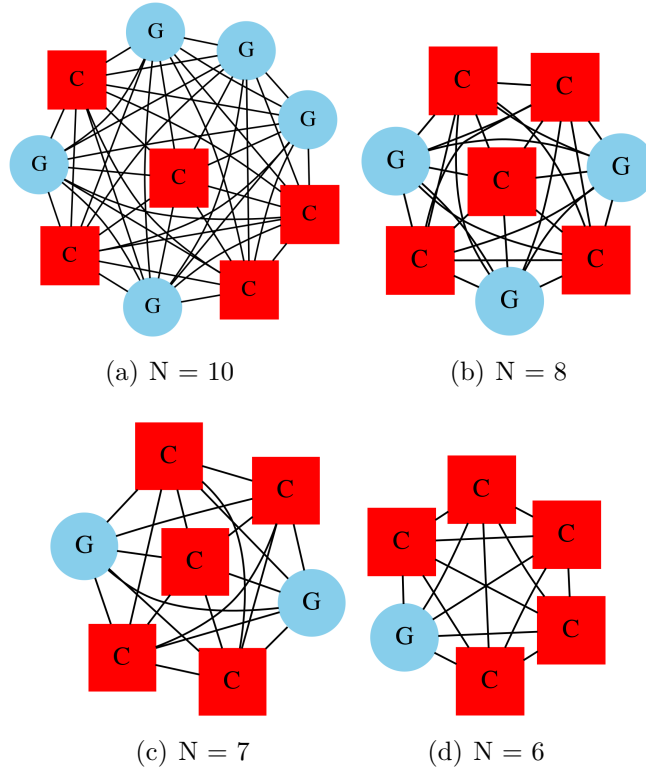
Figure 3.6 - (a) Phase of generator (blue) and consumer (red), (b) angular velocity of oscillator 1 (generator) and 2 (consumer) and (c) order parameter as a function of time for a fixed coupling $P_{max} = 1.49$.



Source: Author production.

way that small energy sources are added but the total power generated remains the same. We use the networks represented in Figure 3.7 where there is a fixed number of consumers, five, each consuming a power $P_C = -1$, so, $\sum P_C = -5$. The number of generators varies between five Figure 3.7(a) and one Figure 3.7(d), in a way that they always provide the same amount of power $\sum P_G = 5$.

Figure 3.7 - Fully connected networks with 5 consumers (C, red square) each consuming a power $P_C = -1$ and (a) 5 generators (G, blue circle), each providing a power $P_G = 1$, (b) 3 generators with $P_{G1} = P_{G2} = 2, P_{G3} = 1$, (c) 2 generators with $P_{G1} = 3, P_{G2} = 2$ and (d) 1 generator with $P_G = 5$.



Source: Author production.

The coupling required for synchronization is given by P_{max}^* (Equation 3.37), P_{max}^{**} (Equation 3.57) and P_{max}^{***} (Equation 3.61 with $\Delta\nu_{max} = 20$) was then calculated for each of the configurations presented in Figure 3.7. The results are found in Table 3.1. We can observe that the values of P_{max}^* , P_{max}^{**} and P_{max}^{***} grow as the energy production becomes more centralized, which means that in order to keep the proper function of the system with the phase locking state or for the recovery of the synchronous state after a disturbance, a greater maximum transmission capacity is

required when comparing to a system where the energy generation is decentralized.

Table 3.1 - Comparison between different coupling values required for synchronization as a function of the network topologies shown in Figure 3.7.

	$\max (P_m - P_n)$	N	P_{max}^*	P_{max}^{**}	P_{max}^{***}
(a)	2	10	0.11	0.12	0.36
(b)	3	8	0.29	0.24	0.56
(c)	4	7	0.50	0.37	0.75
(d)	6	6	1.00	0.68	1.14

3.4 Network topology and system stability

In this section, we study how power transmission networks modeled by the second order Kuramoto model respond to perturbations and how the topology of the networks affects it. We also introduce the concept of basin stability.

We study how the network topology influences the size of the synchronous state's basin of attraction, that is, how the topology influences the network response to large disturbances (MENCK et al., 2014).

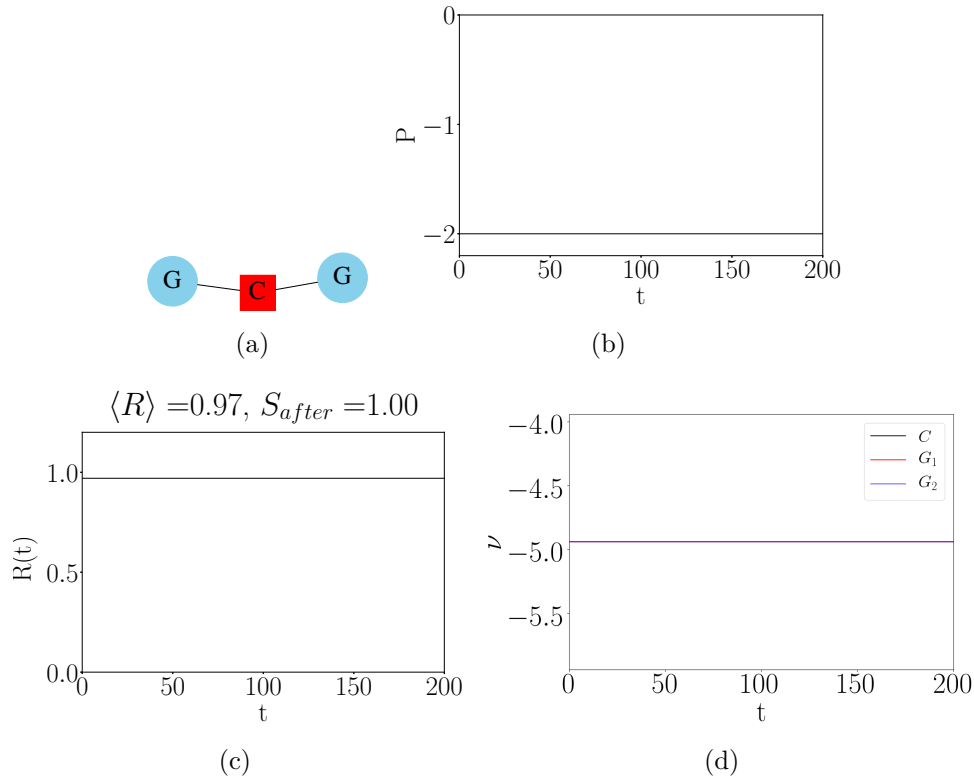
When the electrical transmission network is fully operational, all components of the network are in a synchronous state where there is a uniform flow of energy that supplies the demand (MACHOWSKI et al., 1997). When, for some reason, there is a failure in some component of the network, some of its parts lose synchronization and, to avoid damage, the affected components are turned off. However, the loss of these components, even temporarily, can cause other network components to come out of the synchronous state, which can cause a cascading failure and, eventually, a blackout (BULDYREV et al., 2010; MOTTER; LAI, 2002).

Power grids are designed not to lose the synchronous state by a cascade fault when some small disturbance occurs, that is, its synchronous state is locally stable. However, even with the synchronous state being locally stable with respect to small disturbances, there are several stable non-synchronous states in the power grid state space to which the grid can be driven due to large disturbances that can be caused for example by short circuits or fluctuations in power generation due to renewable energy sources (MENCK et al., 2014; FILATRELLA et al., 2008; CHIANG, 2011).

3.4.1 Perturbations

We start by considering a simple transmission network composed by two generators (whose generated power is $P_G = 1$ for each) connected to a consumer (that absorbs $P_C = -2$), Fig 3.9(a). Setting the coupling $P_{max} = 3$ we integrate the system and calculate the partial synchronization index, which is equal to one, $S = 1$. As this system is subjected to perturbations, we define S_{after} as being the partial synchronization index calculated after this perturbation hits the system, more specifically, after a transient. In Figures 3.8 (b), (c) and (d) the power consumed, order parameter and instantaneous frequency are plotted, respectively. These measures are all constant over time because the system is synchronized, the mean over time of the order parameter is $\langle R \rangle = 0.97$ and $S_{after} = S$, of course, as no perturbation has hit the system yet.

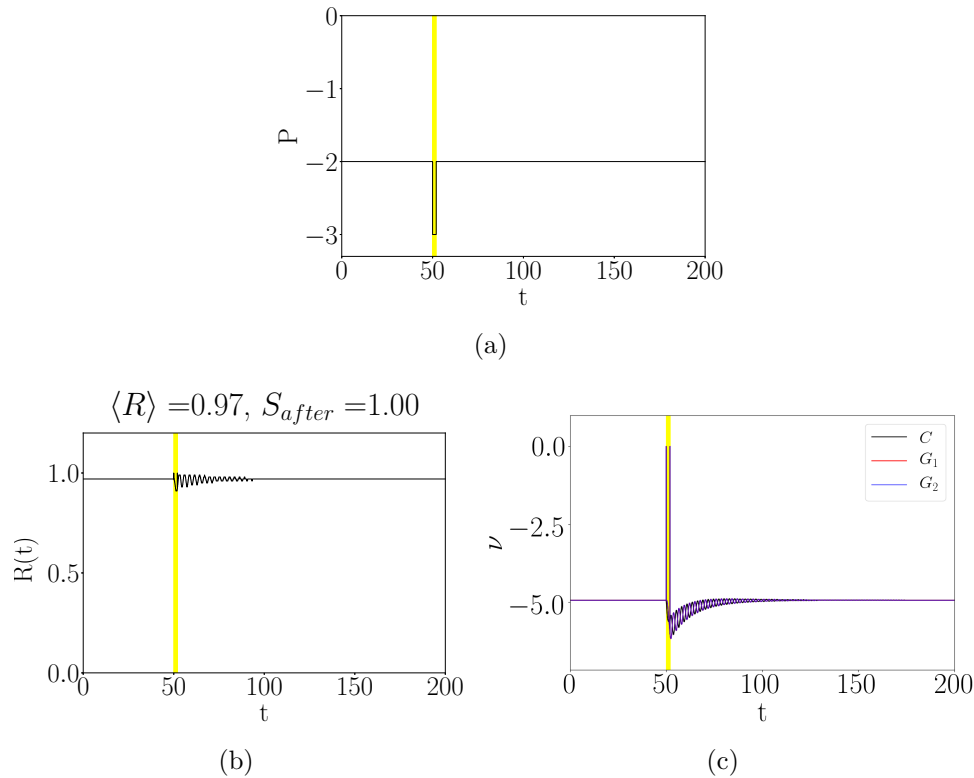
Figure 3.8 - System without perturbation. (a) Three node transmission network composed of a consumer (C, red) connected to two generators (G, blue). (b) is the power absorbed by the consumer, (c) the order parameter as a function of time and (d) is the instantaneous frequency of all nodes as a function of time.



Source: Author production.

Now, consider that the system is in this synchronous state when it is suddenly hit by a perturbation. More specifically, at $t = 50$ time units, the consumer requires an extra power ΔP_C for a short period of time $\Delta t = 2$. After this period, the consumer starts to absorb again two power units. In the first scenario, we consider $\Delta P_C = -1$, the result can be seen in Figure 3.9. The yellow rectangle represents the duration of the perturbation. Note that the system loses synchronization for a few moments, even after the perturbation has ceased, but manages to go back to the synchronous state after a transient, as $S_{after} = 1$ (calculated in this case for $t > 100$). Note that the perturbation hits just one node, but manages to destabilize the entire system as the instantaneous frequency ν of all nodes are disturbed.

Figure 3.9 - System with perturbation $\Delta P_C = -1$ during (marked in yellow) $\Delta t = 2$ time units. (a) Three node transmission network composed of a consumer (C, red) connected to two generators (G, blue). (b) is the power absorbed by the consumer, (c) the order parameter as a function of time and (c) is the instantaneous frequency of all nodes as a function of time.

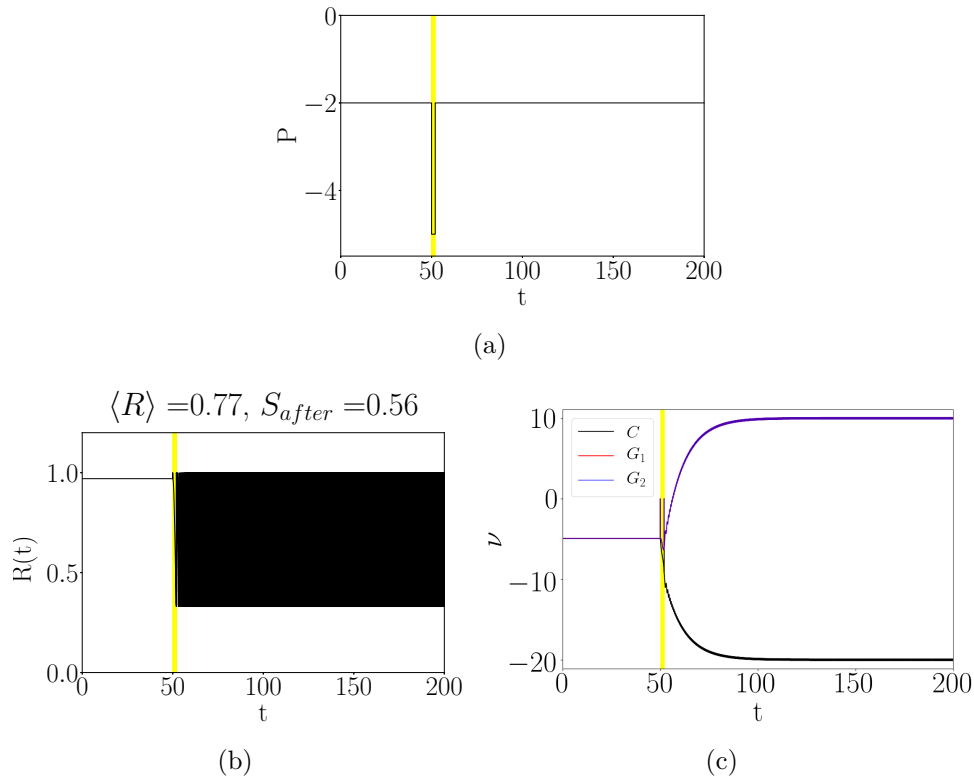


Source: Author production.

Considering now a greater perturbation as the consumer absorbs an extra power of

$\Delta P = -3$ for the same amount of time, $\Delta t = 2$. The results are shown in Figure 3.10. Note how the order parameter varies over time after the perturbation and how the instantaneous frequencies approach distinct values as both generators are on the upper part of Figure 3.10(c), while the consumer is on the bottom. The partial synchronization index after the perturbation is $S_{after} = 0.56$, indicating that, after losing the synchronization the system is unable to return to this state.

Figure 3.10 - System with perturbation $\Delta P_C = -3$ during (marked in yellow) $\Delta t = 2$ time units. (a) Three node transmission network composed of a consumer (C, red) connected to two generators (G, blue). (b) is the power absorbed by the consumer, (c) the order parameter as a function of time and (c) is the instantaneous frequency of all nodes as a function of time.

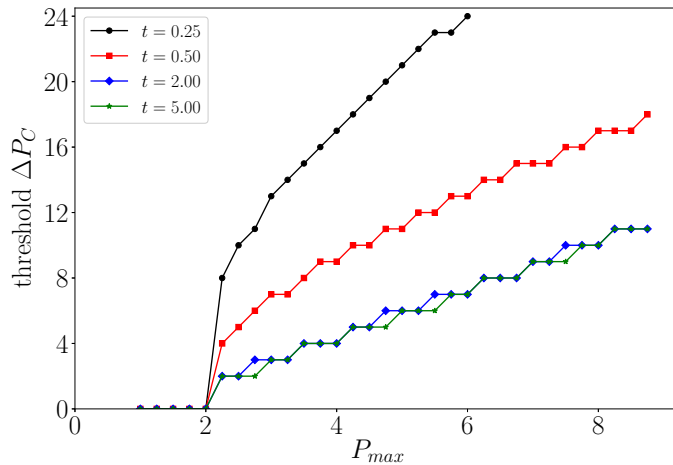


Source: Author production.

So far, the duration of the perturbation Δt and the coupling P_{max} were both fixed. Now, both are set to vary and as we calculate the minimum value of ΔP_C that leads the system out of the synchronous state we name it *threshold* ΔP_C . The results are shown in Figure 3.11. One can clearly see that the threshold ΔP_C heavily depends on the duration of the perturbation, especially when the duration is relatively short. The

lower the duration of the perturbation, the greater is the value of ΔP_C required to destabilize the system, that is, if the consumer perturbs the system by increasing its absorbed power by a great amount, the system is likely to go back to the synchronous state if this perturbation ends soon enough. For relatively large values of Δt , like 2 and 5 units of time, the behavior of threshold ΔP_C is very similar, indicating that perturbations that last longer present similar threshold ΔP_C . Note that the coupling $P_{max} < 2$ is not strong enough to synchronize the system, even without perturbation.

Figure 3.11 - Minimum value (threshold) of ΔP_C that leads the system out of the synchronous state as a function of the coupling P_{max} for distinct values of the duration of the perturbation Δt that hits the system.



Source: Author production.

3.4.2 Basin stability

In the previous section, we showed that when affected by a certain perturbation, the whole system is disturbed but sometimes manages to go back to the synchronous state, as it depends on the magnitude of the perturbation and its duration. The reason for the system occasionally lose the synchronous state has to do with the system's basin of attraction, which is the set of initial conditions that tends to an attracting fixed point as the system evolves in time (STROGATZ, 2014). In this section, we calculate this basin of attraction for a one-node model and present a method to calculate the volume of this basin of attraction, called basin stability, to a multi-node model.

3.4.2.1 One-node model

Large disturbances that affect a power grid usually involve an imbalance in the grid's local energy flow. For example, imagine that a generator is producing a steady stream of energy flowing through a single transmission line that suddenly shorts out. Control devices quickly interrupt the transmission line to stop the network failure and, with this, the rate of mechanical energy injected by the turbine into the generator causes its rotational energy to increase, thus increasing its rotation frequency. Therefore, when the transmission line is reconnected to the grid, the generator is no longer working as it was before the failure, which causes a disturbance in the network. Starting from this disturbed state, would the network be able to return to the synchronous state? (MENCK et al., 2014) To try to answer this question, we first adopt a simple one-node model, analyzing only the dynamics of a network generator.

Considering Equations 3.23 and 3.24 the one-node model can be written as:

$$\dot{\theta} = \nu, \quad (3.64)$$

$$\dot{\nu} = P - \alpha\nu + P_{max} \sin(\theta_{net} - \theta), \quad (3.65)$$

where θ and ν are the phase and angular velocity of the generator in a reference frame that rotates with the nominal frequency of the network and, therefore, here the angular velocity in the synchronous state is given by $\nu_S = 0$. The phase in the synchronous state θ_S is given by Equation 3.33 and $\alpha = 0.1$. Also, θ_{net} represents the phase of the rest of the network. This one oscillator model assumes that the network is not affected by the generator in question, so we set $\theta_{net} = 0$.

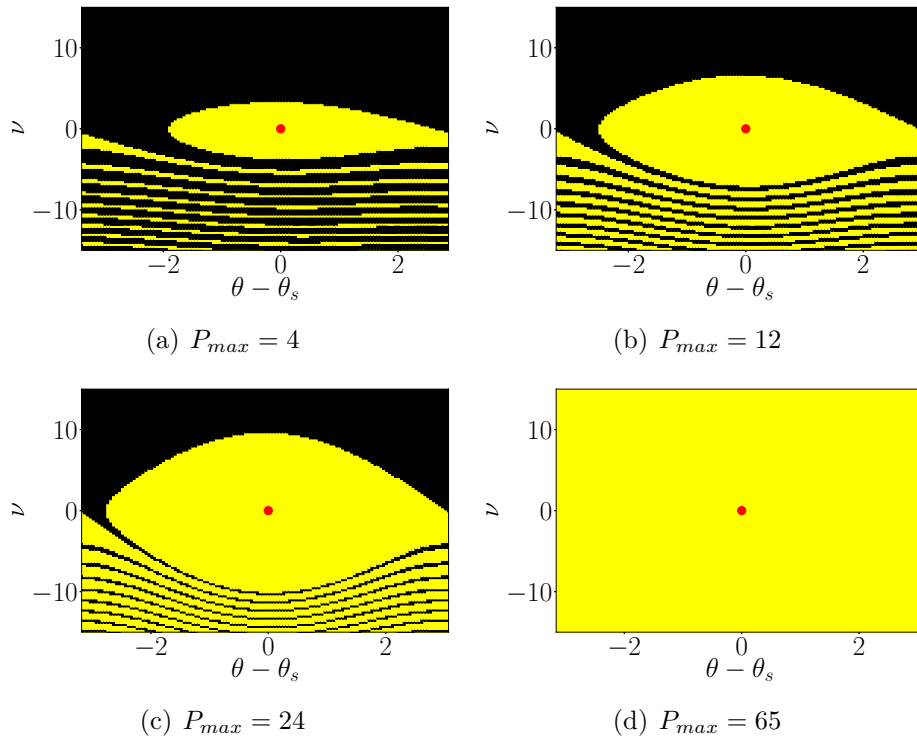
Assume that the generator is initially (at time t_0) in the synchronous state, described by $(\theta(t_0), \nu(t_0)) = (\theta_S, \nu_S)$. Then, in time t_1 , the transmission line that connects the generator to the grid is disconnected, that is, the coupling is set to $P_{max} = 0$. This causes ν to move away from the synchronous angular velocity ν_S and increase until the line is reconnected in time t_2 to the network. The generator converges from the disturbed state $(\theta(t_2), \nu(t_2))$ to the synchronous state (θ_S, ν_S) if the disturbed state is within the basin of attraction B of the synchronous state. For this reason, the synchronous state's basin of attraction must be as large as possible (MENCK et al., 2014).

In order to find the basin of attraction of this one-node model, we integrate Equations

3.64 and 3.65 for distinct values of the coupling $P_{max} = \{4, 12, 24, 65\}$, where the power generated is fixed at $P = 1$. The initial conditions are drawn randomly from a normal distribution, $\theta(0) \in [-\pi, \pi]$ and $\nu(0) \in [-15, 15]$. For each set of initial conditions $(\theta(0), \nu(0))$, we annotate when the system evolves to the synchronous state and when it does not. The basin of attraction can be seen in Figure 3.12, the points marked in yellow represent the initial conditions that led the system to the synchronous state, the black ones represent those that do not. The red dot represents the attracting fixed point which describes this synchronous state. Note that the greater the coupling P_{max} , the greater is the basin of attraction.

Returning to the previous situation, suppose that a component of the system is hit by a perturbation in time t_1 and, in time t_2 , this perturbation ceases. This component is able to return to the synchronous state if the point $(\theta(t_2), \nu(t_2))$ is within its basin of attraction.

Figure 3.12 - Basin of attraction (yellow) of a single node dynamics for the coupling P_{max} equal to (a) 4, (b) 12, (c) 24 and (d) 65. The attracting fixed point is plotted as a red dot.



Source: Author production.

To quantify how stable the synchronous state is when subjected to large perturbations, we use a measure of the volume of the basin of attraction, defined as the *basin stability* E : (MENCK et al., 2013)

$$E(B) = \int \chi_B(\theta, \nu) \rho(\theta, \nu) d\theta d\nu, \quad (3.66)$$

where ρ is a probability density, with $\int \rho(\theta, \nu) d\theta d\nu = 1$, which tells us which states in the state space of the system can be affected by large disturbances, and is defined as:

$$\rho = \begin{cases} \frac{1}{|Q|}, & \text{if } (\theta, \nu) \in Q, \text{ where } Q = [-\pi, \pi] \times [-100, 100], \\ 0, & \text{otherwise.} \end{cases} \quad (3.67)$$

On the other hand, χ_B is the indicator function of the synchronous basin of attraction B , given by:

$$\chi_B = \begin{cases} 1, & \text{if } (\theta, \nu) \in B. \\ 0, & \text{otherwise.} \end{cases} \quad (3.68)$$

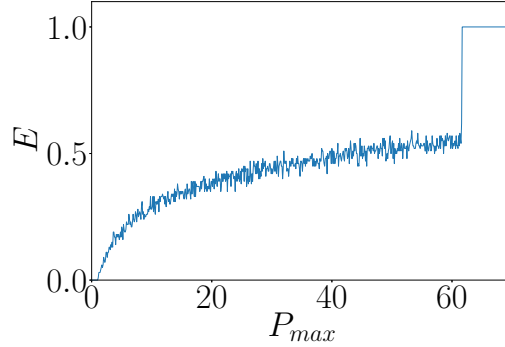
The basin stability $E(B) \in [0, 1]$ expresses the chance of the system to return to the synchronous state after being hit by a large randomly occurring perturbation with a probability density ρ . If $E = 0$, the synchronous state is unstable and, if $E = 1$, the synchronous state is globally stable. To estimate E , we use the Monte-Carlo method (WILEY et al., 2006), where T initial states are randomly chosen according to ρ , their trajectories in phase space are simulated and the number of times U at which the system converges to the synchronous state is annotated. The basin stability is then given by

$$E = \frac{U}{T}, \quad (3.69)$$

with an standard error of $e = \sqrt{\frac{E-E^2}{T}}$ (MENCK et al., 2014).

The basin stability E of the one-node model, with $P = 1$, as a function of coupling P_{max} can be seen in Figure 3.13. Note that E grows as we increase the coupling, until the synchronous state becomes the only possible state with $E = 1$. Note that E calculates how big the basin of attraction B is, for example, at $P_{max} = 65$, one can see that Figure 3.12(d) has its entire yellow area filled and in Figure 3.13 we have $E = 1$.

Figure 3.13 - Basin stability E of the one-node model as a function of the maximum capacity of the transmission line (coupling) P_{max} .



Source: Author production.

3.4.2.2 Multi-node model

In the one-node model (Equations 3.64 and 3.65), we assume that the rest of the network was not affected by the oscillator in question. To make the model more realistic, we now consider that there is an interaction between all nodes that make up the network and we analyze how the location of the node that suffers a disturbance influences the response that the network presents to this local loss of synchronization.

We now consider the second order Kuramoto model presented at the beginning of Section 3.2, given by Equations 3.23 and 3.24. As we assume that we are in a reference frame that rotates with the nominal frequency of the network, when the system is synchronized, the oscillators have an angular velocity $\nu_m = \nu_S = 0$ and constant phases $\theta_m = \theta_S$ with $m = 1, \dots, N$.

In this section, we use a set of fifty randomly generated networks with $N = 100$ nodes and 135 edges (transmission lines). These networks have an average degree $\langle g \rangle = 2.7$ which is a typical value found in real power grids (SUN, 2005; WITTHAUT; TIMME, 2013). The number of generators is given by $\frac{N}{2}$ where each one produces a power equal to $P_G = 1$, and the number of consumers is given by $\frac{N}{2}$ where each one consumes a power equal to $P_C = -1$. The coupling is fixed at $P_{max} = 8$. In each network, for each node m , the value of its basin stability is calculated

$$E_m = E(B_m) \in [0, 1], \quad (3.70)$$

where E is given by Equation 3.66 and E_m expresses the probability of the network

to return to its synchronous state after node m is disturbed, and B_m is a two-dimensional slice of the synchronous state's $2N$ -dimensional basin of attraction B that determines the response of the network to a disturbance that reaches node m , defined as:

$$B_m = \{(\theta_m, \nu_m) : (\theta_n, \nu_n)_{n=1, \dots, N} \in B \text{ com } \theta_n = \theta_n^S \text{ e } \nu_n = \nu_n^S = 0 \text{ para todo } n \neq m\}. \quad (3.71)$$

To estimate E_m , $T = 100$ initial conditions (θ_T, ν_T) are chosen randomly according to ρ (given by Equation 3.67) and, for each of these initial conditions, the initial condition of all nodes in the network is then set to

$$(\theta_n(0), \nu_n(0)) = \begin{cases} (\theta_T, \nu_T), & \text{if } n = m, \\ (\theta_n^S, \nu_n^S), & \text{otherwise,} \end{cases} \quad (3.72)$$

that is, all nodes start their trajectories in the phase space inside the basin of attraction B , except for node m , which is the node suffering the perturbation. We then use the Monte-Carlo method to calculate the basin stability of node m :

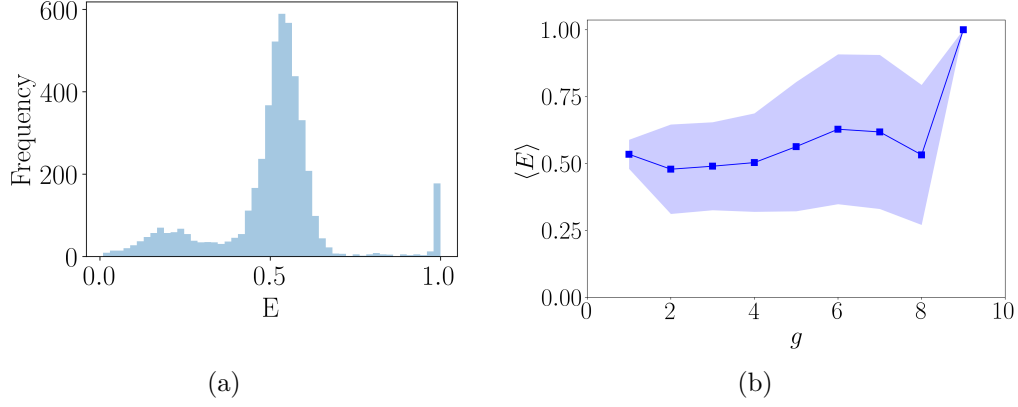
$$E_m = \frac{U_m}{T} \quad (3.73)$$

which has a standard error of $e = \sqrt{\frac{E - E^2}{T}} \leq 5\%$.

As there is a set of fifty networks and each network has $N = 100$ oscillators, we then obtain five thousand measures of the basin stability E_m which is plotted in the histogram of Figure 3.15(a), where most nodes present a reasonable value of basin stability and one can see the existence of two peaks with low and high values of E_m .

In the one oscillator model, we observed in Figure 3.13 that the basin stability was increasing as we increased the coupling P_{max} . In the multi-node model, the total coupling felt by a node m grows linearly with its degree g_m as it is given by $g_m P_{max}$. To calculate how the basin stability varies as a function of this total coupling, we calculate the average value of the basin stability $\langle E \rangle$ of all nodes and plot them as a function of their degree in Figure 3.15(b). Note that $\langle E \rangle$ does not grow much with the increase of g (except for $g = 9$), and the observed standard deviation is high. In a new approach, we investigate the role of the neighbors of a node on its basin

Figure 3.14 - (a) Histogram of the basin stability E . (b) Mean and standard deviation (light color) of basin stability $\langle E \rangle$ of all networks as a function of the nodes' degree g . Light colors indicate standard deviation.



Source: Author production.

stability. The average degree of the neighbors of a node m is defined as

$$g_{av,m} = \frac{1}{g_m} \sum_{n=1}^N A_{mn} g_n. \quad (3.74)$$

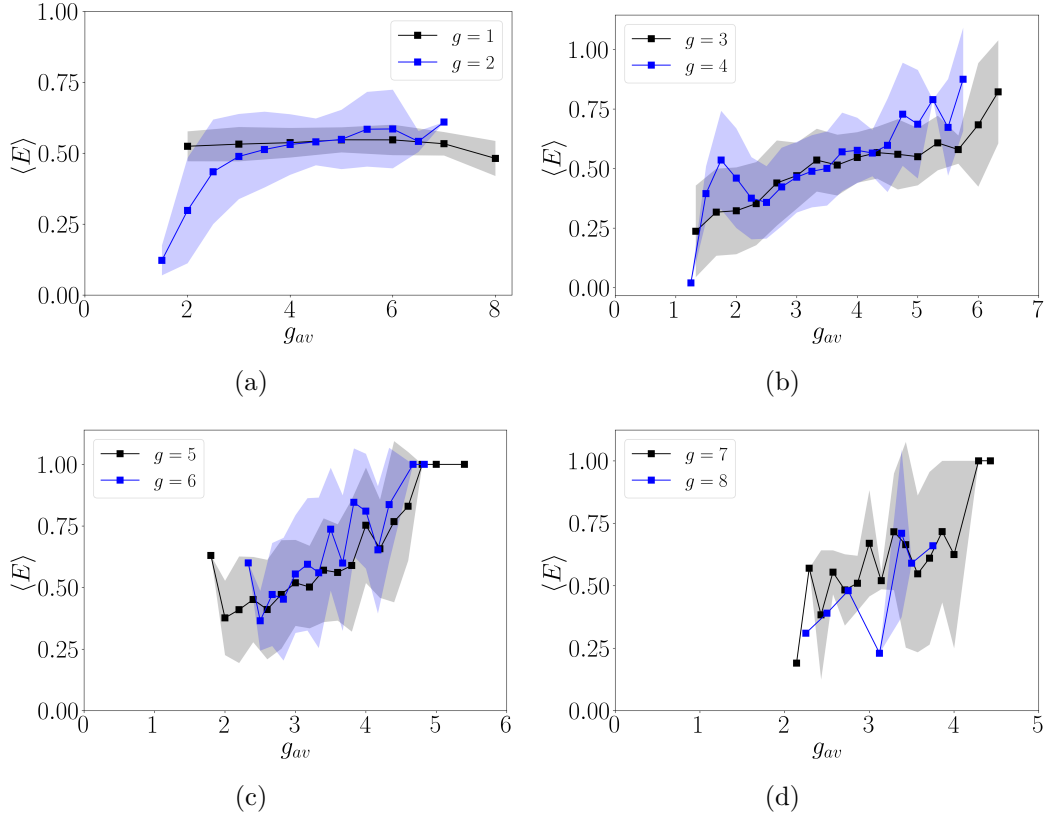
In Figure 3.15, we have the mean value of the basin stability $\langle E \rangle$ of nodes with degree $g_m = \{1, 2, 3, 4, 5, 6, 7, 8\}$, plotted as a function of the average degree of its neighbors g_{av} . With the exception of the node with degree one, the basin stability presents a linear grow, so, although this measure is not much affected by the node's own degree, it is greatly affected by its neighbors' degree.

To better understand how topology influences the behavior of the basin stability, we use the complex network metric called *betweenness centrality* b , defined as (NEWMAN, 2003b):

$$b_m = \sum_{n \neq m \neq q, q > n} \frac{\sigma_{nq}^m}{\sigma_{nq}}, \quad (3.75)$$

where σ_{nq} is the total number of shortest paths between node n and node q and σ_{nq}^m is the number of those paths that pass through node m . We then calculate $\langle E \rangle$ as a function of the betweenness b of the nodes, the result is shown in Figure 3.17(a), where one can see that there is no clear relationship between betweenness values and the basin stability, however, it can be noted that for some specific values of b , the basin stability presents low peaks. Some of these specific low betweenness values

Figure 3.15 - (a) Average of the basin stability $\langle E \rangle$ of nodes with degree 1 and 2, (b) 3 and 4, (c) 5 and 6 and (d) 7 and 8, as a function of the average degree of the neighbors g_{av} . Light colors indicate standard deviation.

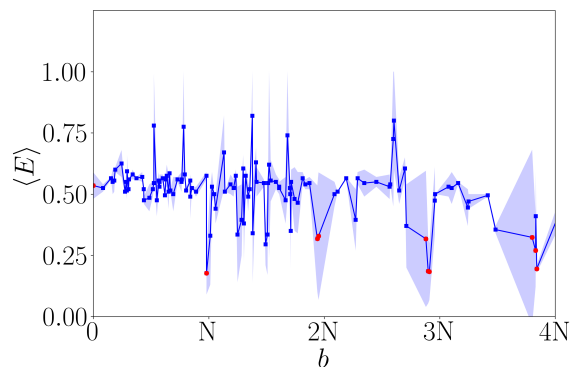


Source: Author production.

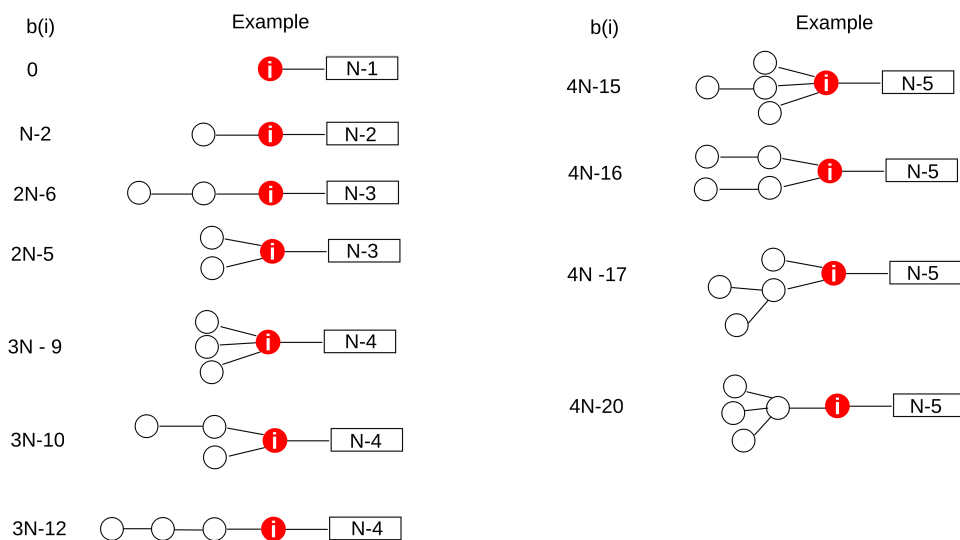
are plotted as red dots in Figure 3.17(a). One can see what these values represent in Figure 3.17(b), where the value of the betweenness of node m is represented in the left column and its location in the network (red) is represented in the right column (the square connected to the right of the node in red represents the number of nodes remaining in the network). We then can clearly see that the synchronous state presents a high instability in relation to perturbations that reach nodes located in certain places that are called *dead ends* or *dead trees* whose betweenness values are characteristic.

To take a closer look at the impact that dead ends and dead trees have on network synchronization, in Figure 3.18(a) we have the average of the basin stability $\langle E \rangle$ of the set of all the networks generated as a function of the degree g of the nodes that are adjacent or not to these dead trees. Note that $\langle E \rangle$ is on average always

Figure 3.16 - (a) Average basin stability $\langle E \rangle$ as a function of the betweenness b . Light colors indicate standard deviation. (b) Typical examples of nodes (red) that have certain distinct betweenness values b , this values of betweenness are marked as red points in (a); the boxes on the right of the red nodes represent the rest of the network whose number of nodes is written inside them.



(a)



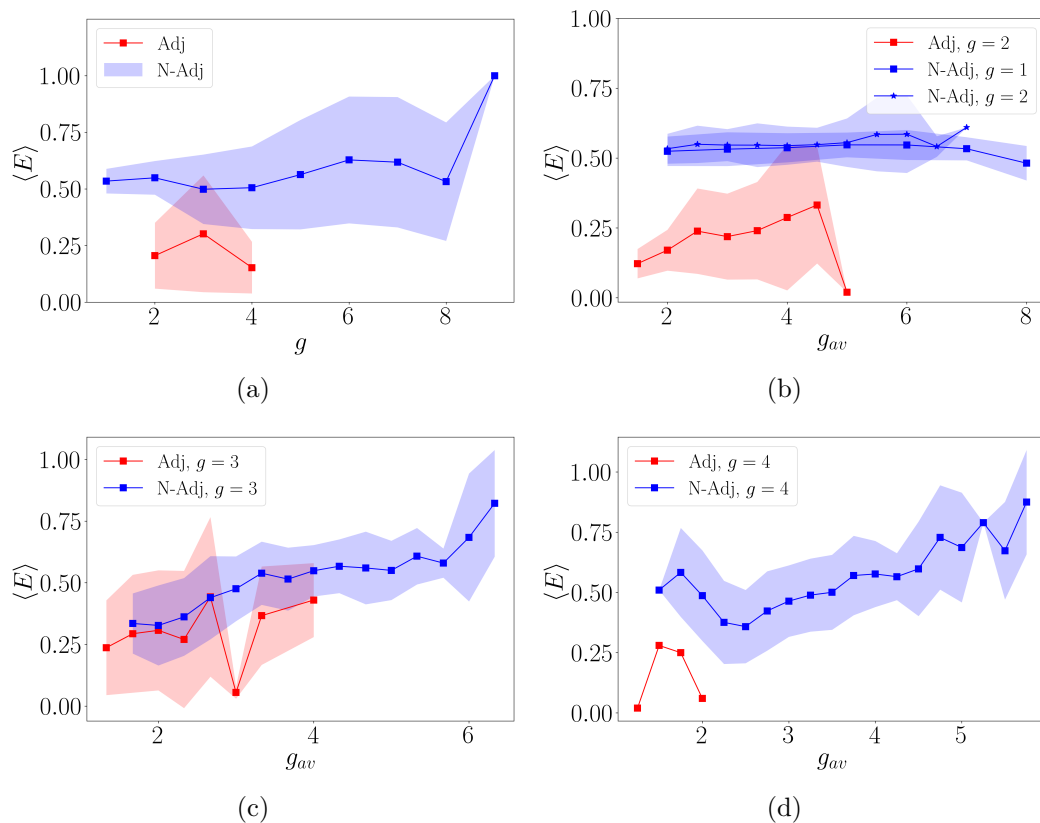
(b)

Source: Author production.

larger for nodes that are not adjacent to dead trees. That is, when a large disturbance, given by Equation 3.72, reaches a node m of the network, if this node has only nodes next to it with reasonable stability, this perturbation causes it to lose synchronization with the rest of the network causing its angular velocity to deviate from its synchronous velocity, $\nu_m \neq \nu_S$, while all other nodes remain very close to the synchronous state with $\nu \approx \nu_S$. However, if m is adjacent to a dead end or dead tree, that is, nodes with low stability, the perturbation tends to enter that alley and

destroy the synchronization of the nodes it contains. Note that $\langle E \rangle$ as a function of node degree has already been shown in Figure 3.15(b) but only when we differentiate nodes adjacent to dead trees or not is that we can see a pattern (MENCK et al., 2014).

Figure 3.17 - (a) Average of the basin stability $\langle E \rangle$ of all generated networks as a function of the degree g of the nodes that are adjacent (red) or not (blue) of dead trees and dead ends. Lighter colors indicate standard deviation. (b)-(d) Average basin stability $\langle E \rangle$ as a function of the neighbors degree plotted for nodes with distinct degrees and that are adjacent (red) and not adjacent (blue) to dead trees.



Source: Author production.

We can now redo Figure 3.15, separating the plots not only by node degree, but also by being adjacent to a dead tree or not. The result can be seen in Figure 3.17(b)-(d), where nodes adjacent to dead ends and trees are plotted in red and nodes not adjacent are plotted in blue. Remember that, in Figure 3.15, $\langle E \rangle$ had a linear increase with g_{av} and this does not seem to happen when we take into account only the value of $\langle E \rangle$ of the nodes adjacent to dead trees.

Finally, in Figure 3.18, we can observe closely the difference between nodes adjacent to dead trees or dead ends and those nodes that are not. In Figure 3.19(a) and 3.19(b), the histogram and the values of E of each node are plotted, respectively, and divided now into these two groups where the nodes adjacent to dead trees and dead ends are marked as Y and plotted in red and those that are not are marked as N and plotted in blue. One can note that the nodes adjacent to dead trees present, most of the time, low values of basin stability as most of them is below 0.3. The degree, betweenness and average neighbor degree, Figure 3.18(b)-(e), are expected to be lower for the nodes adjacent to dead trees as, by definition, they are in or near an "outskirt"¹ of the network. Therefore, they are connected to less nodes, have less shortest paths passing through them and do not have highly connected nodes as neighbors, as their neighbors are in or near the same "edge".

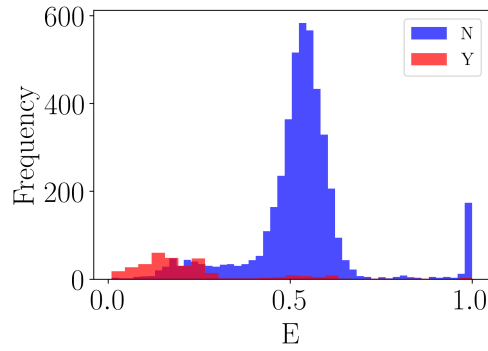
3.4.3 Braess's paradox

As shown in Section 3.4.2, dead trees and dead ends must be avoided in power grids, so, one might think that a good way to avoid these configurations in the topology of the network is just to add some new transmission lines to it. Also, the basin stability of the nodes in power grids tends to grow as one increases the maximum transmission capacity P_{max} of the transmission lines and it was also stated that the total coupling felt by a node is directly proportional to its degree, so, if one needs to add a new transmission line to an already existing and functional power grid there is not concern there since this additional line might actually help to improve the system stability. But is this always the case? Is there any situation in which increasing the coupling or adding a new transmission line has an opposite effect to what one might expect and actually disturbs the system and leads it out of the synchronous state? The answer to this last question is *yes* and this counter-intuitive phenomenon was first observed in traffic networks by Dietrich Braess (BRAESS et al., 2005; BRAESS, 1968), so it is referred to as Braess' Paradox.

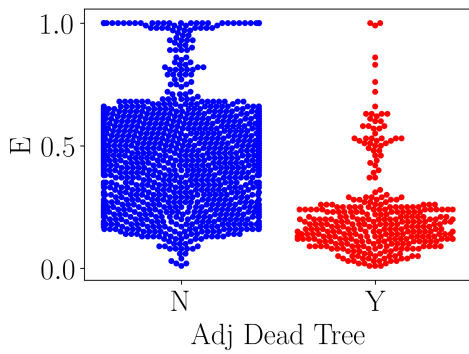
We consider in this section simple topologies, the same used in (WITTHAUT; TIMME, 2012), composed by four generators (generating $P_G = 1$ units of power each) and four consumers (absorbing $P_C = -1$ units of power each). More specifically, the coupling value is fixed as $P_{max} = 3.2$ and we consider three models, *Model A* (Figure 3.20(a)), *Model B* where the coupling constant of the upper dashed green edge is set as $P_{max}^B = 2P_{max}$ and *Model C* where all edges have again the same constant coupling value $P_{max} = 3.2$ but an extra transmission line (dashed) is inserted between two

¹structures like the ones presented in Figure 3.17(b).

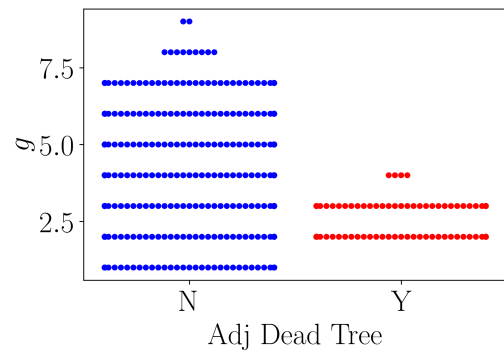
Figure 3.18 - (a) Histogram of basin stability E and measure of nodes' (b) basin stability, (c) degree, (d) betweenness and (e) average neighbors' degree values, divided between nodes adjacent (Y, red) and not (N, blue) to dead trees or dead ends.



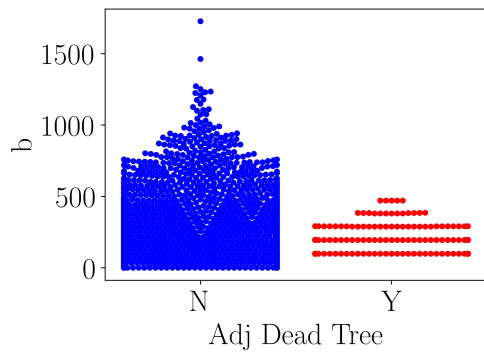
(a)



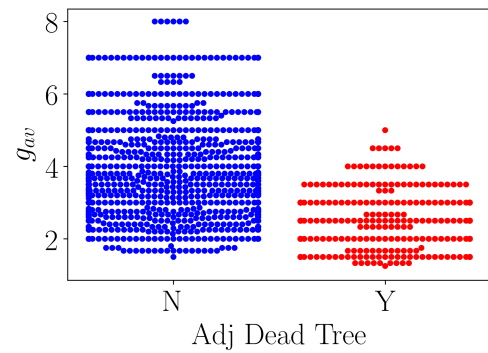
(b)



(c)



(d)



(e)

Source: Author production.

generators.

As the transmission capacity of one line is set to have a distinct value from all the others in Model B, the dynamics of the nodes is given by a modified version of Equations 3.20 and 3.21:

$$\dot{\theta}_m = \nu_m, \quad (3.76)$$

$$\dot{\nu}_m = P_m - \alpha \nu_m + \frac{1}{g_m} \sum_{n=1}^N P_{max}^{mn} A_{mn} \sin(\theta_n - \theta_m). \quad (3.77)$$

After integrating Equations 3.76 and 3.77 for all the three models, the instantaneous frequency is plotted in Figure 3.19. The instantaneous frequency of Model A is plotted in Figure 3.19(b) where one can note that after a transient, the system reaches the synchronous state as the instantaneous frequency of all the nodes are the same and remains constant (the partial synchronization index is calculated below). As for models C and D, one sees in Figures 3.19(d) and (f), respectively, that the consumers and generators are divided into two groups and have their instantaneous frequencies far apart from each other.

The partial synchronization index S is then calculated for all the three models and plotted in Fig 3.20(g) as a function of the coupling. Model A is the first one to reach the synchronous state, at $P_{max} = 3.2$. Note that for this value of coupling, models B and C present a low value of S , which is approximately 0.5. As the coupling is increased, Model B reaches the synchronous state and then, for a greater coupling value, Model C finally synchronizes.

So, a very simple change in the topology, like the addition of a new line or the increase in the power transmission capacity of a one existing line, can cause serious damage to the network as it may lose the synchronous state. In power grids, this process can cause nonlocal failures and even blackouts (PADE; PEREIRA, 2015). The reason behind this counter-intuitive phenomenon is that when these changes are made in the network, the power flows rearrange in a way that an overload may be induced in some transmission lines and the synchronous state is lost (WITTHAUT; TIMME, 2012).

Analytically, the loss of the synchronous state can be explained by the *geometric frustration*. There are two conditions for the existence of the synchronous phase locked state, one dynamical and one geometric. In relation to the dynamical one, consider the power flow defined in Equation 3.22, the dynamics of ν given in Equation

3.77 and the fact that the system is in the synchronous state, so $\nu_m = \nu_S = 0$ for all m , we have

$$0 = P_m + \frac{1}{g_m} \sum_{n=1}^N F_{L_{mn}}, \quad (3.78)$$

where $F_{L_{mn}}$ is the flow of power between nodes n and m , defined in Equation 3.22. Then, the dynamical condition is given by the conservation of the flow (WITTHAUT; TIMME, 2013):

$$|P_m| = \frac{1}{g_m} \left| \sum_{n=1}^N F_{L_{mn}} \right|. \quad (3.79)$$

The geometric condition relates to the fact that the sum of all phase differences around a cycle must be equal to zero, so that all phases are well defined (WITTHAUT; TIMME, 2012):

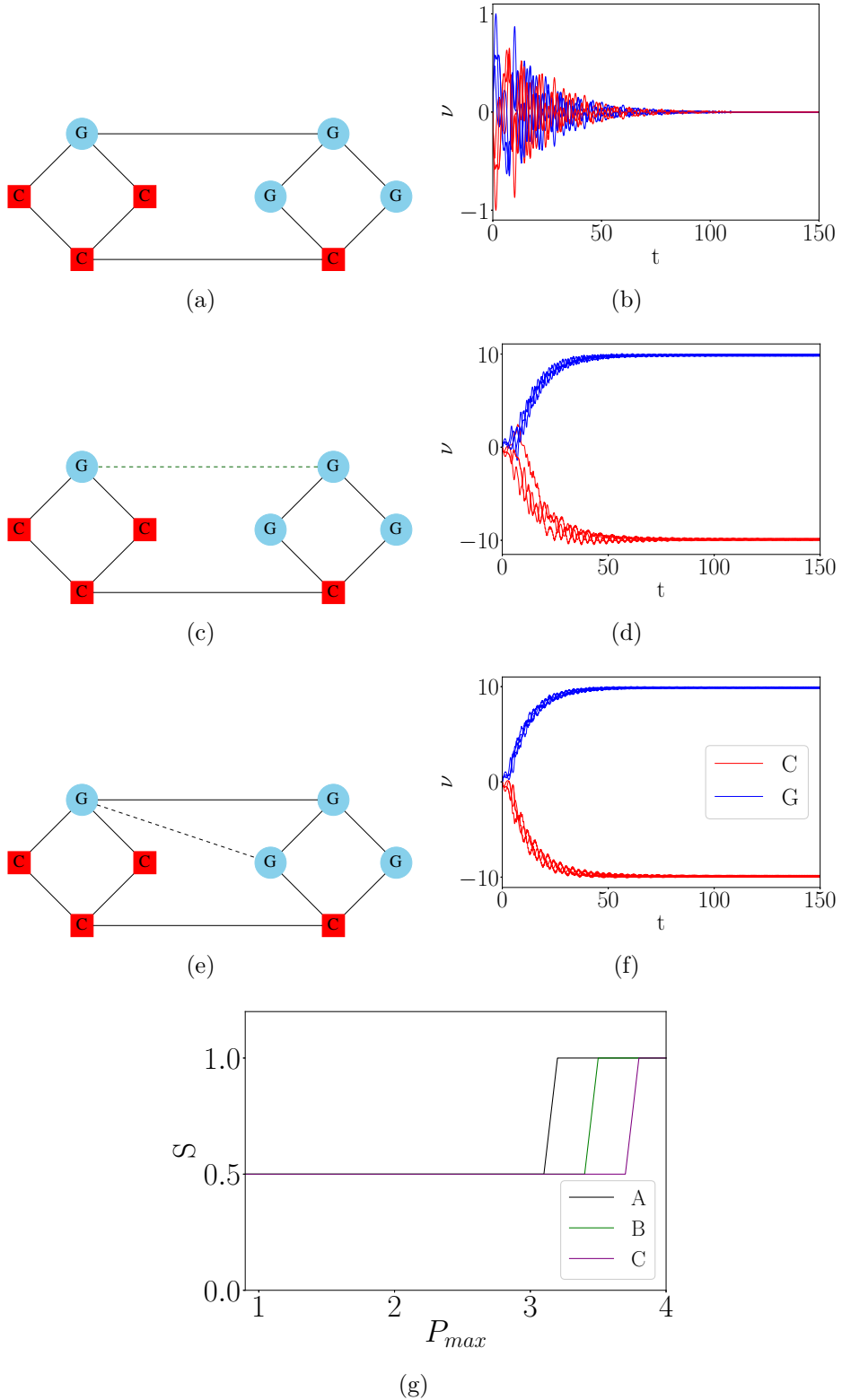
$$\sum^{\circ} (\theta_m - \theta_n) = \sum^{\circ} \arcsin \left(\frac{F_{L_{mn}}}{A_{mn} P_{max}} \right) = 0. \quad (3.80)$$

where \circ indicates that the sum is taken along the cycle. When the system is not able to satisfy this condition, no steady state exists. For the models A, B and C, Equation 3.79 is always satisfied but the condition given by Equation 3.80 is not when models B and C are considered (WITTHAUT; TIMME, 2012).

3.5 Conclusion

In this chapter, a bibliographical review on power grids in the context of the second order Kuramoto model was presented. We showed that, from some approximations, it is possible to describe electrical transmission networks with the use of the second-order Kuramoto model. From this approach, necessary conditions for network synchronization were deduced and the influence of the network topology on its stability was also presented.

Figure 3.19 - (a) Model A, with $P_{max} = 3.2$, (c) Model B with $P_{max} = 3.2$ in the edges marked in black and $P_{max}^B = 2P_{max}$ in the dashed green edge and (e) Model C with $P_{max} = 3.2$. The instantaneous frequencies of models A, B and C are plotted in (b), (d) and (f), respectively. (g) Partial synchronization index for all the three models as a function of the coupling.



Source: Author production.

4 SYNCHRONIZATION OF ENERGY TRANSMISSION NETWORKS AT LOW VOLTAGE LEVELS

In this chapter, we present an extended version of the original contribution published in the journal **Applied Mathematical Modelling** with the title *Synchronization of energy transmission networks at low voltage levels*, (LACERDA et al., 2021a). This paper can be found on Appendix B.

A brief introduction is made in Section 4.1, in Section 4.2 we refer to the models and methods already presented in this work, the results and discussions are shown in Section 4.3 and, finally, the final remarks are made in Section 4.4.

4.1 Introduction

The evolutionary optimization technique called evolutionary edge-snapping (DELELLIS et al., 2010; SCAFUTI et al., 2015b), discussed in Section 2.3, is used in this chapter to generate a network topology that favors synchronization for rather small values of coupling, we call it the ES network. This method creates networks with a relatively small number of edges and these topologies would be of great interest in the design of power grids, due to the costs involved in the construction of transmission lines. The dynamics of the nodes are given by the second order Kuramoto model, given by Equation 2.6.

Also, as the power grid generated by this method reaches the synchronous state at a low coupling value (when compared to the coupling required by a random network composed of the same number of nodes and edges), it means that lower voltage levels are needed in the transmission lines (KUNDUR et al., 1994; MONTICELLI; GARCIA, 2011), which is also a desirable characteristics. After studying and analyzing the behavior of the power grid topology created by the Edge Snapping method, we use the basin stability method (MENCK et al., 2014), presented in Section 3.4.2, to analyze the stability of this topology when subjected to perturbations. We find that the ES network nodes' present in average a higher basin stability when compared to a random one.

4.2 Models and methods

In order for a power grid to be fully functional, all of its components must be frequency synchronized (GRZYBOWSKI et al., 2018). So we begin this section by referring to the metrics that quantify the level of synchronization of a dynamical system. The order parameter R (Equation 2.9) (DANIELS, 2005) shows the level of the

collective behavior of a system by measuring the amount of phase synchronization.

The parameter partial synchronization index S (Equations 2.10 and 2.11) (GÓMEZ-GARDENES et al., 2007) presents the level of the frequency synchronization (or phase locking) (LACERDA et al., 2020; LACERDA et al., 2019) between a pair of a system' units.

In order for power to flow in a power grid, there must be a phase difference between the components of the grid (FILATRELLA et al., 2008). So, we want our system to be phase locked, thus having the same instantaneous frequency, and not phase synchronized, that is, we want $S = 1$ and $R \neq 1$, and we are always referring to this configuration when we say that the system is synchronized.

In order to model the dynamics of generators and consumers, we make use of the second order Kuramoto model (ÓDOR; HARTMANN, 2018) in a way that the dynamics of a power grid component is given by Equations 3.20 and 3.21.

The phase and the angular velocity of a node m in the synchronous state are defined as $(\theta_m = \theta^S, \nu_m = \nu^S)$. The phase in the synchronous state is given by Equation 3.33 and the angular velocity is defined in Equation 3.32 (MENCK et al., 2014; ROHDEN et al., 2012)

In this work, there are $\frac{N}{2}$ consumers ($P_m < 0$) and $\frac{N}{2}$ generators ($P_m > 0$) in a way that all power generated is consumed, so $\sum_{m=1}^N P_m = 0$ and, therefore, $\nu^S = 0$.

The Edge Snapping method (Section 2.3) (DELELLIS et al., 2010; SCAFUTI et al., 2015a) is used in this work in order to generate topologies that model a power grid. This method is an adaptive strategy that drives the evolution of an unweighted network, in which a second order equation is associated with each edge of the graph. In this model, the equation associated with the edge between nodes m and n is given by Equation 2.13. By using the Edge Snapping method to generate network topologies, the second order Kuramoto model is written as

$$\ddot{\theta}_m = -\alpha\dot{\theta}_m + P_m + \frac{P_{max}}{g_m} \sum_{n=1}^N k_{mn} \sin(\theta_n - \theta_m). \quad (4.1)$$

Note that here that adjacency matrix A is replaced by the coupling gain k . So, in order to study the dynamics of our power grid, we integrate Equations 2.13 and 4.1

simultaneously. Although, k_{mn} replaces the adjacency matrix, it can take continuous values between 0 and 1.

The Edge Snapping method is used in the context of evolutionary optimization where rules of variation and selection are applied in order to generate network topologies. The Evolutionary Edge Snapping is composed of two fundamental rules, given in Section 2.3.1. Where the probability of activation of an edge F_{mn} is defined in Equation 2.15 and only edges whose probability of activation higher than a threshold f^* are marked as active (are present) in the network. The value of f^* is chosen in a way that the entire network is connected and present the smallest possible number of edges, we call this network *edge-snapping network (ES network)*.

The basin stability method, presented in Section 3.4.2, is used in this work to study the stability of all the nodes of the network generated by the Edge Snapping method. The results are compared to the ones calculated for a random network with the same number of edges and nodes.

4.3 Results and discussion

We use the Edge Snapping method to generate a $N = 50$ node (due to high computational cost) power grid whose nodes' delivered or consumed power P are given by a Gaussian distribution with zero mean and standard deviation $\sigma_P = 0.2$, in a way that $\frac{N}{2}$ nodes have their frequencies set randomly by this distribution and $\frac{N}{2}$ nodes have the exact opposite power, so all the power generated is consumed as $\sum_{m=1}^N P_m = 0$.

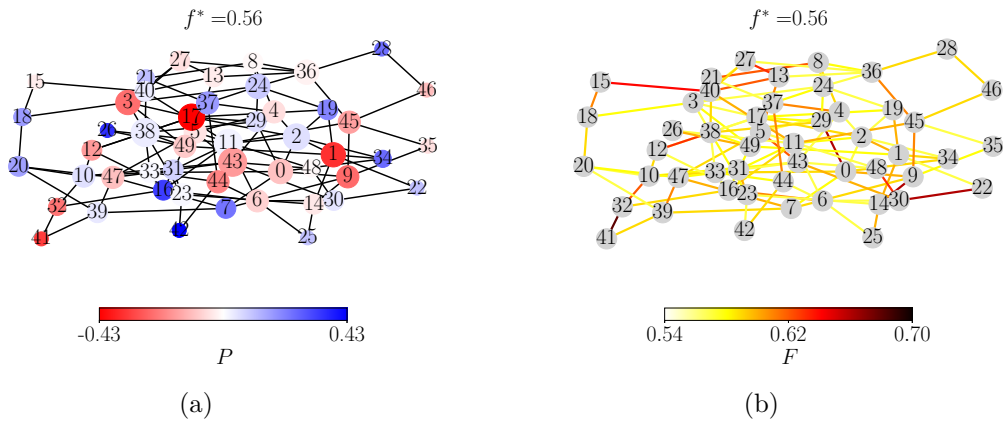
Following the two steps presented in Section 2.3.1, we simultaneously integrate Equations 2.13 and 2.16 with a fixed coupling $P_{max} = 1.5$ for $n_T = 100$ distinct sets of initial conditions. We then annotate the fraction of times each of the $\frac{N(N-1)}{2}$ possible edges were present at the final topology. This fraction F is a $N \times N$ matrix called probability of activation of the edges. We then have a fully connected network whose the edges' probability of activation are given by F_{mn} .

The edges with the lowest values of F start being removed from the network, in a way that one edge is removed at a time and two conditions are always checked: whether no node has been disconnected from the network and whether the partial synchronization is still equal to one, that is, if the network is still in the synchronous state. This procedure is repeated until one of those conditions is false. Then, the value of the probability of activation of the last snapped edge in which both conditions

were true is marked as f^* and is said to be the threshold, as all the edges that remained in the final topology have a probability of activation greater than that value.

The topology of the 50 node ES network is plotted in Figure 4.1, where in Figure 4.1(a) the size of the nodes is proportional to their degree and the color relates to the amount of power P generated (blue) or consumed (red), while in Figure 4.1(b) the probability of activation F is represented by edge colors, as the threshold for this configuration is $f^* = 0.56$, leaving the final topology with 108 edges. This is a relatively low number of edges as only a fraction of around 9% of all possible edges were marked as active in the final topology. It is a characteristics of the Edge Snapping method to generate networks with a relatively low number of edges (SCAFUTI et al., 2015b), which is an advantage when it comes to power grids due to the costs involved in the construction of transmission lines.

Figure 4.1 - Network topology generated by the Edge Snapping method. (a) Shows the power generated or consumed by all nodes and (b) shows the probability of activation of all edges.

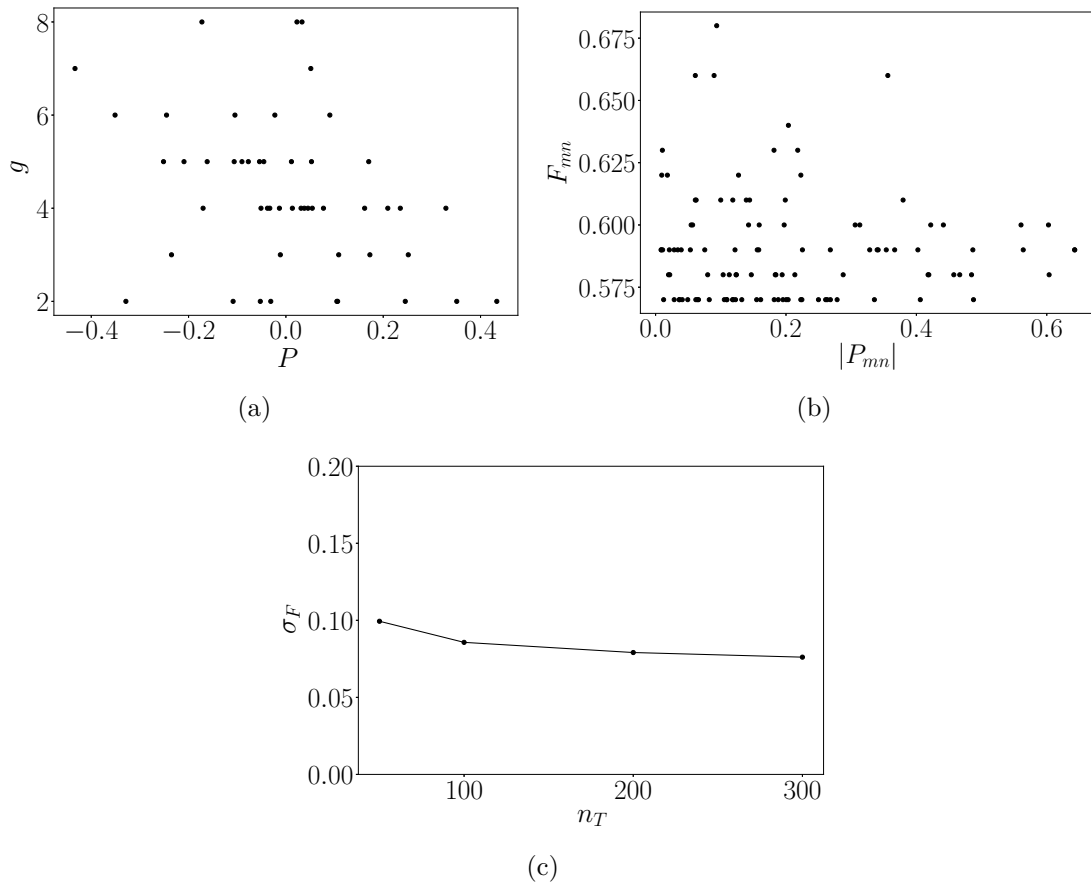


Source: Author production.

More details of the ES network can be seen in Figure 4.2, where, Figure 4.2(a), the degree g of all nodes are plotted as a function of their power P generated or consumed, the probability of activation of all edges are plotted as a function of the absolute value power difference of the nodes these edges are connecting $|P_{mn}| = |P_m - P_n|$, is plotted in Figure 4.2(b), and, finally, the standard deviation of the activation probability F is plotted against the number of trials n_T , Figure 4.2(c).

The degree g of the nodes seem to be distributed mostly at random, as for the probability of activation F , it doesn't display a well defined behavior, although there is roughly a band-like structure and as $|P_{mn}|$ grows, the band structure gets narrower. The standard deviation of the activation probability presents a constant like value for n_T equal or greater than 100 and this is the reason we chose $n_T = 100$.

Figure 4.2 - (a) Nodes degree g as a function of the power generated or consumed P . (b) Probability of edge activation of each edge of the network F_{mn} as a function of the absolute value of the power difference between nodes m and n , $|P_{mn}|$. (c) Standard deviation of the probability of activation σ_F of all edges as a function of the number of trials n_T .

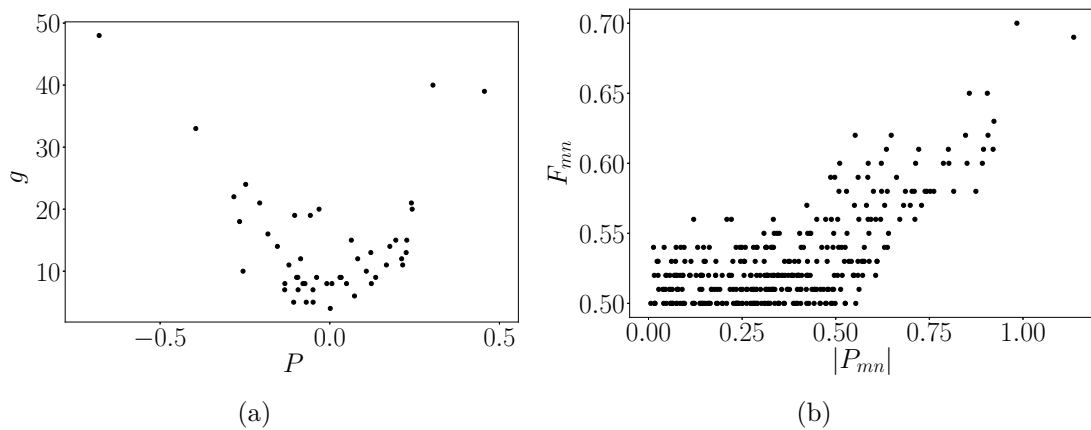


Source: Author production.

The behavior of the degree and the probability of activation found here is not the same of what was found in (SCAFUTI et al., 2015b) by using the Edge Snapping method along with the first order Kuramoto model. In that work, the authors show that the degree and the probability of activation are related to the power P , in a

way that the nodes with the value of P far from the mean present higher degree and the probability of activation of the edges are greater for higher values of $|P_{mn}|$. As shown in Figure 4.3, where the degree is plotted as a function of the power and the probability of activation of the edges are plotted against P_{mn} , for a network generated by the Edge Snapping method along with the second order Kuramoto model where the power consumed or generated are set by a Gaussian distribution with zero mean and standard deviation equal to 0.2, without the constraint $\sum_{m=1}^N P_m = 0$. One can see that we also obtained this behavior for both measures in our simulations. Although, when the condition $\sum_{m=1}^N P_m = 0$ is added to the power distribution, this correlation seems to be lost. This condition is of utmost importance in this work as we are simulating the behavior of power grids in which all power generated is consumed.

Figure 4.3 - Characteristics of a network topology generated by the Edge Snapping method along with the second order Kuramoto model where the power consumed or generated are set by a Gaussian distribution with zero mean and standard deviation equal to 0.2, without the constraint $\sum_{m=1}^N P_m = 0$. (a) Nodes degree g as a function of the power generated or consumed P . (b) Probability of edge activation of each edge of the network F_{mn} as a function of the absolute value of the power difference between nodes m and n , $|P_{mn}|$.



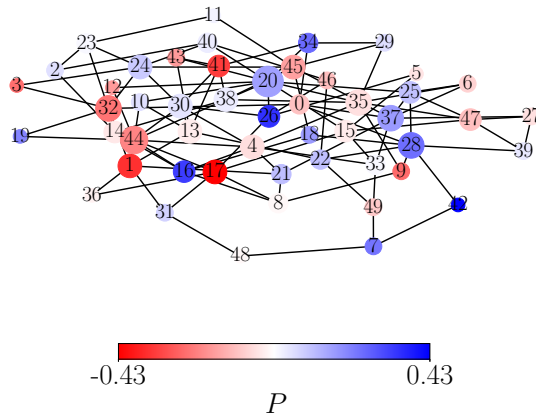
Source: Author production.

Now that the ES network topology is defined, our interest is to study how it affects the synchronization of the power grid and, in order to make some kind of comparison, we generate a random network with the same number of edges (108), nodes (50) and power generated and consumed. This network topology is represented in Figure 4.4. Both network topologies are then integrated for several distinct values of P_{max} . The

average instantaneous frequency ν_{avg} (the mean in time for a fixed value of P_{max}) of each node is plotted in Figure 4.5(a) for the ES network and in Figure 4.5(b) for the random network, where ν_{avg} is marked in red for consumers and in blue for the generators. For the same initial conditions, one can see that a common instantaneous frequency is reached at a lower value of P_{max} for the ES network. In Figure 4.5(c), the order parameter and the partial synchronization index are plotted as a function of the coupling P_{max} for both networks, showing that the ES network reaches the synchronous state at a lower value of coupling when compared to the random one as we have $P_{max} = 0.60$ for the ES network synchronization and $P_{max} = 0.75$ for the random one. Note that for higher values of coupling, the value of the order parameter R is close but never equal to one, which is desired because, as mentioned in Chapter 3, it is a condition in order to have a power flow between two nodes of a power grid.

The advantage of reaching synchronization at lower values of coupling comes from the fact that the coupling represents the maximum power transfer capacity of a transmission line and, therefore, lower transfer capacity means lower voltage levels and cheaper transmission lines when building power grids.

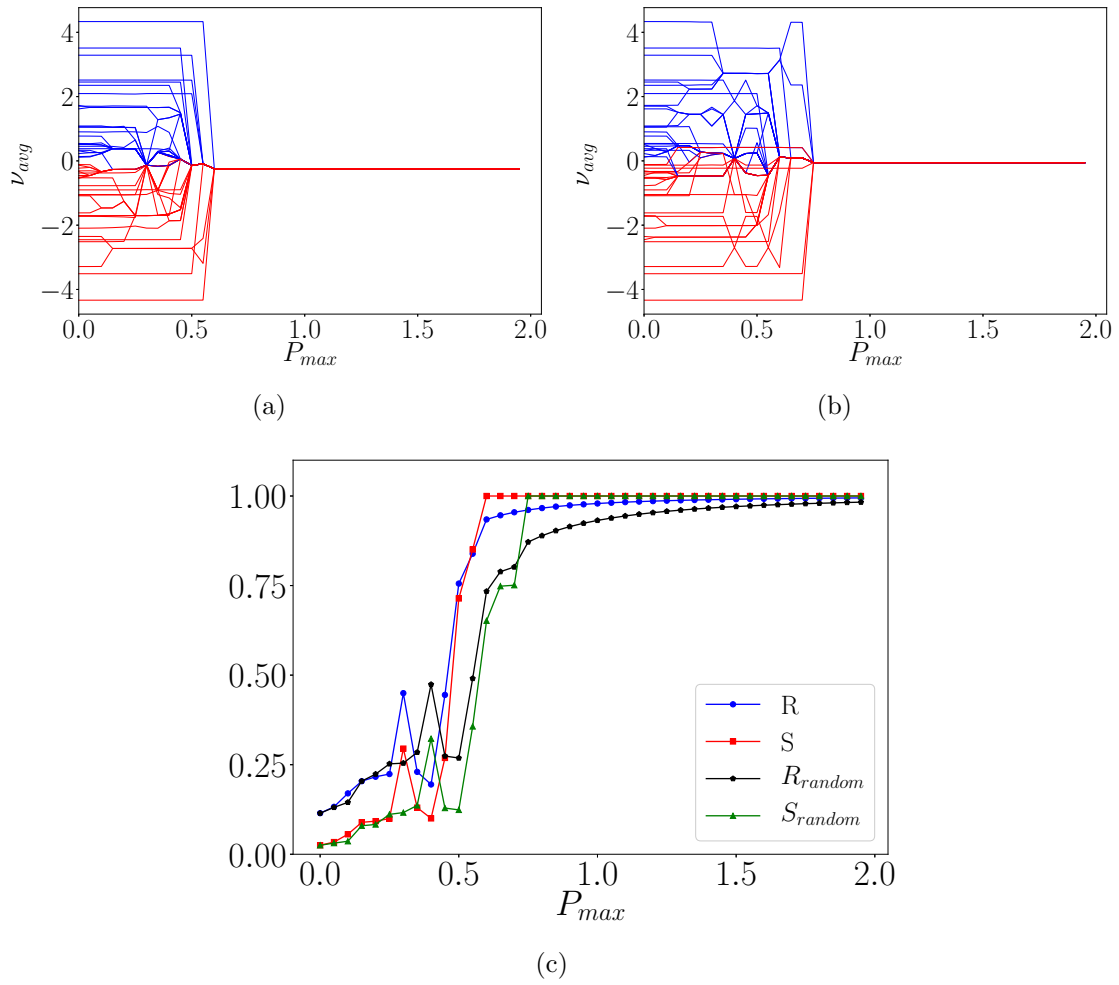
Figure 4.4 - Random network with the same number of nodes, power consumed or generated and edges as the ES network (Figure 4.1).



Source: Author production.

In order to study the stability of the ES network, we use the basin stability method presented in Section 3.4.2, where, for a fixed value of coupling ($P_{max} = 1.5$ is chosen as both topologies are synchronized for this value of coupling), a single node m suffers a perturbation $T = 100$ times. Let U_m be the number of times the system

Figure 4.5 - Average instantaneous frequency ν_{avg} of all nodes as a function of the transmission capacity P_{max} for the (a) ES network and (b) random network where consumers are marked in red and generators in blue. (c) Partial synchronization index S of the ES network (red) and random network (green), order parameter R of the ES network (blue) and random network (black) as a function of the transmission capacity.

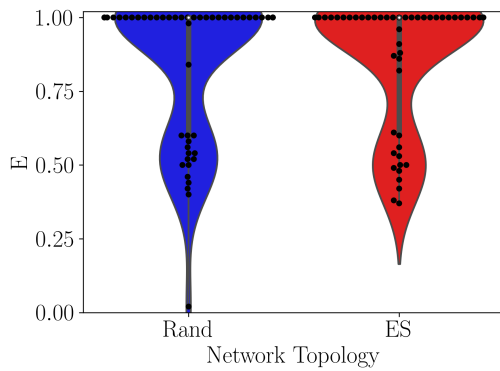


Source: Author production.

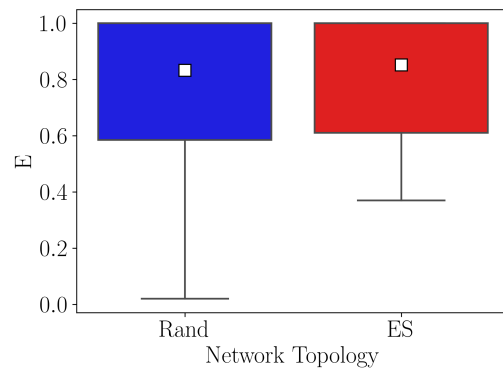
reaches the synchronous state after the perturbation, then the basin stability of node m is defined as $E_m = \frac{U_m}{T}$ (Equation 3.73). The same is done for all nodes of the random network. In Figure 4.6(a), the values of the basin stability of each node are plotted as black dots and we also have the kernel density estimate of those values, in blue for the random network and in red for the ES one and, in Figure 4.6(b), a box plot of the same measure is shown. The kernel density estimate is a non-parametric way to estimate the probability density function of random a variable (WEGLARCZYK, 2018). Note that no node of the ES network presents a relatively low value of basin stability ($E < 0.25$) while the random network presents a node with very low stability. In order to see if these features did not happen by chance, three additional ES networks are generated and also their respective random ones (with the same number of nodes and edges). The basin stability of all nodes of the four ES networks and four random networks are then plotted in Figure 4.6(c-d), where the same pattern can be noted, as the random networks present nodes with relatively low values of E , which still does not happen with the ES networks. Presenting a high value of stability is crucial for power grids as they are often subject to disturbances and component failures. A high basin stability of a node expresses the likelihood of a generator or a consumer to go back to the synchronous state after being taken away from it.

Going back to the original ES and random networks, represented in Figures. 4.1 and 4.4, respectively, the values of the nodes' basin stability E , degree g , average neighbor degree g_{av} and betweenness centrality b are plotted as a function of each other in Figure 4.7, the histogram in the form of the kernel density estimate is plotted in the diagonal. The values of these metrics for the ES network are plotted in red and the random ones are plotted in blue. Note that the histogram of E presents a higher peak at $E = 1$ for the ES network, showing that this network presents a high number of stable nodes when compared to the random one. Also, the random network presents a higher number of nodes with E very close to zero, which is was also presented in Figure 4.6(a-b). Looking at the histogram of the average degree of the nodes' neighbors g_{av} , one sees that they tend to have lower values for the ES network, while the histogram of the betweenness centrality shows that the nodes in the ES network tend to have a little higher values of b . About the figures outside of the diagonal, there is no specific pattern differentiating between the nodes of the ES and the random networks.

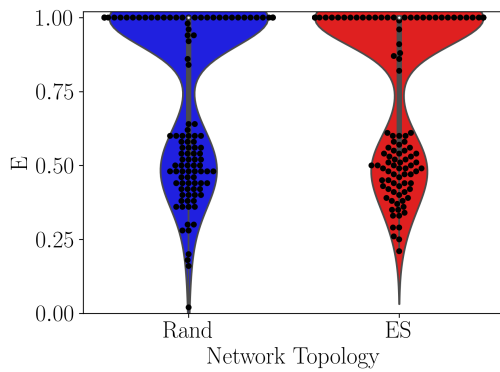
Figure 4.6 - (a) Distribution of the values, their kernel density estimate and (b) box plot of the basin stability E of all nodes of the ES (red) and random (blue) networks presented in Figures. 4.1 and 4.4, respectively. (c-d) The same as (a-b), but now with of four ES and random networks. The median of the boxplots is 1, the mean is shown as a white square.



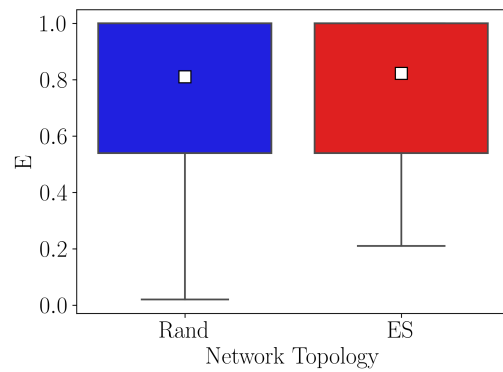
(a)



(b) Rand: Mean = 0.832. ES: Mean = 0.852



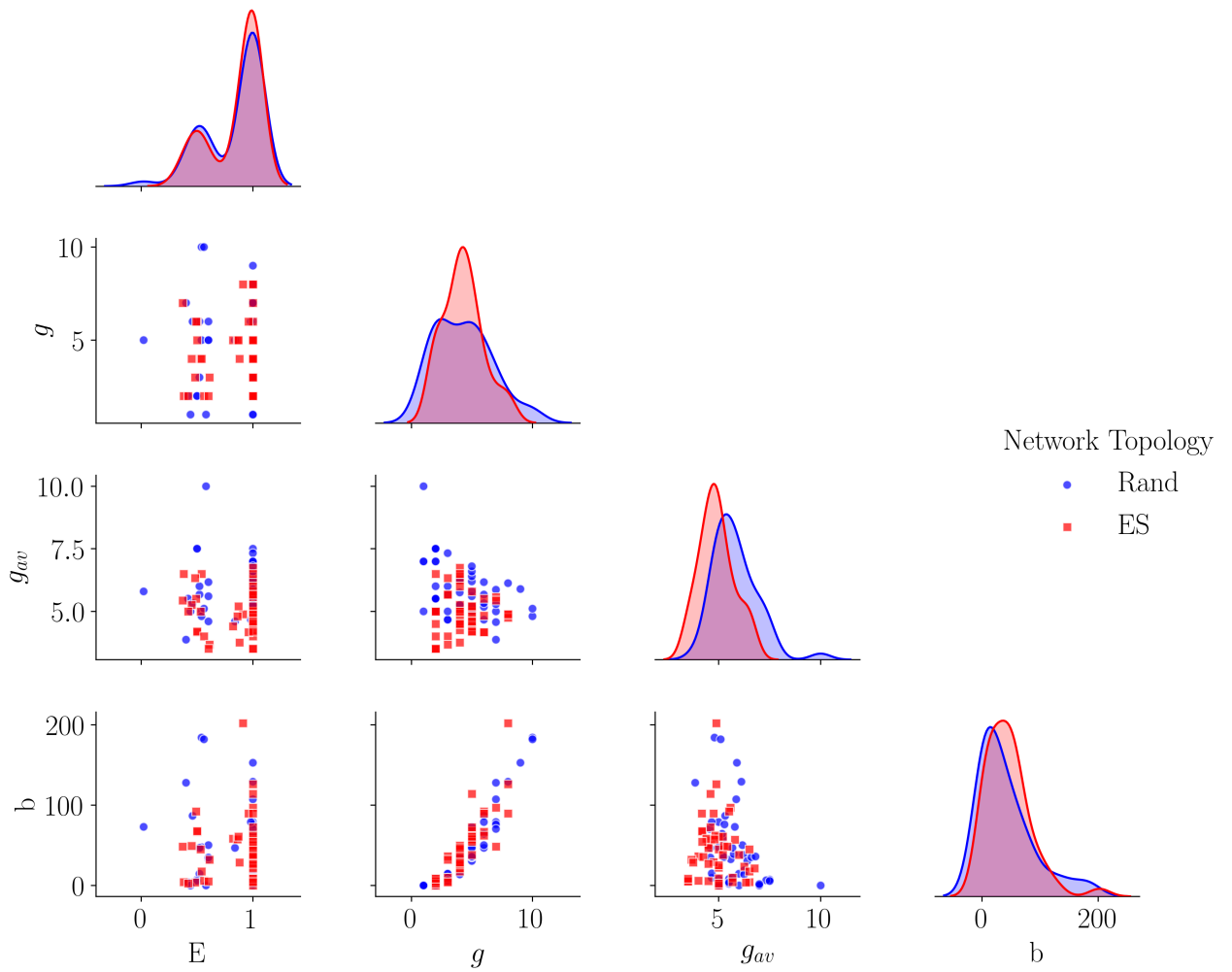
(c)



(d) Rand: Mean = 0.810. ES: Mean = 0.823

Source: Author production.

Figure 4.7 - Degree g , neighbors degree g_{av} and betweenness centrality b of the nodes as a function of each other and kernel density estimate of the histogram in the diagonal for the ES (red) and random (blue) networks.



Source: Author production.

4.4 Conclusion

In this chapter, we used the Edge Snapping method to generate power grid topologies whose units are modeled by the second order Kuramoto oscillator model. A fifty node power grid was generated, being that half of the nodes were set to be consumers and the other half generators, in a way that all power produced is consumed by the grid. The topologies generated by the Edge Snapping method have a characteristic of presenting a relatively low number of edges, which is desirable in our case study since it means building a less amount of transmission lines. Also, the network generated by this method favors synchronization in a way that it reaches phase locking at a lower value of coupling when compared to a random network with the same number of nodes and edges. As the coupling in the second order Kuramoto model is related to the maximum transmission capacity of a transmission line, lower coupling implies lower voltage levels in the transmission lines which is also a desirable characteristics in a power grid, as it is cheaper to build. The nodes of the ES network present in general higher stability when compared to a random network of the same size and this fact is also relevant because if a node can not go back to the synchronous state after being hit by a perturbation, local, nonlocal failures and even blackouts may occur.

5 ELEMENTARY CHANGES IN TOPOLOGY AND POWER TRANSMISSION CAPACITY CAN INDUCE FAILURES IN POWER GRIDS

In this chapter, we present our original contribution published in the journal **Physica A: Statistical Mechanics and its Applications** with the title *Elementary Changes in Topology and Power Transmission Capacity Can Induce Failures in Power Grids*, (LACERDA et al., 2021a). This paper can be found on Appendix C.

An introduction is made in Section 5.1, in Section 5.2 we refer to the models and methods already presented in this work, the results and discussions are shown in Section 5.3 and, finally, the final remarks are made in Section 5.4.

5.1 Introduction

In this chapter, we explore the Braess's paradox phenomenon in power grids by taking into account not only if a removal, addition or increase in the transmission capacity of an edge affects the synchronous state of the grid, but also the nature of the pair of nodes this edge is connecting, taking also into consideration the effect of the level of centralization of energy generation. Distinct network topologies are used in order to calculate the most probable outcome when these simple changes are made to the power grid.

For example, does the addition or removal of an edge between two consumers induces a desynchronization of the grid more often than the adding or removal of an edge that connects two generators? How is this affected by the decentralization of the grid? Can the increase of a transmission line capacity connecting a consumer and a generator cause a failure in the network? How often?

5.2 Models and methods

The dynamics of a component of a power grid considered in this chapter is similar to Equations 3.20 and 3.21, but here we allow the coupling to vary if needed, so they are given by

$$\dot{\theta}_m = \nu_m, \tag{5.1}$$

$$\dot{\nu}_m = P_m - \alpha\nu_m + \frac{1}{g_m} \sum_{n=1}^N P_{max}^{mn} \sin(\theta_n - \theta_m). \tag{5.2}$$

where P_{max}^{mn} is the maximum power transmission capacity on the line connecting nodes m and n and has zero value if these nodes are not connected. Initial conditions

$\theta(0)$ and $\nu(0)$ are fixed at zero for all nodes and the dissipation parameter fixed at $\alpha = 0.1$ (FILATRELLA et al., 2008; MENCK et al., 2014). The flow or power transmitted between two nodes for a varying coupling constant is defined as

$$F_{Lmn} = P_{max}^{mn} \sin(\theta_n - \theta_m) \quad (5.3)$$

In the phase locking state, the synchronous instantaneous frequency is then defined as $\nu_m = \nu_S$ for all $m = 1, \dots, N$, where ν_S is the synchronous angular velocity and is defined by Equation 3.32 as $\nu_S = \frac{\bar{P}}{\alpha}$ where $\bar{P} = \frac{\sum_{m=1}^N P_m}{N}$ is the mean between all consumed and generated power. In this work, no power is stored at any node, that is, all power generated is consumed, so $\sum_{m=1}^N P_m = 0$, and, therefore, $\nu_S = 0$.

A necessary coupling value for the synchronization of the power grid P_{max}^* is given by Equation 3.37 (GRZYBOWSKI et al., 2016; CHOPRA; SPONG, 2005; CARARETO et al., 2013). That is, there is not a synchronous state where the power grid properly works in which the coupling has a value lower than P_{max}^* . We emphasize that Equation 3.37 is a necessary but not sufficient condition for synchronization. The sufficient condition for synchronization $P_{max}^c \geq P_{max}^*$ is calculated numerically in the next section.

To properly measure the synchronization of the grid, we make use of the partial synchronization index S, Equation 2.11 (GÓMEZ-GARDENES et al., 2007).

There are two conditions for the existence of the phase locked state, one dynamical Equation 3.79 and one geometric Equation 3.80. The dynamical relates to the conservation of the flow and the geometric condition relates to the fact that the sum of all phase differences around a cycle must be equal to zero, so that all phases are well defined (WITTHAUT; TIMME, 2012).

In order to simulate the behavior of power grids, we describe them as complex networks (MENCK et al., 2014; SUN, 2005) and a random model (ERDÖS; RÉNYI, 1959) is used to generate their topologies in this chapter. We generate sixteen distinct topologies where each one has $N = 50$ nodes and $E = 68$ edges, which gives an average degree of 2.72, that is a typical value of the average degree of power grids (WITTHAUT; TIMME, 2013; MENCK et al., 2014; SUN, 2005).

In each of these sixteen topologies, four combinations of generators and consumers are used:

- 25 generators and 25 consumers.
- 12 generators and 38 consumers.
- 5 generators and 45 consumers.
- 3 generators and 47 consumers.

So we go from a decentralized grid ($N_G = 25$ generators) to a centralized one ($N_G = 3$ generators). The consumed power is defined as $P_C = -1$ and the generated power is given by

$$P_G = \frac{\sum_1^{N_C} |P_C|}{N_G}. \quad (5.4)$$

To analyze how a simple change in the topology can affect synchronization, first, we calculate P_{max}^c for the original network topology (one of the sixteen mentioned above), being this the minimum coupling for which the network is synchronized ($S = 1$). Then, one edge is added, removed or selected randomly to double its power transmission capacity, P_{max}^c is computed for this new configuration and compared to the P_{max}^c of the original network. The value can be either greater (marked here as *Increases*), lower (marked here as *Decreases*) or equal (marked as *Unchanged*) to the original value. We then go back to the original topology and the process is repeated. Note that when the value of P_{max}^c of the modified network is greater than that of the original network, the current coupling with which the original network was operating is not sufficient enough to maintain the synchronous state so the proper function of the grid is lost. In the case of the decrease situation, the change has a beneficial effect on synchronization, yet this situation is not the aim of this study as we look for possible causes of failures.

In the case of edge addition, we add randomly 50 new edges, one at a time, in each of the sixteen network configurations. Note that one edge is added at random, P_{max}^c is calculated, the original network is then considered again and a new edge is added and so on. In the case of edge removal, all edges from the original networks are removed, one at a time (always considering again the original network before removing a new one) and P_{max}^c is calculated. The selected edge is removed as long as the final network topology is still connected, that is, no node is isolated from the others.

We also check how the increase of the maximum capacity of the transmission of a

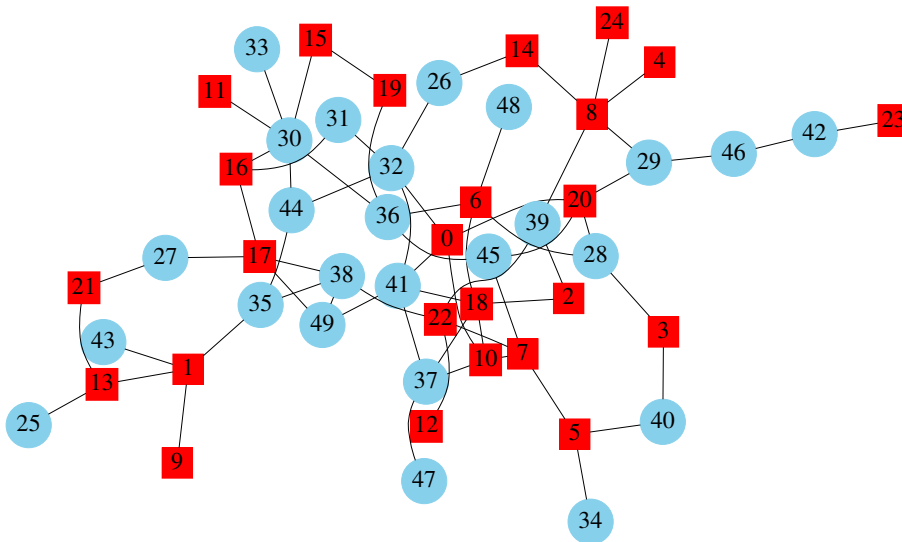
single line affects the proper working of the network, so, in this case, for the edge linking nodes m and n , we consider $P_{max}^{mn} = 2P_{max}$ and, for the rest of the edges, P_{max} is fixed, as it was before. This new capacity is applied to all edges of the original network, one at a time (always considering again the original network configuration before changing the capacity of a new line), for the sixteen distinct topologies.

5.3 Results and discussion

5.3.1 A fixed network topology

We start by analyzing how the decentralization of power generation, that is, how the distinct number of generators affects the proper function of the grid, while maintaining the same topology; that is, we just replace a generator by a consumer, for example, without changing any of the connections of the network. One out of the sixteen topologies with a fixed number of generators $N_G = 25$ and consumers $N_C = 25$ is considered in this section and can be seen in Figure 5.1.

Figure 5.1 - Original random network with $N = 50$ nodes, $N_G = 25$ generators (blue circle) and $N_C = 25$ consumers (red square).



Source: Author production.

Equation 3.37 gives a necessary condition for the synchronization of the system. As $\bar{P} = 0$ by definition, we have $P_{max}^* = \max|P_i|$ ¹, as m stands for all the consumers (C)

¹In the second order Kuramoto model considered in this chapter, we have $P_{max} = \frac{P_{max}}{g_m}$ in

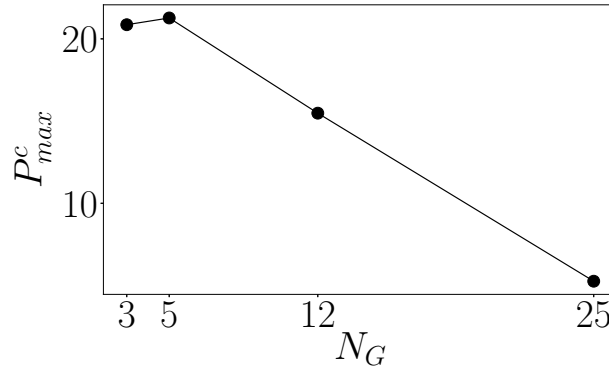
and generators (G). As $P_C = 1$ is fixed for all consumers, the value of P_{max}^* is defined by the value of the power generated P_G , given by Equation 5.4, which is equal to (when $N_G = N_C$) or greater than P_C (when $N_G < N_C$). So, the necessary condition for synchronization in our case depends only on the amount of the power generated by a single generator, the fewer the number of generators, the great is the power they have to provide and so the great is the value of P_{max}^* . We expect the critical coupling P_{max}^c (sufficient condition to achieve synchronization) to behave the same way, that is, to decrease with the increase of the number of generators (ROHDEN et al., 2012). This fact can be seen in Figure 5.2, where the topology presented in Figure 5.1 is considered and some generators are replaced at random by consumers. P_{max}^c is numerically calculated and plotted against the number of generators of the grid. One can see that the decentralization of the grid plays an important role on the synchronization of the network as the critical coupling decreases with the increase of the number of generators of the grid and we investigate further how this decentralization also affects the Braess's Paradox.

Considering the network presented Figure 5.1, with 25 generators and consumers, for the critical coupling $P_{max}^c = 5.26$, we plot the instantaneous frequency ν of all nodes as a function of time in Figure 5.3(a), where the consumers are plotted in red and the generators in blue, note that after a transient time, all nodes tend to the same value of ν . $P_{max}^c = 5.26$ is chosen because it is the minimum value for which the partial synchronization index S is equal to one (Figure 5.3(b)) and, therefore, it is the minimum power transfer capacity of the transmission lines for which the synchronous state exists. In Figure 5.3(c) the average instantaneous frequency of all nodes is plotted as a function of the coupling, note that they are all the same and equal to zero as the system enters the synchronous state.

Now, one new transmission line is added at a random position in this network (between nodes 38 (G) and 36 (G), the red edge in Figure 5.4). The system is then integrated again for the same value of coupling $P_{max}^c = 5.26$ and one can note that the synchronous state is lost in Figure 5.5(a), where the instantaneous frequency is plotted against time. Note that instead of a fixed null value, the instantaneous frequency of all nodes are divided into two branches and vary in time with two distinct means. The partial synchronization index for this configuration is $S = 0.78$ and the partial synchronization matrix, given by Equation 2.10, is represented in Figure 5.5(b), where the color yellow represents a low value of S and dark purple a high one. Note that a few nodes totally lose the synchronous state in relation to the

Equations 5.1 and 5.2, so, from Equation 3.37, $P_{max}^* = \max|P_i|$.

Figure 5.2 - Critical coupling P_{max}^c as a function of the number of generators for the power grid topology presented in Figure 5.1 with some generators being replaced at random by consumers.



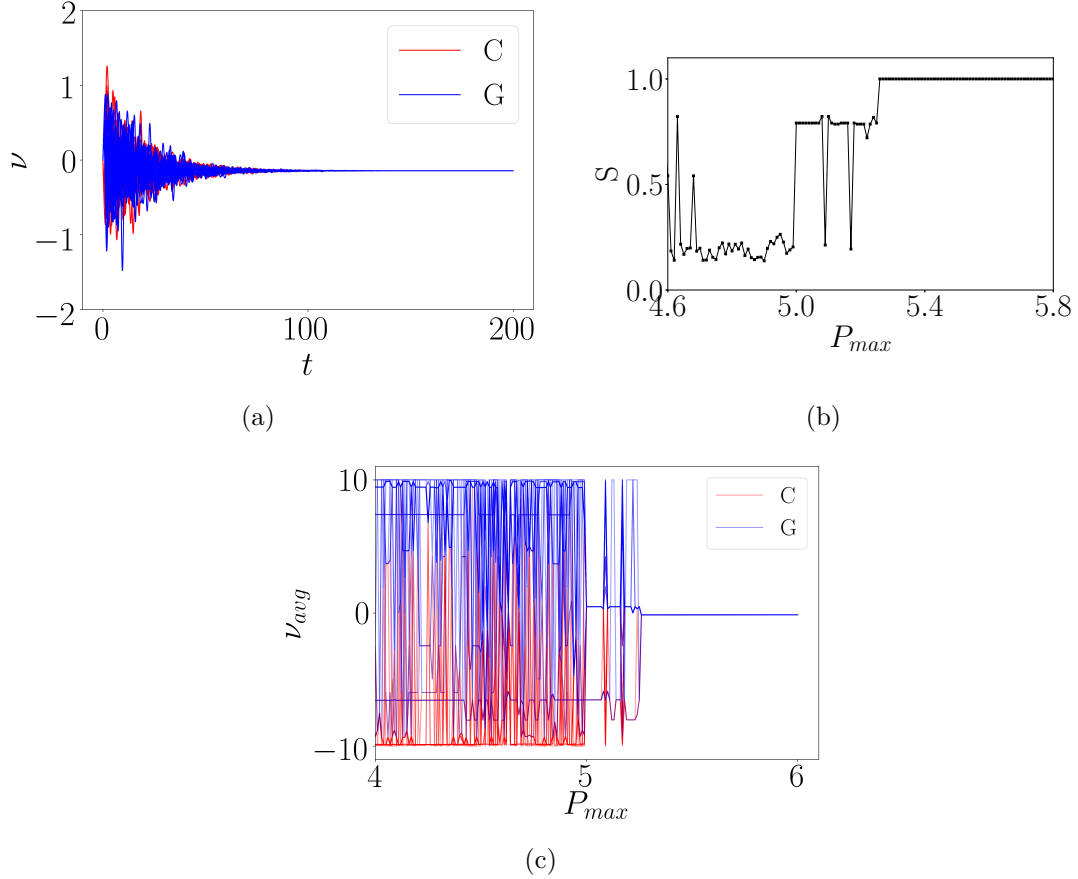
Source: Author production.

rest of the network (nodes 1,9,13,21,25,43) and none of them are the nodes connected by the new link nor are they one of their neighbors. In fact, these nodes are all part of a small group located at the lower left of the network and are depicted in black in Figure 5.5(c). This edge addition is then causing a nonlocal failure (WITTHAUT; TIMME, 2013). So, although the dynamical conditions for synchronization given by Equation 3.79 are satisfied, the synchronous state does not exist anymore due to a geometric frustration, defined in Equation 3.80. Therefore, in the case of this edge addition, the critical coupling P_{max}^c required for the existence of the phase locked state is increased.

We now calculate the partial synchronization index as a function of the coupling P_{max} for the following configurations: *Original*, the original random network (Figure 5.3). *Add*, the topology discussed in the previously, connecting nodes 36 (G) and 38 (G) (the red edge in Figure 5.4). *Remove*, where an edge is randomly removed from the original topology that disconnects nodes 0 (C) and 20 (C) (green dashed edge in Fig 5.4). *Double*, where an edge is selected at random and the power transmission capacity of this line is doubled (edge that connects nodes 1 (C) and 13 (C) and is depicted by the purple edge in Figure 5.4).

The results are shown in Figure 5.6(a). Note that the first one to synchronize is the original network (red), then the Double (green), Remove (black) and Add (blue) configurations, respectively. Against our intuition, the configuration in which one

Figure 5.3 - (a) Instantaneous frequency of all nodes as a function of time for the coupling fixed at $P_{max} = P_{max}^c = 5.26$, (b) partial synchronization index S and (c) average instantaneous frequency as a function of the coupling P_{max} for the original network topology.

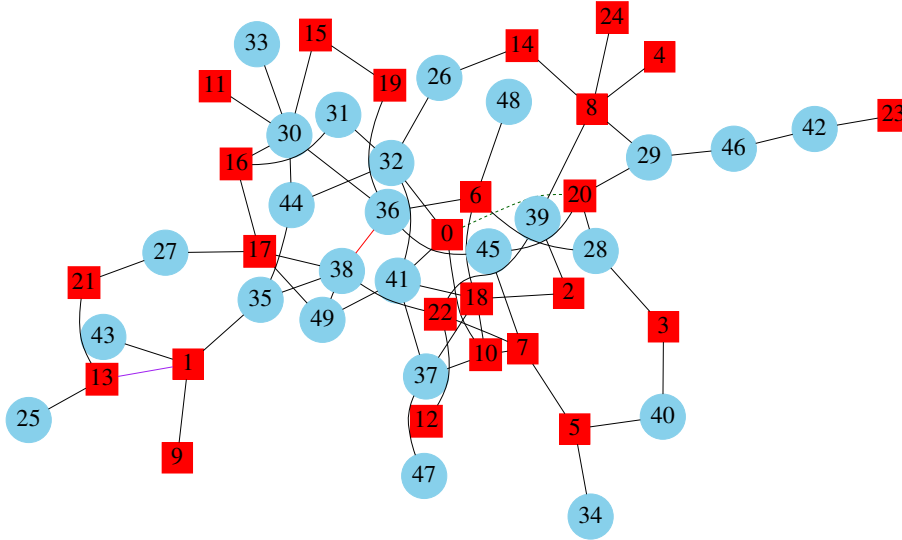


Source: Author production.

edge is added to the network requires the greatest critical coupling P_{max}^c to reach the synchronous state. This odd phenomenon called Braess's Paradox was first detected in traffic networks and an explanation for it is the redistribution of flows in the network which may induce an overload in some transmission lines which then leads to a loss of the synchronous state (WITTHAUT; TIMME, 2012).

We must make it clear that this increase of the critical coupling does not always occur, as can be seen in Figure 5.6(b), where the configurations are: *Original*, the original random network. *Add*, connecting nodes 2 (C) and 31 (G). *Remove*, disconnects nodes 1 (C) and 13 (C). *Double*, doubled the maximum transmission capacity of the line connecting nodes 0 (C) and 20 (C). Note that now, the Remove config-

Figure 5.4 - Original network (Figure 5.1) with a few changes: a new transmission line (red) connecting nodes 36 (G) and 38 (G), a removed transmission line (dashed green) disconnecting nodes 0 (C) and 20 (C) and a transmission line (purple) with doubled transmission capacity between nodes 1(C) and 13(C). Note that none of these changes are considered together.



Source: Author production.

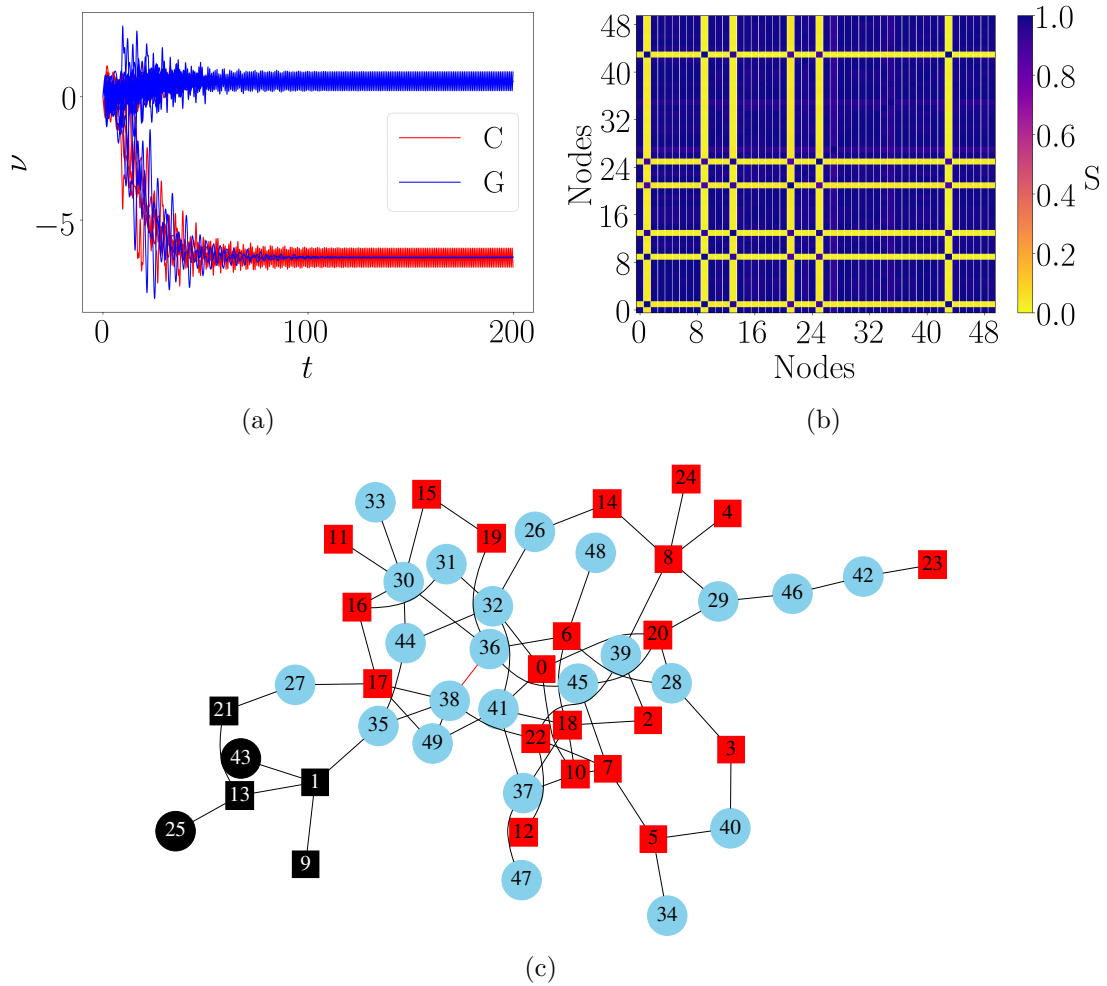
uration is the one to first reach synchronization, followed by the Add, Double and Original configurations, respectively. So all the topological changes made here favor synchronization when compared to the original network topology. One might wonder if there is a way to predict when a topological change will favor synchronization or not. From now on, we try to shed a light on this question.

5.3.2 Several network topologies

All the previous discussions were made only by using a single random network composed of 25 generators and 25 consumers. Now, sixteen different topologies are used, and each one of them goes from a centralized to a decentralized configuration. More specifically, we have sixteen distinct topologies with 3 generators, sixteen topologies with 5 generators, sixteen topologies with 12 generators and, finally, sixteen distinct topologies with 25 generators, giving a total of 64 network configurations. For each of these configurations, we randomly add edges, remove them and double the transmission line capacity, as explained in the Section 5.2.

We now check how these elementary changes affect the synchronous state of the system by calculating the fraction of edges that increases, decreases and leaves P_{max}^c

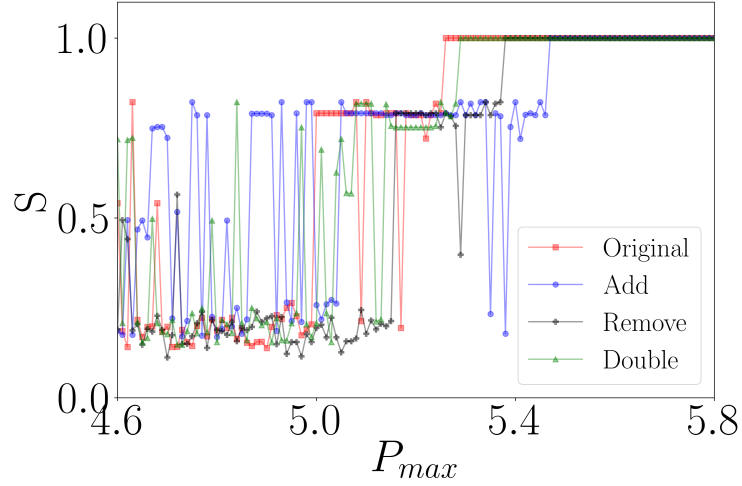
Figure 5.5 - (a) Instantaneous frequency as a function of time for the coupling fixed at $P_{max} = 5.26$, (b) partial synchronization index S_{mn} of all nodes, for a coupling also fixed at $P_{max} = 5.26$ for the network topology depicted in Figure 5.4 taking into account only the added edge (red) and (c) the same network topology but with the nodes that lost the synchronous state marked in black. The partial synchronization index for this configuration is $S = 0.78$.



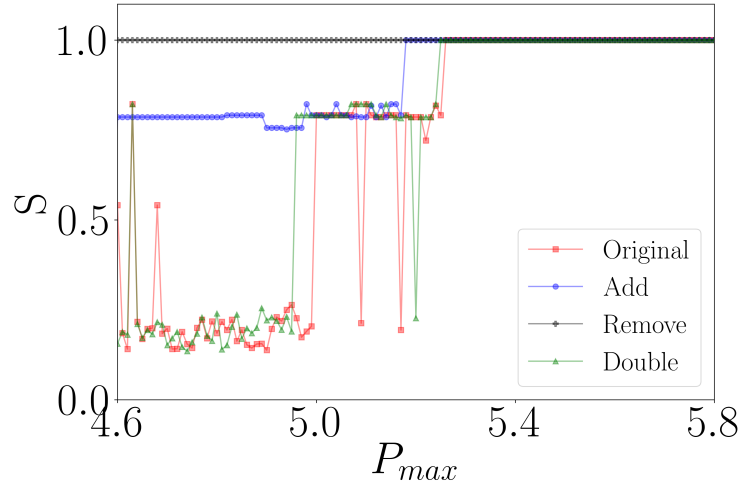
Source: Author production.

unchanged in relation to the addition (Add), removal (Remove) and increase of the maximum transmission capacity (Double). Reminding the reader that the increase in P_{max}^c leads the system to a desynchronized state. For the case of edge addition, for a fixed number of generators, 50 new edges are added (remember that one edge is added, P_{max}^c is calculated, then the original network topology is considered again so a new edge is added and the process is repeated) to each of the sixteen network topologies, giving a total of $N_{edge} = 800$ new added edges. Then, for each of these

Figure 5.6 - Partial synchronization index S as a function of coupling P_{max} for network configurations that present an advantage and disadvantage into reaching the synchronous state when compared to the original network topology. In (a) all the topology modifications leads the system out of the synchronous state, while in (b), all the modifications performed improve the synchronization of the system as a lower coupling is required to reach this state.



(a) Add: connected nodes 36 (G) and 38 (G). Remove disconnected nodes 0 (C) and 20 (C). Double: doubled the transmission capacity of the line connecting nodes 1 (C) and 13 (C).



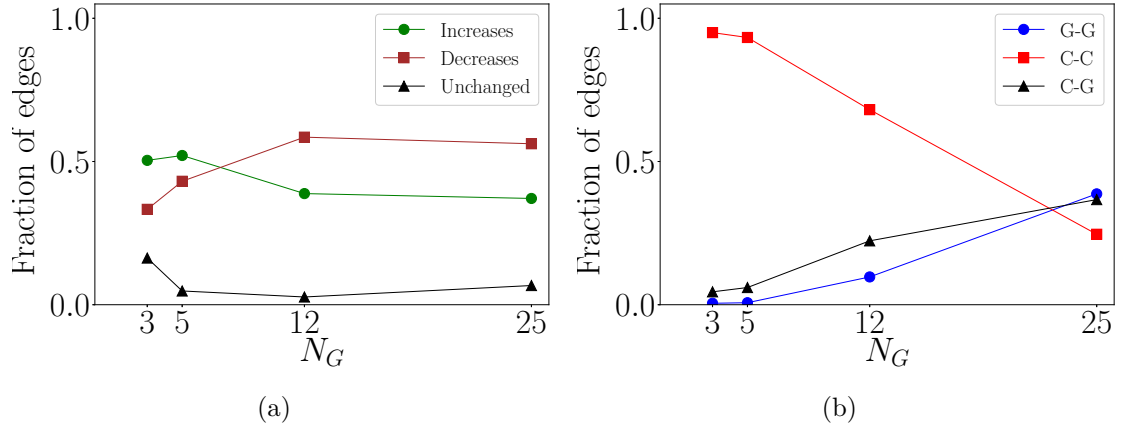
(b) Add: connected nodes 2 (C) and 31 (G). Remove disconnected nodes 1 (C) and 13 (C). Double: doubled the transmission capacity of the line connecting nodes 0 (C) and 20 (C).

Source: Author production.

modified configurations with one additional edge, we compute how many times have the value of P_{max}^c increased N_{inc} , decreased N_{dec} and remained unchanged N_{unc} . The

fraction of edges is then given by N_{inc} , N_{dec} and N_{unc} divided by N_{edge} , which are plotted in Figure 5.7(a) in green, brown and black, respectively. A similar procedure is done for the Remove and the Double situations and are plotted in Figures 5.8(a) and 5.9(a), respectively.

Figure 5.7 - (a) Fraction of edges that increases (green), decreases (brown) and does not change (black) the value of P_{max}^c as a function of the number of generators of the network when one new edge is added at a random position in all of the sixteen topologies. (b) Fraction of edges that connect a generator to another generator (blue), a consumer to a consumer (red) and a consumer to a generator (black), only in relation to those who increase P_{max}^c .

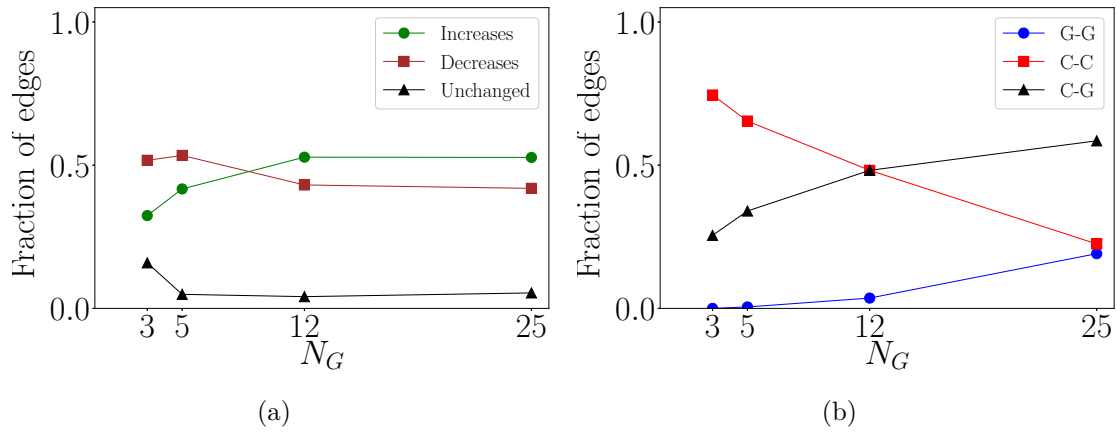


Source: Author production.

In relation to the Add situation, Figure 5.7(a), most of the edge addition results in an increase of P_{max}^c when centralized networks are being considered ($N_G = 3$ and 5). With the increase of the number of generators, most of the edges added result in a decrease of P_{max}^c . As expected, the Remove approach, Figure 5.8(a), shows an inverse situation as most of the edges removed from the networks decreases P_{max}^c for a centralized configuration and increases P_{max}^c for a decentralized configuration. In relation to the Double set up, Figure 5.9(a) shows that most of the edges selected that have their maximum capacity doubled do not change the value of P_{max}^c for the most centralized configuration ($N_G = 3$) and decreases P_{max}^c as the topology becomes decentralized, although the difference between the fractions that decreases, increases and leaves the the critical coupling unchanged is very low in these two scenarios, in comparison to the two previous analysis. Note that the level of centralization of energy generation plays a very important role here, as it dictates which is the most probable scenario that can take place after a simple change in the topology, like

adding or removing a single transmission line of the network.

Figure 5.8 - (a) Fraction of edges that increases (green), decreases (brown) and does not change (black) the value of P_{max}^c as a function of the number of generators of the network when an edge is removed at a random position in all of the sixteen topologies. (b) Fraction of edges that connect a generator to another generator (blue), a consumer to a consumer (red) and a consumer to a generator (black), only in relation to those who increase P_{max}^c .



Source: Author production.

In all of the three situations presented here (*Add*, *Remove* and *Double*) one can note that the system leaves the synchronous state between 29% to 53% of the times, which is something our intuition can not predict, so, one must be very careful when making topological changes to a functional energy transmission network.

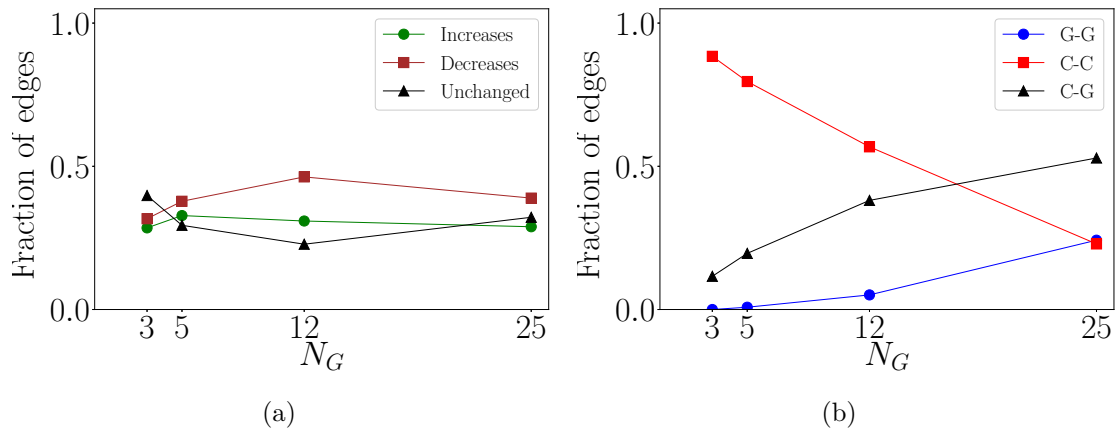
Now that we know that adding, removing or increasing the transmission capacity of edges can cause failures in a power grid with, in some cases, a relatively high probability, we ask the following: which nodes are these edges connecting? Does it make any difference if one adds a new edge connecting two consumers or two generators when it comes to maintaining the synchronous state? To answer these questions, we take into consideration now only the fraction of edges that increase P_{max}^c but analyze which pair of nodes are these edges connecting. Our results are presented in Figures 5.7(b), 5.8(b) and 5.9(b) for the *Add*, *Remove* and *Double* situations, respectively.

The results show that for a relatively low number of generators in the network, in all the three situations, the great part of the fraction of edges that destroys the

synchronous state are caused by edges connecting two consumers (plotted in red). When a random centralized network is being considered, it is a fact that most of the connections are between two consumers, since they are the majority of the nodes, so it is expected to have a higher fraction of edges that cause failures by connecting them, but it is still a valuable information since most power grids are still centralized.

On the other hand, when a decentralized network is being considered, the results differ for the three scenarios. In the *Add* one, new connections between two generators (plotted in blue) and between a consumer and a generator (plotted in black) cause trouble more often. By far, the connection whose removal is the most dangerous is the one linking a consumer to a generator and increasing the transmission capacity of this same kind of connection may also not be an appropriate engineering operation.

Figure 5.9 - (a) Fraction of edges that increases (green), decreases (brown) and does not change (black) the value of P_{max}^c as a function of the number of generators of the network when the maximum transmission capacity of an edge is doubled at a random position in all of the sixteen topologies. (b) Fraction of edges that connect a generator to another generator (blue), a consumer to a consumer (red) and a consumer to a generator (black), only in relation to those who increase P_{max}^c .



Source: Author production.

5.4 Conclusion

In this chapter, we have shown that very simple changes in the network topology can cause failures and lead the system out of the synchronous state which is crucial for

the power grid to work properly. When adding, removing or increasing the capacity of a transmission line, one changes the flux of the power transmitted in the network and this change may induce nonlocal failures due to overloads on some transmission lines. The most probable scenario to what happens when these elementary changes in transmission networks are made depends on the level of centralization of the power generated in the network and also on the nature of the nodes being connected by the edge in question.

When considering a centralized power grid, that is, one grid whose power is supplied by just a few generators, one must be very careful when contemplating a change between two consumers, being an addition, removal or increase in the transmission capacity of the transmission line connecting them, as there is a considerable probability that this change may cause a failure in the network. In the decentralized power grid, the modification that cause most of the failures in the grid is between a consumer and a generator when the removal or increase in the transmission capacity is being considered.

It would be of extreme importance to analyze carefully the effects of elementary changes in real-world power grids before actually making them as these changes can reduce the stability and also cause failures which may generate great economic costs.

We wish to emphasize that this is a first approach to this problem and, as for future work, a more complex model should be used instead of Equations 5.1 and 5.2, for example, a model that includes admittance (NISHIKAWA; MOTTER, 2015).

6 HOW HETEROGENEITY IN CONNECTIONS AND CYCLES MATTER FOR SYNCHRONIZATION OF COMPLEX NETWORKS

In this chapter, we present our original contribution published in the journal **Chaos: An Interdisciplinary Journal of Nonlinear Science** with the title *How Heterogeneity In Connections And Cycles Matter For Synchronization Of Complex Networks*, (LACERDA et al., 2021b). This paper can be found on Appendix D.

An introduction is presented in Section 6.1, in Section 6.2 we refer to the models and methods already presented in this work, the results and discussions are shown in Section 6.3 and, finally, the final remarks are made in Section 6.4.

6.1 Introduction

Biological and social studies have shown that in some situations, like when it comes to choosing friends, people prefer to gather with similar minded ones (PARKINSON et al., 2018; URBERG et al., 1998; KUPERSMIDT et al., 1995; HASELAGER et al., 1998). On the other hand, when it comes to mating preferences some species prefer to mate with dissimilar ones, which may provide the offspring with good genes (PENN; POTTS, 1999; JORDAN; BRUFORD, 1998; BERNATCHEZ; LANDRY, 2003; PIERTNEY; OLIVER, 2006). We can refer to the former behavior as *Similar* (\mathcal{S}), and to the latter as *Dissimilar* (\mathcal{D}) neighborhood patterns. If an ensemble presents no strong bias towards any of these extremes, it is called *Neutral* (\mathcal{N}) (FREITAS et al., 2015).

In this work, we explore the idea of Similarity and Dissimilarity described above by means of the structure properties and synchronization of complex networks of Kuramoto non-identical phase oscillators. In order to quantify these patterns, we use a measure related to classical *dissonance* (PIKOVSKY et al., 2003; FREITAS et al., 2015), which measures the difference of the natural frequencies of a pair of oscillators.

In reference to related material on synchronization of complex networks, Pinto et al. (PINTO; SAA, 2015) employs a dimensional reduction approach proposed by (GOTTWALD, 2015) and derive a sufficient analytical condition, considering an ansatz, to optimize a topology of a network in order to favor synchronization using the Kuramoto model. They also showed that when this method is applied to a network with random natural frequencies, the final topology presents a negative correlation between the natural frequencies of adjacent vertices in a way that we can call a network with a Dissimilar pattern. Even though, the approach in (PINTO; SAA, 2015) does not exhaust the problem, especially for small and intermediate coupling

values, which are commonly found in nature (PIKOVSKY et al., 2003). A numerical study made by Freitas et al. (FREITAS et al., 2015) showed that Similar patterns favor weaker forms of synchronization but Dissimilar ones exhibit explosive synchronization, reaching global synchronization faster than the Similar pattern. (SCAFUTI et al., 2015b) use an evolutionary strategy to find a minimal network structure that guarantees global synchronization and show that the heterogeneity in the nodes' natural frequency is the driving force that determines the evolution of the network structure.

We intend to extend the work done by (FREITAS et al., 2015) and add the complex network measures assortativity and clustering coefficient to investigate how the structure of complex networks influences the synchronization of Similar, Dissimilar and Neutral patterns of natural frequencies of oscillators. Assortativity is employed in order to measure how connections between nodes with the same degree influence the emergence of synchronization, while the clustering coefficient measures the impact of loops of size three (small cycles). Therefore, the topology of the networks is dictated by the assortativity and by the clustering coefficient values, while the natural frequency of their nodes are given by the dissonance patterns.

The authors in (PLUCHINO et al., 2005; PLUCHINO et al., 2006) used a modified version of the Kuramoto model in order to study opinion formation and its dynamics through synchronization of complex networks where the phase of a node in this model represents the opinion of an individual, its natural frequency represents the natural opinion changing rate (the tendency of each individual to change its opinion) and the coupling represents the amount of the interaction among them. To illustrate the meaning of the metrics used here, the natural frequency patterns and the synchronization of the network, let us take as an example a large group of individuals having an argument about a polemic subject where each individual has its own opinion changing rate and, due to the number of people involved and the limited time they have, they can only communicate with a limited number of people inside this group. Their discussion ends only when all participants come to an agreement and so reach a common opinion.

We can model this situation by using a complex network approach where each individual is represented by a node whose behavior is dictated by a dynamical system model, the interaction between them is represented by an edge. As so, reaching a common opinion is associated with a synchronized state. The natural frequency patterns Similar, Dissimilar and Neutral here relate to the level of homogeneity

(Similar) or heterogeneity (Dissimilar) of the opinion changing rate of communicating individuals, as, for example, if the individuals only communicate with similar minded ones, the Similar pattern is used to model this dynamics. We also refer the reader to Noorazar et al. (NOORAZAR, 2020) and Deffuant et. al. (DEFFUANT et al., 2001) for a more detailed discussion on opinion dynamics.

The rules of who can communicate with whom are given by the metrics assortativity and clustering coefficient. If individuals who interact with a lot of people prefer to communicate with the ones that are also popular and individuals who interact with a few people prefer to communicate with ones that are also less popular, the network is said to be assortative and has a high value of the metric assortativity. The opposite can also happen, when popular individuals tend to talk with less popular ones the network is said to be disassortative. Looking at another aspect of the rules of communication within this group of people, we can also allow two contacts of a person to talk to each other, forming then a small cycle or a loop of size three in the network topology. When there is a high number of two contacts of the same individuals communicating to each other, we say that this network presents a high clustering coefficient and, on the other hand, it presents a low clustering coefficient if the opposite happens.

In this scenario, one can ask the following: how strong the interactions (represented here by the coupling of the Kuramoto model) between individuals must be in order to reach an agreement? Is it easier to be achieved if individuals only communicate with similar minded ones or is it the opposite? Is it easier if popular individuals only talk to each other or when they talk to less popular ones? Or if contacts of individuals communicate with each other?

Our results show that the Similar pattern of natural frequency distribution favors weaker forms of synchronization but, as we increase the coupling constant, the Dissimilar pattern is the first to reach the synchronized state, agreeing with (FREITAS et al., 2015). The Erdős-Rényi model presented itself as the easiest to reach the phase locking state when compared to Watts-Strogatz and Barabási-Albert network models. In relation to the network metrics assortativity and clustering coefficient, one can see that low values of both metrics favors the reaching of a synchronized state. As for the questions raised about the best strategy to conduct an argument among a group of people, we find that the best strategy would be to encourage individuals with distinct opinion changing rates to communicate to each other and, at the same time, encourage popular individuals to talk to less popular ones and discour-

age the interaction among contacts of individuals in order to avoid small cycles of interactions.

6.2 Models and methods

In this work, we consider complex networks of Kuramoto phase oscillators whose dynamics is described by the first order Kuramoto model (Equation 2.5). The models of complex networks analyzed here are Erdős-Rényi (ER) (ERDÖS; RÉNYI, 1959), Watts-Strogatz (WS) (WATTS; STROGATZ, 1998) and Barabási-Albert (BA) (BARABÁSI; ALBERT, 1999) as they are widely used in the literature (ARENAS et al., 2008; COSTA et al., 2007). For the ER model we set the probability of edge creation is 0.15, and for the WS networks the probability of rewriting each edge is 0.2. The number of nodes is fixed as $N = 50$, due to computational costs.

6.2.1 Total dissonance

In order to characterize the Similar, Dissimilar and Neutral natural frequency patterns on complex networks, we make use of the total dissonance measure (FREITAS et al., 2015)

$$V = \frac{1}{N} \sqrt{\sum_{i,j=1}^N A_{ij} (\omega_i - \omega_j)^2}. \quad (6.1)$$

For the Similar pattern, the natural frequencies of adjacent nodes are close to each other such that, the value of V is small and it is zero only if all oscillators have identical natural frequencies. If the natural frequencies of adjacent nodes are very different from each other, that is, Dissimilar pattern, the value of V is higher. The Neutral pattern is characterized as intermediate values of V . To calculate these frequency patterns, the stochastic optimization algorithm called Simulated Annealing (LAARHOVEN; AARTS, 1987) is used. In order to optimize the objective function V , this method makes permutations of the natural frequencies set until it finds an optimal local value of the objective function, in correspondence with the desired Similar or Dissimilar patterns. Considering the outputs of this algorithm, the minimization of V corresponds to the Similar pattern, the maximization to the Dissimilar one and the random initial natural frequency set is called Neutral. In practice, for each network topology considered in this work, a set of natural frequencies is chosen from a random uniform distribution in $[-\pi, \pi]$ and the total dissonance ν_{ini} is calculated, this one is called the Neutral frequency pattern. Then an optimization algorithm is applied in order to maximize (ν_{max}) and minimize (ν_{min}) the total dissonance of each network, giving rise to the Dissimilar and Similar patterns, respectively.

6.2.2 Assortativity and clustering coefficient

Our aim is to analyze how network structure influences the emergency of synchronization on complex networks. For this purpose, the network measures called assortativity and clustering coefficient are used in order to select distinct network topologies in each of the three models (ER, WS, BA).

Assortativity measures the similarity of connections in a network with respect to a certain characteristics of a node. In this work, the assortativity is determined by the degree of the nodes and it is given by the use of the Pearson correlation coefficient (NEWMAN, 2003a; NOLDUS; MIEGHEM, 2015)

$$\rho = \frac{\sum_{ij} ij(f_{ij} - a_i b_j)}{\sigma_a \sigma_b}, \quad (6.2)$$

where a_i and b_j are the fraction of edges that start and end at nodes with degree values i and j , respectively, f_{ij} is the fraction of edges between nodes of degree i and j , σ_a and σ_b are the standard deviations of the distributions a and b , respectively. a_i , b_j and f_{ij} satisfy the sum rules

$$\begin{aligned} \sum_{ij} f_{ij} &= 1, \\ \sum_j f_{ij} &= a_i, \\ \sum_i f_{ij} &= b_j. \end{aligned} \quad (6.3)$$

The graph assortativity $\rho \in [-1, 1]$ represents how nodes in a network associate with each other, that is, it shows whether nodes prefer to connect to nodes of the same sort or of opposing sort. When, on average, high degree nodes connect to high degree ones or low degree nodes connect to low degree ones, ρ is close to 1 and the network is said to be *assortative*. On the other hand, if on average high degree nodes connect to low degree ones, ρ is close to -1 and the network is said to be *disassortative*. If ρ is close to 0, the connections are considered to be completely random (NOLDUS; MIEGHEM, 2015). The reader should notice that there are two different mechanisms of preferential attachment here: assortativity takes into account only the node degree, while neighborhood patterns consider both graph structure and node's natural frequency.

Another basic network measure that is used in this work is the *clustering coefficient*, which measures the presence of loops of size three inside a network, that is, it

measures the tendency of two neighbours of a certain vertex to also be connected to each other. In a real world network it can be seen as the likelihood of friends of a certain person also to be friends of each other (WASSERMAN; FAUST, 1994). The clustering coefficient of a node i is given by

$$c_i = \frac{2Tr_i}{g_i(g_i - 1)}, \quad (6.4)$$

where Tr_i is the number of triangles involving node i and g_i is the degree of node i . So, the clustering of a node $c_i \in [0, 1]$ is the number of triangles that pass through that node normalized by the maximum number of such triangles, in a way that if none of the neighbours of node i are connected to each other $c_i = 0$ and $c_i = 1$ if all neighbours are connected (SARAMÄKI et al., 2007). The average clustering coefficient of the network composed of N nodes is given by

$$C = \frac{1}{N} \sum_{i=1}^N c_i. \quad (6.5)$$

A large clustering coefficient indicates that there are many redundant paths in the network and a low clustering indicates the opposite.

6.2.3 Generating network configurations

The main contribution of this work is to analyze the impact on synchronization considering the assortativity and clustering coefficients in association with neighborhood patterns in terms of total the dissonance ($\mathcal{S}/\mathcal{N}/\mathcal{D}$). To do so, we proceed as follows.

Network configurations considered here are represented by the pair (A, ω) , where A stands for the adjacency matrix of the network and ω is the set of natural frequencies. For each network model (BA, ER, WS), three corresponding network topologies are considered that present low $A^{\rho_{min}}$, intermediate $A^{\rho_{middle}}$ and high $A^{\rho_{max}}$ values of assortativity and three that present low $A^{C_{min}}$, intermediate $A^{C_{middle}}$ and high $A^{C_{max}}$ values of clustering and, also, three patterns of the distribution of natural frequencies are considered: Neutral $\omega^{\mathcal{N}}$, Similar $\omega^{\mathcal{S}}$ and Dissimilar $\omega^{\mathcal{D}}$. In all, 27 configurations are studied for assortativity and 27 for the clustering coefficient. As an example, consider a BA network with low value of assortativity $A^{\rho_{min}}$. For this network, a random set of natural frequencies is generated from a uniform distribution (Neutral dissonance pattern), giving rise to the Configuration $(A^{\rho_{min}}, \omega^{\mathcal{N}})$. Then the Simulated Annealing algorithm is used to optimize the values of the total dissonance with a low value giving rise to the set of natural frequencies of the Similar pattern

and the configuration $(A^{\rho_{min}}, \omega^S)$ and a high value generating the set of natural frequencies of the Dissimilar pattern and the Configuration $(A^{\rho_{min}}, \omega^D)$. Recall that dissonance patterns do not alter the physical configuration of networks, it only interchanges the natural frequencies. The distinct assortativity/clustering values are the only ones that come from a different network configuration. The choosing of $A^{\rho_{min}}$, $A^{\rho_{middle}}$ and $A^{\rho_{max}}$ is discussed in the next session.

In order to measure how the total dissonance combined with assortativity and clustering coefficients affect the global synchronization of the networks, the Kuramoto model (Equation 2.5) is numerically integrated and the mean value of the order parameter is calculated $R(t)$ over the integration time and is denoted by $\langle R \rangle$. We call $\langle R \rangle_{PL}$ and λ_{PL} the values of the order parameter and the coupling constant, respectively, at the emergence of synchronization, that is, phase locking ($S = 1$). The initial conditions are the same for all networks used in this work and were all set as $\theta_i(0) = 0.5$ for $i = 1, \dots, N$, where N is the total number of nodes. This choice was intentional because as shown in previous works (LACERDA et al., 2019), the set of initial conditions can also play an important role in the synchronization of the system, but this is not the scope of this work. The distribution of the natural frequencies for the Neutral patterns are drawn randomly by a uniform distribution over $[-\pi, \pi]$.

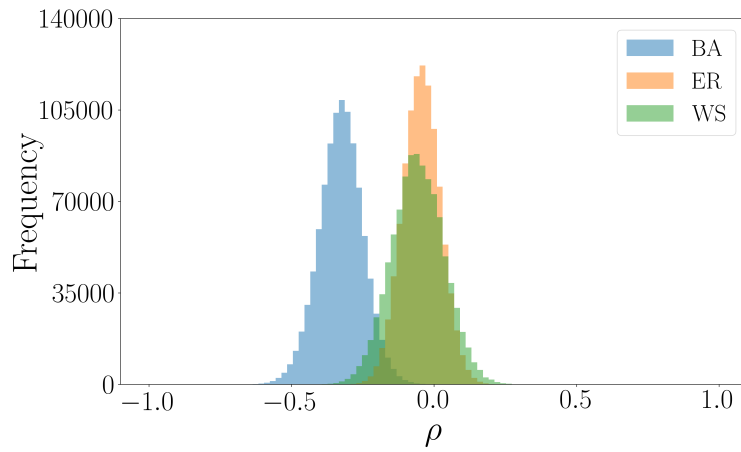
6.3 Results and discussion

ER, WS, and BA topology models are used in this work. Each of them has a specific topology and in order to obtain networks with low and high values of assortativity and clustering coefficient, we chose to create one million networks of each type and pick three of each model which present lowest, intermediate and highest values of the measures being considered. In this way, we make sure to keep the topology of the network models.

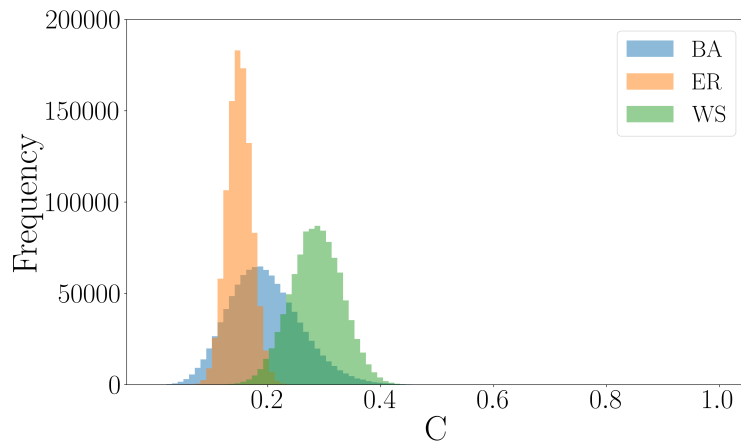
The histograms of all networks generated as a function of assortativity and clustering coefficients can be seen in Figure 6.1. By construction, the BA model has a preferential attachment rule when building the network, so the probability of a new node to connect with an existing one is proportional to the existing node degree. Therefore, these networks are characterized by having a few nodes highly connected (called *hubs*) and the rest of the nodes with few connections. It is by construction a network with a negative value of assortativity where nodes with low degree tend to connect to the ones with high degree. On the other hand, ER and WS do not have a preferential attachment rule and the nodes have a rather random pattern

of connections. So the average assortativity is expected to be around zero. When it comes to clustering coefficient, the WS model is the one expected, in average, to have the higher number of loops of size three as it is constructed by rewriting some edges of a regular network, that are known to have high clustering coefficient (COSTA et al., 2007; SARAMÄKI et al., 2007; NOLDUS; MIEGHEM, 2015).

Figure 6.1 - Histograms of Erdős-Rényi (orange), Watts-Strogatz (green) and Barabási-Albert (blue) networks in relation to (a) assortativity (ρ) and (b) clustering coefficient (C). One million networks were generated to compute each histogram.



(a)



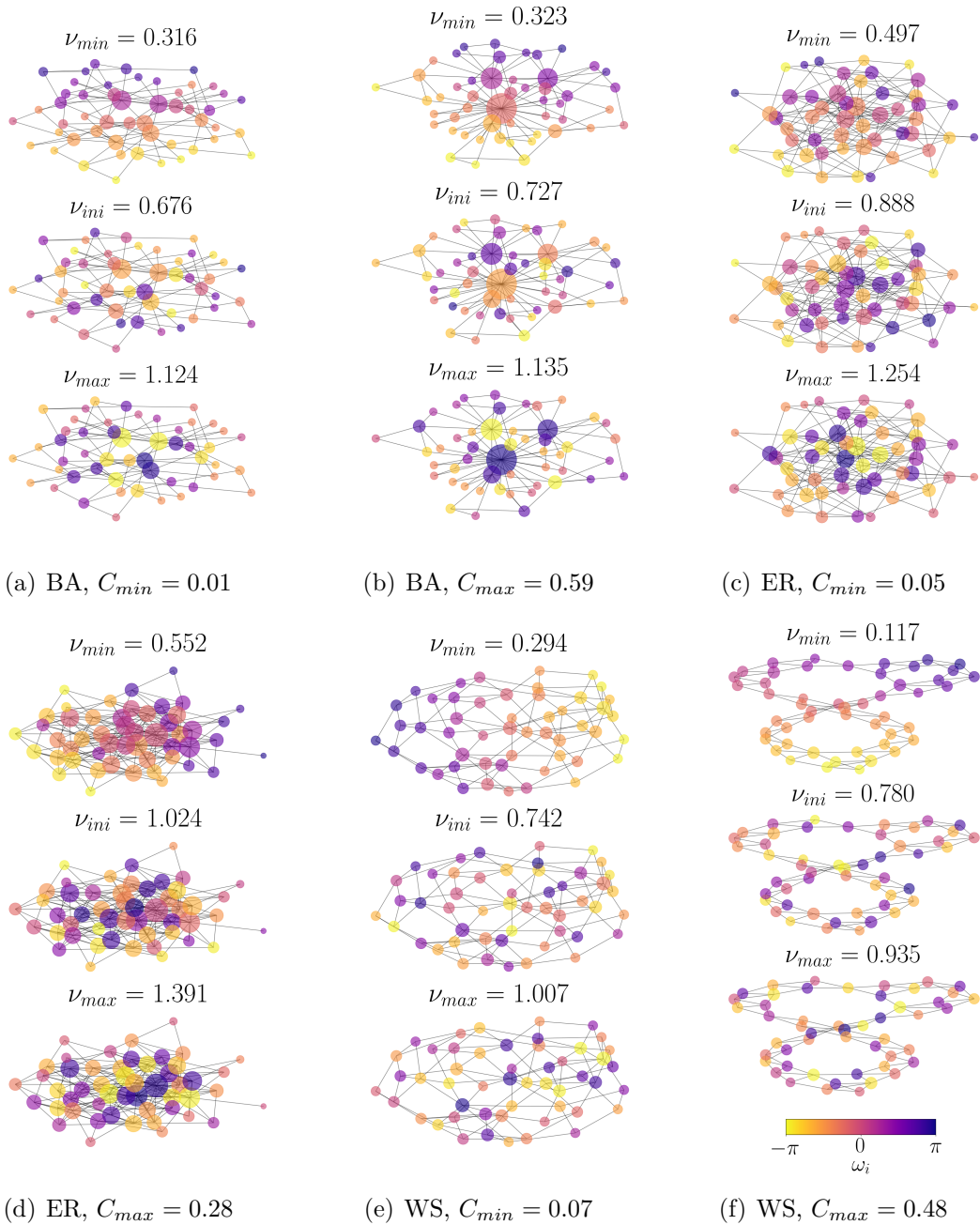
(b)

Source: Author production.

We then pick the extreme values of ρ and C from the histogram in Figure 6.1 and a value approximately in the middle of them to be the ρ_{middle} and C_{middle} . So we have: BA model with $\rho_{min} = -0.7354$, $\rho_{middle} = -0.2898$, $\rho_{max} = 0.1034$; ER model with $\rho_{min} = -0.3560$, $\rho_{middle} = -0.0505$, $\rho_{max} = 0.2584$; WS model with $\rho_{min} = -0.5079$, $\rho_{middle} = -0.0515$, $\rho_{max} = 0.4032$.

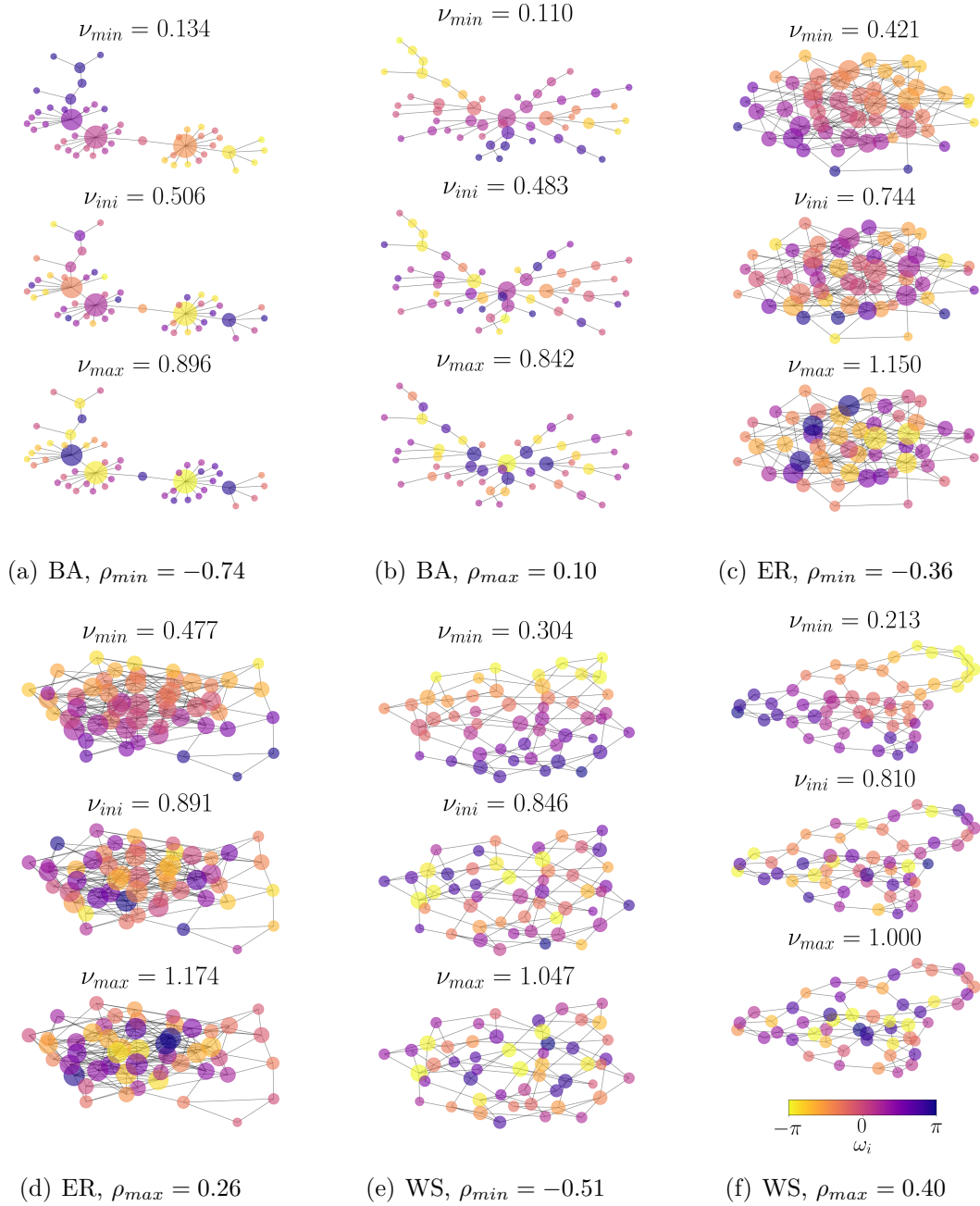
The topologies related to the minimum and maximum values of ρ and C , along with the three dissonance patterns (\mathcal{N} , \mathcal{S} , \mathcal{D}) can be seen on Figures 6.2 and 6.3. One can notice that for the Similar pattern, nodes tend to be connected to ones that have similar natural frequency (similar node color) and that for the Dissimilar pattern they tend to be connected with nodes with different natural frequencies. This is expected, so we can confirm that our optimization algorithm is working (the algorithm used to generate these patterns converges to a local, not global, value of the objective function that it is trying to maximize/minimize). The Neutral pattern stays in the middle as some nodes connect with nodes with similar frequencies and some connect with nodes with dissimilar frequencies. Recall that that dissonance patterns do not alter the physical configuration of the networks, it only interchanges the natural frequencies. The low and high assortativity/clustering values are the only ones that come from a different network configuration.

Figure 6.2 - (a)-(b) BA, (c)-(d) ER and (e)-(f) WS networks with low and high values of clustering coefficient C . The Similar $\mathcal{S}(\nu_{min})$, Neutral $\mathcal{N}(\nu_{ini})$ and Dissimilar $\mathcal{D}(\nu_{max})$ patterns of dissonance ν are also showed for each network (from top to bottom, respectively). ω_i is the natural frequency of the nodes and the size of the nodes is proportional to the degree.



Source: Author production.

Figure 6.3 - (a)-(b) BA, (c)-(d) ER and (e)-(f) WS networks with low and high values of assortativity ρ . The Similar \mathcal{S} (ν_{min}), Neutral \mathcal{N} (ν_{ini}) and Dissimilar \mathcal{D} (ν_{max}) patterns of dissonance ν are also showed for each network (from top to bottom, respectively). ω_i is the natural frequency of the nodes and the size of the nodes is proportional to the degree.



Source: Author production.

The mean of the order parameter $\langle R \rangle$ and the total partial synchronization index S as a function of the overall coupling for networks with high and low values of assortativity and clustering coefficient and all three dissonance patterns for the BA, ER and WS models are presented in Figures 6.4 and 6.5, respectively.

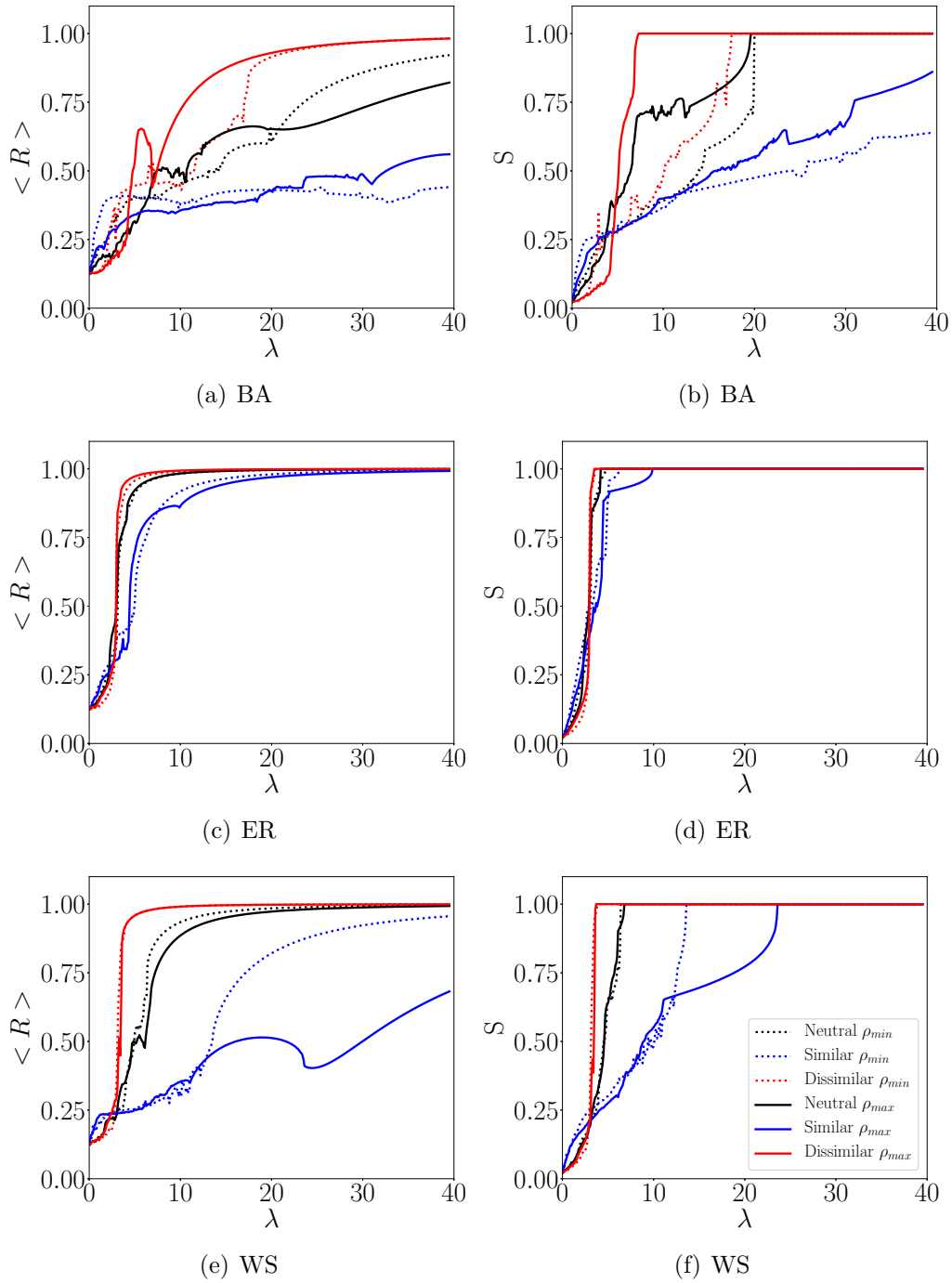
In relation to the patterns Similar, Neutral and Dissimilar, one can note that, for small coupling, the Similar pattern favors weaker forms of synchronization both to a phase locked state (higher value of S) and to phase synchronized state (higher value of $\langle R \rangle$) for the BA, ER and WS models, since the growth of these measures are more protuberant at first, for small values of coupling. The dissimilar pattern appears to be the harder to achieve synchronization, while the Neutral one stays in the middle. As the coupling λ is increased, the Dissimilar pattern presents a higher growth on both $\langle R \rangle$ and S and is the first of the patterns to reach the synchronous state. As the coupling increases even more, it is time of the Neutral pattern to reach the phase locking state and then, for greater λ , the Similar pattern also synchronizes. So, the Dissimilar natural frequency distribution pattern is the one that mostly favors the achievement of the synchronized state. This behaviour was also observed by Freitas et al. (FREITAS et al., 2015) and Scafuti et al. (SCAFUTI et al., 2015b).

In relation to the illustrative example given at the beginning of the paper about the discussion of a polemic subject, we can conclude that if mostly similar minded people talk to each other, an agreement seems to be close by people making only a small effort but at some point the discussion somehow does not advance anymore and more effort is needed in order to reach an agreement. On the other hand, when people tend to talk with the ones that have distinct opinion changing rate, there is a huge discussion at first and, despite the increasing effort of all individuals, it seems like an agreement is not reachable but, after more effort is made by the individuals, a common opinion can finally be reached and all individuals arrive at the same conclusion.

Now, we investigate how the measures assortativity and clustering coefficient along with the dissonance patterns affect synchronization. In order to do this, we annotate the value of λ for which all configurations in Figures 6.4 and 6.5 reach phase locking (λ_{PL}). This result is presented on the first column in Figures 6.6 (related to assortativity) and 6.7 (related to clustering). On the second column there is the value of the order parameter (R_{PL}) for this λ_{PL} . The order parameter R_{PL} represents the amount of phase synchronization of the system at this phase locking state. By definition, the partial synchronization index S at $\lambda = \lambda_{PL}$ is equal to one, so the

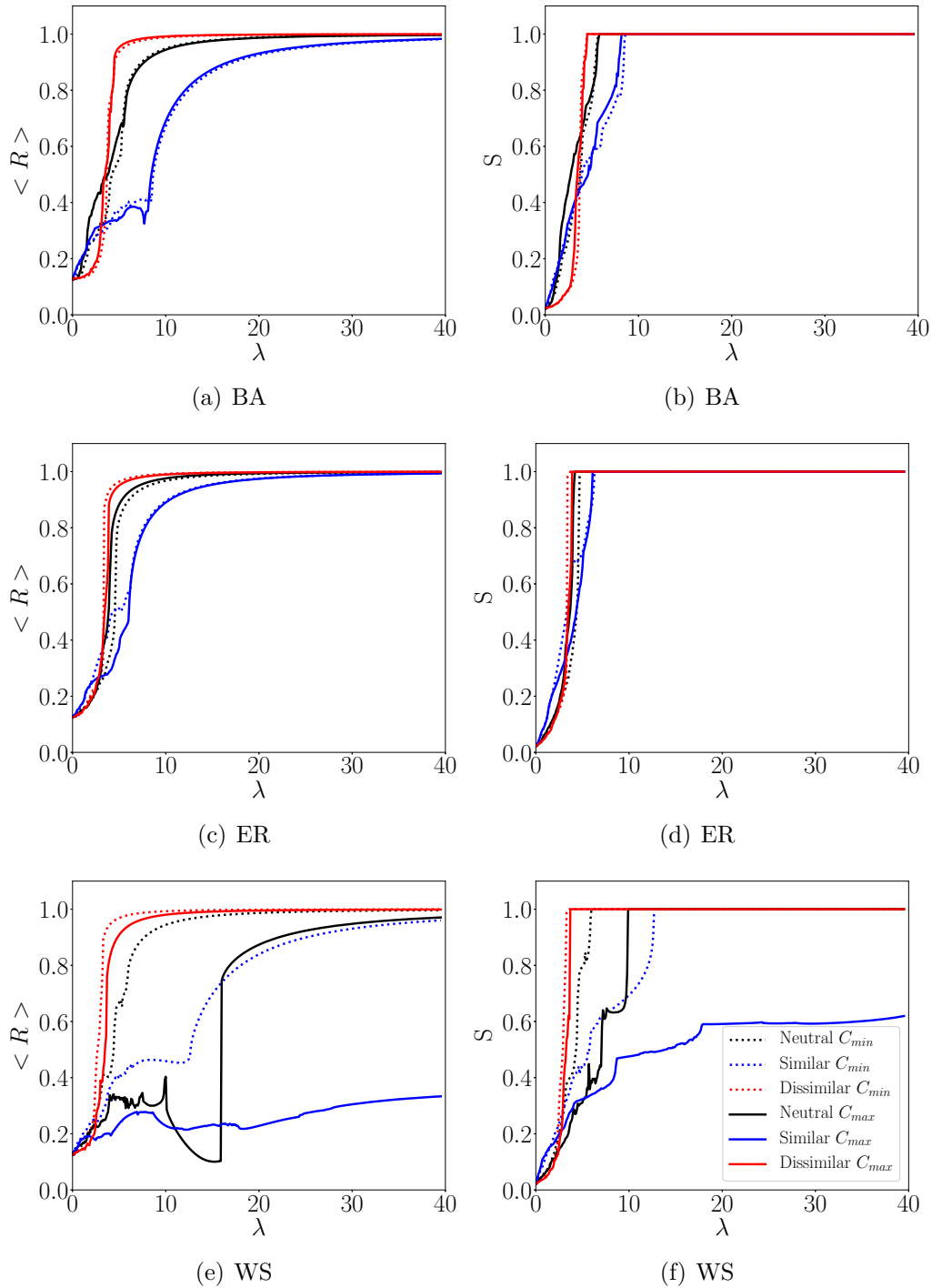
system is synchronized.

Figure 6.4 - (a-c) Mean of the order parameter $\langle R \rangle$ and (d-f) the total partial synchronization index S as a function of the coupling for networks with low (dashed line) and high (continuous line) values of assortativity ρ and patterns Neutral (black), Similar (blue) and Dissimilar (red) of natural frequency distribution.



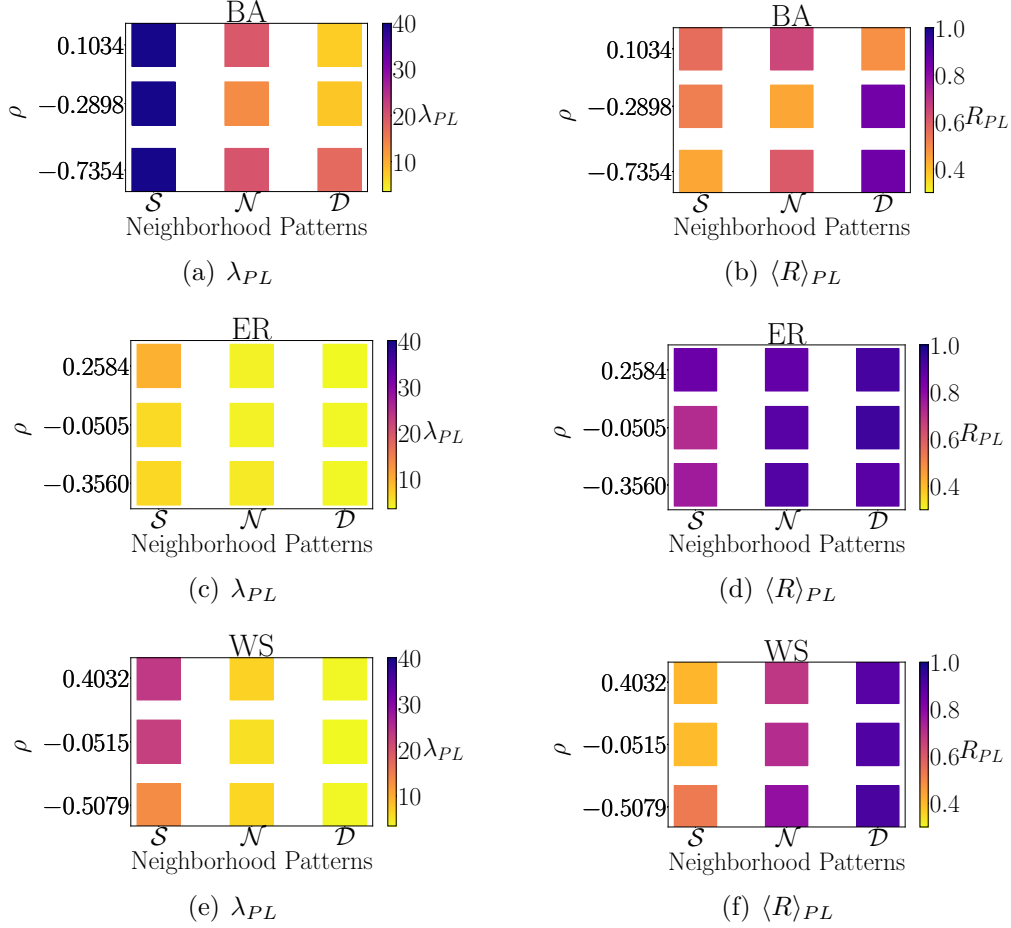
Source: Author production.

Figure 6.5 - (a-c) Mean of the order parameter $\langle R \rangle$ and (d-f) the total partial synchronization index S as a function of the coupling for networks with low (dashed line) and high (continuous line) values of clustering coefficient C and patterns Neutral (black), Similar (blue) and Dissimilar (red) of natural frequency distribution.



Source: Author production.

Figure 6.6 - Contour plot of the assortativity ρ and the neighborhood patterns in relation to the (a,c,e) coupling λ_{PL} and (b,d,f) order parameter R_{PL} at phase locking for the models BA, ER and WS of networks.

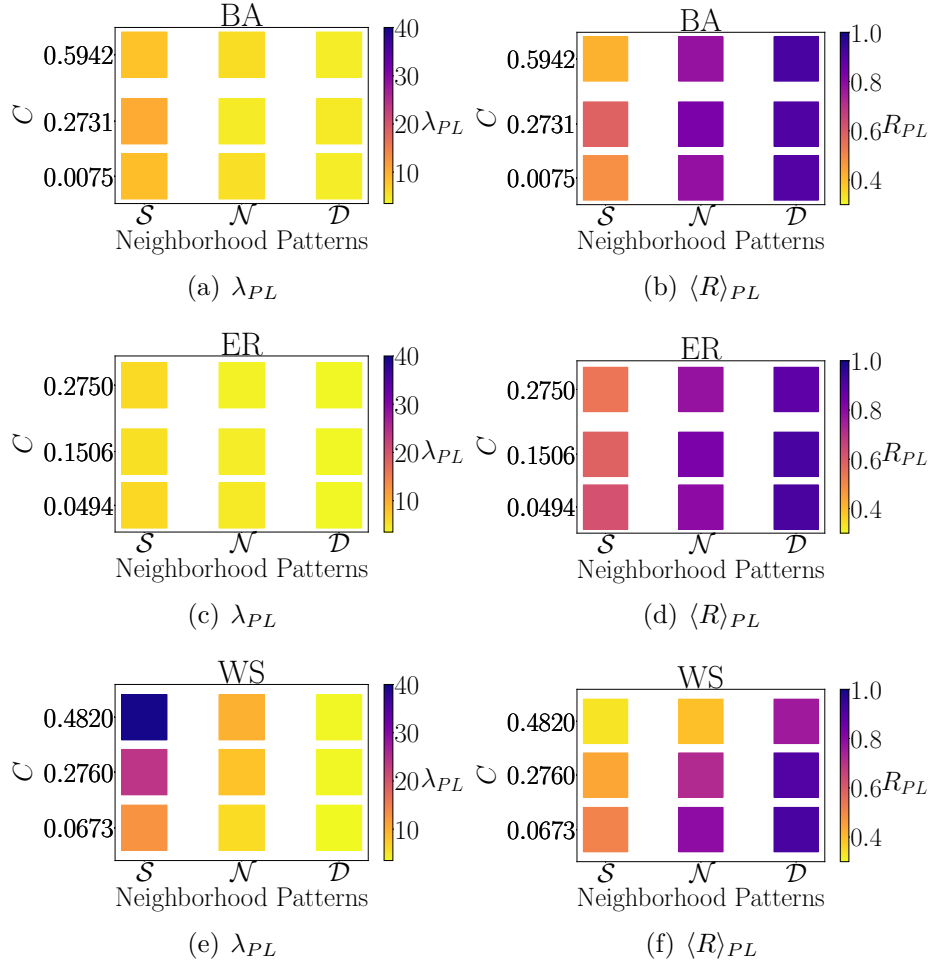


Source: Author production.

In relation to the network models considered in this work, in average, the ER model is the one that reaches phase locking with lower coupling values (light yellow) when considering the measures assortativity and clustering coefficient in Figures 6.6 and 6.7 (a,c,e). The BA network topology needs in average a high coupling constant to reach the phase locking state when considering assortativity, being then the hardest to synchronize in relation to this measure. WS networks are an intermediate between these two in relation to assortativity but requires the highest values of coupling to reach phase locking when the clustering coefficient is taken into account.

In regard to the network structure, we can infer that disassortative networks seem to favor synchronization for, in general, networks with negative values of ρ require

Figure 6.7 - Contour plot of the clustering coefficient C and the neighborhood patterns in relation to the (a,c,e) coupling λ_{PL} and (b,d,f) order parameter $\langle R \rangle_{PL}$ at phase locking for the models BA, ER and WS of networks.



Source: Author production.

a lower coupling value in order reach phase locking. In this way, when high degree nodes connect with low degree ones it favors synchronization (this does not seem to apply to the BA model). As already mentioned before, the Dissimilar natural frequency pattern tends to favor synchronization and we can think of the distribution of the nodes in a disassortative network also as being a dissimilar topological distribution as nodes with different degree tend to connect to each other. So, when analyzing our example, instead of having popular individuals communicating among each other, it is best if popular individuals talk to less popular ones.

In relation to the clustering coefficient, networks with fewer loops of size three seem

to favor synchronization as, in average, networks with the lowest value of C tend to be easier to synchronize. This fact could be explained by the *Braess's paradox* 3.4.3, which shows that inserting edges into networks may destroy synchronization, as these new edges can create new cycles (loops) which can lead to *geometric frustration*. A condition for the synchronization of a network is that the sum of the phase differences along every cycle must be equal to zero (WITTHAUT; TIMME, 2013) and when a new cycle is created in the network, for the same value of coupling, this condition may no longer be satisfied. When it comes to our example, this means that it is best to avoid the contacts of an individual to communicate with each other, avoiding then the creation of a small cycle of discussion as this may create unnecessary debates and therefore, increase the effort to achieve an agreement.

In general, the measures assortativity and clustering coefficient seem to have a stronger effect on the synchronization of the Similar dissonance patterns (especially when considering the WS model), having a modest effect on the Neutral pattern and a very low effect on the Dissimilar one.

6.4 Conclusion

The influence of the structure of complex networks of non-identical oscillators on global synchronization was studied. The total dissonance metric for neighbourhood similarity was employed and, with the help of an optimization algorithm, three patterns of natural frequency distributions were created, one where adjacent nodes have similar frequencies (Similar pattern), one where they have different frequencies (Dissimilar) and one that is a blend of both (Neutral). Network topologies of the models Erdős-Rényi, Watts-Strogatz and Barabási-Albert with high, intermediate and low values of the network measures assortativity and clustering coefficient were created and along with the frequency patterns were used to study the synchronization of these systems.

In relation to the emergency of phase locking, at low values of the coupling constant, the Similar pattern clearly favors weaker synchronization regimes but, as the coupling is increased, the Dissimilar pattern presents a rapid growth and is the first to reach synchronization, which corroborates previous works (FREITAS et al., 2015; SCAFUTI et al., 2015b). As for the complex network models used in this work, the Erdős-Rényi showed itself as the easiest to reach the regime of synchronization when compared to Watts-Strogatz and Barabási-Albert but this has yet to be confirmed by future experiments by comparing for example these three models where each one has the same values of assortativity and/or clustering coefficient. In relation to

the network measures employed here, in general, both low values of assortativity and clustering coefficient appear to favor synchronization, especially for the Similar dissonance pattern.

In summary, answering the questions raised at the beginning of this paper, based on our findings, we can state that the best way to conduct a discussion on a polemic subject is by encouraging individuals with distinct opinion changing rates to talk to each other and also encourage popular individuals to talk to less popular ones. It is also a good idea to avoid contacts of individuals to talk to each other, avoiding then small cycles of discussions. This hypothesis has yet to be confirmed by futures experiments.

As for future work, we consider to use the BA model with distinct degree exponents. We also intend to investigate the role that the average degree of the networks has on synchronization. The behavior of the WS configuration $(A^{C_{min}}, \omega^S)$, which does not reach the synchronous state even for high values of λ , as shown in Figure 6.2, has also to be better analyzed.

7 CONCLUSION

This thesis is focused on the impact topology has on the synchronization of networks of non-identical oscillators whose dynamics are described by the first and second order Kuramoto models. Most of this work is focused on the second order Kuramoto model as which is often used to approximate the dynamics of power grids. The first order Kuramoto model is used in a more general approach to study the influence of cycles and the heterogeneity in connections, which relates to the degree of the nodes, in the synchronization of a network of oscillators.

The first part of this thesis presented the theoretical foundations and is composed of the first two chapters. The following three chapters compose the second part, where the contributions of this work is presented.

Our first contribution, presented in Chapter 4 (LACERDA et al., 2021a), was the use of an evolutionary optimization technique to generate power grid topologies that favors synchronization and presents a relatively low number of transmission lines. It favors the synchronous state in a way that for a proper function of the grid, a lower maximum transmission capacity is required for transmission lines, which implies lower voltage levels. Having a low number of transmission lines which require lower voltage levels is desirable for economic reasons, as a lower number of transmission lines would need to be constructed and lower voltage levels lines are cheaper to build. The nodes of the network constructed with this method presented in general higher stability when compared to a random network of the same size, so their synchronous state is more stable against perturbations.

Our second contribution, presented in Chapter 5, shows that very simple changes in the topology of power grids can cause failures in the network and lead the system out of the synchronous state. The flux of the power being transmitted between nodes changes when adding, removing or increasing the capacity of a transmission line which can induce nonlocal failures due to overloads in a phenomenon known as Braess's paradox. We show that the most probable scenario as to what happens when these elementary changes in power grids are made depends on the level of centralization of the power generated in the network and also on the nature of the nodes being connected by the edge in question. Therefore, it would be of extreme importance to carefully analyze the effects of elementary changes in real-world power grids before even considering making them as these changes can reduce the stability of the grid and also cause failures which may generate great economic costs.

Finally, the last main contribution of this work was presented in Chapter 6. Where we study the influence of the structure of complex networks of non-identical oscillators, whose dynamics is given by the first order Kuramoto model, along with distinct patterns of natural frequencies on synchronization. We generate topologies with high, intermediate e low values of the metrics assortativity and clustering coefficient. We report a behavior that was already studied before that states that the connection between oscillators with distinct natural frequencies favors synchronization. Also, we find that heterogeneous connections (which relates to assortativity), that is, connecting nodes with distinct values of degree, favors the emergency of the synchronous state and that the presence of loops of size three (which relates to clustering coefficient) have the opposing effect. In general, the network measures clustering coefficient and assortativity seem to have a stronger effect on the synchronization of the Similar dissonance patterns, having a modest effect on the Neutral patter and a very low effect on the Dissimilar one. It is a general result and can be applied for example in social systems in a way that in order for a group (network) of people (oscillators) to reach an agreement (synchronous state) on a polemic subject it is wise to conduct this discussion encouraging individuals with distinct opinion changing rates (natural frequencies) to talk to each other and also encourage popular individuals to talk to less popular ones (heterogeneous connections). It is also a good idea to avoid contacts of individuals to talk to each other, avoiding then small cycles of discussions (loops of size three).

As for future research, we suggest analyzing real power grids topologies in order to give some guidance in relation to the addition of new generators. Also, a more complex model should be used instead of the second order Kuramoto one, for example, a model that includes admittance ([NISHIKAWA; MOTTER, 2015](#)). And, in relation to the last contribution mentioned here, we suggest modeling the interaction between groups with opposed political views on Twitter.

REFERENCES

- ACEBRÓN, J. A.; BONILLA, L. L.; VICENTE, C. J. P.; RITORT, F.; SPIGLER, R. The kuramoto model: a simple paradigm for synchronization phenomena. **Reviews of Modern Physics**, v. 77, n. 1, p. 137, 2005. 1, 11, 12
- ALHELOU, H. H.; HAMEDANI-GOLSHAN, M. E.; NJENDA, T. C.; SIANO, P. A survey on power system blackout and cascading events: research motivations and challenges. **Energies**, v. 12, n. 4, p. 682, 2019. 3
- ARENAS, A.; DÍAZ-GUILERA, A.; KURTHS, J.; MORENO, Y.; ZHOU, C. Synchronization in complex networks. **Physics Reports**, v. 469, n. 3, p. 93–153, 2008. 1, 90
- BARABÁSI, A.-L.; ALBERT, R. Emergence of scaling in random networks. **Science**, v. 286, n. 5439, p. 509–512, 1999. 90
- BERNATCHEZ, L.; LANDRY, C. Mhc studies in nonmodel vertebrates: what have we learned about natural selection in 15 years? **Journal of Evolutionary Biology**, v. 16, n. 3, p. 363–377, 2003. 87
- BOCCALETTI, S.; LATORA, V.; MORENO, Y.; CHAVEZ, M.; HWANG, D.-U. Complex networks: structure and dynamics. **Physics Reports**, v. 424, n. 4, p. 175–308, 2006. 1
- BOCCALETTI, S.; PISARCHIK, A. N.; GENIO, C. I. D.; AMANN, A. **Synchronization: from coupled systems to complex networks**. Cambridge: Cambridge University Press, 2018. 11
- BORGHETTI, A.; NUCCI, C. A.; PAOLONE, M.; BERNARDI, M. A statistical approach for estimating the correlation between lightning and faults in power distribution systems. In: IEEE. **Probabilistic Methods Applied to Power Systems, 2006. PMAPS 2006. International Conference on**. [S.l.], 2006. p. 1–7. 3
- BRAESS, D. Über ein paradoxon aus der verkehrsplanung. **Unternehmensforschung**, v. 12, n. 1, p. 258–268, 1968. 55
- BRAESS, D.; NAGURNEY, A.; WAKOLBINGER, T. On a paradox of traffic planning. **Transportation Science**, v. 39, n. 4, p. 446–450, 2005. 55

BULDYREV, S. V.; PARSHANI, R.; PAUL, G.; STANLEY, H. E.; HAVLIN, S. Catastrophic cascade of failures in interdependent networks. **Nature**, v. 464, n. 7291, p. 1025, 2010. [41](#)

BULLMORE, E.; SPORNS, O. Complex brain networks: graph theoretical analysis of structural and functional systems. **Nature Reviews Neuroscience**, v. 10, n. 3, p. 186–198, 2009. [1](#)

CARARETO, R.; BAPTISTA, M. S.; GREBOGI, C. Natural synchronization in power-grids with anti-correlated units. **Communications in Nonlinear Science and Numerical Simulation**, v. 18, n. 4, p. 1035–1046, 2013. [23](#), [24](#), [28](#), [35](#), [74](#)

CHIANG, H.-D. **Direct methods for stability analysis of electric power systems: theoretical foundation, BCU methodologies, and applications**. New Jersey: John Wiley & Sons, 2011. [41](#)

CHOPRA, N.; SPONG, M. W. On synchronization of kuramoto oscillators. In: **IEEE. Decision and Control, 2005 and 2005 European Control Conference. CDC-ECC'05. 44th IEEE Conference on**. [S.l.], 2005. p. 3916–3922. [32](#), [33](#), [74](#)

COSTA, L. d. F.; RODRIGUES, F. A.; TRAVIESO, G.; BOAS, P. R. V. Characterization of complex networks: a survey of measurements. **Advances in Physics**, v. 56, n. 1, p. 167–242, 2007. [90](#), [94](#)

DANIELS, B. C. **Synchronization of globally coupled nonlinear oscillators: the rich behavior of the Kuramoto model**. [S.l.: s.n.], 2005. [13](#), [14](#), [15](#), [61](#)

DEFFUANT, G.; NEAU, D.; AMBLARD, F.; WEISBUCH, G. Mixing beliefs among interacting agents. **Advances in Complex Systems**, n. 3, p. 11, 2001. [89](#)

DELELLIS, P.; GAROFALO, F.; PORFIRI, M. Evolution of complex networks via edge snapping. **IEEE Transactions on Circuits and Systems I: Regular Papers**, v. 57, n. 8, p. 2132–2143, 2010. [14](#), [15](#), [16](#), [61](#), [62](#)

DONETTI, L.; HURTADO, P. I.; MUNOZ, M. A. Entangled networks, synchronization, and optimal network topology. **Physical Review Letters**, v. 95, n. 18, p. 188701, 2005. [15](#)

DONGES, J. F.; ZOU, Y.; MARWAN, N.; KURTHS, J. The backbone of the climate network. **EPL (Europhysics Letters)**, v. 87, n. 4, p. 48007, 2009. [1](#)

- ERDÖS, P.; RÉNYI, A. On random graphs, i. **Publicationes Mathematicae (Debrecen)**, v. 6, p. 290–297, 1959. [74](#), [90](#)
- ERMENTROUT, B. An adaptive model for synchrony in the firefly pteroptyx malacca. **Journal of Mathematical Biology**, v. 29, n. 6, p. 571–585, 1991. [2](#), [13](#)
- ESPINOZA, S.; PANTELI, M.; MANCARELLA, P.; RUDNICK, H. Multi-phase assessment and adaptation of power systems resilience to natural hazards. **Electric Power Systems Research**, v. 136, p. 352–361, 2016. [3](#)
- FILATRELLA, G.; NIELSEN, A. H.; PEDERSEN, N. F. Analysis of a power grid using a kuramoto-like model. **The European Physical Journal B**, v. 61, n. 4, p. 485–491, 2008. [1](#), [13](#), [23](#), [24](#), [25](#), [26](#), [28](#), [41](#), [62](#), [74](#)
- FOLLMANN, R.; MACAU, E. E.; ROSA, E.; PIQUEIRA, J. R. Phase oscillatory network and visual pattern recognition. **IEEE Transactions on Neural Networks and Learning Systems**, v. 26, n. 7, p. 1539–1544, 2015. [1](#)
- FORTUNA, L.; FRASCA, M. Experimental synchronization of single-transistor-based chaotic circuits. **Chaos: an Interdisciplinary Journal of Nonlinear Science**, v. 17, n. 4, p. 043118, 2007. [1](#)
- FREITAS, C.; MACAU, E.; VIANA, R. L. Synchronization versus neighborhood similarity in complex networks of nonidentical oscillators. **Physical Review E**, v. 92, n. 3, p. 032901, 2015. [87](#), [88](#), [89](#), [90](#), [98](#), [103](#)
- FREITAS, V. L.; LACERDA, J. C.; MACAU, E. E. Complex networks approach for dynamical characterization of nonlinear systems. **International Journal of Bifurcation and Chaos**, v. 29, n. 13, p. 1950188, 2019. [1](#)
- GIL, S.; ZANETTE, D. H. Coevolution of agents and networks: opinion spreading and community disconnection. **Physics Letters A**, v. 356, n. 2, p. 89–94, 2006. [1](#)
- GÓMEZ-GARDENES, J.; MORENO, Y.; ARENAS, A. Paths to synchronization on complex networks. **Physical Review Letters**, v. 98, n. 3, p. 034101, 2007. [14](#), [62](#), [74](#)
- GOROCHOWSKI, T. E.; BERNARDO, M. di; GRIERSON, C. S. Evolving enhanced topologies for the synchronization of dynamical complex networks. **Physical Review E**, v. 81, n. 5, p. 056212, 2010. [15](#)

GOTTWALD, G. A. Model reduction for networks of coupled oscillators. **Chaos: An Interdisciplinary Journal of Nonlinear Science**, v. 25, n. 5, p. 053111, 2015. 87

GRZYBOWSKI, J.; MACAU, E.; YONEYAMA, T. On synchronization in power-grids modelled as networks of second-order kuramoto oscillators. **Chaos: An Interdisciplinary Journal of Nonlinear Science**, v. 26, n. 11, p. 113113, 2016. 1, 2, 13, 27, 28, 30, 31, 32, 34, 35, 74

GRZYBOWSKI, J.; MACAU, E. E.; YONEYAMA, T. Power-grids as complex networks: emerging investigations into robustness and stability. In: **Chaotic, Fractional, and Complex Dynamics: New Insights and Perspectives**. [S.l.]: Springer, 2018. p. 287–315. 3, 61

HASELAGER, G. J.; HARTUP, W. W.; LIESHOUT, C. F.; RIKSEN-WALRAVEN, J. M. A. Similarities between friends and nonfriends in middle childhood. **Child Development**, v. 69, n. 4, p. 1198–1208, 1998. 87

HOPPENSTEADT, F. C.; IZHIKEVICH, E. M. Synchronization of laser oscillators, associative memory, and optical neurocomputing. **Physical Review E**, v. 62, n. 3, p. 4010, 2000. 1

HUYGENS, C. **Christiaan Huygens' the pendulum clock, or, Geometrical demonstrations concerning the motion of pendula as applied to clocks**. [S.l.]: Iowa State Pr, 1986. 11

INFIELD, D.; FRERIS, L. **Renewable energy in power systems**. New Jersey: John Wiley & Sons, 2020. 3

JORDAN, W.; BRUFORD, M. New perspectives on mate choice and the mhc. **Heredity**, v. 81, n. 2, p. 127, 1998. 87

KOÇ, Y.; WARNIER, M.; KOOLIJ, R. E.; BRAZIER, F. M. An entropy-based metric to quantify the robustness of power grids against cascading failures. **Safety Science**, v. 59, p. 126–134, 2013. 2

KUNDUR, P.; BALU, N. J.; LAUBY, M. G. **Power system stability and control**. New York: McGraw-Hill, 1994. 25, 61

KUPERSMIDT, J. B.; DEROSIER, M. E.; PATTERSON, C. P. Similarity as the basis for children's friendships: the roles of sociometric status, aggressive and withdrawn behavior, academic achievement and demographic characteristics.

Journal of Social and Personal Relationships, v. 12, n. 3, p. 439–452, 1995. 87

KURAMOTO, Y. Self-entrainment of a population of coupled non-linear oscillators. In: **International symposium on mathematical problems in theoretical physics**. Berlin: Springer-Verlag Berlin Heidelberg: Haraki, H., 1975. p. 420–422. 1, 11

_____. **Chemical oscillations, waves, and turbulence**. New York: Springer Science & Business Media, 2012. 1

LAARHOVEN, P. J. V.; AARTS, E. H. Simulated annealing. In: **Simulated annealing: theory and applications**. [S.l.]: Springer, 1987. p. 7–15. 90

LACERDA, J.; FREITAS, C.; MACAU, E. Remote synchronization and multistability in a star-like network of oscillators. In: INTERNATIONAL CONFERENCE ON DYNAMICAL SYSTEMS THEORY AND APPLICATIONS. Lodz, 2017. p. 1–12. 1

_____. Multistable remote synchronization in a star-like network of non-identical oscillators. **Applied Mathematical Modelling**, v. 69, p. 453–465, 2019. 1, 62, 93

LACERDA, J.; FREITAS, V.; MACAU, E. Dynamical characterization of nonlinear systems through complex networks. In: INTERNATIONAL CONFERENCE ON NONLINEAR SCIENCE AND COMPLEXITY. São José dos Campos, 2016. p. 1–4. 1

LACERDA, J. C.; DIAS, J.; FREITAS, C.; MACAU, E. Synchronization of energy transmission networks at low voltage levels. **Applied Mathematical Modelling**, v. 89, p. 627–635, 2021. 4, 5, 61, 105

_____. Vulnerability and stability of power grids modeled by second-order kuramoto model: a mini review. **The European Physical Journal Special Topics**, p. 1–9, 2021. 1, 5, 23

LACERDA, J. C.; FREITAS, C.; MACAU, E. E. Symbolic dynamical characterization for multistability in remote synchronization phenomena. **Frontiers in Applied Mathematics and Statistics**, v. 6, p. 15, 2020. 1, 62

_____. Elementary changes in topology and power transmission capacity can induce failures in power grids. **Physica A: Statistical Mechanics and its Applications**, p. 126704, 2021. 73

LACERDA, J. C.; FREITAS, C.; MACAU, E. E.; KURTHS, J. How heterogeneity in connections and cycles matter for synchronization of complex networks. **Chaos: An Interdisciplinary Journal of Nonlinear Science**, v. 31, n. 11, p. 113134, 2021. 6, 87

LEEUWEN, P. V.; GEUE, D.; THIEL, M.; CYSARZ, D.; LANGE, S.; ROMANO, M.; WESSEL, N.; KURTHS, J.; GRÖNEMEYER, D. Influence of paced maternal breathing on fetal–maternal heart rate coordination. **Proceedings of the National Academy of Sciences**, v. 106, n. 33, p. 13661–13666, 2009. 1

MACHOWSKI, J.; BIALEK, J.; BUMBY, J. R.; BUMBY, J. **Power system dynamics and stability**. New Jersey: John Wiley & Sons, 1997. 41

MACHOWSKI, J.; LUBOSNY, Z.; BIALEK, J. W.; BUMBY, J. R. **Power system dynamics: stability and control**. New Jersey: John Wiley & Sons, 2020. 9, 10, 11, 23

MAGRINI, L. A.; DOMINGUES, M. O.; MACAU, E. E.; KISS, I. Z. Synchronization in populations of electrochemical bursting oscillators with chaotic slow dynamics. **Chaos: An Interdisciplinary Journal of Nonlinear Science**, v. 31, n. 5, p. 053125, 2021. 1, 13

MARTINHO, E. **Distúrbios da energia elétrica**. São Paulo: Saraiva Educação SA, 2009. 2

MATTHEWS, P. C.; MIROLLO, R. E.; STROGATZ, S. H. Dynamics of a large system of coupled nonlinear oscillators. **Physica D: nonlinear phenomena**, v. 52, n. 2-3, p. 293–331, 1991. 12

MENCK, P. J.; HEITZIG, J.; KURTHS, J.; SCHELLNHUBER, H. J. How dead ends undermine power grid stability. **Nature Communications**, v. 5, p. 3969, 2014. 4, 30, 41, 46, 48, 54, 61, 62, 74

MENCK, P. J.; HEITZIG, J.; MARWAN, N.; KURTHS, J. How basin stability complements the linear-stability paradigm. **Nature Physics**, v. 9, n. 2, p. 89, 2013. 4, 48

MONTICELLI, A.; GARCIA, A. **Introdução a sistemas de energia elétrica**. Campinas: Editora UNICAMP, 2011. 61

MORENO, Y.; PACHECO, A. F. Synchronization of kuramoto oscillators in scale-free networks. **EPL (Europhysics Letters)**, v. 68, n. 4, p. 603, 2004. 2

- MOTTER, A. E.; LAI, Y.-C. Cascade-based attacks on complex networks. **Physical Review E**, v. 66, n. 6, p. 065102, 2002. [41](#)
- NÉDA, Z.; RAVASZ, E.; BRECHET, Y.; VICSEK, T.; BARABÁSI, A.-L. Self-organizing processes: the sound of many hands clapping. **Nature**, v. 403, n. 6772, p. 849–850, 2000. [1](#)
- NEWMAN, M. E. Mixing patterns in networks. **Physical Review E**, v. 67, n. 2, p. 026126, 2003. [91](#)
- _____. The structure and function of complex networks. **SIAM Review**, v. 45, n. 2, p. 167–256, 2003. [51](#)
- NISHIKAWA, T.; MOTTER, A. E. Comparative analysis of existing models for power-grid synchronization. **New Journal of Physics**, v. 17, n. 1, p. 015012, 2015. [86](#), [106](#)
- NOLDUS, R.; MIEGHEM, P. V. Assortativity in complex networks. **Journal of Complex Networks**, v. 3, n. 4, p. 507–542, 2015. [91](#), [94](#)
- NOORAZAR, H. Recent advances in opinion propagation dynamics: a 2020 survey. **The European Physical Journal Plus**, v. 135, n. 6, p. 1–20, 2020. [89](#)
- ÓDOR, G.; HARTMANN, B. Heterogeneity effects in power grid network models. **Physical Review E**, v. 98, n. 2, p. 022305, 2018. [62](#)
- OSIPOV, G. V.; KURTHS, J.; ZHOU, C. **Synchronization in oscillatory networks**. New York: Springer Science & Business Media, 2007. [1](#)
- PACHAURI, R. K.; ALLEN, M. R.; BARROS, V. R.; BROOME, J.; CRAMER, W.; CHRIST, R.; CHURCH, J. A.; CLARKE, L.; DAHE, Q.; DASGUPTA, P. **Climate change 2014: synthesis report. Contribution of Working Groups I, II and III to the fifth assessment report of the Intergovernmental Panel on Climate Change**. Geneva: IPCC, 2014. [3](#)
- PADE, J. P.; PEREIRA, T. Improving network structure can lead to functional failures. **Scientific Reports**, v. 5, n. 1, p. 1–6, 2015. [57](#)
- PAGANI, G. A.; AIELLO, M. The power grid as a complex network: a survey. **Physica A: Statistical Mechanics and its Applications**, v. 392, n. 11, p. 2688–2700, 2013. [13](#)

PANTALEONE, J. Synchronization of metronomes. **American Journal of Physics**, American Association of Physics Teachers, v. 70, n. 10, p. 992–1000, 2002. 1

PANTELI, M.; MANCARELLA, P. Influence of extreme weather and climate change on the resilience of power systems: impacts and possible mitigation strategies. **Electric Power Systems Research**, v. 127, p. 259–270, 2015. 3

PARKINSON, C.; KLEINBAUM, A. M.; WHEATLEY, T. Similar neural responses predict friendship. **Nature Communications**, v. 9, n. 1, p. 332, 2018. 87

PENN, D. J.; POTTS, W. K. The evolution of mating preferences and major histocompatibility complex genes. **The American Naturalist**, v. 153, n. 2, p. 145–164, 1999. 87

PICKETT, J. P. **The American heritage dictionary of the English language**. Boston: Houghton Mifflin Harcourt, 2018. 11

PIERTNEY, S.; OLIVER, M. The evolutionary ecology of the major histocompatibility complex. **Heredity**, v. 96, n. 1, p. 7, 2006. 87

PIKOVSKY, A.; ROSENBLUM, M.; KURTHS, J. **Synchronization: a universal concept in nonlinear sciences**. Cambridge: Cambridge University Press, 2003. 1, 11, 12, 87, 88

PINTO, R. S.; SAA, A. Optimal synchronization of kuramoto oscillators: a dimensional reduction approach. **Physical Review E**, v. 92, n. 6, p. 062801, 2015. 87

PLUCHINO, A.; BOCCALETTI, S.; LATORA, V.; RAPISARDA, A. Opinion dynamics and synchronization in a network of scientific collaborations. **Physica A: Statistical Mechanics and its Applications**, v. 372, n. 2, p. 316–325, 2006. 88

PLUCHINO, A.; LATORA, V.; RAPISARDA, A. Changing opinions in a changing world: a new perspective in sociophysics. **International Journal of Modern Physics C**, v. 16, n. 04, p. 515–531, 2005. 1, 88

POURBEIK, P.; KUNDUR, P. S.; TAYLOR, C. W. The anatomy of a power grid blackout-root causes and dynamics of recent major blackouts. **IEEE Power and Energy Magazine**, v. 4, n. 5, p. 22–29, 2006. 23

- RAD, A. A.; JALILI, M.; HASLER, M. Efficient rewirings for enhancing synchronizability of dynamical networks. **Chaos: An Interdisciplinary Journal of Nonlinear Science**, v. 18, n. 3, p. 037104, 2008. 15
- RIBEIRO, A. E. D.; AROUCA, M. C.; COELHO, D. M. Electric energy generation from small-scale solar and wind power in brazil: the influence of location, area and shape. **Renewable Energy**, v. 85, p. 554–563, 2016. 2
- RODRIGUES, F. A.; PERON, T. K. D.; JI, P.; KURTHS, J. The kuramoto model in complex networks. **Physics Reports**, v. 610, p. 1–98, 2016. 2, 27
- ROHDEN, M.; SORGE, A.; TIMME, M.; WITTHAUT, D. Self-organized synchronization in decentralized power grids. **Physical Review Letters**, v. 109, n. 6, p. 064101, 2012. 30, 62, 77
- ROHDEN, M.; SORGE, A.; WITTHAUT, D.; TIMME, M. Impact of network topology on synchrony of oscillatory power grids. **Chaos: An Interdisciplinary Journal of Nonlinear Science**, v. 24, n. 1, p. 013123, 2014. 4
- SARAMÄKI, J.; KIVELÄ, M.; ONNELA, J.-P.; KASKI, K.; KERTESZ, J. Generalizations of the clustering coefficient to weighted complex networks. **Physical Review E**, v. 75, n. 2, p. 027105, 2007. 92, 94
- SCAFUTI, F.; AOKI, T.; BERNARDO, M. di. An evolutionary strategy for adaptive network control and synchronization and its applications. **IFAC-PapersOnLine**, v. 48, n. 18, p. 193–198, 2015. 15, 16, 17, 62
- _____. Heterogeneity induces emergent functional networks for synchronization. **Physical Review E**, v. 91, n. 6, p. 062913, 2015. 15, 17, 18, 61, 64, 65, 88, 98, 103
- SKARDAL, P. S.; TAYLOR, D.; SUN, J. Optimal synchronization of complex networks. **Physical Review Letters**, v. 113, n. 14, p. 144101, 2014. 15
- STROGATZ, S. H. From kuramoto to crawford: exploring the onset of synchronization in populations of coupled oscillators. **Physica D: Nonlinear Phenomena**, v. 143, n. 1, p. 1–20, 2000. 11
- _____. **Nonlinear dynamics and chaos: with applications to physics, biology, chemistry, and engineering**. Boulder: Westview Press, 2014. 2, 9, 13, 45
- SUN, K. Complex networks theory: a new method of research in grid. In: IEEE. **Transmission and Distribution Conference and Exhibition: Asia and Pacific, 2005 IEEE/PES**. New York, 2005. p. 1–6. 49, 74

TANAKA, H.-A.; LICHTENBERG, A. J.; OISHI, S. First order phase transition resulting from finite inertia in coupled oscillator systems. **Physical Review Letters**, v. 78, n. 11, p. 2104, 1997. [13](#), [27](#)

_____. Self-synchronization of coupled oscillators with hysteretic responses. **Physica D: Nonlinear Phenomena**, v. 100, n. 3-4, p. 279–300, 1997. [27](#)

TANAKA, T.; AOYAGI, T. Optimal weighted networks of phase oscillators for synchronization. **Physical Review E**, v. 78, n. 4, p. 046210, 2008. [15](#)

TREES, B. R.; SARANATHAN, V.; STROUD, D. Synchronization in disordered josephson junction arrays: small-world connections and the kuramoto model. **Physical Review E**, v. 71, n. 1, p. 016215, 2005. [2](#)

ULLNER, E.; KOSESKA, A.; KURTHS, J.; VOLKOV, E.; KANTZ, H.; GARCÍA-OJALVO, J. Multistability of synthetic genetic networks with repressive cell-to-cell communication. **Physical Review E**, v. 78, n. 3, p. 031904, 2008. [1](#)

URBERG, K. A.; DEGIRMENCIOGLU, S. M.; TOLSON, J. M. Adolescent friendship selection and termination: The role of similarity. **Journal of Social and Personal Relationships**, v. 15, n. 5, p. 703–710, 1998. [87](#)

VARELA, F.; LACHAUX, J.-P.; RODRIGUEZ, E.; MARTINERIE, J. The brainweb: phase synchronization and large-scale integration. **Nature Reviews Neuroscience**, v. 2, n. 4, p. 229–239, 2001. [1](#)

VICKHOFF, B.; MALMGREN, H.; ÅSTRÖM, R.; NYBERG, G.; ENGVALL, M.; SNYGG, J.; NILSSON, M.; JÖRNSTEN, R. Music structure determines heart rate variability of singers. **Frontiers in Psychology**, v. 4, p. 334, 2013. [1](#)

WARD, D. M. The effect of weather on grid systems and the reliability of electricity supply. **Climatic Change**, v. 121, n. 1, p. 103–113, 2013. [3](#)

WASSERMAN, S.; FAUST, K. **Social network analysis: methods and applications**. Cambridge: Cambridge University Press, 1994. [92](#)

WATTS, D. J.; STROGATZ, S. H. Collective dynamics of small-world networks. **Nature**, v. 393, n. 6684, p. 440–442, 1998. [90](#)

WEGLARCZYK, S. Kernel density estimation and its application. v. 23, 2018. [69](#)

WILEY, D. A.; STROGATZ, S. H.; GIRVAN, M. The size of the sync basin. **Chaos: An Interdisciplinary Journal of Nonlinear Science**, v. 16, n. 1, p. 015103, 2006. [48](#)

WINFREE, A. T. Biological rhythms and the behavior of populations of coupled oscillators. **Journal of Theoretical Biology**, v. 16, n. 1, p. 15–42, 1967. 11

WITTHAUT, D.; TIMME, M. Braess's paradox in oscillator networks, desynchronization and power outage. **New Journal of Physics**, v. 14, n. 8, p. 083036, 2012. 4, 55, 57, 58, 74, 79

_____. Nonlocal failures in complex supply networks by single link additions. **The European Physical Journal B**, v. 86, n. 9, p. 1–12, 2013. 49, 58, 74, 78, 103

YANAGITA, T.; MIKHAILOV, A. S. Design of easily synchronizable oscillator networks using the monte carlo optimization method. **Physical Review E**, v. 81, n. 5, p. 056204, 2010. 15

YANG, L.-x.; JIANG, J. Impacts of link addition and removal on synchronization of an elementary power network. **Physica A: Statistical Mechanics and its Applications**, v. 479, p. 99–107, 2017. 4

YANG, L.-x.; JIANG, J.; LIU, X.-j. Influence of edge additions on the synchronizability of oscillatory power networks. **Communications in Nonlinear Science and Numerical Simulation**, v. 41, p. 11–18, 2016. 4

ZHU, L.; HILL, D. J. Synchronization of power systems and kuramoto oscillators: a regional stability framework. **arXiv preprint arXiv:1804.01644**, 2018. 3

**APPENDIX A - VULNERABILITY AND STABILITY OF POWER
GRIDS MODELED BY SECOND ORDER KURAMOTO MODEL - A
MINI REVIEW**

Vulnerability and Stability of Power Grids Modeled by Second Order Kuramoto Model - A Mini Review

Juliana C. Lacerda^{1,a}, Jussara Dias¹, Celso Freitas¹, and Elbert Macau²

¹ Associated Laboratory for Computing and Applied Mathematics, National Institute for Space Research, INPE, São José dos Campos, SP, 12243-010, Brazil.

² Institute of Science and Technology, Federal University of São Paulo, São José dos Campos, SP, 12247-014, Brazil.

Abstract. In this work, we derive a model to study and simulate the dynamics of power grids that, after a few approximations, turns out to be the second order Kuramoto model. We then use this model to perform some numerical simulations that relate to the vulnerability and stability of energy transmission networks. In relation to the stability, assuming the grid is fully functional and, therefore, is in the synchronous state, we analyze how the grid responds to large perturbations and, also, how this response can be influenced by the location of the node being perturbed. We also show how a simple change in the topology or in the transmission capacity of a line can affect the synchronization of the grid. Regarding the vulnerability, some indexes to identify dynamically vulnerable nodes and edges are presented.

1 Introduction

Power grids or energy transmission networks are dynamical systems where transmission lines connect generators and consumers [1] that can be far apart from each other. The growing demand in power supply by consumers and the feature that now a consumer can also input energy to the network or have a demand that may dramatically change over time brings new challenges that requires innovative strategies for proper expansion and system stability evaluation. Power transmission occurs mostly by the means of alternated current, which is by definition oscillatory. For a power system to be fully functional, it is mandatory for all elements of this network to be operating with the same frequency, that is, all of its elements must be synchronized [2,3]. If there is a higher demand in power consumption and it is not properly supplied or some failure occurs, some component of the network may lose this synchronized state which may lead to a blackout [4]. Energy transmission networks are not static, they evolve through time as they expand with the addition of new consumers and generators. These generators many times are small energy sources like solar boards. These topology changes can be relevant in the synchronization of the system as they can change the stability and induce cascade failures [5].

^a e-mail: juliana.lacerda@inpe.br

In order to study and simulate the dynamics of power grids, one can make use of complex networks [6] where consumers and generators are modeled as nodes and transmission lines as edges [7,8]. The dynamics of the nodes are often modeled by the second order Kuramoto model [9] where the coupling constant relates to the maximum power transmission capacity of the transmission line. In this work, we use this model to evaluate the power grid vulnerability and stability.

Several research have development studies for assesses electric power grids vulnerabilities [10], mainly motivated by significant blackouts. One way to evaluate this is creating indexes to discover the weak nodes and edges in the network. This index can be created using only the network topology [11] or using dynamics [12] and power flow analyses [13]

This review is organized as follows: Section 2 derives a power grid model based on a two node system, composed of a consumer and a generator. By making a few assumptions and approximations, we arrive in the second order Kuramoto model. A measure to quantify the synchronization of a power grid is also presented. Section 3 explores some numerical results related to vulnerability and stability and conclusions are presented in Section 4.

2 Model and methods

An electric power plant (Fig. 1) is characterized by having a mechanical power input (P_s) and is equipped with a generator G (rotor) that converts this mechanical power source into electrical power. A consumer C , on the other hand, does the exact opposite. The generator produces electrical power with a constant frequency Ω and has a phase given by

$$\theta_1 = \Omega t + \tilde{\theta}_1, \quad (1)$$

where $\tilde{\theta}_1$ is a small perturbation.

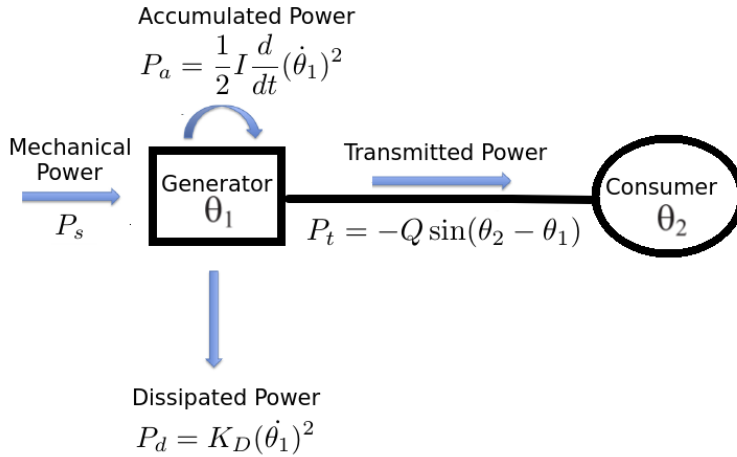


Fig. 1. Diagram of an electric power plant composed by a generator (G) with phase θ_1 and a consumer (C) with phase θ_2 connected by a transmission line.

In the process of converting mechanical to electrical power, some of this power is dissipated due to friction

$$P_d = K_D (\dot{\theta}_1)^2, \quad (2)$$

where K_D is a constant. Also some power is accumulated as kinetic energy at a rate

$$P_a = \frac{1}{2}I\frac{d}{dt}(\dot{\theta}_1)^2 = I\dot{\theta}_1\ddot{\theta}_1, \quad (3)$$

where I is the moment of inertia. The power that remains is transmitted P_t to a consumer C . In Fig. 1 the generator has a phase θ_1 and the consumer θ_2 and power will flow between them as long as there is a difference between these two phases as it is given by

$$P_t = -Q \sin(\theta_2 - \theta_1), \quad (4)$$

where Q is a constant.

We can then describe the dynamics of a generator (or consumer) by writing the power balance equation [4]

$$\begin{aligned} P_s &= P_d + P_a + P_t \\ &= K_D(\dot{\theta}_1)^2 + I\dot{\theta}_1\ddot{\theta}_1 - Q \sin(\theta_2 - \theta_1) \end{aligned} \quad (5)$$

Let us assume that the power grid is operating under the limit of small perturbations

$$\dot{\theta}_1 \ll \Omega. \quad (6)$$

By substituting Eq. 1 into Eq. 5 we have

$$\begin{aligned} P_s &= K_D(\Omega + \dot{\theta}_1)^2 + I[(\Omega + \dot{\theta}_1)\ddot{\theta}_1] - Q \sin(\tilde{\theta}_2 - \tilde{\theta}_1) \\ &= K_D(\dot{\theta}_1)^2 + I\Omega\ddot{\theta}_1 + \dot{\theta}_1(I\ddot{\theta}_1 + 2K_D\Omega) + K_D\Omega^2 - Q \sin(\theta_2 - \theta_1). \end{aligned} \quad (7)$$

Note that $\ddot{\theta}_1 = \frac{d}{dt}(\Omega) + \ddot{\theta}_1 = \ddot{\theta}_1$ and that $\theta_2 - \theta_1 = (\Omega t + \tilde{\theta}_2) - (\Omega t + \tilde{\theta}_1) = \tilde{\theta}_2 - \tilde{\theta}_1$. Considering Eq. 6, the term $K_D(\dot{\theta}_1)^2$ can be neglected:

$$P_s \cong I\Omega\ddot{\theta}_1 + \dot{\theta}_1(I\ddot{\theta}_1 + 2K_D\Omega) + K_D\Omega^2 - Q \sin(\theta_2 - \theta_1). \quad (8)$$

In mechanical systems, it is a common fact that the rate of kinetic energy accumulated ($P_a \approx I\Omega\ddot{\theta}_1$) is much less than the rate at which the energy is dissipated by friction ($P_d \approx K_D(\dot{\theta}_1)^2$) [4] that, according to Eq 6, is much smaller than $K_D\Omega^2$:

$$I\Omega\ddot{\theta}_1 \ll K_D(\dot{\theta}_1)^2 \ll K_D\Omega^2. \quad (9)$$

So, the power accumulated is much smaller than $K_D\Omega^2$:

$$I\Omega\ddot{\theta}_1 \ll K_D\Omega^2. \quad (10)$$

We can then neglect the term $I\ddot{\theta}_1$ in the coefficient of the first derivative in Eq. 8 and this equation then becomes

$$P_s \cong I\Omega\ddot{\theta}_1 + 2K_D\Omega\dot{\theta}_1 + K_D\Omega^2 - Q \sin(\theta_2 - \theta_1). \quad (11)$$

Isolating $\ddot{\theta}_1$ and neglecting the approximation sign, we have:

$$\ddot{\theta}_1 = \frac{P_s}{I\Omega} - \frac{2K_D}{I}\dot{\theta}_1 - \frac{K_D\Omega}{I} + \frac{Q}{I\Omega} \sin(\theta_2 - \theta_1). \quad (12)$$

Normalizing time with respect to the common frequency Ω^{-1} in Eq. 12 [4]:

$$\ddot{\theta}_1 = \left(\frac{P_s \Omega}{I} - \frac{K_D \Omega^3}{I} \right) - \frac{2K_D \Omega}{I} \dot{\theta}_1 + \frac{Q \Omega}{I} \sin(\theta_2 - \theta_1). \quad (13)$$

To better visualize this equation, we define the following constants:

$$P_1 = \frac{P_s \Omega}{I} - \frac{K_D \Omega^3}{I}, \quad (14)$$

$$\alpha = \frac{2K_D \Omega}{I}, \quad (15)$$

$$P_{max} = \frac{Q \Omega}{I}, \quad (16)$$

where P_1 is the power generated, α is a dissipation parameter and P_{max} is the maximum power transfer capacity of the transmission line. Eq. 13 can then be written as

$$\ddot{\theta}_1 = P_1 - \alpha \dot{\theta}_1 + P_{max} \sin(\theta_2 - \theta_1). \quad (17)$$

Eq. 17 dictates the dynamics of the generator at Fig. 1 that is connected to just one consumer. The dynamics of the consumer is governed by the equation

$$\ddot{\theta}_2 = P_2 - \alpha \dot{\theta}_2 + P_{max} \sin(\theta_1 - \theta_2). \quad (18)$$

Generalizing this equation to a network of N dynamical systems (assuming that all transmission lines have the same maximum transmission capacity):

$$\ddot{\theta}_m = P_m - \alpha \dot{\theta}_m + \frac{P_{max}}{g_m} \sum_{n=1}^N A_{mn} \sin(\theta_n - \theta_m), \quad (19)$$

where $m = 1, \dots, N$ and g_m is the degree, that is, the number of elements connected to node m . A_{mn} is the adjacency matrix with bidirectional edges.

Eq. 19 is the celebrated second order Kuramoto model [14–17], in which the dynamics of generators and consumers is described as oscillators. Eq. 19 can also be written as two first order differential equations (for a better visualization, we will now remove the tilde from the notation)

$$\dot{\theta}_m = \nu_m, \quad (20)$$

$$\dot{\nu}_m = P_m - \alpha \nu_m + \frac{P_{max}}{g_m} \sum_{n=1}^N A_{mn} \sin(\theta_n - \theta_m). \quad (21)$$

To summarize, θ_m and ν_m are the phase and angular velocity (instantaneous frequency) of oscillator m , respectively, α is the dissipation parameter, P_m denotes the power consumed ($P_m < 0$) or generated ($P_m > 0$) which corresponds to the natural frequency of oscillator m . P_{max} is the coupling constant of the Kuramoto model and in our case it corresponds to the maximum power capacity of the transmission line (here we assume that all transmission lines have the same capacity), A is the adjacency matrix with entry $A_{mn} = 1$ if oscillators m and n are connected and $A_{mn} = 0$ otherwise. More specifically, $\dot{\nu}_m$ accounts for the accumulated power, $\alpha \nu_m$ represents the dissipated power due to friction, $P_{max} \sin(\theta_n - \theta_m)$ is the power flow between nodes m and n . [5]

For a power grid to be fully functional, all of its components must be operating with the same instantaneous frequency, so the synchronous state must be maintained

even when its components are subjected to perturbations, such as an increase in the consumption or some failure on some of its components [7].

In order to quantify the synchronous state of the power grid, a measure called *partial synchronization index* [18] is often used. It measures a state called *phase locking* [19] where all oscillators have the same instantaneous frequency and is given by

$$S_{mn} = \left| \lim_{\Delta t \rightarrow \infty} \frac{1}{\Delta t} \int_{t_r}^{t_r + \Delta t} e^{i[\theta_m(t) - \theta_n(t)]} dt \right|, \quad (22)$$

where t_r is a long enough transient time and $S_{mn} \in [0, 1]$. It measures the synchronization between two elements of the grid, when m and n are in phase locking, $S_{mn} = 1$. In order to measure the partial synchronization index of the entire network, we calculate the arithmetic mean

$$S = \frac{1}{N^2} \sum_{m,n=1}^N S_{mn}. \quad (23)$$

3 Numerical results and discussions

We now present some results regarding the study of power grids by the use of the second order Kuramoto model.

3.1 Stability

In this section, we analyze how power grids modeled by the second order Kuramoto model respond to perturbations. First, consider a simple transmission network composed by two generators connected to a consumer, Fig. 2(a), where the consumer absorbs two power units ¹ $P_C = -2$ and each generator produces one power unit $P_G = 1$. At first, the system is in the synchronous state as the partial synchronization index before the perturbation is $S = 1$, then suddenly at $t = 50$ time units, the consumer requires an extra power ΔP from the generators for a short period of time $\Delta t = 2$. After this period, the consumer goes back into consuming two power units.

We consider two cases, one where the extra power consumed is $\Delta P = -1$, Fig. 2(b), and one where the extra power is $\Delta P = -3$, Fig. 2(d). One can see that when $\Delta P = -1$, the entire system feels the perturbation but manages to return to the synchronous state as the partial synchronization index, calculated after the transient ($t > 100$), is $S_{after} = 1.0$. We can also notice that the instantaneous frequency goes back to the same value as it had before the perturbation, Fig 2(c). However, for $\Delta P = -3$, the system is taken out from the synchronous state and is not able to come back to it, as $S_{after} = 0.67$ as for the instantaneous frequency, Fig 2(e), instead of all components presenting the same value, the system is divided into two where both generators tend to an instantaneous frequency close to 10 and the consumers tends to one close to -20 .

In order to understand and be able to predict why and how some perturbations lead a power system out of the synchronous state and some do not, a concept of basin stability E in relation to large perturbations was proposed by Menck et al. [20,21]. Assuming the transmission network is in the synchronized state, after a component of the grid is hit by a large perturbation, it quantifies the probability of this element to remain in this state after a transient. It is related to the volume of the basin of

¹ power units are short for normalized power units

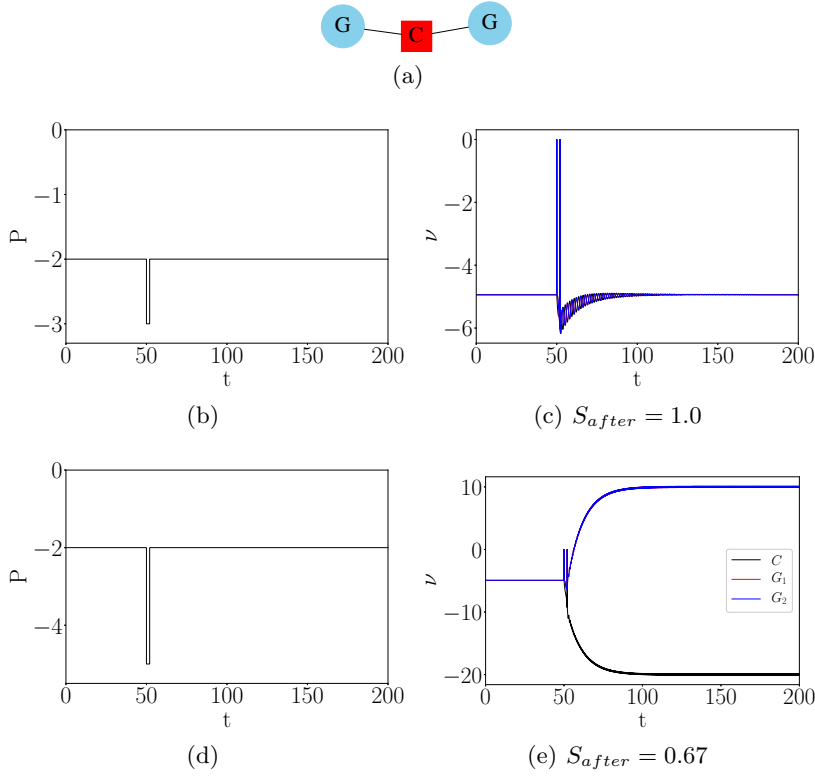


Fig. 2. (a) Three node transmission network composed of a consumer (C, red) connected to two generators (G, blue). (b) and (d) are the power absorbed by the consumer and (c) and (e) are its instantaneous frequency as a function of time.

attraction (B) and can be numerically calculated by means of a Monte-Carlo method [22,23] where Eq. 19 is integrated for T different initial conditions in relation to node m and the number U_m of times that this node converges to the synchronous state is annotated, that is:

$$E_m = \frac{U_m}{T}. \quad (24)$$

Node m is said to be globally stable if $E_m = 1$ and unstable when $E_m = 0$.

In order to compute the basin stability of node m , it was considered the one-node model which is given by Eq. 19, where $\theta_n = 0$ for all $n \neq m$, in a way that the rest of the grid is not affected by node m . The basin of attraction of this node can be seen in yellow in Fig. 3 (a-c) along with the basin stability Fig. 3(d) as a function of the transmission capacity. One can notice that the higher the transmission capacity, the greater is the basin of attraction and, of course, the basin stability. So, the higher the transmission capacity of the transmission lines, the harder it gets to desynchronize the system.

To study the role the topology plays in the synchronization of the system, Menck et al. [21] randomly generated 1000 network topologies composed of 100 nodes and 135 transmission lines, having average degree equal to 2.7 (which is a typical value for power grids [8]) and found that some patterns called dead ends and dead trees play an important role on the basin stability of the network. In Fig.3(e) a small part of a network is depicted, where color represents the value of the basin stability E

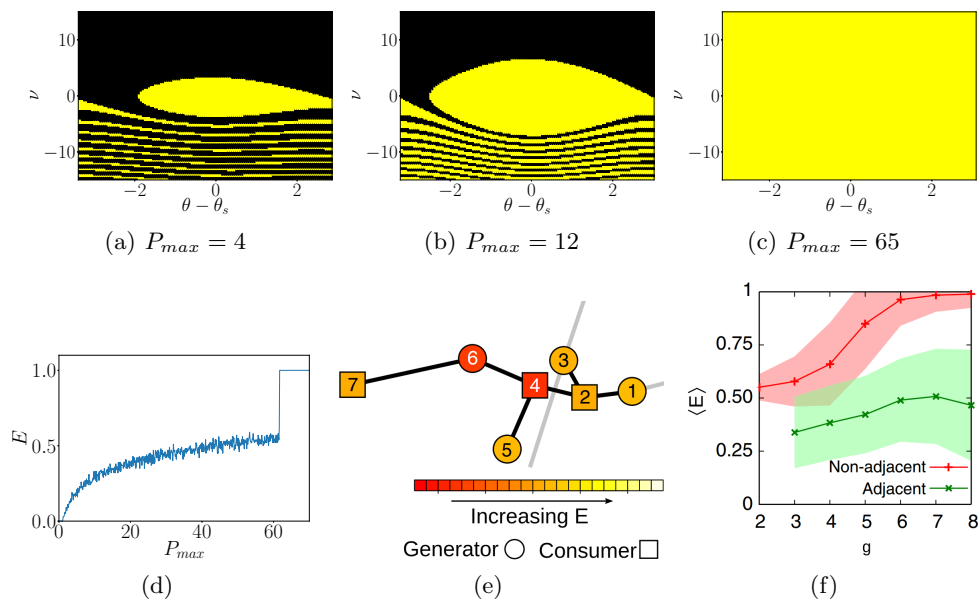


Fig. 3. (a)-(c) Basin of attraction B (yellow) of a single node dynamics given by Eq. 19 with $\theta_n = 0$ for different values of transmission capacity P_{max} and (d) basin stability E of a single node dynamics as a function of P_{max} . The parameters used are $\alpha = 0.1$, $P_m = 1$ and $\theta_S = \sin^{-1}(P_m/P_{max})$, which is the value of the phase at the synchronous state [21]. (e) The dead tree is composed of nodes $\{4, 5, 6, 7\}$ and includes two dead ends $\{5\}$ and $\{6, 7\}$. (f) Mean value and standard deviation of basin stability of nodes as a function of their degree g divided into two groups, nodes that are non-adjacent (red) and adjacent to dead trees (green). Figures (e) and (f) were adapted from [21].

of each node. The dead tree is composed of nodes $\{4, 5, 6, 7\}$ and is composed of two dead ends, $\{5\}$ and $\{6, 7\}$. Node 4 is adjacent to two dead ends and node 6 is adjacent to one and we can see that their basin stability is lower than the average. When the mean and standard deviation of the basin stability $\langle E \rangle$ was calculated for all network topologies as a function of the nodes' degree and were divided into two groups, one group are the nodes that are not adjacent to a dead tree or dead end (red) and one where the ones that are adjacent (green), Fig.3(f), one can clearly see that those nodes that are adjacent to dead trees present a lower value of basin stability and must be avoided in the building of power grids.

3.2 Braess's Paradox

In Section 3.1 it was mentioned that dead trees and dead ends must be avoided in order to maintain the synchronous state, so, one might think that a good way to avoid that from happening would be just to add some new edges at the network. However, in fact, might not be a good idea because of what is known as Braess's Paradox [24], which actually shows that inserting edges into network topologies can destroy synchronization. This fact was explored by Witthaut et al. [25] in the context of energy transmission networks, where, in fact, they pointed out that not only adding a transmission line may destroy the synchronous state but also, increasing the maximum transmission capacity of a transmission line may also perturb this synchronous state.

In Fig. 4 tree models of power grids are presented, *Model A* which is composed of four generators (G, blue circle) whose power generated by each is $P_G = 1$ and four consumers (C, red square) whose power consumed by each is $P_C = -1$, all transmission lines have the same transmission capacity $P_{max} = 3.2$. *Model B* presents the same topology as Model A but one line has a higher transmission capacity (dashed green) $P_{max}^{green} = 2P_{max}$, in *Model C* all lines have the same transmission capacity but, when comparing to Model A, there is an extra transmission line (dashed black).

When Model A is integrated, one can see that all the phases tend to a constant value 4(d) and that the instantaneous frequency of all nodes tend to the same constant value (zero) 4(g) which indicates that the system is frequency synchronized for this value coupling P_{max} . When doubling the power transmission capacity of just one transmission line (Model B) the synchronous state is lost as the instantaneous frequency of consumers and generators tend to different values. The same behavior of the instantaneous frequency can be observed for Model C when a new transmission line is added to the grid.

Considering now all the three models, we calculate the partial synchronization index given by Eq. 23 for different values of P_{max} , Fig. 4. One can note that Model A is the first to synchronize ($S = 1$) at $P_{max} = 3.1$. Then Model B reaches synchronization at $P_{max} = 3.4$ and, finally, Model C synchronizes at $P_{max} = 3.7$.

3.3 Dynamic vulnerability in power grids

Cascade failure is a sequence of failures and disconnections triggered by an initial event, which can be generated by natural phenomena (strong winds, lightning, etc.), human actions, such as errors in operation or execution, or the appearance of imbalances between load and generation. To mitigate the effects of cascading failure, avoiding the famous blackouts, it is important to identify the points of vulnerability in the transmission networks. Many studies have been carried out associating transmission networks to complex networks and, in this case, centrality measures are used to indicate the most vulnerable nodes and edges. But the topological analysis approach takes into account only the topology of the network and its connections [26], which may not be applicable in a real transmission network, which must guarantee sufficient load flow throughout the system. Thus, other studies analyze points of vulnerability and take into account, in addition to the network topology, the load flow [10, 27, 28].

Another way to locate vulnerability points is with the analysis of the stability of the network as a whole, with the location of nodes or edges that, if disturbed or removed, cause the network to lose its synchronization so that the entire system goes to a blackout. The Work of [29] developed the index DVI (Dynamic Vulnerability Index) to estimates the vulnerability of a node through stochastic signals using the Fourier spectrum of the conduction signal due to its Power Spectral Density characteristics and the nodal response amplitude for each Fourier component. This index can be used to identify vulnerable point exposed by fluctuating inputs from renewable energy sources and fluctuating power output to consumers.

The work of [30] assesses the vulnerability of an electrical network against random and focused disturbances, and uses vulnerability measures in terms of the topological and dynamic properties of nodes and edges of the network. Using a percolation method, nodes and edges are evaluated based on these topological and dynamic indexes. In this way, the network's ability to maintain its functioning after successive removals, randomized or directed by the indexes, is evaluated until it is brought to a complete blackout.

The topological indexes used to measure the vulnerability of the network are based on centrality measures for complex networks. The indexes used are:

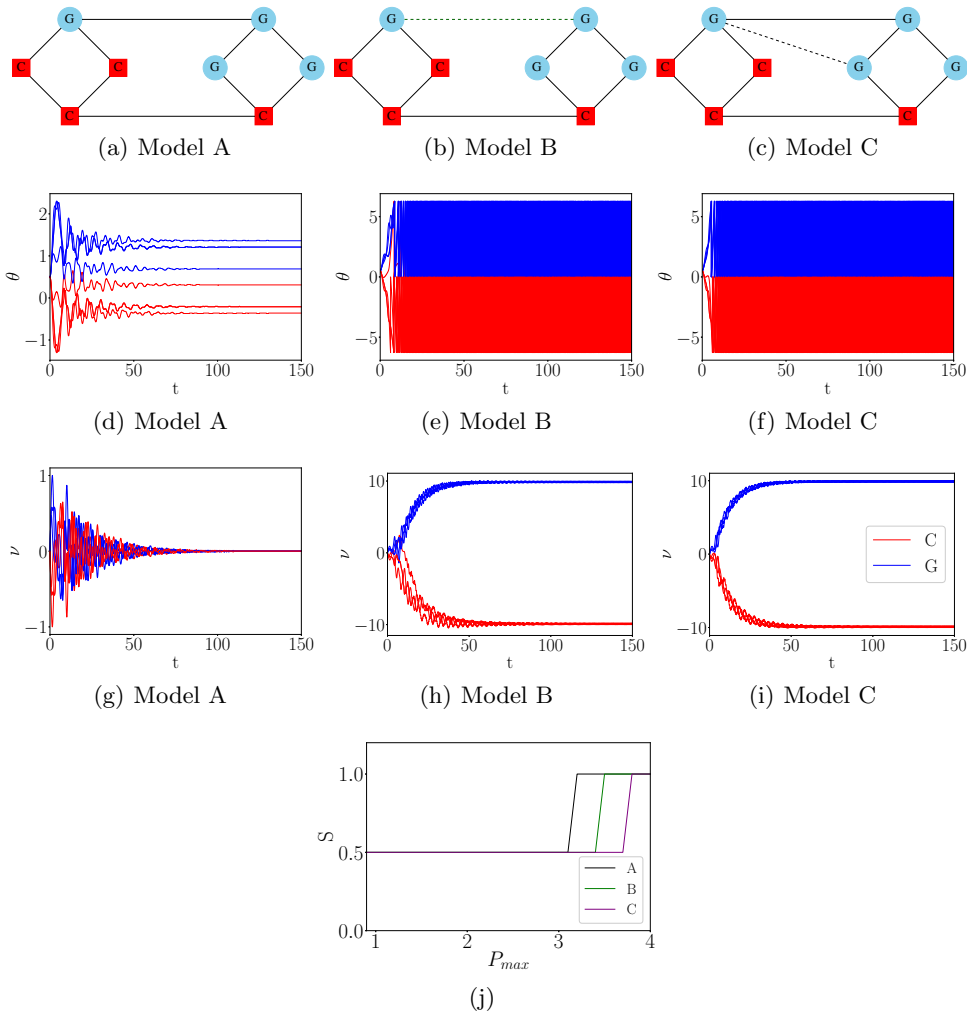


Fig. 4. (a)-(c) Topology power grid models composed of four generators G (circle blue) and four consumers C (square red), where in (b) the power transmitted at the dashed green line is the double of the power transmitted by the same line at (a) and in (c) there is an extra edge (dashed black line) when compared to Model A. (d)-(f) Phases and (g)-(i) instantaneous frequency of all oscillators. (j) Partial synchronization index of Models A (black), B (green) and C (purple) as a function of the maximum capacity of the transmission line.

- Degree centrality $g_k^{(i)}$: measures the number of connections that each node has on the network. This standardized measure is used here [31];
- Clustering coefficient $c_k^{(i)}$: measures the degree to which the nodes of a graph tend to group together [32];
- Node betweenness centrality $b_k^{(i)}$: measures how far a vertex is in the shortest path among other vertices. This measure indicates the node that most shares the information flow in the network[31];
- Edge betweenness centrality $e_k^{(i)}$: similar to the betweenness for a node, but here is measured the importance of the edge for the flow of information[33].

The indices that measure the dynamic vulnerability of nodes and edges use the second-order kuramoto model [9] to capture the synchronization status of the network, as well as the desynchronized points. From this to the vulnerability measure of transmission lines (edges) it can be approximated:

$$\Delta_{\theta} \approx \frac{1}{K} B^T L^{\dagger} P, \quad (25)$$

Where L^{\dagger} is the laplacian pseudo-inverse, B is a incidence matrix, K is the coupling strength and P is the power injected. To guarantee a single and stable solution with synchronized frequencies and cohesive phases if the following condition is met:

$$\|\Delta_{\theta}\|_{\infty} < \sin(\gamma) \quad (26)$$

Edge (i, j) is considered weak when $|\Delta_{\theta}(i, j)|$ is close to 1, and considered more stable when closer to 0, with $0 \leq \gamma < \frac{\pi}{2}$

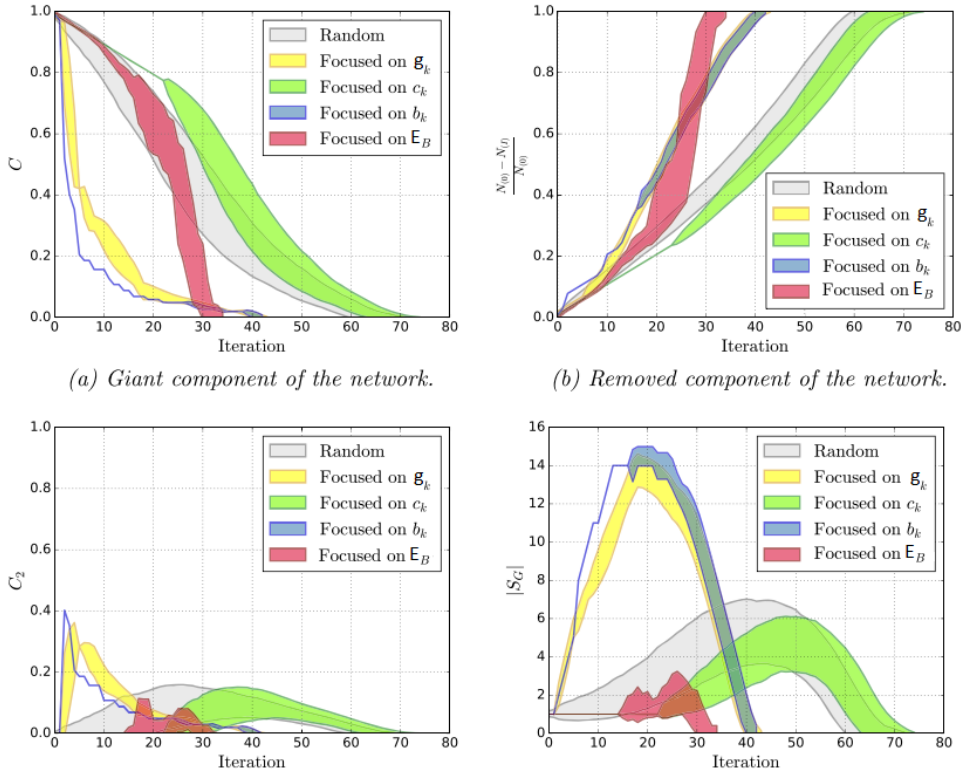


Fig. 5. Result of the nodal elimination algorithm for topological and dynamic indexes. Adapted from [30].

For the vertex, the concept of the single node basin stability is presented in Sub-section 3.1. In this section we call the basin stability of node i $E_B^{(i)}$.

For the tests, a real Colombian energy distribution network with 159 edges and 102 nodes was used, that represent are 28 generators and 74 consumers [30]. A randomly generated network [34] was also used for testes in work of [30], this network simulates

properties of real distribution networks. The results for the topological and dynamics indexes were similar for this two networks.

Using a percolation algorithm [30], Fig. 5 represents the result of the simulation for removing nodes, selected randomly or according to the selection based on the vulnerability indices. Two phase transitions are analyzed during the elimination process. Transition T1: Iteration where the graph has become disconnected, but still functional, with at least 1 generator in each subgraph, and transition 2, which is the final iteration where the blackout is verified.

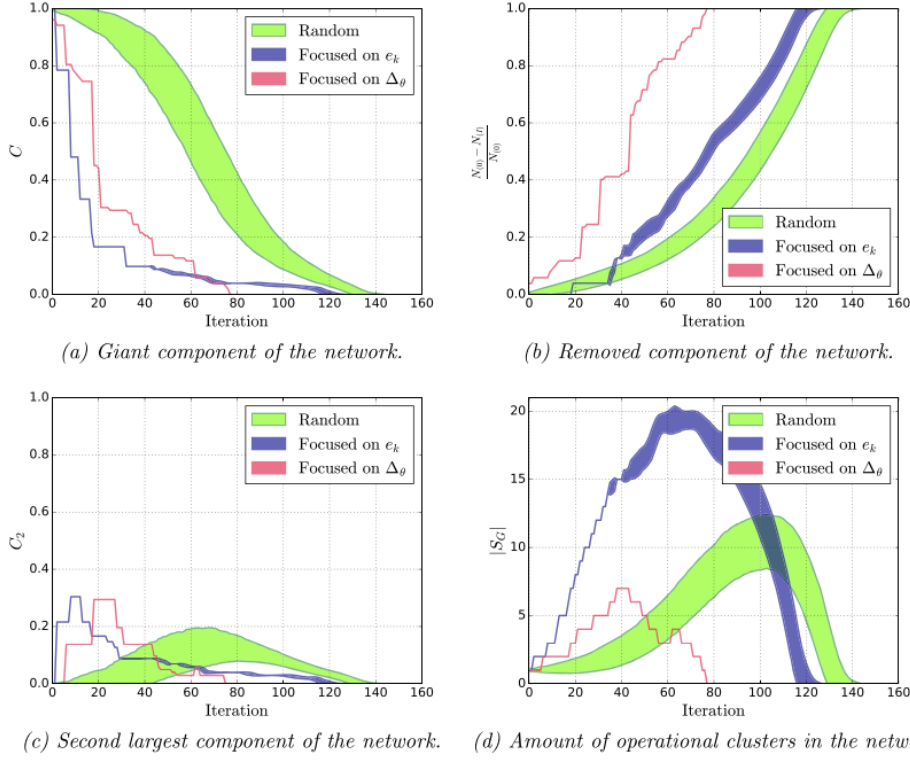


Fig. 6. Result of the edge elimination algorithm for topological and dynamic indexes. Adapted from [30].

Fig. 5(a) shows the fraction of nodes in the largest cluster in the network. Fig. 5(b) shows the fraction of nodes removed after each iteration in relation to the original size, with $N_{(0)}$ and $N_{(I)}$ being the original size of G and its size after I iterations of removal, respectively, which allows detecting the phase transition T2. It is observed as soon as the grid goes to complete blackout around the 30th removal iteration for the case of focal attack in E_B before than other metrics. In Fig. 5(c) it shows the size of the second largest component, that shown the iteration for the T1 transition. And finally, Fig. 5(d) shows the amount of cluster generated, it is verified that the E_B metric generates less cluster compared to the other techniques, since the nodes located in dead-tree present a lower value of basin stability [21].

In Fig. 6, the same analysis is performed to remove the edges (transmission lines) in this Colombian transmission network, where the metrics Δ_θ and e_K are used, as

shown, with the focus on the highest Δ_{Θ} the network reaches the complete state of blackout before the other techniques.

4 Conclusions

In this review, we showed that by making a few assumptions and approximations one can use the second order Kuramoto model to simulate the dynamics of power grids. We then used this model to study the stability and vulnerability of transmission networks. In relation to stability, it was shown that if the system is hit by a large perturbation in a single node, the whole grid may come out of the synchronous state if this perturbation is large enough to take the node out of its basin of attraction. Not only the size of the perturbation matters in this case, as also, the location of the node inside the network also plays an important role as nodes that are adjacent to dead ends and dead trees present a lower value of basin stability. It was further shown that changing the topology of a grid by adding a new transmission line, as well as increasing the power transmission capacity, may destroy the synchronization of the system. A new index to identify vulnerabilities was also introduced, where the index with dynamics properties obtained better results for the indication of edges and nodes vulnerable in comparison to the indexes based only on the network topology.

Acknowledgments

The authors would like to thank Conselho Nacional de Desenvolvimento Científico e Tecnológico - CNPq for the financial support, including grant 307714/2018-7. This research is also supported by grants 2015/50122 and 2018/03211-6 of São Paulo Research Foundation (FAPESP).

References

1. P. Kundur, N. J. Balu, M. G. Lauby, *Power system stability and control* (McGraw-hill, New York 1994) 1-1200
2. P. Pourbeik, P. S. Kundur, S. Prabha, C. W. Taylor, *IEEE Power and Energy Magazine* **4**, (2006) 22-29
3. F. Dorfler, F. Bullo, *SIAM Journal on Control and Optimization* **50**, (2012) 1616-1642
4. G. Filatrella, A. H. Nielsen, N. F. Pedersen, *The European Physical Journal B* **61**, (2008) 485-491
5. R. Carareto, M.S. Baptista, C. Grebogi, *Communications in Nonlinear Science and Numerical Simulation* **18**, (2013) 1035-1046
6. S. Boccaletti, V. Latora, Y. Moreno, M. Chavez, D-U Hwang, *Physics reports* **424**, (2006) 175-308
7. J. Grzybowski, E. Macau, T. Yoneyama, *Chaotic, Fractional, and Complex Dynamics: New Insights and Perspectives*, Springer, New York, (2018) 287-315
8. G. A. Pagani, M. Aiello, *Physica A: Statistical Mechanics and its Applications* **392**, (2013) 2688-2700
9. G. Ódor, B. Hartmann, *Physical Review E* **98**, (2018) 022305
10. Chopade, Pravin and Bikdash, Marwan, *International Journal of Critical Infrastructure Protection* **12**, (2016) 29-45
11. Cuadra, Lucas and Salcedo-Sanz, Sancho and Del Ser, Javier and Jiménez-Fernández, Silvia and Geem, Zong Woo. *Chaos: An Interdisciplinary Journal of Nonlinear Science* **19**, (2009) 013119

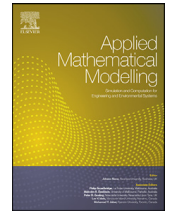
12. Nitzbon, Jan and Schultz, Paul and Heitzig, Jobst and Kurths, Jürgen and Hellmann, Frank. *New Journal of Physics* **19**, (2017) 033029
13. Cuadra, Lucas and Salcedo-Sanz, Sancho and Del Ser, Javier and Jiménez-Fernández, Silvia and Geem, Zong Woo, *Energies* **8**, (2015) 9211-9265
14. F. A. Rodrigues, T. K. Peron, P. Ji, J. Kurths, *Physics Reports* **610**, (2016) 1-98
15. J. M. V. Grzybowski, E. E. N. Macau, T. Yoneyama, *Chaos: An Interdisciplinary Journal of Nonlinear Science* **26**, (2016) 113113
16. H. Tanaka, A. J. Lichtenberg, S. Oishi, *Physical review letters* **78**, (1997) 2104
17. H. Tanaka, A. J. Lichtenberg, S. Oishi, *Physica D: Nonlinear Phenomena* **100**, (1997) 279-300
18. J. Gómez-Gardenes, Y. Moreno, A. Arenas, *Physical review letters* **98**, (2007) 034101
19. B. Daniels, *Ohio Wesleyan Physics Dept.* **7**, (2005) 20
20. J. P. Menck, J. Heitzig, N. Marwan, J. Kurths, *Nature physics* **9**, (2013) 89
21. P. J. Menck, J. Heitzig, J. Kurths, H. J. Schellnhuber, *Nature communications* **5**, (2014) 3969
22. D. A. Wiley, S. H. Strogatz, M. Girvan, *Chaos: An Interdisciplinary Journal of Nonlinear Science* **16**, (2006) 015103
23. N. Metropolis, S. Ulam, *Journal of the American statistical association* **44**, (1949) 335-341
24. D. Braess, *Unternehmensforschung* **12**, (1968) 258-268
25. D. Witthaut, M. Timme, *New journal of physics* **14**, (2012) 083036
26. Xu, Shouzhi and Zhou, Huan and Li, Chengxia and Yang, Xiaomei. 2009 Asia-Pacific Power and Energy Engineering Conference, **1**, (2009) 1-4
27. Cavaleri, Francesco and Franchin, Paolo and Buriticá. *Computer-Aided Civil and Infrastructure Engineering*, **29**, (2014) 590-607
28. Gutierrez, Francisco and Barocio, E and Uribe, F and Zuniga, P. *Discrete Dynamics in Nature and Society*, **2013**, (2013) 1-12
29. Zhang, Xiaozhu and Ma, Cheng and Timme, Marc. *Chaos: An Interdisciplinary Journal of Nonlinear Science*, **30**, (2020) 063111
30. Galindo-González, Cristian Camilo and Angulo-García, David and Osorio, Gustavo. *New Journal of Physics*, **22**, (2020) 103033
31. Freeman, Linton C. *Sociometry*, **1**, (1977) 35-41
32. Costa, L da F and Rodrigues, Francisco A and Travieso, Gonzalo and Villas Boas, Paulino Ribeiro. *Advances in physics*, **56**, (2007) 167-242.
33. Vukičević, Damir and Škrekovski, Riste and Tepeh, Aleksandra. *Ars Mathematica Contemporanea*, **12**, (2016) 261-270
34. Schultz, Paul and Heitzig, Jobst and Kurths, Jürgen. *The European Physical Journal Special Topics*, **223**, (2014) 2593-2610

**APPENDIX B - SYNCHRONIZATION OF ENERGY TRANSMISSION
NETWORKS AT LOW VOLTAGE LEVELS**



Contents lists available at ScienceDirect

Applied Mathematical Modelling

journal homepage: www.elsevier.com/locate/apm

Synchronization of energy transmission networks at low voltage levels

Juliana C. Lacerda^{a,*}, Jussara Dias^a, Celso Freitas^a, Elbert Macau^b^a Associated Laboratory for Computing and Applied Mathematics, National Institute for Space Research, INPE, São José dos Campos, SP 12243-010, Brazil^b Institute of Science and Technology, Federal University of São Paulo, São José dos Campos, SP 12247-014, Brazil

ARTICLE INFO

Article history:

Received 29 April 2020

Revised 24 June 2020

Accepted 12 July 2020

Available online 6 August 2020

Keywords:

Power grid

Synchronization

Kuramoto model

ABSTRACT

Power grids or energy transmission networks are among the biggest and more complex man made constructions ever made and are a typical example of a complex system. Its components need to be in a synchronous state in order to be fully functional and avoid cascade failures and blackouts. Power grids can be modeled as a complex network of oscillators, where each node represents a generator or a consumer and the transmission lines are represented by edges. In this work, we show how to build a power grid topology that presents relatively low number of edges and favors synchronization as a low value of coupling is required to reach the synchronous state. As the coupling is related to the maximum transmission capacity of a transmission line, lower coupling in this context means lower voltage levels. The basin stability of this network is also calculated as it appears to have a higher quantity of stable nodes when compared to a random network. The methodology presented in this work is based on an evolutionary optimization framework and would be of great interest when building power grids due to the costs involved in the construction of transmission lines, as there would be less lines and they would be required to operate in a lower voltage level.

© 2020 Elsevier Inc. All rights reserved.

1. Introduction

Power transmission systems are crucial to economic prosperity worldwide as interruptions in the transmission and generation in electricity networks can cause economic and social problems for the whole society [1]. Power grids are naturally complex as they are one of the biggest constructions ever made, and, in order to be fully functional, all of its components must be in a synchronous state and they must be robust enough to go back to this state even when subjected to failures and disturbances [2], which represents an enormous challenge for stability analysis. Therefore, engineers and researchers must be able to accurately analyze the stability of power systems taking into consideration scenarios that can cause disturbances in the network implying local failures and in some cases, blackouts of high proportions [3].

Instabilities in power grids can be caused, for example, by the malfunctioning of some of its components, due to climatic factors such as fire, rain and lightning [4,5] or if a renewable source of energy becomes unavailable [6] due to its proper characteristics. Interruptions in energy transmission due to climatic problems have a great impact on the network infrastructure, being considered one of the main causes of problems in power grids world wide [5]. The growing integration of

* Corresponding author.

E-mail addresses: juliana.lacerda@inpe.br (J.C. Lacerda), elbert.macau@unifesp.br (E. Macau).

renewable energy sources in transmission networks is stimulated by environmental and economic issues. Microgrid is one of the technologies that can integrate large amounts of renewable energy such as solar, wind and geothermal systems, and fulfills the distributed generation potential of a system [7]. However, the generation of renewable energy is intermittent, stochastic and subject to climatic conditions, so it can cause unforeseen fluctuations in the system and is one of the major causes of instability in transmission networks today [8].

A way to properly study power grids is by using the concepts of complex networks. In this representation, the transmission lines are modeled by edges and the generators and consumers are represented by nodes. The second order Kuramoto model is often applied in frequency synchronization problems, for example, in networks of electric power transmission [9] and forced pendulum dynamics [10] and is used in this work to describe the dynamics of generators and consumers. In this model, the coupling constant relates to the maximum power transmission capacity of the transmission lines, while the phase and the angular velocity evolve as time passes and the synchronization is damped by a term of inertia [11].

By using the second order Kuramoto model to study power grids, a model of basin stability in relation to strong perturbations was proposed in order to study the stability of electric networks that also may be applied to other dynamical systems [12]. It was shown that there are some patterns called dead ends and dead trees in power grids that reduce the overall dynamic stability of the system [13].

The evolutionary optimization technique called evolutionary edge-snapping [14,15] is used in this work to generate a network topology that favors synchronization for rather small values of coupling. This method creates networks with a relatively small number of edges and these topologies would be of great interest in designing of power grids, due to the costs involved in the construction of transmission lines. Further, as the system enters the synchronous state at a low coupling (compared to the coupling obtained when studying a random network with the same number of nodes and edges), it means that lower voltage levels are needed in the transmission lines [16,17], which is also a desirable characteristics. After studying and analyzing the behavior of the power grid topology created by the Edge Snapping method, we use the one-node basin stability method [13] to analyze the stability of this topology when subjected to large perturbations. We find that this network appears to have a higher number of stable nodes when compared to a random network.

2. Model and methods

In this section, we present the model used to describe the dynamics of the components (generator and consumers) of a power grid, metrics to quantify the level of synchronization of this system, both in Section 2.1, and a model to generate topologies of power grids in Section 2.2. In Section 2.3, a method to study the stability of the components of this power grid is presented.

2.1. Synchronization metrics and second order Kuramoto model

In order for a power grid to be fully functional, all of its components must be frequency synchronized [2]. So we begin this section by presenting metrics that quantify the level of synchronization of a dynamical system. The *order parameter* $R(t)$ [18] shows the level of the collective behavior of a system by measuring the amount of phase synchronization. It is defined as

$$R(t) = \left| \frac{1}{N} \sum_{m=1}^N e^{i\theta_m(t)} \right|, \quad (1)$$

where i is the imaginary unit, $\theta(t)$ is the phase of oscillator m and N is the total number of nodes. $R(t) \in [0, 1]$, in a way that when all oscillators have the same phase, that is, when the system presents phase synchronization, $R(t) = 1$. The mean over time of the order parameter $R(t)$ will be called R .

The parameter *partial synchronization index* [19] presents the level of the frequency synchronization (or phase locking) [20,21] between a pair of a system' units and is given by

$$S_{mn} = \left| \lim_{\Delta t \rightarrow \infty} \frac{1}{\Delta t} \int_{t_r}^{t_r + \Delta t} e^{i[\theta_m(t) - \theta_n(t)]} dt \right|, \quad (2)$$

where m and n are the label of the nodes and t_r is a transient time. In order to measure the level of frequency synchronization of the whole network, we calculate the arithmetic mean

$$S = \frac{1}{N^2} \sum_{m,n=1}^N S_{mn}. \quad (3)$$

$S \in [0, 1]$ and when $S = 1$, the system is phase locked, meaning that the phase difference between all pair of nodes is constant through time, thus having the same instantaneous frequency.

In order for power to flow in a power grid, there must be a phase difference between the components of the grid [11]. So, we want our system to be phase locked, thus having the same instantaneous frequency, and not phase synchronized, that is, we want $S = 1$ and $R \neq 1$, and we will be referring to this configuration when we say that the system is synchronized.

In order to model the dynamics of generators and consumers, we make use of the second order Kuramoto model [22] in a way that the dynamics of a power grid component m is given by:

$$\ddot{\theta}_m = -\alpha \dot{\theta}_m + \omega_m + \frac{\lambda}{g_m} \sum_{n=1}^N A_{mn} \sin(\theta_n - \theta_m), \tag{4}$$

for $m = 1, \dots, N$, $\alpha \in \mathbb{R}$ is the dissipation parameter ($\alpha = 0.1$ is used in this work), λ is the coupling constant and it represents the maximum power transmission capacity of the transmission line that connects the nodes in a power grid (note that λ is the same for our entire network), ω_m is the natural frequency of oscillator m and here it represents the amount of power delivered by ($\omega_m > 0$, generator) or consumed by ($\omega_m < 0$, consumer) node m , g_m and θ_m are the degree and phase of oscillator m , respectively. The degree g of a node m represents the number of edges that are incident to this node. A_{mn} are the entries of the adjacency matrix, being equal to 1 if oscillators m and n are connected (there is a transmission line between them) and 0 otherwise. Eq. (4) can be also written as:

$$\dot{\theta}_m = \nu_m, \tag{5}$$

$$\dot{\nu}_m = -\alpha \nu_m + \omega_m + \frac{\lambda}{g_m} \sum_{j=1}^N A_{mj} \sin(\theta_j - \theta_m), \tag{6}$$

where ν_m is the angular velocity (instantaneous frequency) of node m .

The phase and the angular velocity of a node m in the synchronous state are defined as (θ_m^S, ν_m^S) . The phase in the synchronous state is [13,23]

$$\theta_m^S = \arcsin \frac{\omega_m}{\lambda}, \tag{7}$$

and the synchronous angular velocity is given by [9,11]

$$\nu_m^S = \sum_{m=1}^N \frac{\omega_m}{N\alpha}. \tag{8}$$

In this work, there are $\frac{N}{2}$ consumers ($\omega_m < 0$) and $\frac{N}{2}$ generators ($\omega_m > 0$) in a way that all power generated is consumed, so $\sum_{m=1}^N \omega_m = 0$ and, therefore, $\nu_m^S = \nu^S = 0$.

2.2. Edge snapping method

The *edge snapping method* [14,24] is used in this work in order to generate topologies that model a power grid. This method is an adaptive strategy that drives the evolution of an unweighted network, in which a second order equation is associated with each edge of the graph. It has been chosen because it generates networks with a relatively low number of edges (transmission lines) [24] and, as will be presented in Section 3, it allows the network to be synchronized at lower values of coupling, thus requiring transmission lines with lower maximum transmission capacity, which, along with the lower number of transmission lines, would be economically desirable.

The equation associated with the edge between nodes m and n is given by

$$\ddot{k}_{mn} + d\dot{k}_{mn} + \frac{\partial V(k_{mn})}{\partial k_{mn}} = h(|\theta_m - \theta_n|), \tag{9}$$

where $d = 1$ is a constant damping factor, h is an external force and k_{mn} is the coupling gain. $V(k_{mn})$ is a double-well potential given by

$$V(k_{mn}) = bk_{mn}^2(k_{mn} - 1)^2, \tag{10}$$

in which $b = 1$ is a constant. $V(k_{mn})$ has two local minima, $k_{mn} = 0$ and $k_{mn} = 1$, in a way that if $k_{mn} = 1$ we define that there is an edge between nodes m and n and if $k_{mn} = 0$ there is not. At the beginning of evolution of Eq. (9), all nodes are disconnected and the initial conditions are $k_{mn}(0) = 0$ and $\dot{k}_{mn}(0) = 0$. Due to the external force h , k_{mn} may come out of its initial equilibrium point $k_{mn} = 0$ (edge is not present) and move to the other local minima $k_{mn} = 1$ (edge is present). The external force in this work is defined as $h(|\theta_m - \theta_n|) = 1 - |\theta(m) - \theta(n)|$.

By using the edge snapping method to generate network topologies, the second order Kuramoto model is written as

$$\ddot{\theta}_m = -\alpha \dot{\theta}_m + \omega_m + \frac{\lambda}{g_m} \sum_{n=1}^N k_{mn} \sin(\theta_n - \theta_m). \tag{11}$$

Note that the only difference between Eqs. (4) and (11) is that in the latter the adjacency matrix A is replaced by the coupling gain k given by Eq. (9). So, in order to study the dynamics of our power grid, we integrate Eqs. (9) and (11) simultaneously.

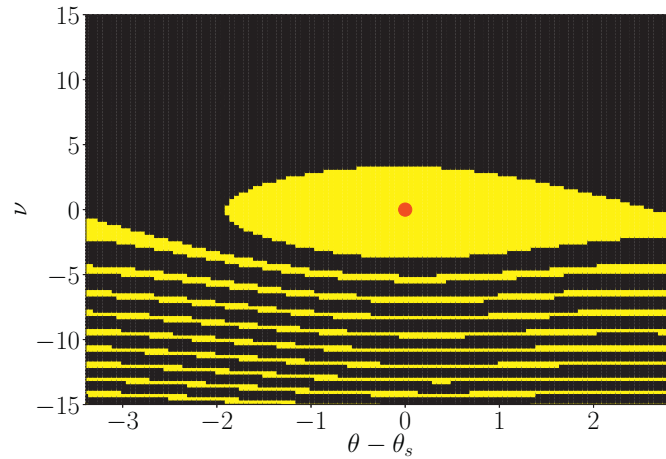


Fig. 1. Basin of attraction (yellow) of a single node dynamics given by Eq. (13). The synchronous state $(\theta_m^S, 0)$ is plotted as a red dot. (For interpretation of the references to color in this figure legend, the reader is referred to the web version of this article.)

2.2.1. Evolutionary edge snapping

The edge snapping method is used in the context of evolutionary optimization where rules of variation and selection are applied in order to generate network topologies. The evolutionary edge snapping is composed of two fundamental rules [15,24]:

Rule 1 – Variation: A set of $n_T = 100$ network topologies is generated by integrating Eqs. (9) and (11), with Eq. (11) starting from n_T distinct initial conditions that are randomly generated by a uniform distribution between $[0, 2\pi)$. From this set of n_T topologies, we calculate the fraction between the number of networks where the edge between the nodes m and n is present (n_{mn}) and the total number of topologies that were generated. This fraction is the probability of activation of the edge between nodes m and n

$$F_{mn} = \frac{n_{mn}}{n_T}, \tag{12}$$

where $0 \leq F_{mn} \leq 1$.

Rule 2 – Selection: Only edges with activation probability F_{mn} higher than a certain threshold f^* are marked as active (are present) in the network. The value of f^* is chosen in a way that the entire network is connected and present the smallest possible number of edges, we call this network *minimal edge-snapping network (ES network)*.

2.3. Basin stability

A basin of attraction B is the set of initial conditions that, as the system evolves in time, tends to an attracting fixed point [10]. In order to visualize the basin of attraction of a node m in a power grid, consider a single node dynamics given by

$$\begin{aligned} \dot{\theta}_m &= \nu_m, \\ \dot{\nu}_m &= -\alpha \nu_m + \omega_m + \lambda \sin(\theta_{grid} - \theta_m), \end{aligned} \tag{13}$$

where $\theta_{grid} = 0$, as we consider that the rest of the network is not affected by node m . In order to find the basin of attraction, we integrate Eq. (13) fixing $\lambda = 4.0$ and $\omega = 1.0$ for distinct values of initial conditions $(\theta(0), \nu(0))$, where $\theta \in [0, 2\pi]$ and $\nu \in [-15, 15]$ and annotate for which conditions the system evolved to the synchronous state $(\theta_m^S, \nu^S = 0)$. This basin of attraction can be seen in Fig. 1, it is colored in yellow and the red dot represents the attracting fixed point describing the synchronous state.

Looking from another perspective, we can assume that at a time t_1 , node m is at the synchronous state $(\theta_m(t_1), \nu_m(t_1)) = (\theta_m^S, 0)$ and suffers a perturbation at time t_2 in a way that $(\theta_m(t_2), \nu_m(t_2)) \neq (\theta_m^S, 0)$. So, if $(\theta_m(t_2), \nu_m(t_2))$ is outside of the basin of attraction, the node will not go back to the synchronous state, and, on the other hand, if $(\theta_m(t_2), \nu_m(t_2))$ is inside the basin of attraction, the dynamics of the node will reach the synchronous state after a certain amount of time.

The single-node basin stability method [13] is applied in study of the stability of the second order Kuramoto network generated by the Edge Snapping method. The basin stability E of a node m is defined as

$$E_m = E(B_m) = \int \chi_B(\theta, \nu) \rho(\theta, \nu) d\theta d\nu, \tag{14}$$

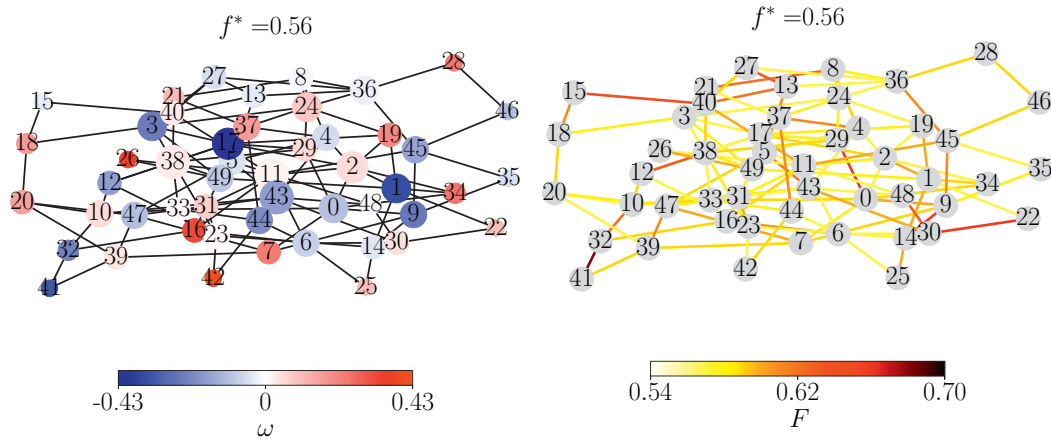


Fig. 2. 50 node ES network with threshold $f^* = 0.56$ and 108 edges. (a) The size of the nodes is proportional to their degree and their color relates to the consumed (blue) or delivered (red) power ω . (b) Probability of activation F of the edges. (For interpretation of the references to color in this figure legend, the reader is referred to the web version of this article.)

where ρ is a probability density ($\int \rho(\theta, \nu) d\theta d\nu = 1$) related to the states that the system can reach due to perturbations and in order to perform our calculations, ρ is defined as

$$\rho = \begin{cases} \frac{1}{|Q|}, & \text{if } (\theta, \nu) \in Q, \text{ where } Q = [0, 2\pi] \times [-100, 100], \\ 0, & \text{otherwise.} \end{cases} \tag{15}$$

χ_B is the indicator function of the basin of attraction B and is given by

$$\chi_B = \begin{cases} 1, & \text{if } (\theta_m, \nu_m) \in B_m. \\ 0, & \text{otherwise.} \end{cases} \tag{16}$$

The basin of attraction B_m in our context is defined as

$$B_m = \{(\theta_m(0), \nu_m(0)) \text{ where } \lim_{t \rightarrow +\infty} \theta_m(t) = \theta_m^S \text{ and } \lim_{t \rightarrow +\infty} \nu_m(t) = 0 : (\theta_n(0), \nu_n(0))_{n=1, \dots, N} \in B \text{ with } \theta_n(0) = \theta_n^S \text{ and } \nu_n(0) = 0 \text{ for all } n \neq m\}, \tag{17}$$

which is a two-dimensional section of the 2N-dimensional synchronous state basin B .

The basin stability E_m express the chance of the system’s component m to return to the synchronous state after a single node perturbation that occurs randomly with a probability density ρ . If $E_m = 0$, the synchronous state is unstable and if $E_m = 1$, the synchronous state is globally stable. In order to estimate E_m we use the Monte-Carlo method [25], where for each node, $T = 100$ initial states $(\theta_m(0), \nu_m(0))$ are chosen randomly according to ρ and their trajectories in phase space are calculated and the number U_m of times in which the system converges to the synchronous state is annotated. The other $N - 1$ nodes have a fixed initial condition $(\theta_n(0), \nu_n(0)) = (\theta_n^S, 0)$ for all $n \neq m$. The basin stability is then $E_m \approx \frac{U_m}{T}$ which has a standard error [12] of $e = \sqrt{\frac{E - E^2}{T}} \leq 5\%$.

3. Results and discussion

We use the Edge Snapping method by simultaneously integrating Eqs. (9) and (11) with a fixed coupling $\lambda = 1.5$ to generate a $N = 50$ node network whose delivered or consumed power ω are given by a Gaussian distribution with zero mean and standard deviation $\sigma_\omega = 0.2$ in a way that $\frac{N}{2}$ nodes have their frequencies set randomly by this distribution and $\frac{N}{2}$ nodes have the exact opposite frequency, so all the power generated is consumed and $\sum_{m=1}^N \omega_m = 0$. The topology of this network is plotted in Fig. 2 where in Fig. 2(a) the size of the nodes is proportional to their degree and the color relates to the amount of power ω delivered (red) or consumed (blue), while in Fig. 2(b) the probability of activation F is represented by edge colors, as the threshold for this configuration is $f^* = 0.56$, leaving the final topology with 108 edges. This is a relatively low number of edges as only a fraction of 0.08817 of all possible edges were marked as active in the final topology. It is a characteristics of the Edge snapping method to generate networks with a relatively low number of edges, which is an advantage when it comes to power grids due to the costs involved in the construction of transmission lines.

The degree of the nodes as a function of their power ω is plotted in Fig. 3(a). Let $|\omega_{mn}| = |\omega_m - \omega_n|$ be the absolute value of power difference between nodes m and n , in Fig. 3(b) the probability of activation of the edge connecting nodes m and n is plotted as a function of $|\omega_{mn}|$. The degree g of the nodes seem to be distributed mostly at random, as for the probability of activation F , it does not display a well defined behavior, although there is roughly a band-like structure and as $|\omega_{mn}|$ grows, the band structure gets narrower. The behavior of the degree and the probability of activation found

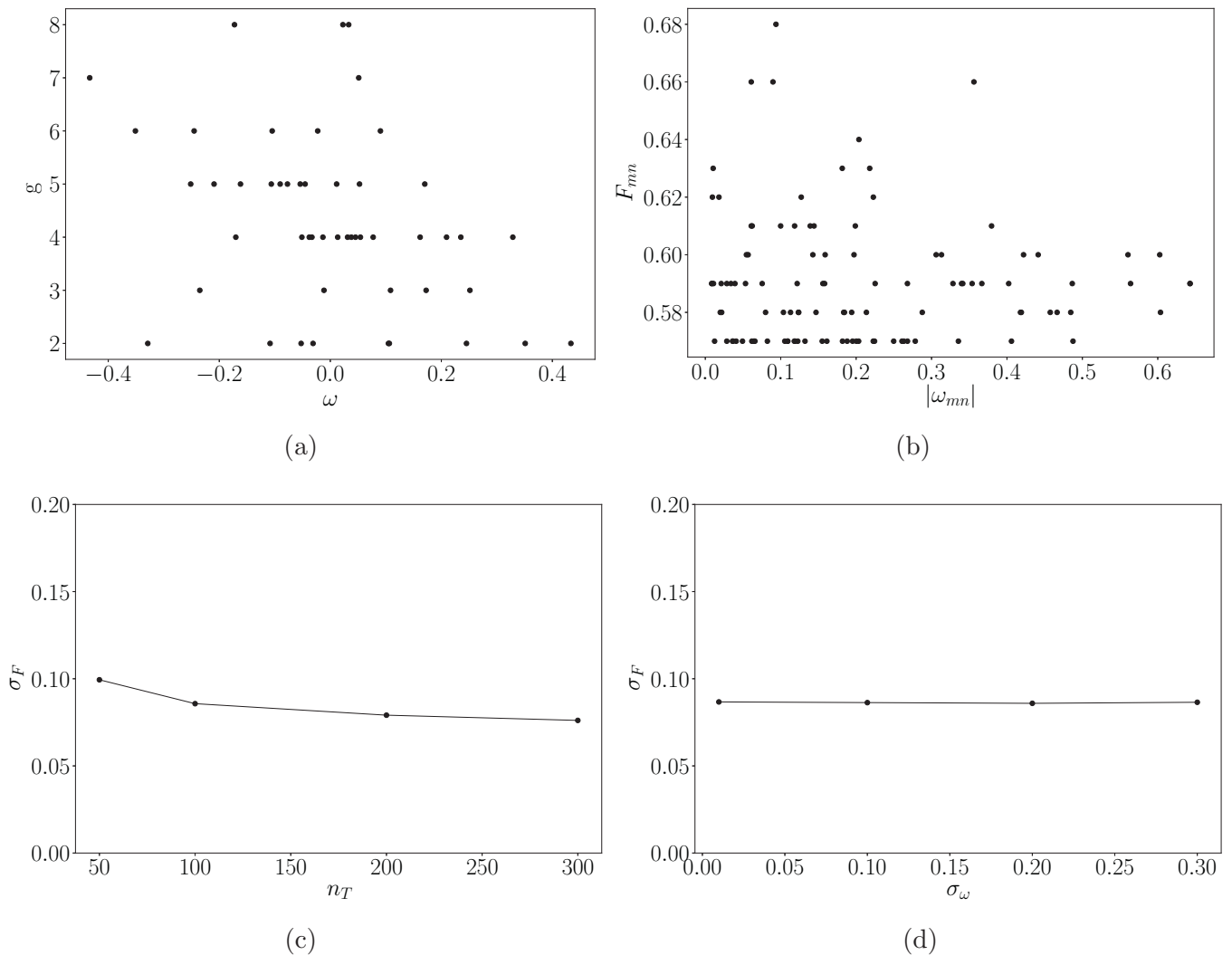


Fig. 3. (a) Node degree distribution as a function of the power ω . (b) Probability of activation F as a function of the power difference between nodes m and n . (c) Standard deviation of the matrix F as a function of the number of topologies n_T . (d) Standard deviation of F as a function of the standard deviation of the Gaussian distribution used to generate the power distribution ω .

here is the opposite of what was found in [15] by using the Edge Snapping method along with the first order Kuramoto model and, most importantly, the distribution of ω was given randomly by the same distribution used here but without the condition $\sum_{m=1}^N \omega_m = 0$. So, in [15], it is shown that the degree and the probability of activation are related to ω , in a way that the nodes with the value of ω far from the mean have higher degree and the probability of activation of the edges are greater for higher values of $|\omega_{mn}|$. We also obtained this behavior for both measures in our simulations for the second order Kuramoto model but when the condition $\sum_{m=1}^N \omega_m = 0$ is added to the distribution of power, this correlation seems to be lost. This condition is of utmost importance in this work as we are simulating a power grid in which all power generated is consumed.

Two parameters were fixed in our simulations, the standard deviation of the Gaussian distribution of ω , $\sigma_\omega = 0.2$, and the number of trials $n_T = 100$ used in the Evolutionary Edge Snapping, which gives the number of network topologies generated in order to calculate the matrix of the probability of activation F . The standard deviation of this matrix F as a function of the number of trials and as a function of the standard deviation of ω are plotted in Fig. 3(c) and (d), respectively. Note that σ_F does not vary much in both cases, so we consider the values of n_T and σ_ω we chose to be satisfactory.

Now that the network topology is defined, our interest is to study how it affects the synchronization of the power grid and in order to make some kind of comparison to see how efficient the ES network is, a random network with the same number nodes (50), edges (108) and with the same power distribution is generated, we name it Random network (since there is no consense when it comes to a network model that can fully represent a power grid topology, several researchers use the random model [26] to represent power grids as they both present exponential degree distribution [13,27]). Eq. (5) is integrated for both topologies, for several values of coupling λ in order to calculate the order parameter R and the partial synchronization index S . The initial conditions are fixed as $\theta_m(0) = 0.5$ and $v_m(0) = 0$ for $m = 1, \dots, N$. The result can be seen in Fig. 4. The ES network reaches phase locking $S = 1$ at $\lambda = 0.60$ and the Random network reaches synchronization for

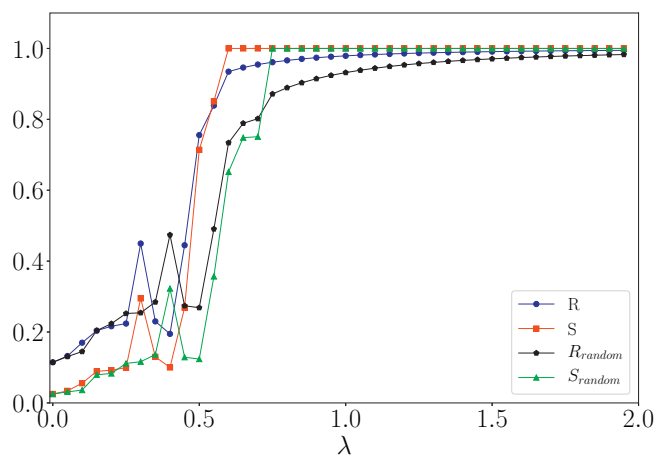
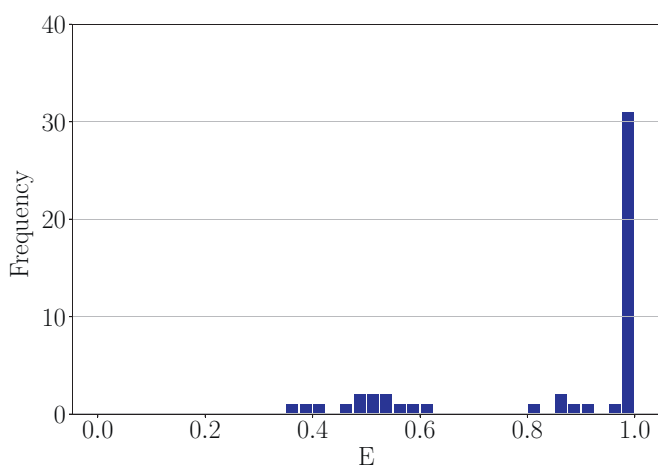
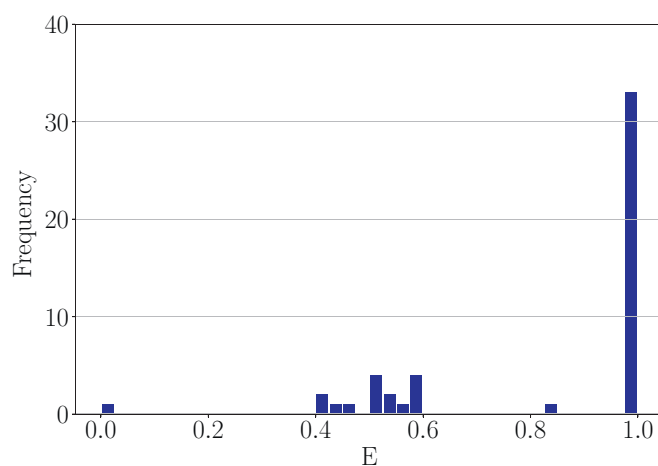


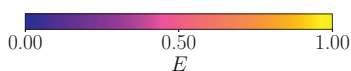
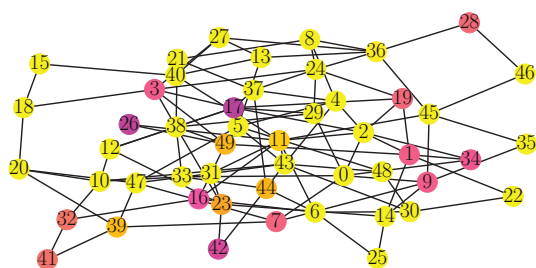
Fig. 4. Order parameter R (blue circle), partial synchronization index S (red square) of the ES network and order parameter (black hexagon) and partial synchronization index (green triangle) of the Random network as a function of the maximum power transmission capacity λ . (For interpretation of the references to color in this figure legend, the reader is referred to the web version of this article.)



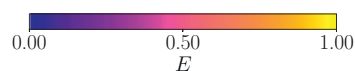
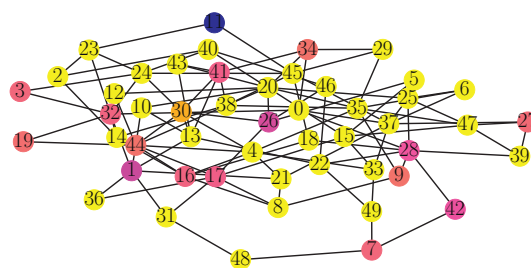
(a)



(b)



(c)



(d)

Fig. 5. Histogram of the basin stability for the (a) ES network and for the (b) Random network. Basin stability of each node for the (c) ES and (d) Random networks.

$\lambda = 0.75$. Note that for higher values of coupling the value of the order parameter R is close but never equal to one, which is expected because, as mentioned in Section 2.1, it is a condition to have a power flow between two nodes of a power grid. The advantage of reaching synchronization at lower values of coupling comes from the fact that the coupling represents the maximum power transfer capacity of a transmission line and, therefore, lower transfer capacity means lower voltage levels and cheaper transmission lines when building power grids.

In order to study the stability of the ES network topology we use the basin stability method presented in Section 2.3, where at a fixed value of coupling ($\lambda = 1.5$) a single node m suffers a perturbation $T = 100$ times. Let U_m be the number of times the system reaches synchronization, then the basin stability of node m is approximately $E_m = \frac{U_m}{T}$. The same is done for the Random network. The histogram and the value of the basin stability of each node for both networks and can be seen in Fig. 5. Note that for the ES network, 74% of the nodes present a relatively high stability, that is, $E \geq 0.8$, as for the Random network, this value drops to 68%.

4. Conclusions

In this paper, we used the Edge Snapping method to generate power grids whose generator and consumers are modeled by the second order Kuramoto oscillator model. A fifty node power grid was generated, being that half of the nodes were set to be consumers and the other half generators in a way that all power produced is consumed by the grid. The topologies generated by the Edge Snapping method have a characteristic of having a relatively low number of nodes, which is desirable in our case study since it means building less transmission lines. Also, the network generated by this method favors synchronization in a way that it reaches phase locking at a lower value of coupling when compared to a random network with the same number of nodes and edges. As the coupling in the second order Kuramoto model is related to the maximum transmission capacity of a transmission line, lower coupling implies lower voltage levels in the transmission lines which is also a desirable characteristics in a power grid. The ES network presented a higher number of stable nodes when compared to the random network of the same size.

Acknowledgments

Juliana C. Lacerda and Jussara Dias would like to thank Conselho Nacional de Desenvolvimento Científico e Tecnológico – CNPq for the financial support. This research is also supported by grant 2015/50122-0 of São Paulo Research Foundation (FAPESP) and DFG-IRTG 1740/2.

References

- [1] Y. Koç, M. Warnier, R.E. Kooij, F.M. Brazier, An entropy-based metric to quantify the robustness of power grids against cascading failures, *Saf. Sci.* 59 (2013) 126–134.
- [2] J. Grzybowski, E.E. Macau, T. Yoneyama, Power-grids as complex networks: emerging investigations into robustness and stability, in: *Chaotic, Fractional, and Complex Dynamics: New Insights and Perspectives*, Springer, 2018, pp. 287–315.
- [3] H. Haes Alhelou, M.E. Hamedani-Golshan, T.C. Njenda, P. Siano, A survey on power system blackout and cascading events: Research motivations and challenges, *Energies* 12 (4) (2019) 682.
- [4] M. Panteli, P. Mancarella, Influence of extreme weather and climate change on the resilience of power systems: Impacts and possible mitigation strategies, *Electr. Power Syst. Res.* 127 (2015) 259–270.
- [5] D.M. Ward, The effect of weather on grid systems and the reliability of electricity supply, *Clim. Change* 121 (1) (2013) 103–113.
- [6] D. Infield, L. Freris, *Renewable Energy in Power Systems*, John Wiley & Sons, 2020.
- [7] P. Piagi, R.H. Lasseter, Autonomous control of microgrids, in: *Proceedings of the 2006 IEEE Power Engineering Society General Meeting*, 2006, p. 8.
- [8] L. Zhu, D.J. Hill, Synchronization of Power Systems and Kuramoto Oscillators: A Regional Stability Framework, arXiv preprint arXiv:1804.01644 (2018).
- [9] J. Grzybowski, E. Macau, T. Yoneyama, On synchronization in power-grids modelled as networks of second-order Kuramoto oscillators, *Chaos: Interdiscip. J. Nonlinear Sci.* 26 (11) (2016) 113113.
- [10] S.H. Strogatz, *Nonlinear Dynamics and Chaos*, Westview Press, Boulder, 2014.
- [11] G. Filatrella, A.H. Nielsen, N.F. Pedersen, Analysis of a power grid using a Kuramoto-like model, *Eur. Phys. J. B* 61 (4) (2008) 485–491.
- [12] P.J. Menck, J. Heitzig, N. Marwan, J. Kurths, How basin stability complements the linear-stability paradigm, *Nat. Phys.* 9 (2) (2013) 89.
- [13] P.J. Menck, J. Heitzig, J. Kurths, H.J. Schellnhuber, How dead ends undermine power grid stability, *Nat. Commun.* 5 (2014) 3969.
- [14] P. DeLellis, F. Garofalo, M. Porfiri, et al., Evolution of complex networks via edge snapping, *IEEE Trans. Circuits Syst. I: Regul. Pap.* 57 (8) (2010) 2132–2143.
- [15] F. Scafuti, T. Aoki, M. di Bernardo, Heterogeneity induces emergent functional networks for synchronization, *Phys. Rev. E* 91 (6) (2015) 062913.
- [16] P. Kundur, N.J. Balu, M.G. Lauby, *Power System Stability and Control*, 7, McGraw-Hill New York, 1994.
- [17] A. Monticelli, A. Garcia, *Introdução a Sistemas de Energia Elétrica*, Editora UNICAMP, 2011.
- [18] B.C. Daniels, Synchronization of Globally Coupled Nonlinear Oscillators: The Rich Behavior of the Kuramoto Model, Ohio Wesleyan Physics Dept., *Essayvol.* 7(2) (2005).
- [19] J. Gómez-Gardenes, Y. Moreno, A. Arenas, Paths to synchronization on complex networks, *Phys. Rev. Lett.* 98 (3) (2007) 034101.
- [20] J.C. Lacerda, C. Freitas, E.E. Macau, Symbolic dynamical characterization for multistability in remote synchronization phenomena, *Front. Appl. Math. Stat.* 6 (2020) 15.
- [21] J. Lacerda, C. Freitas, E. Macau, Multistable remote synchronization in a star-like network of non-identical oscillators, *Appl. Math. Model.* 69 (2019) 453–465.
- [22] G. Ódor, B. Hartmann, Heterogeneity effects in power grid network models, *Phys. Rev. E* 98 (2) (2018) 022305.
- [23] M. Rohden, A. Sorge, M. Timme, D. Witthaut, Self-organized synchronization in decentralized power grids, *Phys. Rev. Lett.* 109 (6) (2012) 064101.

- [24] F. Scafuti, T. Aoki, M. di Bernardo, An evolutionary strategy for adaptive network control and synchronization and its applications, *IFAC-PapersOnLine* 48 (18) (2015) 193–198.
- [25] D.A. Wiley, S.H. Strogatz, M. Girvan, The size of the sync basin, *Chaos: Interdiscip. J. Nonlinear Sci.* 16 (1) (2006) 015103.
- [26] P. Erdős, A. Rényi, On random graphs, I, *Publ. Math. (Debrecen)* 6 (1959) 290–297.
- [27] P. Hines, S. Blumsack, E.C. Sanchez, C. Barrows, The topological and electrical structure of power grids, in: *Proceedings of the 43rd Hawaii International Conference on System Sciences*, IEEE, 2010, pp. 1–10.

**APPENDIX C - ELEMENTARY CHANGES IN TOPOLOGY AND
POWER TRANSMISSION CAPACITY CAN INDUCE FAILURES IN
POWER GRIDS**



Contents lists available at ScienceDirect

Physica A

journal homepage: www.elsevier.com/locate/physa

Elementary changes in topology and power transmission capacity can induce failures in power grids

Juliana C. Lacerda^{a,*}, Celso Freitas^a, Elbert E.N. Macau^b

^a National Institute for Space Research (INPE), São José dos Campos, 12227-010, Brazil

^b Federal University of São Paulo, São José dos Campos, 12247-010, Brazil

ARTICLE INFO

Article history:

Received 28 September 2021

Received in revised form 25 November 2021

Available online 11 December 2021

Keywords:

Synchronization
Power grids
Braess' paradox
Kuramoto model

ABSTRACT

In this work, we show that elementary changes in the topology of power grids, like the addition or removal of a single transmission line or the increase of its maximum transmission capacity can cause failures in the network. Also, we show that the probability of the occurrence of these failures can be related to the level of centralization of energy generation and to the nature of the nodes being connected by the transmission line being considered, although the increase in the transmission capacity does not seem to be much affected by the level of centralization. When considering a centralized power grid, that is, one grid whose power is supplied by just a few generators, one must be very careful when contemplating a change between two consumers, being an addition, removal or increase in the transmission capacity of the transmission line connecting them, as there is a considerable probability that this change may cause a failure in the network. In the decentralized power grid, the modification that cause most of the failures in the grid is between a consumer and a generator when the removal or increase in the transmission capacity is being considered. Therefore, one must be very careful when planning an update in an existing power grid or when building a new one as a single modification in the grid may lead the system out of the synchronous state.

© 2021 Elsevier B.V. All rights reserved.

1. Introduction

Synchronization is a universal phenomenon in natural and technological systems that materializes in a diversity of forms [1], like in the flashing of fireflies [2], the brain [3], mechanical systems [4], social systems [5,6], electrochemical chaotic oscillators [7] and energy transmission networks (power grids) [8–10].

Power grids are one of the biggest constructions ever made by men and, in order to study and simulate their behavior, they can be modeled as complex networks where generators and consumers are modeled as nodes, whose dynamics are governed by differential equations, and transmission lines as edges [11–13]. In order to maintain a stable operation in power grids, the whole system must be synchronized with the same instantaneous frequency, in a state called *phase locking* [14–16].

It is an undeniable fact that the construction of large power plants has gradually been left behind with the growing interest of building small renewable energy sources [17,18]. With their addition to power grids, energy production tends to become more and more decentralized, so one needs to be concerned on how this can affect the synchronization of the existing network. As showed by [19], decentralized transmission networks are more sensitive to dynamical perturbations

* Corresponding author.

E-mail addresses: juliana.lacerda@inpe.br (J.C. Lacerda), cbnfreitas@gmail.com (C. Freitas), elbert.macau@unifesp.br (E.E.N. Macau).

but become more robust in relation to topological failures. This decentralization of power grids promote a change not only in the number of generators but also have an impact in the topology of the network as new transmission lines must be built to take the energy produced in remote locations (like wind turbines) to consumers [20].

The topology of complex networks plays a very important role in the proper function of the grid [21]. For example, nodes that are adjacent to a *dead end* or *dead tree* are more prone to failures [22]. Synchronization of complex networks has been shown, by several different methodologies, to be favored by heterogeneous connections [23–25] (when considering power grids, these heterogeneous connections relate to a generator being connected to a consumer). Also, the addition or removal of a single link or even the increase in a transmission line capacity can induce nonlocal failures in the grid [26,27], due to a phenomenon called Braess's paradox which was first observed in traffic networks [28,29]. The Braess's paradox phenomenon in power grids is further studied in [30] where the impact of heterogeneous edge adding (connects a consumer to a generator) is studied in a ring and tree like topologies of twenty nodes and in [31] where the addition and removal and heterogeneous and homogeneous (connects two consumers or two generators) edges is studied in a twelve node network where the number of generators is the same as the number of consumers. Both works conclude that heterogeneous edge additions has a benefit on the synchronization of a power grid while the effect of homogeneous edge addition was not obvious. The latter work also states that the network exhibits weak synchronization when an heterogeneous edge is removed.

In this work, we explore the Braess's paradox phenomenon in power grids by taking into account not only if a removal, addition or increase in the transmission capacity of an edge affects the synchronous state of the grid, but also considering the nature of the pair of nodes this edge is connecting, taking also into consideration the effect of the level of centralization of energy generation. Distinct network topologies are used in order to calculate the most probable outcome when these simple changes are made to the power grid. For example, does the addition or removal of an edge between two consumers induces a desynchronization of the grid more often than the adding or removal of an edge that connects two generators? How is this affected by the decentralization of the grid? Can the increase of a transmission line capacity connecting a consumer and a generator cause a failure in the network? How often?

Our results show that very simple changes in the topology of power grid, like the adding, removal of a single edge or the increase of the transmission capacity of a single line can induce the loss of the synchronous state thus causing nonlocal failures in the grid. The main contribution of this paper is to show that the probability of these failures to occur depends on the level of centralization of the grid and on the nature of the nodes being connected by the perturbed edge.

2. Model and methods

The dynamics of a component of a power grid is described in this work by the second order Kuramoto model [32–34]

$$\dot{\theta}_i = \nu_i, \tag{1}$$

$$\dot{\nu}_i = -\alpha \nu_i + P_i + \frac{P_{max}}{g_i} \sum_{j=1}^N A_{ij} \sin(\theta_j - \theta_i), \tag{2}$$

where N is the number of nodes of the power grid and $i = 1, \dots, N$. The parameters g_i , θ_i , ν_i , $\dot{\nu}_i$, $\alpha \nu_i$ and P_i are the degree, phase, instantaneous frequency, power accumulated as rotational power, power dissipated due to friction and amount of power consumed ($P_i < 0$, we shall label this node as a consumer or C) or delivered ($P_i > 0$, we shall label this node as a generator or G) by node i , respectively. A_{ij} are the entries of the adjacency matrix, being equal to 1 if nodes i and j are connected (there is a transmission line between them) and 0 otherwise. Also, $\alpha \in \mathbb{R}$ is the dissipation parameter ($\alpha = 0.1$ is used in this work, [22,33]), P_{max} represents the maximum power transmission capacity of a transmission line that connects nodes in a power grid and it its also known as the coupling of the Kuramoto model and

$$F_{ij} = P_{max} A_{ij} \sin(\theta_j - \theta_i), \tag{3}$$

is the flow or power transmitted from node j to node i . As for the initial conditions, $\theta_i(0) = 0$ and $\dot{\theta}_i(0) = 0$ for all nodes.

For a power grid to work properly, the synchronous state must be sustained, in a way that all nodes must present the same instantaneous frequency in a state called phase locking [35]. In this phase locking state, the synchronous instantaneous frequency is then defined as $\nu_i = \nu_s$ for all $i = 1, \dots, N$. Following this definition, ν_s does not vary with time, so $\dot{\nu}_s = 0$. Setting $\nu_i = \nu_s$ and $\dot{\nu}_i = 0$ into Eq. (2):

$$0 = -\alpha \nu_s + P_i + \frac{P_{max}}{g_i} \sum_{j=1}^N A_{ij} \sin(\theta_j - \theta_i), \tag{4}$$

summing for all N :

$$0 = \sum_{i=1}^N [-\alpha \nu_s + P_i] + P_{max} \sum_{i=1}^N \sum_{j=1}^N \left[\frac{A_{ij}}{g_i} \sin(\theta_j - \theta_i) \right]. \tag{5}$$

As the adjacency matrix is symmetrical, the sum $\sum_{i=1}^N \sum_{j=1}^N \frac{A_{ij}}{g_i} \sin(\theta_j - \theta_i)$ is equal to zero.

So, Eq. (5) becomes

$$\sum_{i=1}^N (-\alpha v_S + P_i) = 0. \tag{6}$$

The synchronous instantaneous frequency is then given by

$$v_S = \frac{\sum_{i=1}^N P_i}{N} \left(\frac{1}{\alpha} \right) = \frac{\bar{P}}{\alpha}, \tag{7}$$

where $\bar{P} = \frac{\sum_{i=1}^N P_i}{N}$ is the mean between all consumed and generated power. In this work, no power is stored at any node, that is, all power generated is consumed, so $\sum_{i=1}^N P_i = 0$, and, therefore, $v_S = 0$.

In order to calculate a necessary condition for the synchronization of the power grid [32,34,36], consider Eq. (4) and isolate P_{max}

$$P_{max} = \frac{g_i(\alpha v_S - P_i)}{\sum_{j=1}^N A_{ij} \sin(\theta_j - \theta_i)}. \tag{8}$$

Note that $\sum_{j=1}^N A_{ij} \sin(\theta_j - \theta_i) \in [-g_i, g_i]$, so, a necessary condition for the existence of a synchronous state is given by

$$P_{max} \geq \max(|\alpha v_S - P_i|). \tag{9}$$

By Eq. (7), we know that $\alpha v_S = \bar{P}$:

$$P_{max} \geq \max(|\bar{P} - P_i|) = P_{max}^*. \tag{10}$$

There is not a synchronous state where the power grid properly functions in which the coupling has a value lower than P_{max}^* . We emphasize that Eq. (10) is a necessary but not sufficient condition for synchronization. The sufficient condition for synchronization P_{max}^c is calculated numerically in the next section.

To properly measure the synchronization of the grid, we make use of the partial synchronization index [37]

$$S_{ij} = \left| \lim_{\Delta t \rightarrow \infty} \frac{1}{\Delta t} \int_{t_r}^{t_r + \Delta t} e^{i[\theta_i(t) - \theta_j(t)]} dt \right|, \tag{11}$$

where t_r is a transient time and $S_{ij} \in [0, 1]$. When node i is in phase locking in relation to node j , $S_{ij} = 1$. When this value is lower than unit, there is no synchronization between them. In order to measure the synchronization of the whole network, we calculate the arithmetical mean

$$S = \frac{1}{N^2} \sum_{i,j=1}^N S_{ij}. \tag{12}$$

When all nodes are in phase lock, $S = 1$.

There are two conditions for the existence of the phase locked state, one dynamical and one geometric. In relation to the dynamical one, taking into account that $v_S = 0$ and that the power flow is given by Eq. (3), Eq. (4) becomes:

$$0 = P_i + \frac{1}{g_i} \sum_{j=1}^N F_{ij}. \tag{13}$$

Then the dynamical condition is given by the conservation of the flow [27]:

$$|P_i| = \frac{1}{g_i} \left| \sum_{j=1}^N F_{ij} \right|. \tag{14}$$

The geometric condition relates to the fact that the sum of all phase differences around a cycle must be equal to zero, so that all phases are well defined [26]:

$$\sum^{\circ} (\theta_i - \theta_j) = \sum^{\circ} \arcsin \left(\frac{F_{ij}}{A_{ij} P_{max}} \right) = 0. \tag{15}$$

where \circ indicates that the sum is taken along the cycle. When the system is not able to satisfy this condition, no steady state exists due to what is said to be a *geometric frustration*.

In order to simulate the behavior of power grids, we describe them as complex networks [11,22] and a random model [38] is used to generate their topologies. We generate sixteen distinct topologies where each one has $N = 50$ nodes and $E = 68$ edges, which gives an average degree of 2.72, that is a typical value of the average degree of power grids [11,22,27].

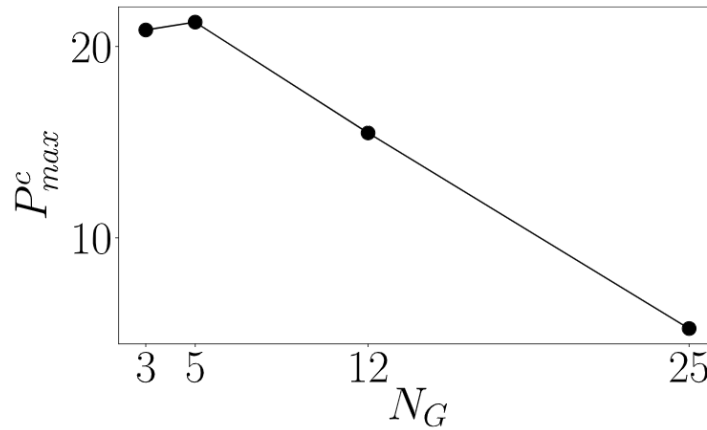


Fig. 1. Critical coupling P_{max}^c as a function of the number of generators for a fixed power grid topology.

In each of these sixteen topologies, four combinations of generators and consumers are used:

- 25 generators and 25 consumers.
- 12 generators and 38 consumers.
- 5 generators and 45 consumers.
- 3 generators and 47 consumers.

So we go from a decentralized grid ($N_G = 25$ generators) to a centralized one ($N_G = 3$ generators). The consumed power is defined as $P_C = -1$ and the generated power is given by

$$P_G = \frac{\sum_1^{N_G} |P_C|}{N_G}. \tag{16}$$

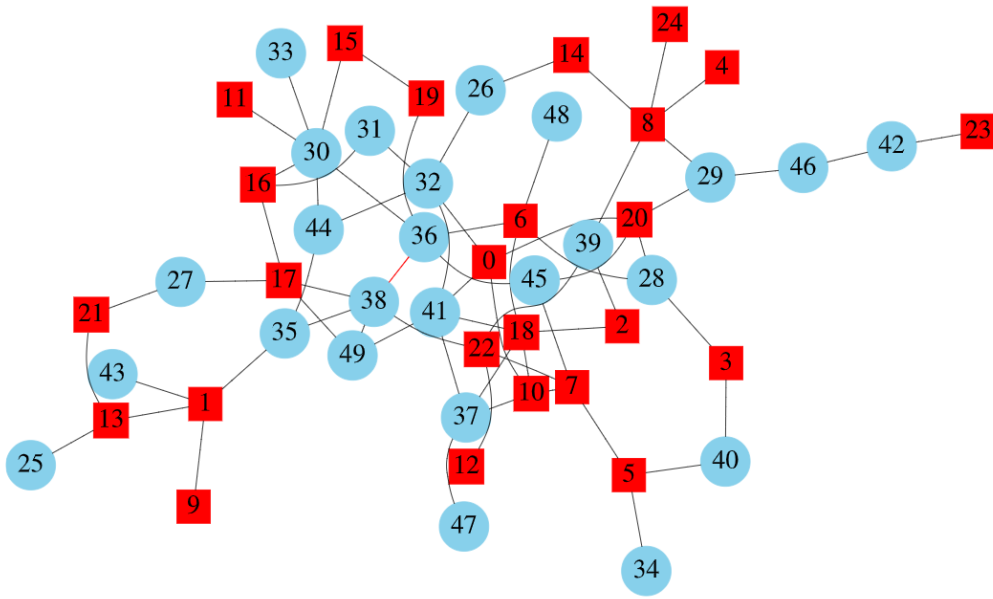
To analyze how a simple change in the topology can affect synchronization, first, we calculate the minimum coupling value for which the original network topology synchronizes, we call this value the critical coupling, P_{max}^c . Then, one edge is added, removed or selected randomly to double its power transmission capacity, P_{max}^c is computed for this new configuration and compared to the P_{max}^c of the original network. The value can be either greater (marked here as *Increases*), lower (marked here as *Decreases*) or equal (marked as *Unchanged*) to the original value. We then go back to the original topology and the process is repeated. Note that when the value of P_{max}^c of the modified network is greater than that of the original network, the current coupling with which the original network was operating is not sufficient enough to maintain the synchronous state so the proper function of the grid is lost. In the case of the *Decreases* situation, the change has a beneficial effect on synchronization, yet this situation is not the aim of this study as we look for possible causes of failures. In the *Unchanged* situation, the critical coupling remains the same being that the change we made did not have an effect on the synchronization of the network.

In the case of edge addition, we add randomly 50 new edges, one at a time, in each of the sixteen network configurations. Note that one edge is added at random, P_{max}^c is calculated, the original network is then considered again and a new edge is added and so on. In the case of edge removal, all edges from the original networks are removed, one at a time (always considering again the original network before removing a new one) and P_{max}^c is calculated. The selected edge is removed as long as the final network topology is still connected, that is, no node is isolated from the others.

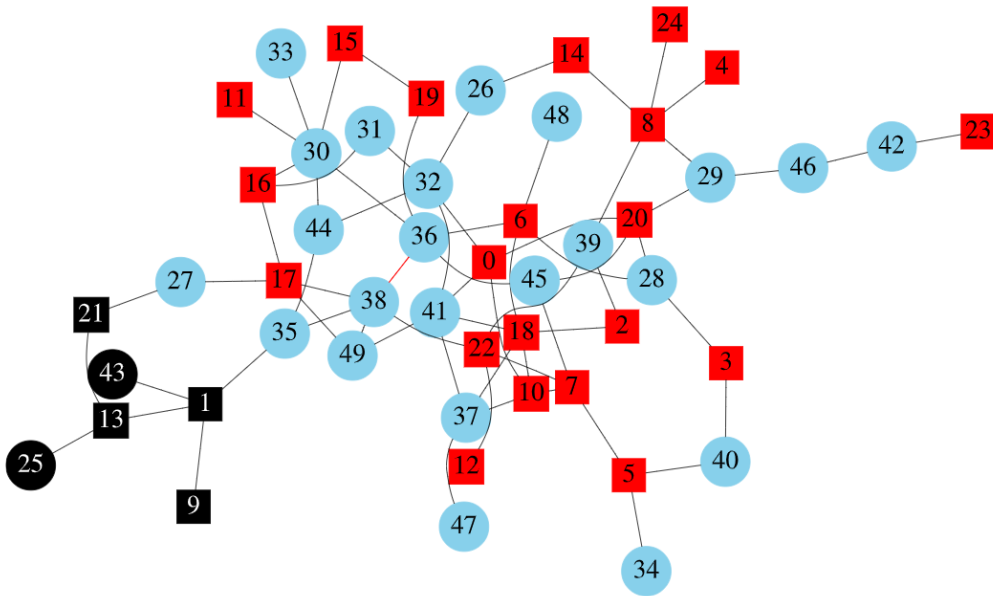
We also check how the increase of the maximum capacity of the transmission of a single line affects the proper working of the network, so, in this case, for the edge linking nodes m and n , we consider $P_{max}^{mn} = 2P_{max}$ and, for the rest of the edges, P_{max} is fixed, as it was before. This new capacity is applied to all edges of the network, one at a time (always considering again the original network configuration before changing the capacity of a new line), for the sixteen distinct topologies.

3. Results and discussion

We start by analyzing how the decentralization of the grid, that is, how the change in the number of generators (while maintaining the same topology) affects the proper function of the grid. Eq. (10) gives a necessary condition for the synchronization of the system. As $\bar{P} = 0$ by definition, we have $P_{max}^* = \max|P_i|$, as i stands for all the consumers (C) and generators (G). As $P_C = -1$ is fixed for all consumers, the value of P_{max}^* is determined by the value of the power generated P_G , given by Eq. (16), which is equal to (when $N_G = N_C$) or greater than P_C (when $N_G < N_C$). So, the necessary condition for synchronization in our case depends only on the amount of the power generated by a single generator, the fewer the number of generators, the great is the power they have to provide and so the great is the value of P_{max}^* . We expect the critical coupling P_{max}^c (sufficient condition to achieve synchronization) to behave the same way, that is, to decrease with the increase of the number of generators [19]. This fact can be seen in Fig. 1, where one of the random topologies



(a)



(b)

Fig. 2. (a) Representation of the original network (black edges) with an additional edge (in red) linking nodes 36 (whose neighbors are 6, 17, 30, 38, 45) and 38 (whose neighbors are 17, 22, 35, 36, 49). Consumers are plotted as red squares and generators as blue circles. Nodes that totally lost synchronization ($S < 0.1$) due to the addition of the red edge are shown in depicted in black (b).

is fixed and P_{max}^c is numerically calculated and plotted against the number of generators of the grid. One can see that the decentralization of the grid plays an important role on the synchronization of the network and we investigate further how this decentralization also affects the Braess's Paradox.

One out of the sixteen topologies with a fixed number of generators $N_G = 25$ is now considered and can be seen in Fig. 2(a) (with black edges), and for the critical coupling $P_{max}^c = 5.26$, we plot the instantaneous frequency ν of all nodes as a function of time in Fig. 3(a), where the consumers are plotted in red and the generators in blue. Note that after a transient time, all nodes tend to the same value of ν . $P_{max}^c = 5.26$ is chosen because it is the minimum value for which the partial synchronization index S is equal to one, so it is the minimum power transfer capacity of the transmission lines for which the synchronous state exists.

Now, as an example, one new transmission line is added at a random position in this network (between nodes 38 and 36, the red edge in Fig. 2(a)). The system is then integrated again for the same value of P_{max}^c and one can note that the synchronous state is lost in Fig. 3(b), where the instantaneous frequency is plotted against time. Note that instead of a

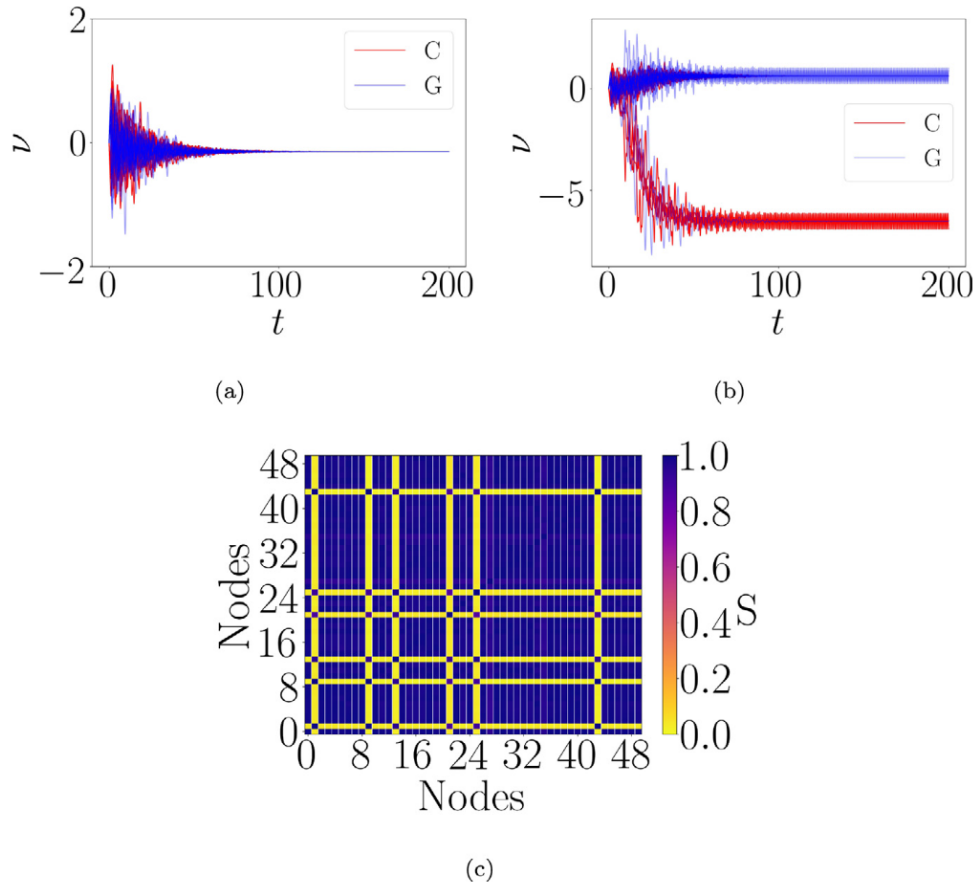


Fig. 3. Instantaneous frequency as a function of time of a 25 generator network (see Fig. 2(a)) for (a) original topology with and (b) when one new link is added to the original network, both integrated with coupling $P_{max}^c = 5.26$. Consumers are plotted in red and generators in blue. In (c) the partial synchronization matrix, Eq. (11), is plotted for all nodes of this network where the first 25 nodes are consumers and the last 25 nodes are generators.

fixed null value, the instantaneous frequency of all nodes are divided into two branches and vary in time with two distinct means. The partial synchronization index for this configuration is $S = 0.78$ and the partial synchronization matrix, given by Eq. (11), is represented in Fig. 3(c), where the color yellow represents a low value of S and purple a high one. Note that a few nodes totally lose the synchronous state in relation to the rest of the network (nodes 1,9,13,21,25,43) and none of them are the nodes connected by the new link nor are they one of their neighbors. In fact, these nodes are all part of a small group located at the lower left of the network and are painted in black in Fig. 2(b). This edge addition is then causing a nonlocal failure [27]. So, although the dynamical conditions for synchronization given by Eq. (14) are satisfied, the synchronous state does not exist anymore due to a geometric frustration, Eq. (15). In the case of this edge addition, the critical coupling P_{max}^c required for the existence of the phase locked state is increased.

Still considering the same network (Fig. 2(a), with black edges), we now calculate the partial synchronization index as a function of the coupling P_{max} for the following configurations: *Original*, the original random network. *Add*, the topology discussed in the previous paragraph (connecting nodes 36 and 38). *Remove*, where an edge is randomly removed from the original topology (connected 0 with 20). *Double*, where an edge is selected at random and the power transmission capacity of this line is doubled (connects 1 with 13). The results are shown in Fig. 4. Note that the first one to synchronize is the original network, then the Double, Remove and Add configurations, respectively. Against our intuition, the configuration in which one edge is added to the network requires the greatest critical coupling P_{max}^c to reach the synchronous state. This odd phenomenon called Braess's Paradox was first detected in traffic networks and an explanation for it is the redistribution of flows in the network which may induce an overload in some transmission lines which then leads to a loss of the synchronous state [26]. We must make it clear that this increase of the critical coupling does not always occur, as it can be the case that the modified topologies all present a lower critical coupling when compared to the original network. One might wonder if there is a way to predict when a topological change will favor synchronization or not. From now on, we try to shed a light on this question.

All the previous discussions were made only by using a single random network composed of 25 generators and 25 consumers. Now, sixteen distinct topologies are used, and each one of them goes from a centralized to a decentralized configuration. More specifically, we have sixteen distinct topologies with 3 generators, sixteen topologies with 5 generators, sixteen topologies with 12 generators and, finally, sixteen distinct topologies with 25 generators, giving a

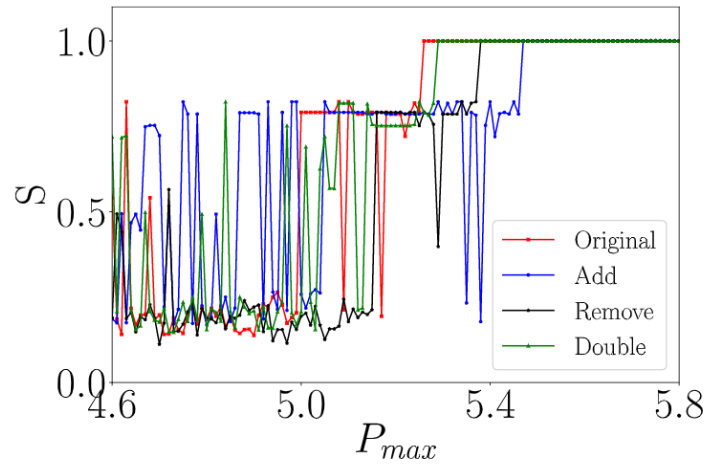


Fig. 4. Partial synchronization index S as a function of the coupling P_{max} .

total of 64 network configurations. For each of these configurations, we add edges randomly, remove them and double the transmission line capacity, as explained in the previous section.

We now check how these elementary changes affect the synchronous state of the system by calculating the fraction of edges that increases, decreases and leaves P_{max}^c unchanged in relation to the addition (Add), removal (Remove) and increase of the maximum transmission capacity (Double). Reminding the reader that the increase in P_{max}^c leads the system to a desynchronized state. Taking the example of the edge addition for a fixed number of generators, 50 new edges are added (remember that one edge is added, P_{max}^c is calculated, then the original network topology is considered again so a new edge is added and the process is repeated) to each of the sixteen network topologies, giving a total of $N_{edge} = 800$ new added edges. Then, we annotate how many times the value of P_{max}^c increased (N_{inc}), decreased (N_{dec}) and remained unchanged (N_{unc}). Finally, the fraction of edges depicted in Fig. 5(a) is given by N_{inc} , N_{dec} and N_{unc} divided by N_{edge} , which are plotted in green, brown and black, respectively. A similar procedure is done for the Remove and the Double situations and are plotted in Figs. 5(b) and 5(c), respectively.

For the Add situation, Fig. 5(a), most of the edge addition results in an increase of P_{max}^c when centralized networks are being considered ($N_G = 3$ and 5). With the increase of the number of generators, most of the edges added result in a decrease of P_{max}^c . As expected, the Remove approach, Fig. 5(b), shows an inverse situation as most of the edges removed from the networks decreases P_{max}^c for a centralized configuration and increases P_{max}^c for a decentralized configuration. In relation to the Double set up, Fig. 5(c) shows that most of the edges selected that have their maximum capacity doubled do not change the value of P_{max}^c for the most centralized configuration ($N_G = 3$) and decreases P_{max}^c as the topology becomes decentralized, although the difference between the fractions that decreases, increases and leaves the critical coupling unchanged is very low in these two scenarios, in comparison to the two previous analysis. Note that the level of centralization of energy generation plays a very important role here, as it dictates which is the most probable scenario that can take place after a simple change in the topology, like adding or removing a single transmission line of the network.

In all of the three situations presented here (Add, Remove and Double) one can note that the system leaves the synchronous state between 29% to 53% of the times, which is something our intuition cannot predict, so, one must be very careful when making topological changes to a functional energy transmission network.

Now that we know that adding, removing or increasing the transmission capacity of edges can cause failures in a power grid with, in some cases, a relatively high probability, we ask the following: which nodes are these edges connecting? Does it make any difference if one adds a new edge connecting two consumers or two generators when it comes to maintaining the synchronous state?

To answer these previous questions, we take into consideration now only the fraction of edges that increase P_{max}^c and analyze which pair of nodes are these edges connecting. Our results are presented in Fig. 5(d)–(f). They show that for a relatively low number of generators in the network, in all the three situations, Add, Remove and Double, the great part of the fraction of edges that destroys the synchronous state are caused by edges connecting two consumers. When a random centralized network is being considered, it is a fact that most of the connections are between two consumers, since they are the majority of the nodes, so it is expected to have a higher fraction of edges that cause failures by connecting them, but it is still a valuable information since most power grids are still centralized.

On the other hand, when a decentralized network is being considered, the results differ for the three scenarios. In the Add one, new connections between two generators and between a consumer and a generator cause trouble more often. By far, the connection whose removal is the most dangerous is the one linking a consumer to a generator and increasing the transmission capacity of this same kind of connection may also not be an appropriate engineering operation.

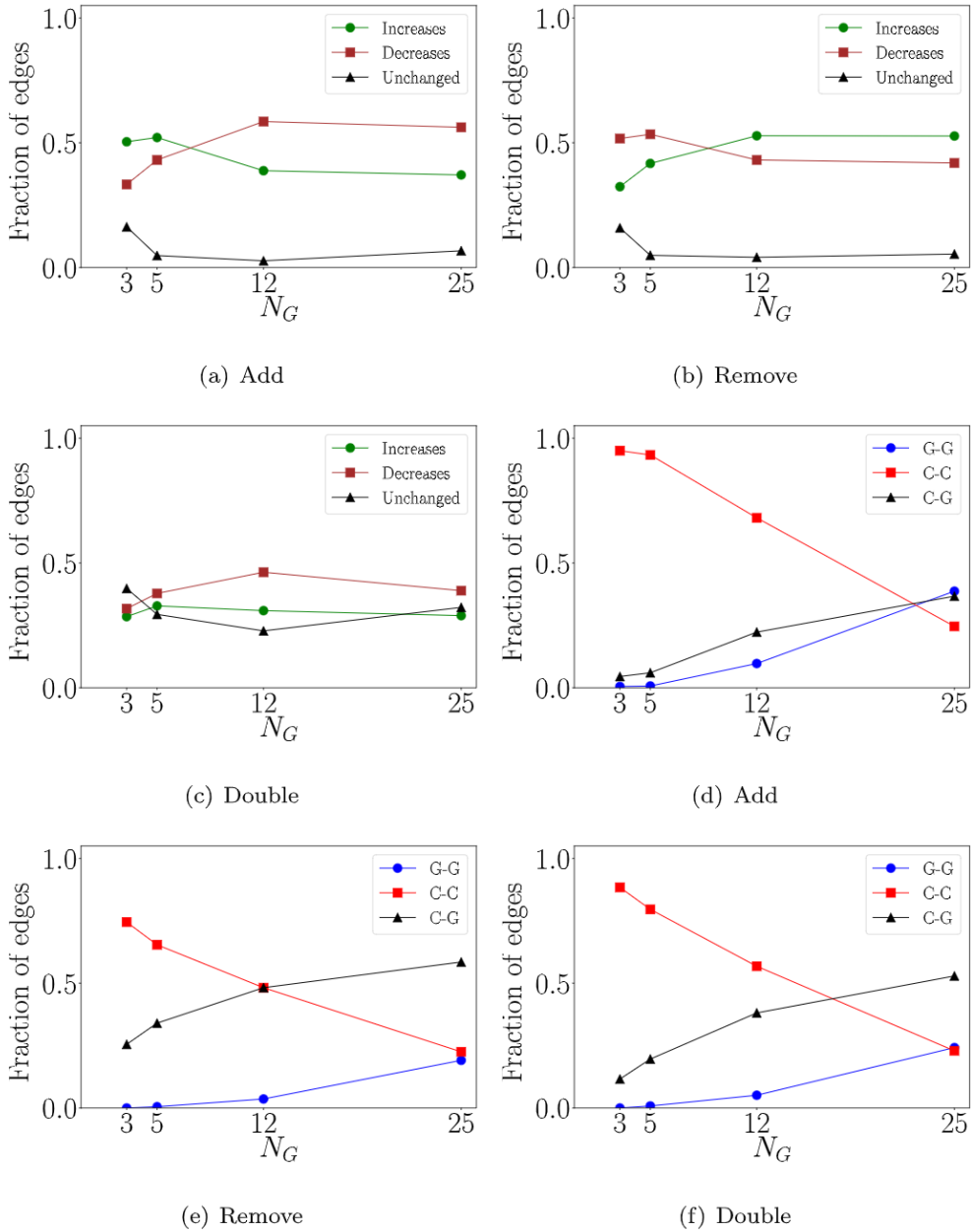


Fig. 5. Fraction of edges that increases (green), decreases (brown) and does not change (black) the value of P_{max}^c as a function of the number of generators when (a) an edge is added, (c) an edge is removed and (e) the maximum transmission capacity of an edge is doubled. (d)–(f) Fraction of edges that connect a generator to another generator (blue), a consumer to a consumer (red) and a consumer to a generator (black), only in relation to those who increase P_{max}^c in (a)–(c), respectively.

4. Conclusion

In summary, we have shown that very simple changes in the network can cause failures and lead the system out of the synchronous state which is crucial for the power grid to work properly. When adding, removing or increasing the capacity of a transmission line, one changes the flux of the power transmitted in the network and this change may induce nonlocal failures due to overloads on some transmission lines. The most probable scenario to what happens when these elementary changes in transmission networks are made depends on the level of centralization of the power generated in the network and also on the nature of the nodes being connected by the edge in question. It would be of extreme importance to analyze carefully the effects of elementary changes on real-world power grids before actually making them as these changes can reduce the stability and also cause failures which may generate great economic costs. We wish to emphasize that this is a first approach to this problem and, as for future work, a more complex model should be used instead of Eqs. (1) and (2), for example, a model that includes admittance [39] and a one that includes phase shift [9].

CRediT authorship contribution statement

Juliana C. Lacerda: Conceptualization, Methodology, Software, Formal analysis, Writing – original draft, Writing – review & editing, Visualization. **Celso Freitas:** Conceptualization, Supervision, Project administration. **Elbert E.N. Macau:** Conceptualization, Supervision, Project administration.

Declaration of competing interest

The authors declare that they have no known competing financial interests or personal relationships that could have appeared to influence the work reported in this paper.

Acknowledgments

The authors would like to thank Conselho Nacional de Desenvolvimento Científico e Tecnológico - CNPq, Brazil for the financial support, including grant 141138/2017-3. This research is also supported by grants 2015/50122 and 2018/03211-6 of São Paulo Research Foundation (FAPESP), Brazil.

References

- [1] S. Boccaletti, A.N. Pisarchik, C.I. Del Genio, A. Amann, *Synchronization: From Coupled Systems to Complex Networks*, Cambridge University Press, Cambridge, 2018.
- [2] J. Buck, Synchronous rhythmic flashing of fireflies. II., *Q. Rev. Biol.* (1988) 265–289.
- [3] M. Avoli, M. de Curtis, Gabaergic synchronization in the limbic system and its role in the generation of epileptiform activity, *Prog. Neurobiol.* 95 (2) (2011) 104–132.
- [4] J. Pantaleone, Synchronization of metronomes, *Amer. J. Phys.* 70 (10) (2002) 992–1000.
- [5] Z. Nédá, E. Ravasz, Y. Brechet, T. Vicsek, A.-L. Barabási, Self-organizing processes: the sound of many hands clapping, *Nature* 403 (6772) (2000) 849–850.
- [6] A. Pluchino, V. Latora, A. Rapisarda, Changing opinions in a changing world: a new perspective in sociophysics, *Internat. J. Modern Phys. C* 16 (04) (2005) 515–531.
- [7] L.A. Magrini, M. Oliveira Domingues, E.E. Macau, I.Z. Kiss, Synchronization in populations of electrochemical bursting oscillators with chaotic slow dynamics, *Chaos* 31 (5) (2021) 053125.
- [8] J.C. Lacerda, J. Dias, C. Freitas, E. Macau, Synchronization of energy transmission networks at low voltage levels, *Appl. Math. Model.* 89 (2021) 627–635.
- [9] F. Hellmann, P. Schultz, P. Jaros, R. Levchenko, T. Kapitaniak, J. Kurths, Y. Maistrenko, Network-induced multistability through lossy coupling and exotic solitary states, *Nature Commun.* 11 (1) (2020) 1–9.
- [10] G.A. Pagani, M. Aiello, The power grid as a complex network: a survey, *Physica A* 392 (11) (2013) 2688–2700.
- [11] K. Sun, Complex networks theory: A new method of research in power grid, in: *Transmission and Distribution Conference and Exhibition: Asia and Pacific, 2005 IEEE/PES, IEEE, 2005*, pp. 1–6.
- [12] P. Kundur, N.J. Balu, M.G. Lauby, *Power System Stability and Control*, Vol. 7, McGraw-hill New York, 1994.
- [13] J. Grzybowski, E.E. Macau, T. Yoneyama, Power-grids as complex networks: emerging investigations into robustness and stability, in: *Chaotic, Fractional, and Complex Dynamics: New Insights and Perspectives*, Springer, 2018, pp. 287–315.
- [14] J. Lacerda, C. Freitas, E. Macau, Remote synchronization and multistability in a star-like network of oscillators, in: *Proceedings of the 14th International Conference on Dynamical Systems Theory and Applications, International Conference on Dynamical Systems Theory and Applications, Lodz, 2017*, pp. 1–12.
- [15] F. Blaabjerg, R. Teodorescu, M. Liserre, A.V. Timbus, Overview of control and grid synchronization for distributed power generation systems, *IEEE Trans. Ind. Electron.* 53 (5) (2006) 1398–1409.
- [16] A. Pikovsky, M. Rosenblum, J. Kurths, *Synchronization*, Vol. 12, Cambridge University Press, Cambridge, 2003.
- [17] G. Pepermans, J. Driesen, D. Haeseldonckx, R. Belmans, W. Dhaeseleer, Distributed generation: definition, benefits and issues, *Energy Policy* 33 (6) (2005) 787–798.
- [18] J.P. Lopes, N. Hatzigiorgiou, J. Mutale, P. Djapic, N. Jenkins, Integrating distributed generation into electric power systems: A review of drivers, challenges and opportunities, *Electr. Power Syst. Res.* 77 (9) (2007) 1189–1203.
- [19] M. Rohden, A. Sorge, M. Timme, D. Witthaut, Self-organized synchronization in decentralized power grids, *Phys. Rev. Lett.* 109 (6) (2012) 064101.
- [20] E. Marris, Energy: Upgrading the grid, *Nat. News* 454 (7204) (2008) 570–573.
- [21] M. Rohden, A. Sorge, D. Witthaut, M. Timme, Impact of network topology on synchrony of oscillatory power grids, *Chaos* 24 (1) (2014) 013123.
- [22] P.J. Menck, J. Heitzig, J. Kurths, H.J. Schellnhuber, How dead ends undermine power grid stability, *Nature Commun.* 5 (2014) 3969.
- [23] F. Scafuti, T. Aoki, M. di Bernardo, Heterogeneity induces emergent functional networks for synchronization, *Phys. Rev. E* 91 (6) (2015) 062913.
- [24] C. Freitas, E. Macau, R.L. Viana, Synchronization versus neighborhood similarity in complex networks of nonidentical oscillators, *Phys. Rev. E* 92 (3) (2015) 032901.
- [25] R.S. Pinto, A. Saa, Optimal synchronization of kuramoto oscillators: A dimensional reduction approach, *Phys. Rev. E* 92 (6) (2015) 062801.
- [26] D. Witthaut, M. Timme, Braess's paradox in oscillator networks, desynchronization and power outage, *New J. Phys.* 14 (8) (2012) 083036.
- [27] D. Witthaut, M. Timme, Nonlocal failures in complex supply networks by single link additions, *Eur. Phys. J. B* 86 (9) (2013) 1–12.
- [28] D. Braess, Über ein paradoxon aus der verkehrsplanung, *Unternehmensforschung* 12 (1) (1968) 258–268.
- [29] D. Braess, A. Nagurney, T. Wakolbinger, On a paradox of traffic planning, *Transp. Sci.* 39 (4) (2005) 446–450.
- [30] L.-x. Yang, J. Jiang, X.-j. Liu, Influence of edge additions on the synchronizability of oscillatory power networks, *Commun. Nonlinear Sci. Numer. Simul.* 41 (2016) 11–18.
- [31] L.-x. Yang, J. Jiang, Impacts of link addition and removal on synchronization of an elementary power network, *Physica A* 479 (2017) 99–107.
- [32] J. Grzybowski, E. Macau, T. Yoneyama, On synchronization in power-grids modelled as networks of second-order kuramoto oscillators, *Chaos* 26 (11) (2016) 113113.
- [33] G. Filatrella, A.H. Nielsen, N.F. Pedersen, Analysis of a power grid using a Kuramoto-like model, *Eur. Phys. J. B* 61 (4) (2008) 485–491.

- [34] R. Carareto, M.S. Baptista, C. Grebogi, Natural synchronization in power-grids with anti-correlated units, *Commun. Nonlinear Sci. Numer. Simul.* 18 (4) (2013) 1035–1046.
- [35] B.C. Daniels, *Synchronization of globally coupled nonlinear oscillators: the rich behavior of the Kuramoto model*, 2005, p. 20, Ohio Wesleyan Physics Dept., Essay, 7, 2.
- [36] N. Chopra, M.W. Spong, On synchronization of Kuramoto oscillators, in: *Decision and Control, 2005 and 2005 European Control Conference. CDC-ECC'05. 44th IEEE Conference on, IEEE, 2005*, pp. 3916–3922.
- [37] J. Gómez-Gardenes, Y. Moreno, A. Arenas, Paths to synchronization on complex networks, *Phys. Rev. Lett.* 98 (3) (2007) 034101.
- [38] P. Erdős, A. Rényi, On random graphs, I, *Publ. Math. (Debrecen)* 6 (1959) 290–297.
- [39] T. Nishikawa, A.E. Motter, Comparative analysis of existing models for power-grid synchronization, *New J. Phys.* 17 (1) (2015) 015012.

APPENDIX D - HOW HETEROGENEITY IN CONNECTIONS AND CYCLES MATTER FOR SYNCHRONIZATION OF COMPLEX NETWORKS

How heterogeneity in connections and cycles matter for synchronization of complex networks

Cite as: Chaos **31**, 113134 (2021); doi: 10.1063/5.0068136

Submitted: 23 August 2021 · Accepted: 3 November 2021 ·

Published Online: 17 November 2021



View Online



Export Citation



CrossMark

Juliana C. Lacerda,^{1,a)} Celso Freitas,^{1,b)} Elbert E. N. Macau,^{2,c)} and Jürgen Kurths^{3,d)}

AFFILIATIONS

¹National Institute for Space Research, São José dos Campos 12227-010, Brazil

²Institute of Science and Technology, Federal University of São Paulo, São José dos Campos 12247-010, Brazil

³Department of Physics, Humboldt University of Berlin, Newtonstr. 15, 12489 Berlin, Germany

Note: This article is part of the Focus Issue, Dynamics of Oscillator Populations.

^{a)}**Author to whom correspondence should be addressed:** juliana.lacerda@inpe.br

^{b)}**Electronic mail:** cbnfreitas@gmail.com

^{c)}**Electronic mail:** elbert.macau@unifesp.br

^{d)}**Also at:** Potsdam Institute for Climate Impact Research (PIK), Member of the Leibniz Association, P.O. Box 60 12 03, D-14412 Potsdam, Germany. **Electronic mail:** juergen.kurths@pik-potsdam.de

ABSTRACT

We analyze how the structure of complex networks of non-identical oscillators influences synchronization in the context of the Kuramoto model. The complex network metrics assortativity and clustering coefficient are used in order to generate network topologies of Erdős–Rényi, Watts–Strogatz, and Barabási–Albert types that present high, intermediate, and low values of these metrics. We also employ the total dissonance metric for neighborhood similarity, which generalizes to networks the standard concept of dissonance between two non-identical coupled oscillators. Based on this quantifier and using an optimization algorithm, we generate Similar, Dissimilar, and Neutral natural frequency patterns, which correspond to small, large, and intermediate values of total dissonance, respectively. The emergence of synchronization is numerically studied by considering these three types of dissonance patterns along with the network topologies generated by high, intermediate, and low values of the metrics assortativity and clustering coefficient. We find that, in general, low values of these metrics appear to favor phase locking, especially for the Similar dissonance pattern.

Published under an exclusive license by AIP Publishing. <https://doi.org/10.1063/5.0068136>

The topology of networks of phase oscillators plays a very important role on the synchronization of the system. The individual dynamics of each oscillator, characterized by their individual frequencies, also play a very important role, which is not completely understood. What effect the emergence of cycles, the connection of nodes with close or very distinct degree have on synchronization? Furthermore, is this affected by the natural frequencies of the oscillators being connected? These questions are also important if we take into consideration the emergence of synchronization phenomena in nature that leads the involved agents from the disorder to order in a scenario in which the agent interconnections are not all-to-all. Here, we investigate these issues.

I. INTRODUCTION

Synchronization is a process in which dynamical systems manage to coordinate some dynamical properties by being connected among themselves or by being driven by a common force.¹ It is a universal behavior that takes place in many natural and artificial multi-agent systems.^{2–7} In order to study synchronization in systems of interacting dynamical units, it has been shown to be useful to describe a system as a complex network of interacting oscillators,^{8,9} where nodes represent the dynamical units and the connections between them express their interacting mechanisms, where nodes only interact with adjacent units. One of the most widely used paradigmatic models of phase oscillators to study synchronization in complex networks is the Kuramoto model.^{10,11}

A great number of natural phenomena where a system is composed of interconnected dynamical units can be modeled by using complex networks to capture its global and emerging properties.^{12–14} For example, it can be used in the study of non-linear dynamical systems,^{15,16} of chemical and biological systems,^{17–21} of power grids,^{22–25} and even in the study of social networks.^{26–28} The synchronization of networks in a multi-layer network has also been the subject of intense studies and can be used, for example, in the study of epidemic models.^{29,30}

Biological and social studies have shown that in some situations, like when it comes to choosing friends, people prefer to gather with similar minded ones.^{31–34} On the other hand, when it comes to mating preferences, some species prefer to mate with dissimilar ones, which may provide the offspring with good genes.^{35–38} Freitas *et al.*²⁶ used an approach based on an interconnected network of Kuramoto oscillators to analyze these scenarios. There, the former kind of behavior is referred to as *Similar* (\mathcal{S}), while the latter one as *Dissimilar* (\mathcal{D}) neighborhood patterns. If an ensemble presents no strong bias toward any of these extremes, it is called *Neutral* (\mathcal{N}).

In this work, we explore the idea of Similarity and Dissimilarity described above by means of structure properties and synchronization of complex networks of Kuramoto non-identical phase oscillators. In order to quantify these patterns, we shall use a measure related to classical *dissonance*,¹ which measures the difference of the natural frequencies of a pair of oscillators.

With reference to related material on synchronization of complex networks, Pinto and Saa³⁹ employs a dimensional reduction approach proposed by Ref. 40 and derive a sufficient analytical condition, considering an ansatz, to optimize a topology of a network in order to favor synchronization using the Kuramoto model. They also showed that when this method is applied to a network with random natural frequencies, the final topology presents a negative correlation between the natural frequencies of adjacent vertices in a way that we can call a network with a Dissimilar pattern, even though the approach in Ref. 39 does not exhaust the problem, especially for small and intermediate coupling values, which are commonly found in nature.¹ A numerical study made by Freitas *et al.*²⁶ showed that Similar patterns favor weaker forms of synchronization, but Dissimilar ones exhibit explosive synchronization, reaching global synchronization faster than the Similar pattern.⁴¹ We use an evolutionary strategy to find a minimal network structure that guarantees global synchronization and show that the heterogeneity in the nodes' natural frequency is the driving force that determines the evolution of the network structure.

We intend to extend the work done by Ref. 26 and add the complex network measures assortativity and clustering coefficient to investigate how the structure of complex networks influences the synchronization of Similar, Dissimilar, and Neutral patterns of natural frequencies of oscillators. Assortativity is employed in order to measure how connections between nodes with the same degree influence the emergence of synchronization, while the clustering coefficient measures the impact of loops of size three (small cycles). Therefore, the topology of the networks is dictated by the assortativity and by the clustering coefficient values, while the natural frequency of their nodes is given by the dissonance patterns.

The authors in Refs. 42 and 43 used a modified version of the Kuramoto model in order to study opinion formation and its

dynamics through synchronization of complex networks where the phase of a node in this model represents the opinion of an individual and the coupling represents the amount of the interaction among them. To illustrate the meaning of the metrics used here, the natural frequency patterns, and the synchronization of the network, let us take as an example a large group of individuals having an argument about a polemic subject where each individual has its own initial opinion, and due to the number of people and the limited time they have, they can only communicate with a limited number of people inside this group. Their discussion ends only when all participants come to an agreement and, therefore, reach a common opinion. We can model this situation by using a complex network approach where each individual is represented by a node whose behavior is dictated by a dynamical system model, the interaction between them is represented by an edge, and the opinion of each individual in relation to the subject being discussed is given by the natural frequency of the nodes. Therefore, reaching a common opinion is associated with a synchronized state. The natural frequency patterns Similar, Dissimilar, and Neutral here relate to the level of homogeneity (Similar) or heterogeneity (Dissimilar) of the opinion of communicating individuals, as, for example, if the individuals only communicate with similar minded ones, the Similar pattern is used to model this dynamics. We also refer the reader to Noorazar⁴⁴ and Deffuant *et al.*⁴⁵ for a more detailed discussion on opinion dynamics.

The rules of who can communicate with whom are given by the metrics assortativity and the clustering coefficient. If individuals who interact with many people prefer to communicate with the ones that are also popular and individuals who interact with a few people prefer to communicate with ones that are also less popular, the network is said to be assortative and has a high value of the metric assortativity. The opposite can also happen; when popular individuals tend to talk with less popular ones, the network is said to be disassortative. Looking at another aspect of the rules of communication within this group of people, we can also allow two contacts of a person to talk to each other, forming then a small cycle or a loop of size three in the network topology. When there is a large number of a couple of contacts of individuals communicating to each other, we say that this network presents a high clustering coefficient, and, on the other hand, it presents a low clustering coefficient if the opposite happens.

In this scenario, one can ask the following: how strong the interactions (represented here by the coupling of the Kuramoto model) between individuals must be in order to reach an agreement? Is it easier to be achieved if individuals only communicate with similar minded ones or is it the opposite? Is it easier if popular individuals only talk to each other or when they talk to less popular ones? Or if contacts of individuals communicate with each other?

Our results show that the Similar pattern of a natural frequency distribution favors weaker forms of synchronization, but, as we increase the coupling constant, the Dissimilar pattern is the first to reach the synchronized state. The Erdős–Rényi model presented itself as the easiest to reach the phase locking state when compared to Watts–Strogatz and Barabási–Albert network models. In relation to the network metrics assortativity and clustering coefficient, one can see that low values of both metrics favors the reaching of the synchronized state. As for the questions raised about the best strategy

to conduct an argument among a group of people, we find that the best strategy would be to encourage individuals with different opinions to communicate to each other and, at the same time, encourage popular individuals to talk to less popular ones and discourage the interaction among contacts of individuals in order to avoid small cycles of interactions.

This paper is organized as follows: Sec. II presents the Kuramoto model, characterize the Similar, Dissimilar, and Neutral frequency patterns, defines synchronization quantifiers, and presents the network metrics used to generate the network topologies. Section III develops a discussion about the results, and the conclusions are presented in Sec. IV.

II. MODEL AND METHODS

In this work, we consider complex networks of Kuramoto phase oscillators whose dynamics is described by a simple but very powerful model as it has proven to accurately approximate a great class of coupled oscillators.^{46,47} The dynamics of the Kuramoto model is described by

$$\dot{\theta}_i = \omega_i + \frac{\lambda}{d_i} \sum_{j=1}^N A_{ij} \sin(\theta_j - \theta_i), \quad (1)$$

where N is the number of oscillators, $\theta_i \in \mathbb{R}$ is the phase variable of each oscillator for $i = 1, \dots, N$, and ω_i is its natural frequency. Communication channels are defined through a coupling graph, a simple and connected graph, which is expressed via its adjacency matrix (A_{ij}); i.e., A_{ij} has value 1 if nodes i and j are connected and 0 otherwise. The symbol d_i denotes the node degree of the i th oscillator, while $\lambda \geq 0$ is the overall coupling constant.

In order to characterize the Similar, Dissimilar, and Neutral natural frequency patterns on complex networks, we make use of the total dissonance measure²⁶

$$\nu = \frac{1}{N} \sqrt{\sum_{i,j=1}^N A_{ij} (\omega_i - \omega_j)^2}. \quad (2)$$

For the Similar pattern, the natural frequencies of adjacent nodes are close to each other such that the value of ν is small and it is zero only if all oscillators have identical natural frequencies. If the natural frequencies of adjacent nodes are very different from each other, that is, the Dissimilar pattern, the value of ν is higher. The Neutral pattern is characterized as intermediate values of ν . To calculate these frequency patterns, the stochastic optimization algorithm called simulated annealing⁴⁸ is used. In order to optimize the objective function ν , it makes permutations of the natural frequencies set until it finds an optimal local value of the objective function, in correspondence with the desired Similar or Dissimilar patterns. Considering the outputs of this algorithm, the minimization of ν corresponds to the Similar pattern, the maximization to the Dissimilar one, and the random initial natural frequency set is called Neutral. In practice, for each network topology considered in this work, a set of natural frequencies is chosen from a random uniform distribution in $[-\pi, \pi]$ and the total dissonance ν_{ini} is calculated, this one is called the Neutral frequency pattern. Then, an optimization algorithm is applied in order to maximize (ν_{max}) and

minimize (ν_{min}) the total dissonance of each network, giving rise to the Dissimilar and Similar patterns, respectively.

A useful way to quantify phase synchronization of networks is by using the order parameter R defined as

$$R(t) = \left| \frac{1}{N} \sum_{i=1}^N e^{i\theta_i} \right|, \quad (3)$$

where $R(t) \in [0, 1]$ measures the amount of collective behavior of the system. When $R(t) = 1$, the system is said to be in the state of phase synchronization and all oscillators present the same phase. On the other hand, when the system presents an incoherent behavior, $R(t) \approx 0$.

As done by Ref. 49, we introduce now an index to quantify the appearance of another type of synchronization, called *phase locking* (PL) that indicates when a pair of oscillators presents a constant phase difference and, therefore, moves as a rigid body. This measure is called *partial synchronization index* S_{ij} given by

$$S_{ij} = \left| \lim_{\Delta t \rightarrow \infty} \frac{1}{\Delta t} \int_{t_r}^{t_r + \Delta t} e^{i[\theta_i(t) - \theta_j(t)]} dt \right|, \quad (4)$$

where $S_{ij} \in [0, 1]$ and t_r is a large enough transient time. When two oscillators have the same instantaneous frequency, they are said to be in phase lock and, in this case, S_{ij} is equal to 1. In order to measure the degree of partial synchronization of the whole network, we calculate the arithmetic mean

$$S = \frac{1}{N^2} \sum_{i,j=1}^N S_{ij}. \quad (5)$$

Therefore, when the whole system is in phase lock, that is, when the phase difference between all pair of nodes is constant in time, $S = 1$. As for the order parameter in this case, $R(t)$ is constant in time but not necessarily equal to 1 as it is not mandatory that the phases are the same. If $S \approx 0$, the system presents a low coherent behavior.

Our aim is to analyze how network structure influences the emergence of synchronization on complex networks. For this purpose, the network measures called assortativity and clustering coefficient are used in order to generate different network topologies.

Assortativity measures the similarity of connections in a network with respect to a certain characteristics of a node. In this work, the assortativity is determined by the degree of the nodes, and it is given by the use of the Pearson correlation coefficient^{50,51}

$$\rho = \frac{\sum_{ij} ij(f_{ij} - a_i b_j)}{\sigma_a \sigma_b}, \quad (6)$$

where a_i and b_j are the fraction of edges that start and end at nodes with degree values i and j , respectively, f_{ij} is the fraction of edges between nodes of degree i and j , and σ_a and σ_b are the standard deviations of the distributions a and b , respectively. a_i , b_j , and f_{ij} satisfy the sum rules: $\sum_{ij} f_{ij} = 1$, $\sum_j f_{ij} = a_i$, and $\sum_i f_{ij} = b_j$.

The graph assortativity $\rho \in [-1, 1]$ represents how nodes in a network associate with each other; i.e., it shows whether nodes prefer to connect to nodes of the same sort or of opposing sort. When, on average, high degree nodes connect to high degree ones or low degree nodes connect to low degree ones, ρ is close to 1 and the

network is said to be *assortative*. On the other hand, if on average, high degree nodes connect to low degree ones, ρ is close to -1 and the network is said to be *disassortative*. If ρ is close to 0, the connections are considered to be completely random.⁵¹ The reader should notice that there are two different mechanisms of preferential attachment here: assortativity takes into account only the node degree, while neighborhood patterns consider both graph structure and node's natural frequency.

Another basic network measure that is used in this work is the *clustering coefficient*, which measures the presence of loops of size three inside a network; i.e., it measures the tendency of two neighbors of a certain vertex to also be connected to each other. In a real world network, it can be seen as the likelihood of friends of a certain person also to be friends with each other.⁵² The clustering coefficient of a vertex is given by

$$c_i = \frac{2T_i}{d_i(d_i - 1)}, \quad (7)$$

where T_i is the number of triangles involving node i and d_i is the degree of node i . Therefore, the clustering of a node $c_i \in [0, 1]$ is the number of triangles that pass through that node normalized by the maximum number of such triangles in a way that if none of the neighbors of node i are connected to each other, $c_i = 0$, and $c_i = 1$ if all neighbors are connected.⁵³ The average clustering coefficient of the network is given by

$$C = \frac{1}{N} \sum_{i=1}^N c_i. \quad (8)$$

A large clustering coefficient indicates that there are many redundant paths in the network and a low clustering indicates the opposite.

The models of complex networks analyzed in this work are Erdős–Rényi (ER),⁵⁴ Watts–Strogatz (WS),²⁷ and Barabási–Albert (BA)⁵⁵ as they are widely used in the literature.^{8,56} For the BA model, the degree exponent is fixed as $\gamma = 3$. In the ER model, we set the probability of edge creation to be 0.15, and for the WS networks, the probability of rewriting each edge is 0.2. The number of nodes is fixed as $N = 50$.

The main contribution of this work is to analyze the impact on synchronization considering the assortativity and clustering coefficients in association with neighborhood patterns ($\mathcal{S}/\mathcal{N}/\mathcal{D}$). To do so, we proceed as follows.

Network configurations considered here are represented by the pair (A, ω) , where A stands for the adjacency matrix of the graph and ω is the set of natural frequencies. For each network model (BA, ER, WS), the three corresponding network topologies are considered for assortativity and clustering (representing low, intermediate, and high values of each) $A^{\rho_{min}}, A^{\rho_{middle}}, A^{\rho_{max}}, A^{C_{min}}, A^{C_{middle}}, A^{C_{max}}$, and three patterns of the distribution of natural frequencies are considered: Neutral $\omega^{\mathcal{N}}$, Similar $\omega^{\mathcal{S}}$, and Dissimilar $\omega^{\mathcal{D}}$. In all, 27 configurations are studied for assortativity and 27 for the clustering coefficient. As an example, consider a BA network with low value of assortativity $A^{\rho_{min}}$. For this network, a random set of natural frequencies is generated from a uniform distribution (Neutral dissonance pattern), giving rise to the Configuration $(A^{\rho_{min}}, \omega^{\mathcal{N}})$. Then, the simulated annealing algorithm is used to optimize the

values of the total dissonance with a low value, giving rise to the set of natural frequencies of the Similar pattern and the configuration $(A^{\rho_{min}}, \omega^{\mathcal{S}})$ and a high value generating the set of natural frequencies of the Dissimilar pattern and the Configuration $(A^{\rho_{min}}, \omega^{\mathcal{D}})$. Recall that dissonance patterns do not alter the physical configuration of networks, it only interchanges the natural frequencies. The low and high assortativity/clustering values are the only ones that come from a different network configuration. The choosing of $A^{\rho_{min}}, A^{\rho_{middle}}, A^{\rho_{max}}, A^{C_{min}}, A^{C_{middle}},$ and $A^{C_{max}}$ is discussed in Sec. III.

In order to measure how the total dissonance combined with assortativity and clustering coefficients affect the global synchronization of the networks, the Kuramoto model [Eq. (1)] is numerically integrated and the mean value of the order parameter is calculated $\langle R \rangle$ over the integration time and is denoted by $\langle R \rangle$. We call $\langle R \rangle_{PL}$ and λ_{PL} the values of the order parameter and the coupling constant, respectively, at the emergence of phase locking ($S = 1$). The initial conditions are the same for all networks used in this work and were all set as $\theta_i(0) = 0.5$ for $i = 1, \dots, N$, where N is the total number of nodes. This choice was intentional because as shown in previous works,³ the set of initial conditions can also play an important role in the synchronization of the system, but this is not the scope of this work. The distribution of the natural frequencies for the Neutral patterns is drawn randomly by a uniform distribution over $[-\pi, \pi]$.

III. RESULTS AND DISCUSSION

ER, WS, and BA topology models are used in this work. Each of them has specific topology, and in order to obtain networks with low and high values of assortativity and clustering coefficient, we chose to create 1×10^6 networks of each type and pick three of each model, which present lowest, intermediate, and highest values of the measures being considered. In this way, we make sure to keep the topology of the network models. The histograms of all networks generated as a function of assortativity and clustering coefficients can be seen in Fig. 1.

By construction, the BA model has a preferential attachment rule when building the graph; therefore, the probability of a new node to connect with an existing one is proportional to the existing node degree. Therefore, these networks are characterized by having a few nodes highly connected (called *hubs*) and the rest of the nodes with few connections. It is by construction a network with a negative value of assortativity where nodes with low degree tend to connect to the ones with high degree. On the other hand, ER and WS do not have a preferential attachment rule, and the vertices have a rather random pattern of connections. Therefore, the average assortativity is expected to be around zero. When it comes to the clustering coefficient, the WS model is the one expected, in average, to have the higher number of loops of size three as it is constructed by rewriting some edges of a regular network, which are known to have a high clustering coefficient.^{51,53,56}

We then pick the adjacency matrices A that generate extreme values of ρ and C from the histogram in Fig. 1 (ρ_{min} and C_{min} are the smallest and ρ_{max} and C_{max} are the greatest values) and ones that generate values approximately in the middle of them (ρ_{middle} and C_{middle}). Therefore, we have the BA model with $\rho_{min} = -0.7354$, $\rho_{middle} = -0.2898$, $\rho_{max} = 0.1034$; the ER model

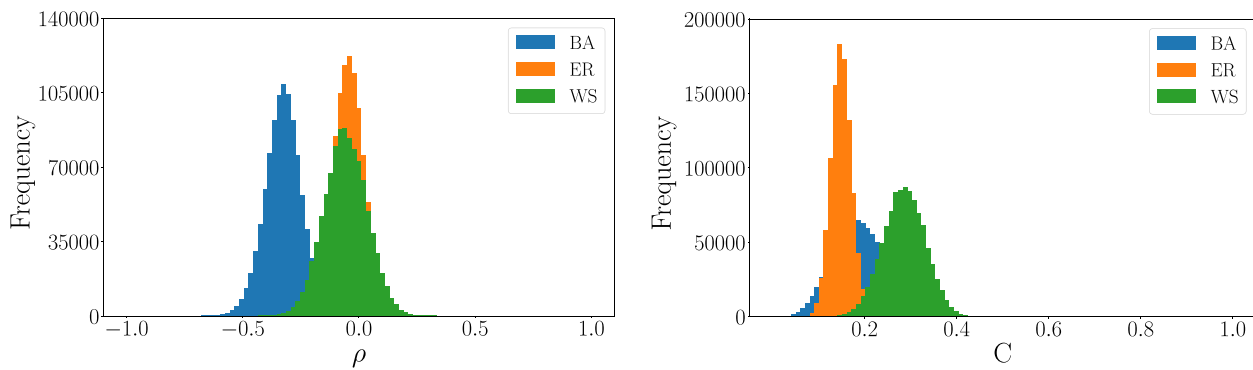


FIG. 1. Histograms of Erdős–Rényi (orange), Watts–Strogatz (green), and Barabási–Albert (blue) networks in relation to (a) assortativity (ρ) and (b) clustering coefficient (C). 1×10^6 networks were generated to compute each histogram.

with $\rho_{min} = -0.3560$, $\rho_{middle} = -0.0505$, $\rho_{max} = 0.2584$; and the WS model with $\rho_{min} = -0.5079$, $\rho_{middle} = -0.0515$, $\rho_{max} = 0.4032$.

The topologies related to the minimum and maximum values of ρ and C , along with the three dissonance patterns, can be seen in Figs. 2 and 3. One can notice that for the Similar pattern, nodes tend to be connected to ones that have a similar natural frequency (similar node color) and that for the Dissimilar pattern, they tend to be connected with nodes with different natural frequencies. This is expected; therefore, we can confirm that our optimization algorithm is working (the algorithm used to generate these patterns converges to a local, not global, value of the objective function that it is trying to maximize/minimize). The Neutral pattern stays in the middle as some nodes connect with nodes with similar frequencies and some connect with nodes with dissimilar frequencies. Recall that dissonance patterns do not alter the physical configuration of the networks, it only interchanges the natural frequencies. The low and high assortativity/clustering values are the only ones that come from a different network configuration.

The mean of the order parameter (R) and the total partial synchronization index S as a function of the overall coupling for networks with high and low assortativity and clustering coefficient and all three dissonance patterns for the BA, ER, and WS models are presented in Figs. 4 and 5, respectively. In relation to the patterns Similar, Neutral, and Dissimilar, one can note that, for small coupling, the Similar pattern favors weaker forms of synchronization both to a phase locked state (higher value of S) and to a phase synchronized state (higher value of $\langle R \rangle$) for the BA, ER, and WS models since the growth of these measures is more protuberant at first for small values of coupling. The dissimilar pattern appears to be the harder to achieve synchronization, while the Neutral one stays in the middle. As the coupling λ is increased, the Dissimilar pattern presents a higher growth on both $\langle R \rangle$ and S and is the first of the patterns to reach phase locking. As the coupling increases even more, it is time of the Neutral pattern to reach the phase locking state, and then for greater λ , the Similar pattern also synchronizes. Therefore, the Dissimilar natural frequency distribution pattern is the one that mostly favors the achievement of the synchronized state. This behavior was also observed by Freitas *et al.*²⁶ and Scafuti *et al.*⁴¹

In relation to the illustrative example given at the beginning of the paper about the discussion of a polemic subject, we can conclude that if mostly similar minded people talk to each other, an agreement seems to be close by people making only a small effort, but at some point, the discussion somehow does not advance anymore and more effort is needed in order to reach an agreement. On the other hand, when people tend to talk with the ones that have distinct opinions, there is a huge discussion at first, and, despite the increasing effort of all individuals, it seems like an agreement is not reachable, but, after more effort is made by the individuals, a common opinion can finally be reached and all individuals arrive at the same conclusion.

Now, we investigate how the measures assortativity and clustering coefficient along with the dissonance patterns affect synchronization. In order to do this, we annotate the value of λ for which all configurations in Figs. 4 and 5 reach phase locking, and we name it λ_{PL} . This result is presented in the first column in Figs. 6 (related to assortativity) and 7 (related to clustering). In the second column, there is the value of the order parameter (R_{PL}) for this λ_{PL} . The order parameter R_{PL} shows the amount of phase synchronization of the system at this stage. By definition, the partial synchronization index S at $\lambda = \lambda_{PL}$ is equal to one; therefore, the system is synchronized.

In relation to the network models considered in this work, on average, the ER model is the one that reaches phase locking with lower coupling values (light yellow) when considering the measures assortativity and clustering coefficient in Figs. 6 and 7(a), 7(c), and 7(e). The BA network topology needs on average a high coupling constant to reach the phase locking state when considering assortativity, being then the hardest to synchronize in relation to this measure. WS networks are an intermediate between these two in relation to assortativity but requires the highest values of coupling to reach phase locking when the clustering coefficient is taken into account.

In regard to the network structure, we can infer that disassortative networks seem to favor synchronization for, in general, networks with negative values of ρ require a lower coupling value in order to reach phase locking. In this way, when high degree nodes connect with low degree ones, it favors synchronization (this does

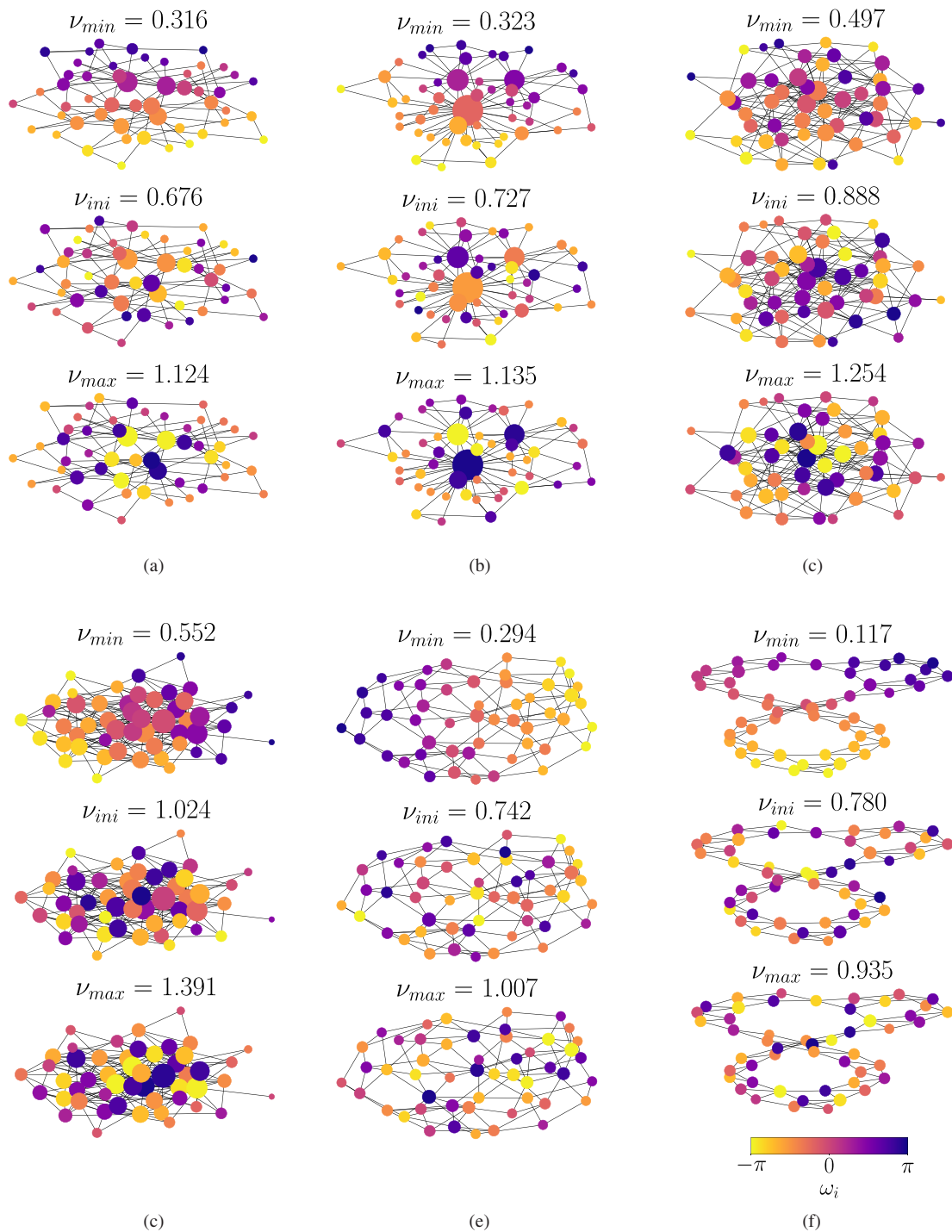


FIG. 2. (a) and (b) BA, (c) and (d) ER, and (e) and (f) WS networks with low and high values of clustering coefficient C . The Similar $\mathcal{S}(\nu_{min})$, Neutral $\mathcal{N}(\nu_{ini})$, and Dissimilar $\mathcal{D}(\nu_{max})$ patterns of dissonance ν are also showed for each network (from top to bottom, respectively). ω_i is the natural frequency of the nodes, and the size of the nodes is proportional to the degree.

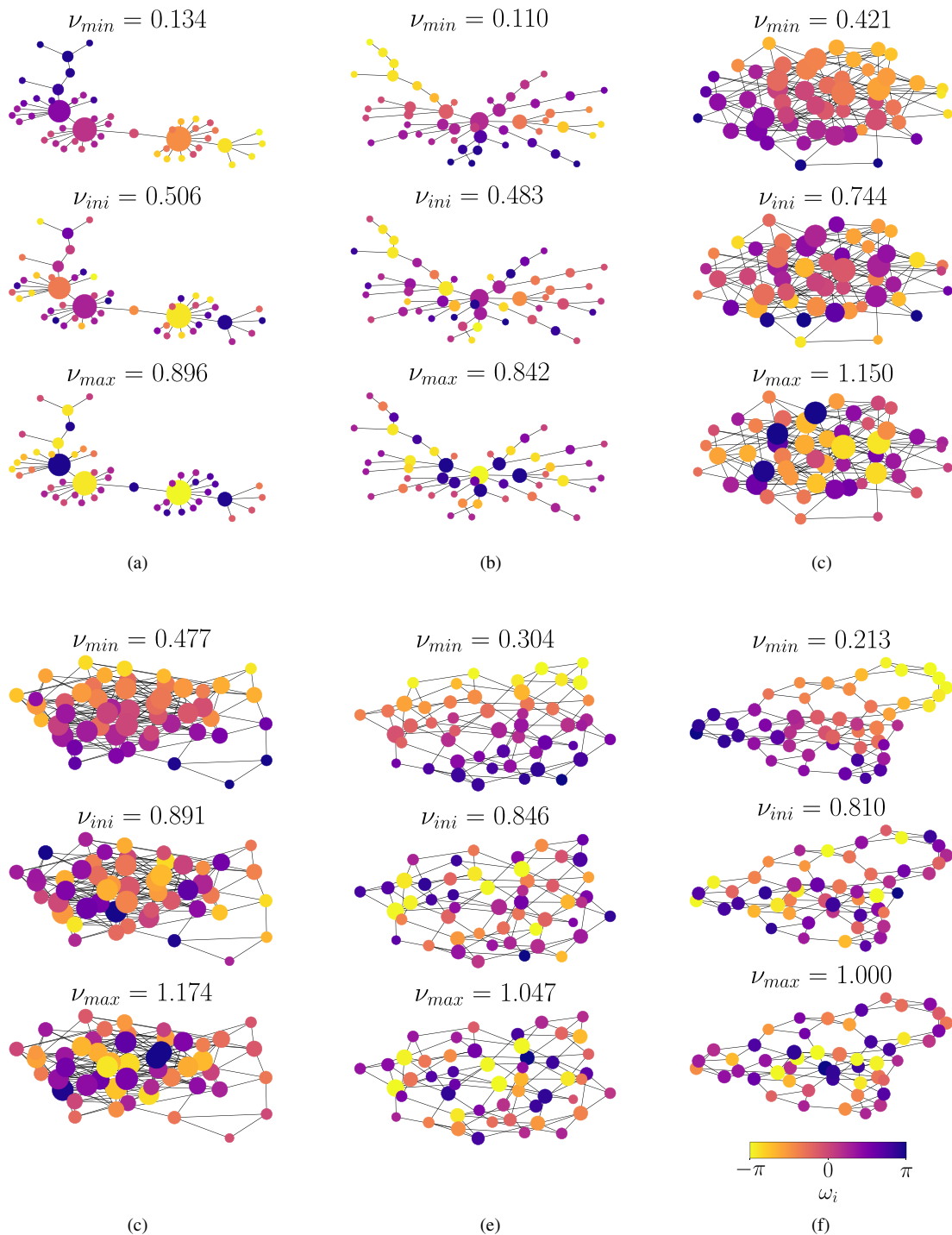


FIG. 3. (a) and (b) BA, (c) and (d) ER, and (e) and (f) WS networks with low and high values of assortativity ρ . The Similar $\mathcal{S}(\nu_{min})$, Neutral $\mathcal{N}(\nu_{ini})$, and Dissimilar $\mathcal{D}(\nu_{max})$ patterns of dissonance ν are also showed for each network (from top to bottom, respectively). ω_i is the natural frequency of the nodes, and the size of the nodes is proportional to the degree.

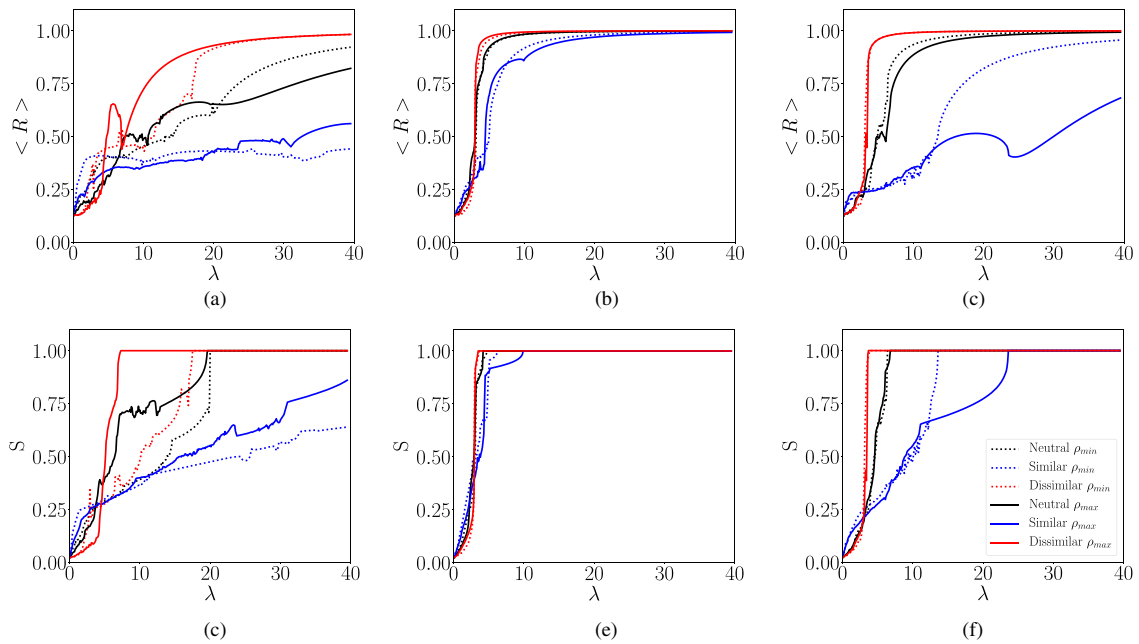


FIG. 4. (a)–(c) Mean of the order parameter $\langle R \rangle$ and (d)–(f) the total partial synchronization index S as a function of the coupling for networks with low (dashed line) and high (continuous line) values of assortativity ρ and patterns Neutral (black), Similar (blue), and Dissimilar (red) of the natural frequency distribution. Note that S converges to 1 for a finite value of λ and $\langle R \rangle$ asymptotically tends to 1.

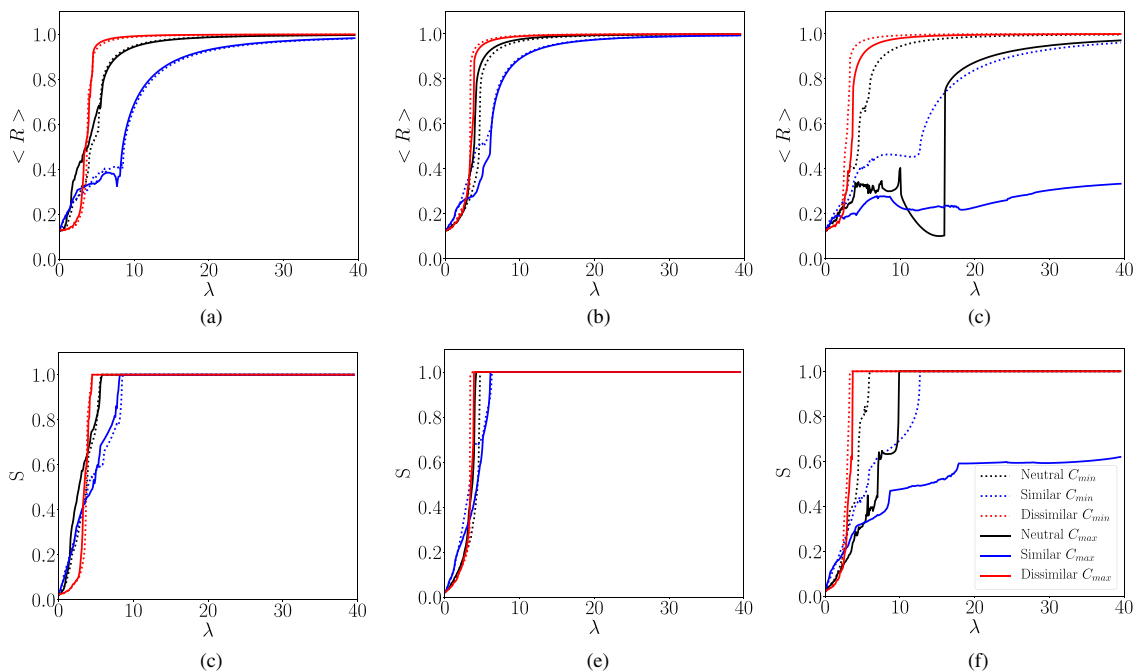


FIG. 5. (a)–(c) Mean of the order parameter $\langle R \rangle$ and (d)–(f) the total partial synchronization index S as a function of the coupling for networks with low (dashed line) and high (continuous line) values of clustering coefficient C and patterns Neutral (black), Similar (blue), and Dissimilar (red) of the natural frequency distribution. Note that S converges to 1 for a finite value of λ (except for the WS Similar C_{max}) and $\langle R \rangle$ asymptotically tends to 1.

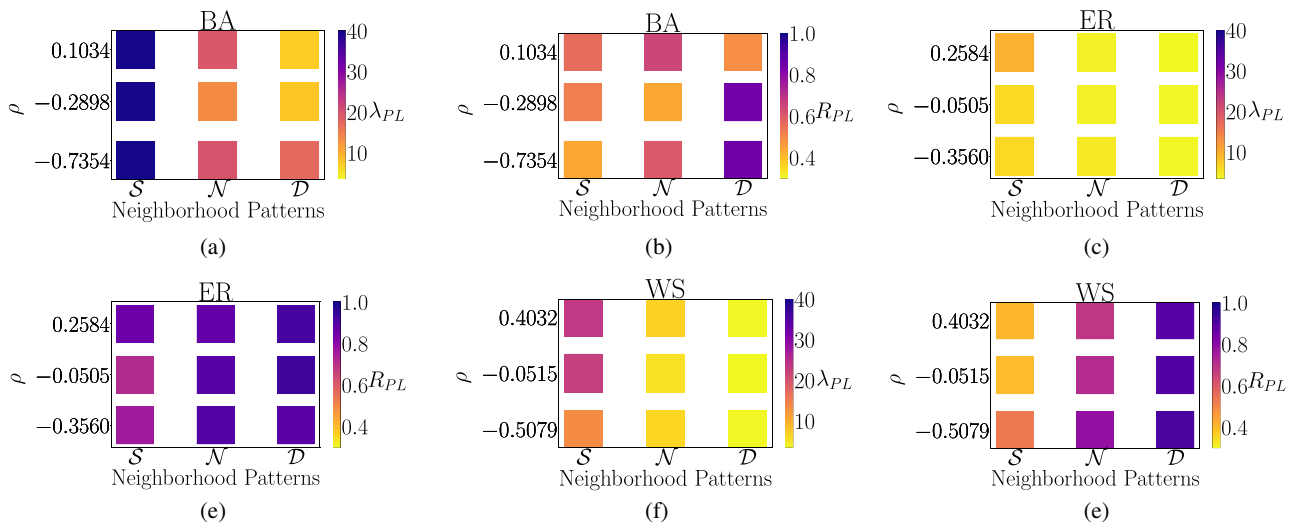


FIG. 6. Contour plot of the assortativity ρ and the neighborhood patterns in relation to the (a), (c), and (e) coupling λ_{PL} and (b), (d), and (f) order parameter R_{PL} at phase locking for the models BA, ER, and WS of networks.

not seem to apply to the BA model). As already mentioned before, the Dissimilar natural frequency pattern tends to favor synchronization, and we can think of the distribution of the nodes in a disassortative network also as being a dissimilar topological distribution as nodes with different degree tend to connect to each other. Therefore, when analyzing our example, instead of having popular

individuals communicating among each other, it is best if popular individuals talk to less popular ones.

In relation to the clustering coefficient, networks with fewer loops of size three seem to favor synchronization as, on average, networks with the lowest value of C tend to be easier to synchronize. When it comes to our example, this means that it is best to avoid the

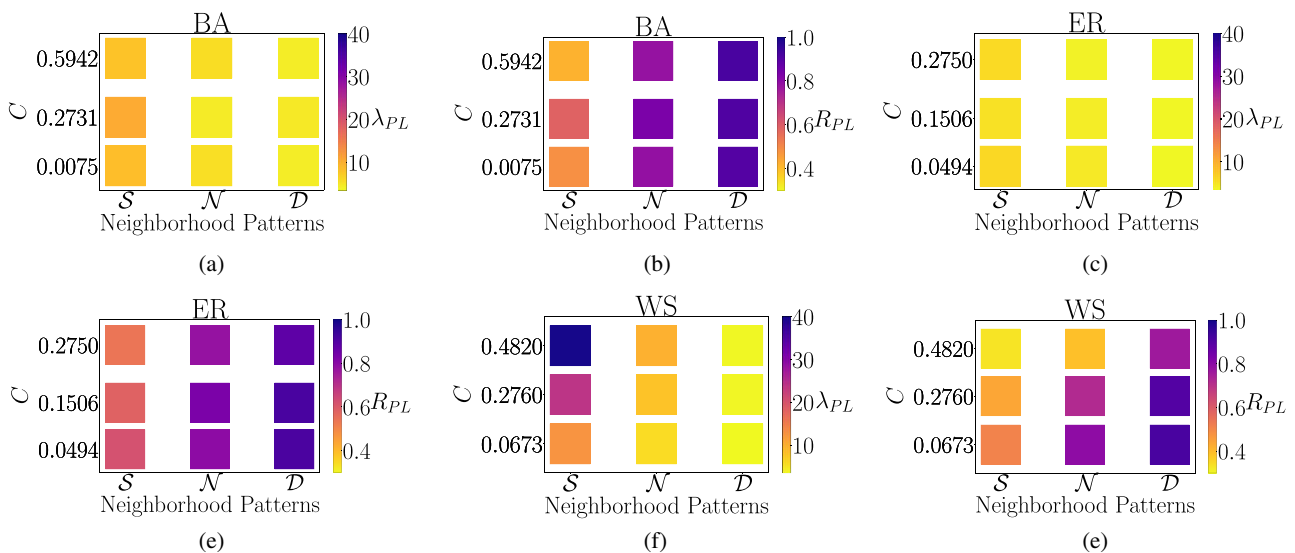


FIG. 7. Contour plot of the clustering coefficient C and the neighborhood patterns in relation to the (a), (c), and (e) coupling λ_{PL} and (b), (d), and (f) order parameter (R) $_{PL}$ at phase locking for the models BA, ER, and WS of networks.

contacts of an individual to communicate with each other, avoiding then the creation of a small cycle of discussion as this may create unnecessary debates and, therefore, increase the effort to achieve an agreement.

In general, the measures assortativity and clustering coefficient seem to have a stronger effect on the synchronization of the Similar dissonance patterns (especially when considering the WS model), having a modest effect on the Neutral pattern and a very low effect on the Dissimilar one.

IV. CONCLUSIONS

The influence of the structure of complex networks of non-identical oscillators on global synchronization was studied. The total dissonance metric for neighborhood similarity was employed, and, with the help of an optimization algorithm, three patterns of natural frequency distributions were created, one where adjacent nodes have similar frequencies (Similar pattern), one where they have different frequencies (Dissimilar), and one that is a blend of both (Neutral). Network topologies of the models Erdős–Rényi, Watts–Strogatz, and Barabási–Albert with high, intermediate, and low values of the network measure assortativity and clustering coefficient were created and along with the frequency patterns were used to study the synchronization of these systems.

In relation to the emergence of phase locking, at low values of the coupling constant, the Similar pattern clearly favors weaker synchronization regimes, but, as the coupling is increased, the Dissimilar pattern presents a rapid growth and is the first to reach synchronization, which corroborates previous works.^{26,41} As for the complex network models used in this work, the Erdős–Rényi showed itself as the easiest to reach the regime of synchronization when compared to Watts–Strogatz and Barabási–Albert, but this has yet to be confirmed by future experiments by comparing, for example, these three models where each one has the same values of assortativity and/or clustering coefficient. In relation to the network measures employed here, in general, both low values of assortativity and clustering coefficient appear to favor synchronization, especially for the Similar dissonance pattern.

In summary, answering the questions raised at the beginning of this paper, based on our findings, we can state that the best way to conduct a discussion on a polemic subject is by encouraging individuals with different opinions to talk to each other and also encourage popular individuals to talk to less popular ones. It is also a good idea to avoid contacts of individuals to talk to each other, avoiding then small cycles of discussions. This hypothesis has yet to be confirmed by future experiments.

As for future work, we consider to use the BA model with distinct degree exponents. We also intend to investigate the role that the average degree of the networks has on synchronization. The behavior of the WS configuration ($A^{C_{min}}, \omega^{\mathcal{S}}$), which does not reach the synchronous state even for high values of λ , as shown in Fig. 2, has also to be better analyzed.

ACKNOWLEDGMENTS

The authors would like to thank Conselho Nacional de Desenvolvimento Científico e Tecnológico (CNPq) for the financial

support (Grant No. 141138/2017-3). This research is also supported by the São Paulo Research Foundation (FAPESP) (Grant Nos. 2015/50122 and 2018/03211-6).

AUTHOR DECLARATIONS

Conflict of Interest

The authors have no conflicts to disclose.

DATA AVAILABILITY

The data that support the findings of this study are available from the corresponding author upon reasonable request.

REFERENCES

- ¹A. Pikovsky, M. Rosenblum, and J. Kurths, *Synchronization* (Cambridge University Press, Cambridge, 2003), Vol. 12.
- ²B. Vickhoff, H. Malmgren, R. Åström, G. Nyberg, M. Engvall, J. Snygg, M. Nilsson, and R. Jörnsten, “Music structure determines heart rate variability of singers,” *Front. Psychol.* **4**, 334 (2013).
- ³J. Lacerda, C. Freitas, and E. Macau, “Multistable remote synchronization in a star-like network of non-identical oscillators,” *Appl. Math. Model.* **69**, 453–465 (2019).
- ⁴C. Batista, J. Szezech, Jr., A. Batista, E. Macau, and R. Viana, “Synchronization of phase oscillators with coupling mediated by a diffusing substance,” *Physica A* **470**, 236–248 (2017).
- ⁵A. Loppini, A. Capolupo, C. Cherubini, A. Gizzi, M. Bertolaso, S. Filippi, and G. Vitiello, “On the coherent behavior of pancreatic beta cell clusters,” *Phys. Lett. A* **378**, 3210–3217 (2014).
- ⁶L. Fortuna and M. Frasca, “Experimental synchronization of single-transistor-based chaotic circuits,” *Chaos* **17**, 043118 (2007).
- ⁷P. Protachevicz, R. Borges, A. Reis, F. Borges, K. Iarosz, I. Caldas, E. Lameu, E. Macau, R. Viana, I. Sokolov *et al.*, “Synchronous behaviour in network model based on human cortico-cortical connections,” *Physiol. Meas.* **39**, 074006 (2018).
- ⁸A. Arenas, A. Díaz-Guilera, J. Kurths, Y. Moreno, and C. Zhou, “Synchronization in complex networks,” *Phys. Rep.* **469**, 93–153 (2008).
- ⁹L. V. Gambuzza, A. Cardillo, A. Fiasconaro, L. Fortuna, J. Gómez-Gardenes, and M. Frasca, “Analysis of remote synchronization in complex networks,” *Chaos* **23**, 043103 (2013).
- ¹⁰Y. Kuramoto, “Self-entrainment of a population of coupled non-linear oscillators,” in *International Symposium on Mathematical Problems in Theoretical Physics*, edited by H. Haraki (Springer-Verlag, Berlin, 1975), pp. 420–422.
- ¹¹J. A. Acebrón, L. L. Bonilla, C. J. P. Vicente, F. Ritort, and R. Spigler, “The Kuramoto model: A simple paradigm for synchronization phenomena,” *Rev. Mod. Phys.* **77**, 137 (2005).
- ¹²S. H. Strogatz, “Exploring complex networks,” *Nature* **410**, 268 (2001).
- ¹³A. T. Winfree, “Biological rhythms and the behavior of populations of coupled oscillators,” *J. Theor. Biol.* **16**, 15–42 (1967).
- ¹⁴S. Boccaletti, V. Latora, Y. Moreno, M. Chavez, and D.-U. Hwang, “Complex networks: Structure and dynamics,” *Phys. Rep.* **424**, 175–308 (2006).
- ¹⁵V. L. Freitas, J. C. Lacerda, and E. E. Macau, “Complex networks approach for dynamical characterization of nonlinear systems,” *Int. J. Bifurcation Chaos* **29**, 1950188 (2019).
- ¹⁶X. Yu, Z. Jia, and X. Jian, “Logistic mapping-based complex network modeling,” *Appl. Math. (Irvine)* **4**, 1558 (2013).
- ¹⁷L. A. Magrini, M. Oliveira Domingues, E. E. Macau, and I. Z. Kiss, “Synchronization in populations of electrochemical bursting oscillators with chaotic slow dynamics,” *Chaos* **31**, 053125 (2021).
- ¹⁸H. Jeong, B. Tombor, R. Albert, Z. N. Oltvai, and A.-L. Barabási, “The large-scale organization of metabolic networks,” *Nature* **407**, 651–654 (2000).

- ¹⁹H. Jeong, S. P. Mason, A.-L. Barabási, and Z. N. Oltvai, “Lethality and centrality in protein networks,” *Nature* **411**, 41–42 (2001).
- ²⁰R. V. Sole and M. Montoya, “Complexity and fragility in ecological networks,” *Proc. R. Soc. London, Ser. B* **268**, 2039–2045 (2001).
- ²¹J. Camacho, R. Guimerà, and L. A. N. Amaral, “Robust patterns in food web structure,” *Phys. Rev. Lett.* **88**, 228102 (2002).
- ²²J. C. Lacerda, J. Dias, C. Freitas, and E. Macau, “Synchronization of energy transmission networks at low voltage levels,” *Appl. Math. Model.* **89**, 627–635 (2021).
- ²³J. Grzybowski, E. Macau, and T. Yoneyama, “On synchronization in power-grids modelled as networks of second-order Kuramoto oscillators,” *Chaos* **26**, 113113 (2016).
- ²⁴J. C. Lacerda, J. Dias, C. Freitas, and E. Macau, “Vulnerability and stability of power grids modeled by second-order Kuramoto model: A mini review,” *Eur. Phys. J. Spec. Top.* **230**, 1–9 (2021).
- ²⁵G. Filatrella, A. H. Nielsen, and N. F. Pedersen, “Analysis of a power grid using a Kuramoto-like model,” *Eur. Phys. J. B* **61**, 485–491 (2008).
- ²⁶C. Freitas, E. Macau, and R. L. Viana, “Synchronization versus neighborhood similarity in complex networks of nonidentical oscillators,” *Phys. Rev. E* **92**, 032901 (2015).
- ²⁷D. J. Watts and S. H. Strogatz, “Collective dynamics of small-world networks,” *Nature* **393**, 440–442 (1998).
- ²⁸L. A. N. Amaral, A. Scala, M. Barthelemy, and H. E. Stanley, “Classes of small-world networks,” *Proc. Natl. Acad. Sci. U.S.A.* **97**, 11149–11152 (2000).
- ²⁹H. Zhang, W. Zhang, and J. Gao, “Synchronization of interconnected heterogeneous networks: The role of network sizes,” *Sci. Rep.* **9**, 1–12 (2019).
- ³⁰M. M. Danziger, I. Bonamassa, S. Boccaletti, and S. Havlin, “Dynamic interdependence and competition in multilayer networks,” *Nat. Phys.* **15**, 178–185 (2019).
- ³¹C. Parkinson, A. M. Kleinbaum, and T. Wheatley, “Similar neural responses predict friendship,” *Nat. Commun.* **9**, 332 (2018).
- ³²K. A. Urberg, S. M. Degirmencioglu, and J. M. Tolson, “Adolescent friendship selection and termination: The role of similarity,” *J. Soc. Pers. Relat.* **15**, 703–710 (1998).
- ³³J. B. Kupersmidt, M. E. DeRosier, and C. P. Patterson, “Similarity as the basis for children’s friendships: The roles of sociometric status, aggressive and withdrawn behavior, academic achievement and demographic characteristics,” *J. Soc. Pers. Relat.* **12**, 439–452 (1995).
- ³⁴G. J. Haselager, W. W. Hartup, C. F. Lieshout, and J. M. A. Riksen-Walraven, “Similarities between friends and nonfriends in middle childhood,” *Child Dev.* **69**, 1198–1208 (1998).
- ³⁵D. J. Penn and W. K. Potts, “The evolution of mating preferences and major histocompatibility complex genes,” *Am. Nat.* **153**, 145–164 (1999).
- ³⁶W. Jordan and M. Bruford, “New perspectives on mate choice and the MHC,” *Heredity* **81**, 127 (1998).
- ³⁷L. Bernatchez and C. Landry, “MHC studies in nonmodel vertebrates: What have we learned about natural selection in 15 years?,” *J. Evol. Biol.* **16**, 363–377 (2003).
- ³⁸S. Pieltney and M. Oliver, “The evolutionary ecology of the major histocompatibility complex,” *Heredity* **96**, 7 (2006).
- ³⁹R. S. Pinto and A. Saa, “Optimal synchronization of Kuramoto oscillators: A dimensional reduction approach,” *Phys. Rev. E* **92**, 062801 (2015).
- ⁴⁰G. A. Gottwald, “Model reduction for networks of coupled oscillators,” *Chaos* **25**, 053111 (2015).
- ⁴¹F. Scafuti, T. Aoki, and M. di Bernardo, “Heterogeneity induces emergent functional networks for synchronization,” *Phys. Rev. E* **91**, 062913 (2015).
- ⁴²A. Pluchino, V. Latora, and A. Rapisarda, “Changing opinions in a changing world: A new perspective in sociophysics,” *Int. J. Mod. Phys. C* **16**, 515–531 (2005).
- ⁴³A. Pluchino, S. Boccaletti, V. Latora, and A. Rapisarda, “Opinion dynamics and synchronization in a network of scientific collaborations,” *Physica A* **372**, 316–325 (2006).
- ⁴⁴H. Noorazar, “Recent advances in opinion propagation dynamics: A 2020 survey,” *Eur. Phys. J. Plus* **135**, 521 (2020).
- ⁴⁵G. Deffuant, D. Neau, F. Amblard, and G. Weisbuch, “Mixing beliefs among interacting agents,” *Adv. Complex Syst.* **3**, 87–98 (2000).
- ⁴⁶I. Z. Kiss, Y. Zhai, and J. L. Hudson, “Emerging coherence in a population of chemical oscillators,” *Science* **296**, 1676–1678 (2002).
- ⁴⁷B. C. Daniels, “Synchronization of globally coupled nonlinear oscillators: The rich behavior of the Kuramoto model,” Ohio Wesleyan Physics Department Essay, Vol. 7, 2005.
- ⁴⁸P. J. Van Laarhoven and E. H. Aarts, “Simulated annealing,” in *Simulated Annealing: Theory and Applications* (Springer, 1987), pp. 7–15.
- ⁴⁹J. Gómez-Gardenes, Y. Moreno, and A. Arenas, “Paths to synchronization on complex networks,” *Phys. Rev. Lett.* **98**, 034101 (2007).
- ⁵⁰M. E. Newman, “Mixing patterns in networks,” *Phys. Rev. E* **67**, 026126 (2003).
- ⁵¹R. Noldus and P. Van Mieghem, “Assortativity in complex networks,” *J. Complex Netw.* **3**, 507–542 (2015).
- ⁵²S. Wasserman and K. Faust, *Social Network Analysis: Methods and Applications* (Cambridge University Press, Cambridge, UK, 1994), Vol. 8.
- ⁵³J. Saramäki, M. Kivelä, J.-P. Onnela, K. Kaski, and J. Kertesz, “Generalizations of the clustering coefficient to weighted complex networks,” *Phys. Rev. E* **75**, 027105 (2007).
- ⁵⁴P. Erdős and A. Rényi, “On random graphs, I,” *Publ. Math. (Debrecen)* **6**, 290–297 (1959).
- ⁵⁵A.-L. Barabási and R. Albert, “Emergence of scaling in random networks,” *Science* **286**, 509–512 (1999).
- ⁵⁶L. D. F. Costa, F. A. Rodrigues, G. Travieso, and P. R. Villas Boas, “Characterization of complex networks: A survey of measurements,” *Adv. Phys.* **56**, 167–242 (2007).

PUBLICAÇÕES TÉCNICO-CIENTÍFICAS EDITADAS PELO INPE

Teses e Dissertações (TDI)

Teses e Dissertações apresentadas nos Cursos de Pós-Graduação do INPE.

Manuais Técnicos (MAN)

São publicações de caráter técnico que incluem normas, procedimentos, instruções e orientações.

Notas Técnico-Científicas (NTC)

Incluem resultados preliminares de pesquisa, descrição de equipamentos, descrição e ou documentação de programas de computador, descrição de sistemas e experimentos, apresentação de testes, dados, atlas, e documentação de projetos de engenharia.

Relatórios de Pesquisa (RPQ)

Reportam resultados ou progressos de pesquisas tanto de natureza técnica quanto científica, cujo nível seja compatível com o de uma publicação em periódico nacional ou internacional.

Propostas e Relatórios de Projetos (PRP)

São propostas de projetos técnico-científicos e relatórios de acompanhamento de projetos, atividades e convênios.

Publicações Didáticas (PUD)

Incluem apostilas, notas de aula e manuais didáticos.

Publicações Seriadas

São os seriados técnico-científicos: boletins, periódicos, anuários e anais de eventos (simpósios e congressos). Constam destas publicações o International Standard Serial Number (ISSN), que é um código único e definitivo para identificação de títulos de seriados.

Programas de Computador (PDC)

São a seqüência de instruções ou códigos, expressos em uma linguagem de programação compilada ou interpretada, a ser executada por um computador para alcançar um determinado objetivo. Aceitam-se tanto programas fonte quanto os executáveis.

Pré-publicações (PRE)

Todos os artigos publicados em periódicos, anais e como capítulos de livros.